12-2019

Fractional Order State Feedback Control for Improved Lateral Stability of Semi-Autonomous Commercial Heavy Vehicles

Rasheed Mazen Abdulkader
University of Arkansas, Fayetteville

Fractional Order State Feedback Control for Improved Lateral Stability of Semi-Autonomous Commercial Heavy Vehicles

A dissertation submitted in partial fulfillment
of the requirements for the degree of
Doctor of Philosophy in Engineering with a concentration in Electrical Engineering

by

Rasheed Mazen Abdulkader
University of St. Thomas
Bachelor of Science in Electrical Engineering, 2011
University of Illinois
Master of Science in Electrical & Computer Engineering, 2012

December 2019
University of Arkansas

This dissertation is approved for recommendation to the Graduate Council.

_____
Roy McCann, Ph.D.
Dissertation Director

_____
Yue Zhao, Ph.D.
Committee Member

_____
Jingxian Wu, Ph.D.
Committee Member

_____
Mark Arnold, Ph.D.
Committee Member

Abstract

With the growing development of autonomous and semi-autonomous large commercial heavy vehicles, the lateral stability control of articulated vehicles have caught the attention of researchers recently. Active vehicle front steering (AFS) can enhance the handling performance and stability of articulated vehicles for an emergency highway maneuver scenario. However, with large vehicles such tractor-trailers, the system becomes more complex to control and there is an increased occurrence of instabilities. This research investigates a new control scheme based on fractional calculus as a technique that ensures lateral stability of articulated large heavy vehicles during evasive highway maneuvering scenarios. The control method is first implemented to a passenger vehicle model with 2-axles based on the well-known “bicycle model”. The model is then extended and applied onto larger three-axle commercial heavy vehicles in platooning operations. To validate the proposed new control algorithm, the system is linearized and a fractional order PI state feedback control is developed based on the linearized model. Then using Matlab/Simulink, the developed fractional-order linear controller is implemented onto the non-linear tractor-trailer dynamic model. The tractor-trailer system is modeled based on the conventional integer-order techniques and then a non-integer linear controller is developed to control the system. Overall, results confirm that the proposed controller improves the lateral stability of a tractor-trailer response time by 20% as compared to a professional truck driver during an evasive highway maneuvering scenario. In addition, the effects of variable truck cargo loading and longitudinal speed are evaluated to confirm the robustness of the new control method under a variety of potential operating conditions.

Acknowledgement

Initially, I would like to thank Allah (God) for making me complete this mission and giving me hope, strength and inspiration throughout my studies in the United States, as this mission would not be accomplished without Allah blessing.

I would like to thank the Saudi Arabian Government and the Saudi Arabian Cultural Mission (SACM) for providing me with this one in a life time opportunity to be sponsored for my study in the United States.

I would like express my deep gratitude and sincere appreciation to my advisor Dr. Roy A. McCann for his support, encouragement, guidance and being a source enlightenment to me throughout my PhD studies, as he has helped me in many aspects to complete this mission. Also, I would like to thank all the committee members for their guidance and support during this process.

This dissertation is dedicated to my parents Mazen and Muna for their constant prayers, love, support, encouragement and motivation throughout my studies period and for their long patience. Also I would like to thank all my sisters Dalia, Layla, Rania and Nouf for their love, support and encouragement. Special thanks for my wife Sultana and my recently born son Mazen for all their patience and support throughout this journey.

I would like to thank all my friends and family members whom have supported and helped throughout thing long journey whether they were located near me or thousands of miles away.

Dedication

This dissertation is dedicated to:

My Father Dr. Mazen

Table of Contents

Chapter 1

Chapter 2

Chapter 3

Chapter 4

Chapter 5

Chapter 6

Chapter 7

List of Figures

List of Tables

List of Symbols

Symbol	Description
a_1	Distance of the front axle to C.G of the tractor
b_1	Distance of the rear axle to C.G of the tractor
b_2	Distance of the trailer axle to C.G of the trailer
e_2	Trailer 5th wheel pivot distance from C.G
d_1	Tractor 5th wheel pivot
C_1/C_2	Tractor front and rear tire cornering stiffness
C_3	Trailer tire cornering stiffness
m_1/m_2	Mass of the tractor/trailer
u_1/u_2	Longitudinal speed of the tractor/trailer
v_1/v_2	Lateral speed at C.G of tractor/trailer
r_1/r_2	Yaw rate of the tractor/trailer
ψ	Articulation angle
δ_f	Front wheel steering angle
I_{z1}/I_{z2}	Yaw moment of inertia of the tractor/trailer
F_x	Longitudinal force applied by the 5th wheel
F_y	Lateral force applied by the 5th wheel
F_{xi}	Longitudinal force applied to the ith wheel
F_{yi}	Lateral force applied to the ith wheel
F_{a1}	Aero-dynamical force applied to the tractor
F_{a2}	Aero-dynamical force applied to the trailer
α_i	Tire slip angle for the ith tire
J_s	Inertia of the steering system
K_s	Self-aligning stiffness of the tires
τ_{hw}	Hand wheel torque
τ_{afs}	Active front steering torque
B_σ	Steering friction
ε	Tire slip angle empirical constant

List of Abbreviations

Symbol	Description
ABS	Anti-lock brake system
ACC	Adaptive cruise control
AFS	Active front steering
ALV	Autonomous land vehicle
BLS	Bureau of Labor Statistics
CFE	Continuous fractional expansion
CG	Center of gravity
DYC	Direct yaw moment control
DOD	Department of Defense
DOT	Department of Transportation
ECU	Electronic control unit
FFT	Fast Fourier transform
FHWA	Federal Highway Administration
FMCSA	Federal Motor Carrier Safety Administration
FO	Fractional order
FOC	Fractional order control
FOPI	Fractional order proportional integral control
FOPID	Fractional order proportional integral derivative control
FOSFB	Fractional order state feedback control
FPAA	Field-programmable analog array
FPGA	Field-programmable gate array
FOTF	Fractional order transfer function
GE	General Motors
GPS	Global positioning system
GVWR	Gross vehicle weight rating
IFT	International transport forum
IO	Integer order
IOPID	Integer order proportional integral derivative
IOPI	Integer order proportional integral

NHTSA	National Highway Transportation Safety Administration
LTI	Linear time invariant
LQR	Linear-quadratic regulator
SBW	Steer-by-wire
SISO	Single-input and single-output
SMC	Sliding mode control
MIMO	Multiple-input and multiple-output
MRAC	Model reference adaptive control
MPC	Model predictive control
PI	Proportional integral
PIC	Peripheral interface controller
PID	Proportional integral derivative
PSE	Power series expansion
PLC	Programmable logic controller
V2I	Vehicle-to-Infrastructure
V2V	Vehicle-to-Vehicle
VSC	Vehicle stability control
VGR	Variable gear ratio
TF	Transfer function
TID	Tilted integral derivative
TTI	Texas A&M Transpiration Institute
TTC	Time to Collison
SAE	Society of Automotive Engineers
SA	Situation awareness

Chapter 1: Introduction

1.1 Background

The development of autonomous and semi-autonomous commercial heavy vehicles are in growing demand by offering improved emissions, passenger comfort and fuel economy, along with the potential to reduce traffic congestion and improve human safety [1]. Large heavy trucks in platooning operations can play an important role in energy saving from aerodynamic drafting, in addition to further reducing highway congestion and safety improvements [2].

Road freight transportation is much needed and significantly dominates other transportation methods such as maritime, air, and rail [3]. Further, in 2015, heavy trucks accounted for 70% of the national freight transportation (U.S DOT), where 10.6 billion tons equaling $10.9 trillion worth of goods were transported by tractor-trailers, with an average of $29 billion worth of goods transported on a daily basis [1].

Lateral stability control is a critical aspect of the vehicle performance which can help a driver maintain control during a sudden or emergency maneuver. Active front steering (AFS) is a technology for increasing vehicle maneuverability and stability by providing an supplemental steering angle that is independent of the driver hand wheel input [4].

From a safety perspective, in the United States it is estimated that 52% of all road traffic fatalities occur due to roadway departures (FHWA) [6]. Statistical data obtained by the National Highway Transportation Safety Administration (NHTSA) estimates that 2016 traffic fatalities in the U.S. were 37,461 of which 19,676 mortalities involved lane departures. Injuries involving tractor-trailers during that same year are estimated to be 116,000 with 4,327 fatalities [5]. These

numbers suggest significant research and improvement needs to be conducted to solve this issue and reduce this tragic number of fatalities happening annually.

A study conducted by the Federal Motor carrier Safety Administration (FMCSA) examined the elements causing these accidents [72]. The factors that impact the incident of a traffic collision might take place hours, days or even months before the collision taking place. Some of these factors include the level of training and expertise of the driver, fatigue, alcohol consumption, weather conditions and excessive speed. The ten most cited causes of accidents involving heavy-duty trucks and passenger automobiles are presented below. It is noted that semi-automated or automated systems could significantly reduce all of these factors [72]:

- Illegal lane departures
- Fatigue
- False assumption of other roadway user actions
- Interruption of traffic flow
- Unfamiliarity with roadway configuration
- Inattention
- Poor observation
- Driving too fast for conditions
- Poor health or illness
- Distraction by object or person inside the automobile

Vehicle dynamics control can be categorized intro three main areas: lateral, longitudinal and yaw control. Varying factors affect the lateral dynamic performance of an automobile such as the road conditions, vehicle parameters, tire steering angle and the initial operation of the vehicle [3]. Vehicle stability control (VSC) is an active safety method which can help in the reduction of the

total wheel slip amount when accelerating. Furthermore, VSC generally includes active front steering (AFS), direct yaw moment control (DYC), anti-lock braking systems (ABS) and active suspension systems [7].

There are two main concerns for achieving lateral stability for an automobile. The first is the inherent nonlinearities in the vehicle dynamics. The second challenge is that the longitudinal velocity varies with time which makes tracking the performance more complex in order to control the lateral dynamics of the automobile [8]. Ensuring lateral stability for heavy duty vehicles remains one of the concerns in safety system design and development [9]. Large tractor-trailers operate under conditions with many types of uncertainty and remains one of the main concerns of applying modern control theory [10].

One of the circumstances that tends to reduce the stability margin of large trucks is abrupt lateral acceleration. This makes articulated vehicles tend to oversteer during an evasive maneuvering situation as shown in Fig. 1.1. Reduced lateral stability margins are further reduced when travelling at increased highway speeds [9, 11]. Several methods have been developed to increase lateral stability. One method uses gain scheduling of state-feedback [12]. Using this method the vehicle lateral stability and handling were improved by combing AFS and DYC control. Another method has been the application of linear quadratic regulator (LQR) theory [13]. In this case it was shown that the controller reduced load transfer and roll angle at high speeds and improved lateral stability on banked surfaces while also preventing oversteer effects. Sliding mode control (SMC) [14] has been suggested such that the rear of the trailer would be required to follow the track of the 5^{th} wheel. In this approach, the stability and handling were improved by applying the SMC controller for the tractor-trailer dynamics under adverse driving conditions.

H_∞ control was also implemented in numerous studies [15, 16] where the vehicle behavior was improved under critical driving situations. It also illustrated robust performance with respect to model uncertainties such changing the road adhesion coefficient, vehicle forward speed, and freight mass in the trailer. In [17], a lead-lag control provided a driver-assistance function in emergency situations in order to mitigate accident sequences.

Researchers have proposed genetic algorithm control [18] for emergency obstacle avoidance situations that account for the distance at which the driver first detects the object. Model reference adaptive control (MRAC) was implemented in [19] to increase the lateral stability of a car-trailer system. Tt was shown to be effective for enhancing lateral stability during several cycles of a sinusoidal steering input maneuver.

Fuzzy neural networks with self-learning functions have been utilized with various fuzzy logic rules. It was demonstrated in [20] that this control technique can be an effective method for lateral control of intelligent vehicles in tracking desired trajectories. Model predictive control (MPC) [28] was implemented in the basis of altering the trend on tire forces over a specified time interval. The prediction functions would indicate the nonlinear features in the process which resulted in improving the stability and handling of the vehicle steering system.

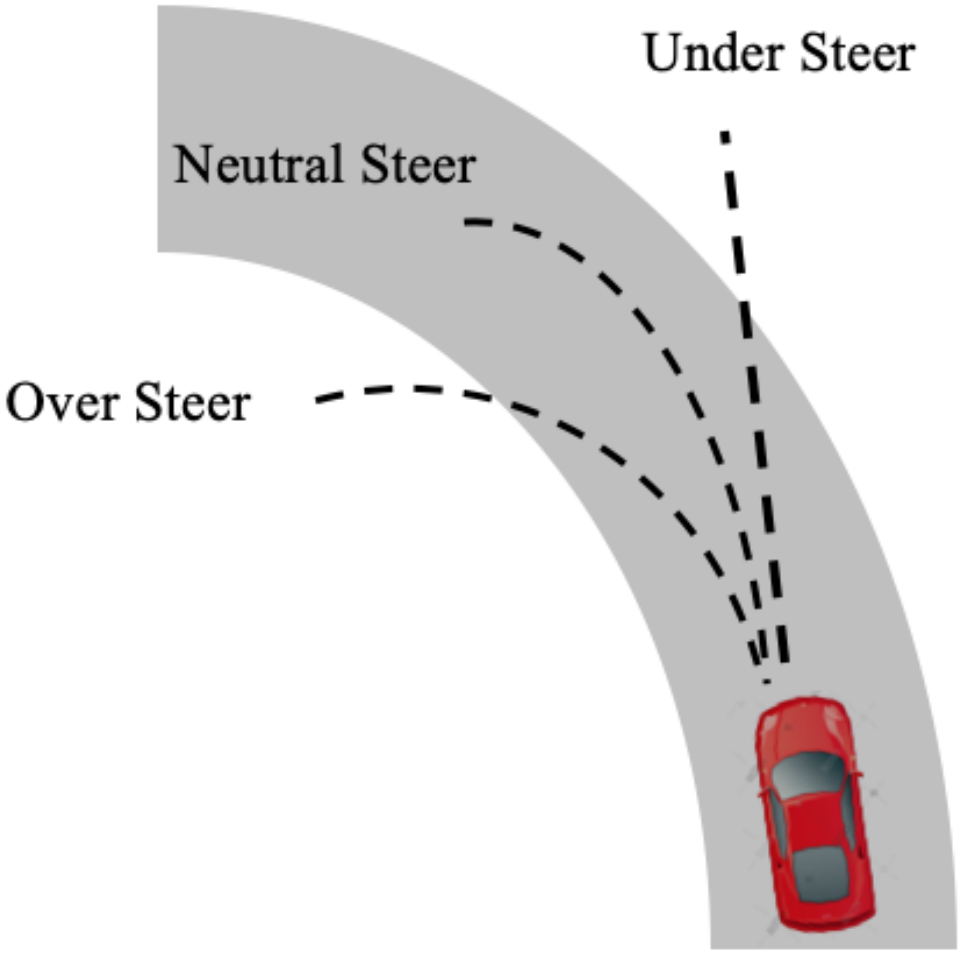

Fig. 1.1. Understeering and oversteering overview.

With today's technologies for automated driving, the vehicle should be able to exceed the human driver capability with improved time response for avoiding collisions. The Society of Automotive Engineers (SAE) six levels of automation is presented in Fig. 1.2. Currently, companies are working on reaching level four and five with the short term goal to reach level six in the near future [3]. For this research, the goal is to achieve the conditional or partial automation (levels two and three) where a driver is still behind the wheel but is not required to monitor the environment at all times but should be ready for intervention when needed.

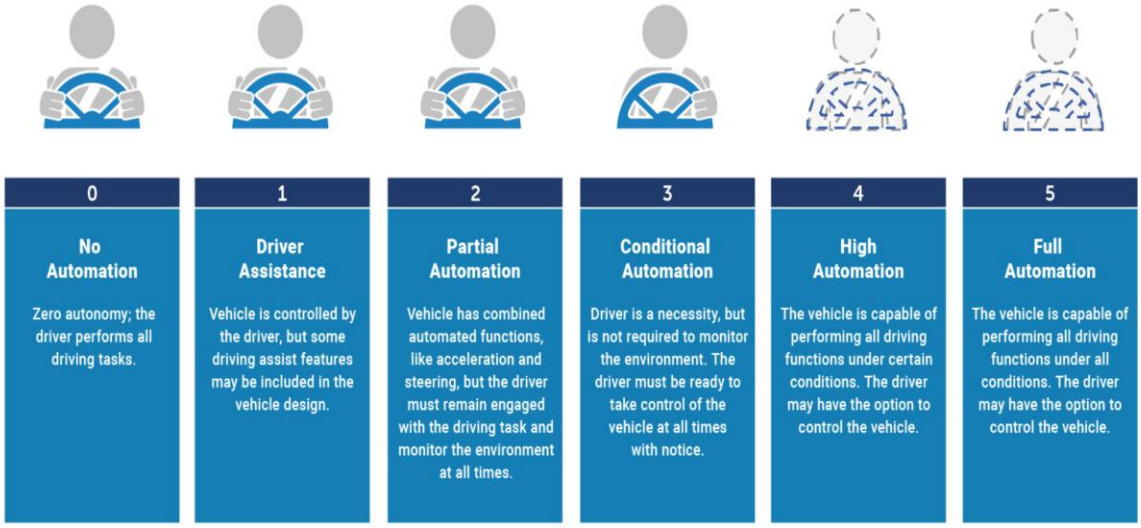

Fig. 1.2. SAE level of automation chart [21].

1.2 Motivation of this Research

Numerous factors can contribute to roadway accidents with human error being estimated to cause 94% of all crashes [22]. Further, tractor-trailer combinations are involved in 72% of fatal crashes involving large trucks [23]. Driving tasks are gradually shifting towards automated driving methods [2, 24] with the expectation of reducing crashes due to human error.

Automated highway systems have attracted researchers' growing attention in recent years [2, 11, 25]. This includes particular attention on lateral stability and is the primary topic of this dissertation. Furthermore, tractor-trailers have the projection of becoming the main beneficiary to automatic control for the following motives [27]:

- The relative equipment price for automated heavy trucks is lower than that for passenger automobiles.

- Tractor-trailers on average travel six times the distance as compared to a passenger automobile. Hence, reducing the number of drivers would reduce the operating price significantly.
- Autonomous heavy trucks can have a substantial influence on improving the overall highway safety.
- Truck drivers have a tedious job and the automation would contribute greatly to reduce the stress levels and thereby would increase safety.

In the U.S., trucks roughly move about 70% of the national freight by weight [1]. Further, goods transport is critical for the economy and transportation volumes are tightly coupled with economic prosperity. However, earlier research on autonomous driving systems was mostly installed on passenger vehicles. It would difficult to deploy autonomous platooning systems for passenger vehicles on public roads since approval by drivers has not been as favorable when compared to tractor-trailers [26]. Overall, autonomous trucks in platooning operations are more likely to be available to the market first due to the major efficiency and safety benefits they can provide [2, 11, 25, 26]

a) Public safety is increased by reducing the number of accidents trucks are involved in.
b) Cost saving by decreasing the cost for shipping companies.
c) Traffic congestion can be significantly reduced.
d) Providing more clean energy saving along with cost reduction from the platooning.
e) Decreasing the workload of the driver with automated driving, is especially effective for truck drivers who tend to drive longer distances than passenger car drivers.

Platooning would offer additional safety and traffic congestion measures along with fuel consumption and greenhouse gas emissions. In a study conducted in 2011 [2] where an observation

of three heavy-duty vehicles in a platooning mode with a distance gap of 6 meters was enforced. The result was an average of 10% reduction in fuel consumption from the platooning operation.

1.3 Objective of this Research

- Develop a new control scheme to improve the lateral stability for an evasive maneuver scenario for tractor-trailers platoons to avoid obstacles and collision while travelling on a highway by accomplishing the following:
    - Achieve a 20% response time improvement over a professional truck driver.
    - Completing an emergency lane change with the tractor-trailer being in the center of the adjacent lane after the maneuver is completed.
    - Integrate lateral steering control design into semi-autonomous heavy vehicles in platooning.

1.4 Scope of this Research

Controlling a moving vehicle requires considerable resources and data collection. For this research, it is assumed that the tractor-trailer is operating in a semi-autonomous platooning mode where the objective is to provide fast lane position control during an evasive maneuver. The requisite sensor measurements are assumed to be available to the control algorithm. This is a reasonable assumption since these sensors are commercially available for supporting existing vehicle technologies. These sensors include:

- Gyroscope.
- Accelerometer.
- Image and GPS.

In addition, the following is assumed while the tractor-trailer is in platooning operation mode:

- Constant longitudinal velocity.
- The tractor-trailer is properly loaded for a balanced cargo weight distribution.
- Road surface conditions are adequate to provide suitable traction for evasive maneuvers.
- No mechanical or equipment failures.
- The roll motion is negligible.

1.5 Contributions and Dissertation Outline

The primary contribution of this research is developing a new control method that achieves the maneuvering requirements for tractor-trailer lateral dynamics. This is achieved with a novel fractional order PI^{λ} state feedback control methodology. This results in improved lateral stability for commercial heavy-vehicles in platooning operations in order to safely change lanes during a highway emergency maneuver situation to avoid an obstacle. The results indicate achieving a 20% time response improvement compared to a skilled human driver. The research also presents a new design method for selecting the optimal fractional order integral value that provides higher stability margin and reduced tracking error for a ramp reference input to a tractor-trailer steering system. It is noted that a fractional order controller has not been previously applied to tractor-trailers and therefore is a new contribution to the field of large track dynamics and control.

The outline of this dissertation is as follows:

- Chapter 1 provides a brief background, the research motivation and objectives.
- Chapter 2 introduces the active front steering mechanism along with passenger vehicle modeling with simulation results.

- Chapter 3 expands the passenger vehicle model to a tractor trailer modeling. The platooning operation is illustrated.
- Chapter 4 presents background information of fractional calculus and the associated theoretical definitions. Fractional order control and its benefits are presented
- Chapter 5 introduces the proposed control method for lateral stability. A fractional order PI state feedback controller is presented and the design method for selecting the optimal fractional order integrator is presented along with the details for implementing the controller. The developed fractional-order controller is initially evaluated with a linearized tractor-trailer model.
- Chapter 6 provides detailed simulation results for a realistic nonlinear model of the tractor-trailer for verification where the proposed control method is compared to a professional truck driver for an evasive maneuver scenario.
- Chapter 7 concludes the major contributions of this dissertation and future research suggestions.

Chapter 2: AFS and Passenger Vehicle Model

2.1 Driver Assistance Devices

Driver assistance technologies can be broadly classified as either passive or active devices. A number of driver assistance devices have been developed by the automotive industry in order to automate driving and minimize the number of highway collisions. Examples of driver assist device include [29]:

- Adaptive cruise control (ACC) that allow a leading vehicle to be followed automatically while maintaining a safe distance.
- Collision avoidance devices which can provide brake assistance to the driver and automatically identify slower moving vehicles to provide a warning.
- Driver condition monitoring devices that can identify objects and obstacles and also deliver warning for the driver in case of a drowsiness.
- Lane departure warning systems.
- Lane keeping systems that provide self-steering during highway environments.
- Vision improvement and night vision devices.

Passive safety devices are classified as vehicle components and systems alert the driver to possible risk conditions. These include in-cab rear-view camera vision systems, blind-spot warning annunciators activated by turn signals, and tire pressure and other dashboard warning lights. To increase the lane change performance, there have been various trailer self-steer axles have been introduced [9]. For minimizing sway motion associated with a trailer, a variety of coupling mechanisms have been suggested [9, 56].

Active safety systems have the goal to prevent collisions by directly modifying vehicle speed and direction through braking, steering and engine controls. In the active control approach, numerous methods have been investigated to enhance vehicle handling by stabilizing the lateral performance of tractor-trailers. These methods include active and rear steering control, active control of the trailer differential breaking, and actively controlling both combination of the tractor-trailers differential breaking system [9]. In general, passive safety systems have reached a well-developed status and are widely sing by vehicle manufactures, whereas active systems have to date been deployed in a small number of commercially available products [9, 56]. The dissertation provides results that would help the future development and deployment of active safety systems.

2.2 Active Front Steering

VSC is an active safety method which is able to diminish tire slip in severe driving situations by modulating braking forces and thereby help drivers maintain directional stability. This helps the driver stay in control of the automobile at the time of an emergency maneuvering situation [7]. AFS can further enhance steering control during an emergency condition by augmenting driver inputs to avoid an oversteer response.

AFS has been heavily studied in both academic and industrial communities [2, 7, 11, 30-35]. Early work was started in the late 1960's by Kasselmann and Keranen [32]. These studies demonstrate the effectiveness of applying an AFS technique to provide a significant yaw disturbance rejection initiated for lane-change maneuvers, high speed turns, and compensating for side wind forces [33]. Moreover, AFS is one of the most effective techniques applied to achieving active safety control since it can deliver an additional steer angle element to the input of the driver. In prior development, the AFS function was implemented as a driver assist ratio of driver to

automatic steering inputs. This ratio would be decreased at high speeds, such as driving on a highway in order to provide more accurate handling to the driver for harsh maneuvers, while the ratio is increased at slow vehicle speeds to diminish steering efforts during parking situations [11, 7].

AFS has been successfully implemented for assisting drivers to avoid a collision or an obstacle [11-34]. A study by Diao et al. [7] demonstrated the effectiveness of AFS in side wind disturbance rejection of a vehicle when completing a single lance change maneuver. Other control methods introduced for AFS include fuzzy logic in a study by March and Shim for a single and double lane change [35]. Sliding mode control (SMC) was demonstrated to be an effective method to handle uncertainties and disturbance rejection [36]. H_∞ control has been shown to minimize the effects of disturbances caused by the steering system hysteresis [37]. Optimal control was applied to improve vehicle handling and stability under severe driving conditions with consideration of nonlinearity of tire character tics [38]. Gain scheduling feedback control was considered for rollover avoidance by AFS while also increasing lateral stability [39, 40]. Quantitative feedback theory demonstrated a robust control design with respect to the mass, speed and center of gravity location [41]. Model predictive control (MPC) has shown good results where the effects of side wind disturbances at high speeds were reduced [42].

The active safety control incorporated in vehicles typically includes yaw moment control, active suspension system, anti-lock braking (ABS) and AFS [7]. AFS technology was originally developed by BMW with ZF Lenksysteme for passenger cars [43, 54] in order to make the front wheels maneuver in a particular angle based on vehicle speed. With this technology, oversteering and understeering can be prevented and thus AFS systems provides more security while driving. In contrast to steer-by-wire technologies, AFS keeps a mechanical connection from the road wheel

and the steering wheel during a fault situation and thereby provides intrinsic fail-safe redundancy [55,101]. Several basic variable gear ratio (VGR) have been implemented for the AFS system design which include a harmonic drive, a differential gear and a bi-planetary gear, where the bi-planetary or planetary gear system imposes an additional steering angle on the out shaft [55]. This configuration is studied in this dissertation and with functional relations illustrated in Fig. 2.1. The mechanical configuration is shown in Fig. 2.2.

For the block diagram shown in Fig. 2.1, the control module gathers information from the sensor package from which the angle through a servo motor is executed [11].

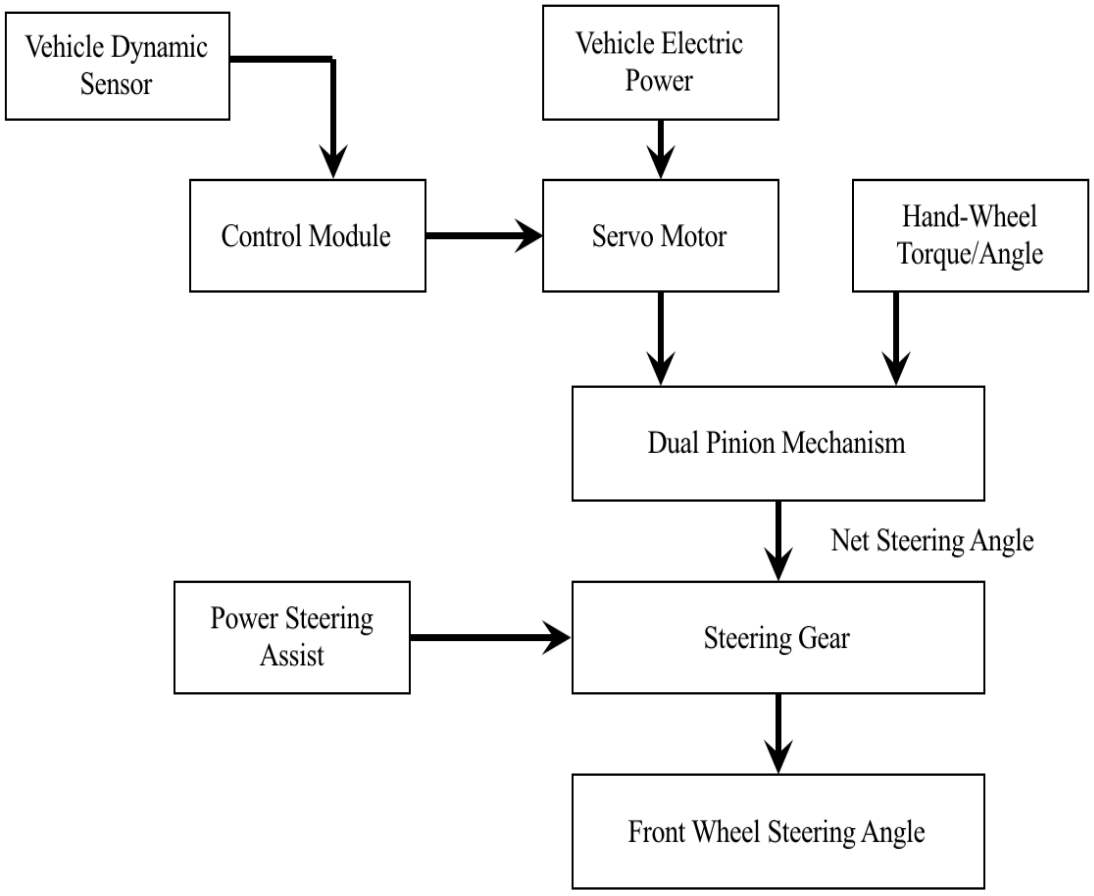

Fig. 2.1. Active front steering configuration.

An AFS assembly typically contains dual planetary gear setting in addition to a separate input torque from the electric motor and an input torque from the hand wheel. The dual input torques are additive at the output shaft, while the two planetary mechanism would allow for isolating the position between the inputs (handwheel and servo motor) that act on the steering column as shown in Fig. 2.2 [44].

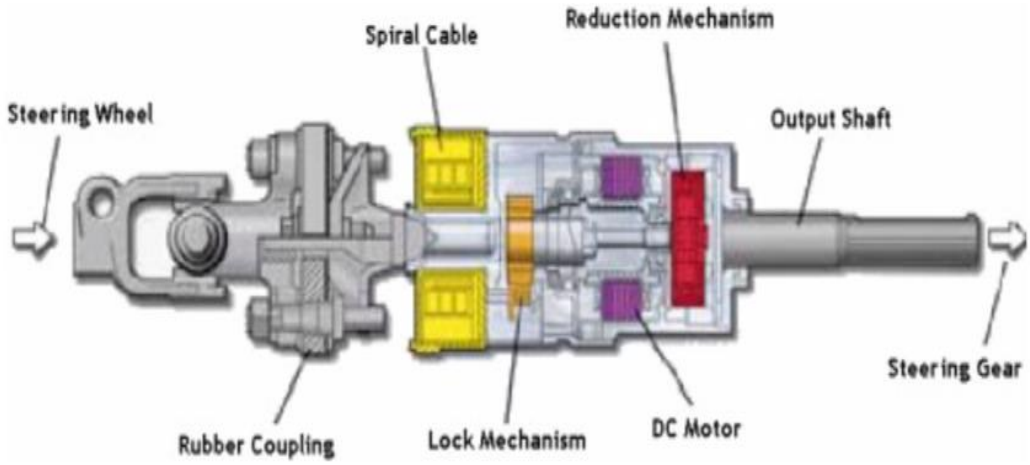

Fig. 2.2. Components of the AFS [11].

An AFS provides the total torque to the steering gear during maneuvering situations. The net torque applied to the front wheel would also include friction and inertial effects [11]. For control system design purposes, the interrelations of an AFS mechanism are given in Fig. 2.3.

The definitions for the AFS steering variables are given by steering wheel angle as δ_s ; the motor angle is denoted by δ_M ; and the steering gear pinion angle as δ_g. The net effective front tire angle is δ_f. Thus δ_g is dependent upon δ_M and δ_s, while δ_f relies on the pinion angle δ_g. It is also noted that the relation between δ_f and δ_g is non-linear and therefore needs to be accounted for in developing a feedback control law.

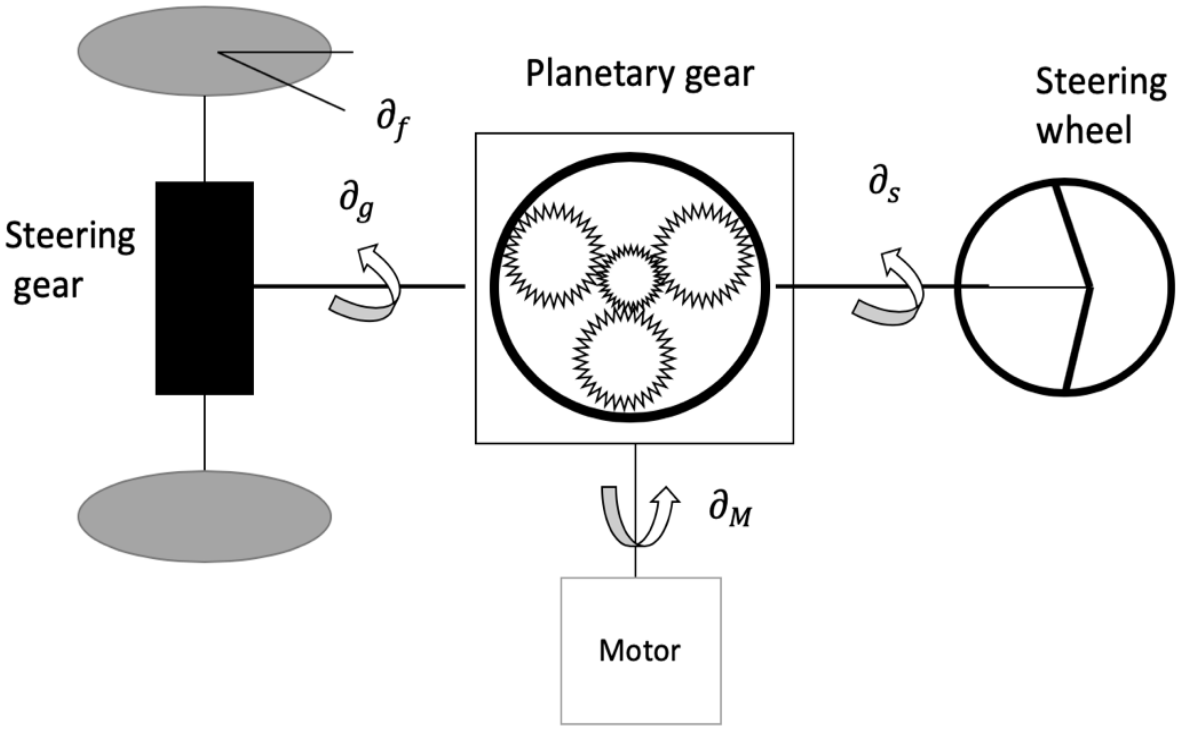

Fig. 2.3. Active front steering mechanism [45].

The components described above are related with the following equations:

$$\delta_f(t) = \delta_s(t)\frac{1}{r} \tag{2.1}$$

$$\delta_f(t) = rg\ \delta_s(t) + \delta_M(t)\ rS \tag{2.2}$$

$$\delta_f(t) = F(\delta_s\ g(t)) \tag{2.3}$$

Where *F* represents the non-linear correlation within the front tire steering angle δ_s and the pinion angle δ_g. The factor r_g is applied from the motor angle to the steer gear pinion angle and r_s is the factor of conversion from the steering wheel angle to the steering gear pinion angle. Hence, the steer gear ratio of the active steering system is defined with the following relationship $r = \frac{\delta_s}{\delta_f}$.

.

The AFS outcome can be summarized in the following relationship

$$\delta_s = \delta_d + \delta_c \tag{2.4}$$

where δ_s is the steering modified angled applied to the front tires, δ_d is the steering input identified from the driver and δ_c is the resulting feedback angle from the control algorithm.

By applying feedback control is possible that understeering and oversteering can be minimized. Understeer is the tendency to have a reduced yaw angle response resulting in the front of the vehicle to continue longitudinally when turning. In contrast, oversteering is defined as the tendency for a larger than expected yaw angle response where the rear of the automobile moves laterally outward which can result in loss of driver control [29]. Recall that a visual representation of oversteering and understeering was given in Fig 1.1. For analytical purposes, Fig. 2.4 shows the associated coordinates for describing under and oversteer conditions. Understeer can occur which when $\alpha_1 > \alpha_2$, while oversteer occurs when $\alpha_1 < \alpha_2$, and a neutral steer is when $\alpha_1 = \alpha_2$.

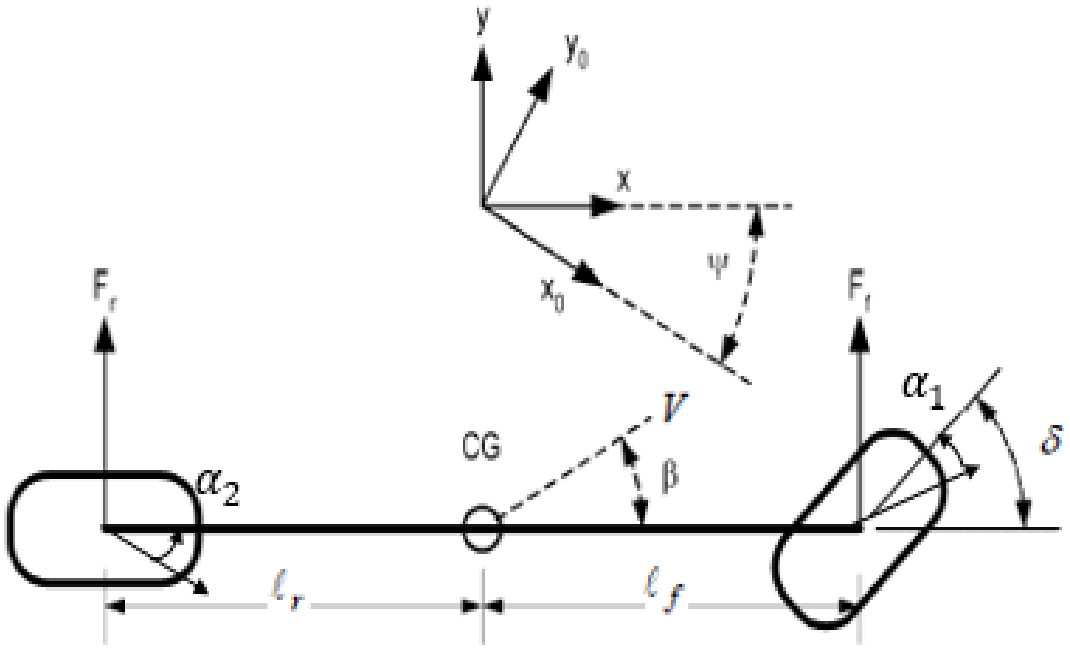

Fig. 2.4. Vehicle coordinate diagram [29].

2.3 Autonomous Vehicles Technology

The history of autonomous vehicles goes back to 1926 when the potential for an automated vehicle was assembled based on radio control and referred to as the "Linriccan Wonder" [49]. Following this, General Motors (GE) introduced another major breakthrough in the Motorama auto show in 1960 by presenting semi-automated cars. Between 1980 -1990 further progress was also accomplished. For example, the "Eureka Prometheus" project received funding as one of the largest research and development projects for automated automobiles. In addition, the automated land vehicle project by the U.S (DOD) through a partnership with other research universities was initiated. Civic and military transportation with automated abilities were explored during the early 2000's [50]. More details on the evolution of the development of automated vehicles can be found in [51].

Automated vehicle technologies are potentially at a transformation phase for the driver experience with advantages to the transport infrastructure. The benefits are compelling from the safety aspect since human error is the primary contributor to the majority of traffic collisions. The other advantage relates to congestion reduction and air pollution decline. In addition a person with a disability could highly benefit from this technology. There is a growing number in the U.S of adults with driving restrictions and according to the U.S Census report in 2010 that those with some type of a disability are estimated to be 56.7 million [47]. As the deployment time frame of automated vehicles is uncertain, the timing depends more on the market demand and regulated policy rather than the technology growth [48].

Today, fully automated vehicles are not available commercially and are only under pilot testing. Investigating innovative methods and evaluating the possible effect of automated automobiles is critical for the future of the automotive industry. For instance, Tesla has the most aggressive

porotype of highly autonomous vehicles with an auto-pilot introduced in 2017, but Tesla anticipates that it will not have software for a fully automated vehicle until the year of 2020 when complete testing and safety measures are met [48].

At the Texas A&M Transportation Institute (TTI) there was an investigation of the experiences of present ride-sharing automobile customers as an assessment for future automated vehicles users [52]. The TTI concluded that present ride-sharing customers using Uber or Lyft are more willing to use automated automobiles than customers whom didn't use ride-sharing services by a margin of two to one. Furthermore, if the customers used ride-sharing services for an extended period, the more likely they will be the first individuals to adopt autonomous automobiles. An alternative report by the University of Texas at Austin [53] indicates that people who are tech-savvy and have green life style preferences are more likely to use car-sharing. These studies are critical to identify the initial users of fully autonomous automobiles for the following reasons [48]:

- Present ride-sharing customers in a metropolis area might be a suitable estimation for the rate of early users of fully automated vehicles.
- Ride-sharing customers can define the characteristics or habits of the early adapters of autonomous automobiles.
- Ride-sharing travel patterns can indicate which cities that might adopt autonomous vehicle technology first.

2.4 Vehicle Dynamics

The behavior of an autonomous land vehicle (ALV) model is inherently nonlinear and uncertain thereby making it challenging to obtain a precise dynamic model. The model for the

system lateral motion is developed based upon the system presented in [46] with the following assumptions:

- Only front wheels to steer is used by the automobile.
- Slip angles cannot be disregarded since the longitudinal velocity is large.
- The lateral tire force are proportional to the slip angles.
- The longitudinal force generated by the tires is disregarded.

In Fig. 2.5 is a diagram of the autonomous land vehicle "bicycle model" where xoy represents the coordinate system of the automobile, whereas XOY denotes the coordinate system based on a fixed earth point of reference. Fig. 2.6 shows the system lateral vehicle dynamics with two degrees of freedom. The model parameters of the passenger vehicle is given in Table 1.

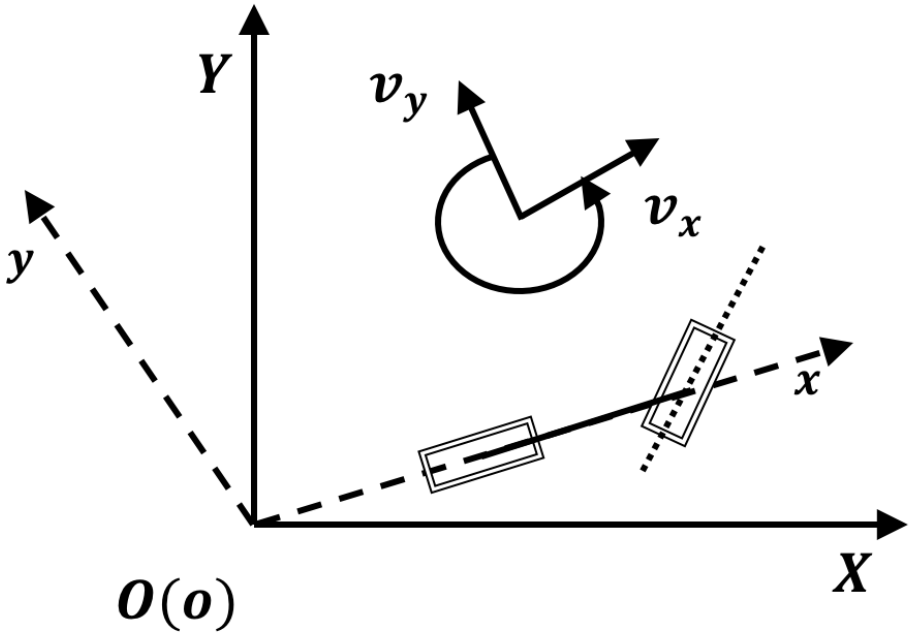

Fig. 2.5. Autonomous land vehicle bicycle model.

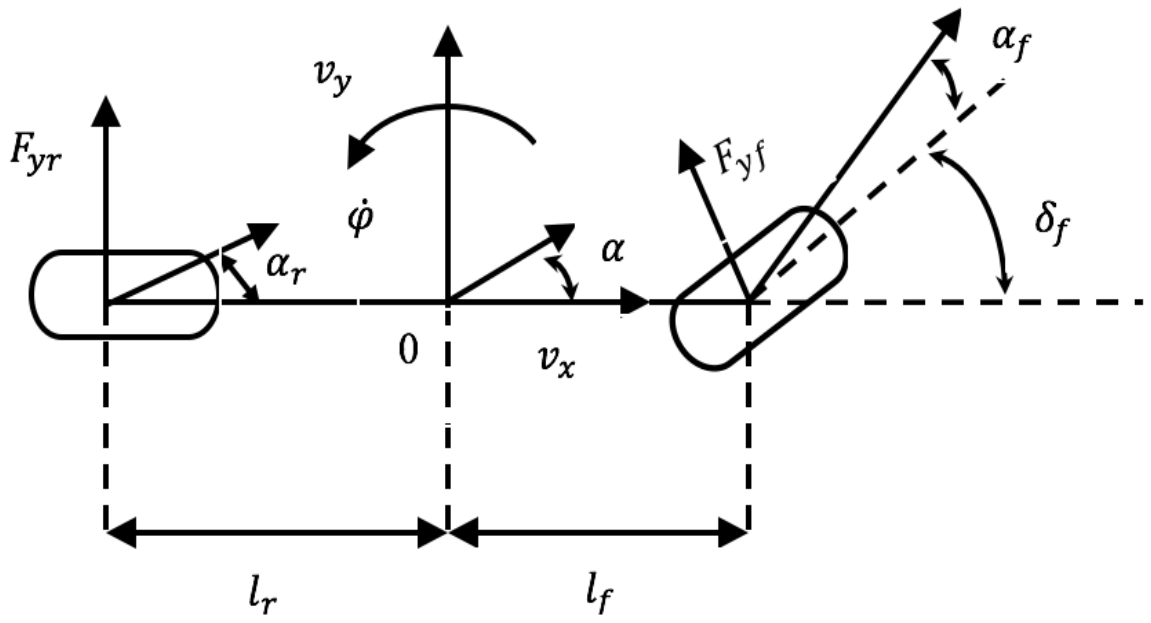

Fig. 2.6. Lateral dynamics of a vehicle.

2.4.1 Passenger vehicle system model

Modeling of the yaw moment of inertia, automobile mass, forward tire cornering stiffness and back tire cornering stiffness are difficult to accurately model due variability in vehicle operating conditions. It is important to develop a robust control that accounts for vehicle uncertainties and external disturbances. The lateral vehicle dynamic model can be written as the following [46]:

$$\begin{cases} \dot{y} = v_x \sin\varphi + v_y cos\,\varphi \\ \dot{\varphi} = r \\ \dot{v_y} = \frac{1}{m}\left(F_{yf} + F_{yr}\right) - v_x r \\ \dot{r} = \frac{1}{I_z}\left(F_{yf} l_f - F_{yr} l_r\right). \end{cases} \tag{2.4}$$

The relationship within the tire slip angle and the tire forces could be obtained as

$$\begin{cases} F_{yf} = -C_f\left(\frac{v_y + r l_f}{v_x} - d_f\right) \\ F_{yr} = -C_r a_r \left(\frac{v_y + r l_f}{v_x}\right). \end{cases} \tag{2.5}$$

Substituting (2) into (1) the lateral dynamic model becomes

$$\begin{cases} \dot{y} = v_x \sin\varphi + v_y cos\,\varphi \\ \dot{\varphi} = r \\ \dot{v_y} = -\frac{C_f + C_r}{m v_x} v_y + \left(\frac{C_r l_r + C_f l_f}{m v_x} - v_x\right) r + \frac{C_f}{m} \\ \dot{r} = \frac{-C_f l_f + C_r l_r}{I_z v_x} v_y - \frac{C_f {l_f}^2 + C_r {l_r}^2}{I_z v_x} r + \frac{l_f C_f}{I_z}\,\delta_f \end{cases} \tag{2.6}$$

where

v_x Longitudinal velocity

v_y Lateral velocity

y Lateral displacement

$\dot{y}$ Lateral velocity

φ Yaw angle

$\dot{\varphi}$ Vehicle yaw rate

F_{yf} Lateral tire force of front wheel

F_{rf} Lateral tire force of rear wheel

C_f Front tire cornering stiffness

C_r Rear tire cornering stiffness

l_f Distance between the center of gravity and the front axle

l_r Distance between the center of gravity and the rear axle

m Vehicle mass

I_z Yaw moment of inertia

With the small angle approximation $\cos(\psi) \approx 1, \sin(\psi) \approx \psi$, the state-space representation of the system can be given as the following:

$$\dot{x} = Ax + Bu\,,\ y = Cx \tag{2.7}$$

$$x_1 = y,\ x_2 = v_y,\ x_3 = \psi,\ x_4 = r. \tag{2.8}$$

$$A = \begin{pmatrix} 0 & v_x & 1 & 0 \\ 0 & 0 & 0 & 1 \\ 0 & 0 & \frac{-\left(\frac{C_f + C_r}{m}\right)}{v_x} & -v_x + \frac{\left(\frac{C_r l_r + C_f l_f}{m}\right)}{v_x} \\ 0 & 0 & \frac{\left(\frac{C_r l_r + C_f l_f}{I_z}\right)}{v_x} & \frac{-\left(\frac{C_f {l_f}^2 + C_r {l_r}^2}{I_z}\right)}{v_x} \end{pmatrix}, \tag{2.9}$$

$$B = \begin{pmatrix} 0 \\ 0 \\ \frac{C_f}{m} \\ \frac{C_f l_f}{I_z} \end{pmatrix}, \tag{2.10}$$

$$C = \begin{pmatrix} 1 & 0 & 0 & 0 \\ 0 & 1 & 0 & 0 \end{pmatrix}. \tag{2.11}$$

Chapter 3: Tractor-Trailer Modeling

3.1 Tractor-Trailers Background

In 2015, tractor-trailers accounted for more than 70% of the national freight transportation in the U.S. Moreover, in that year 10.6 billion tons of goods worth $10.9 trillion were transported on trucks in the United States [1]. Heavy-trucks with a gross vehicle weight rating (GVWR) between 10,000 – 26,000 pounds are classified as medium trucks, and those with a GVWR larger than 26,000 pounds are classified as heavy-duty trucks. Heavy trucks are considered the principle transport vehicle of cargo transportation, moving large quantities of cargo over long distances where the average tractor-trailer travels over 100,000 miles per year [23].

The truck transportation industry plays a major role in freight transportation in the U.S. in terms of the value of the goods being shipped inside the trucks. However, rail transportation tends toward bulk commodities such as coal, mineral ores and agricultural products over lengthy distances [23].

One of the most commonly used modes of transportation for goods in the U.S. is the 18-wheeler tractor-trailer [57]. In a similar configuration to a passenger vehicle model based on the bicycle model (2-axles) described earlier in Fig 2.6, the model can be expanded to a large 18-wheeler tractor-trailer combination with 3-axles as presented in Fig. 3.1.

In this research, the standard bicycle model presented and validated in [11, 68] is used for modeling the tractor-trailer system. In this case, the vehicle roll and pitch effects are neglected. For platooning dynamics, only the lateral and yaw moments are considered. The nonlinear dynamic model can be developed for the tractor-trailer based on the single track bicycle model. From this, a linearized model can be obtained using a small angle approximation.

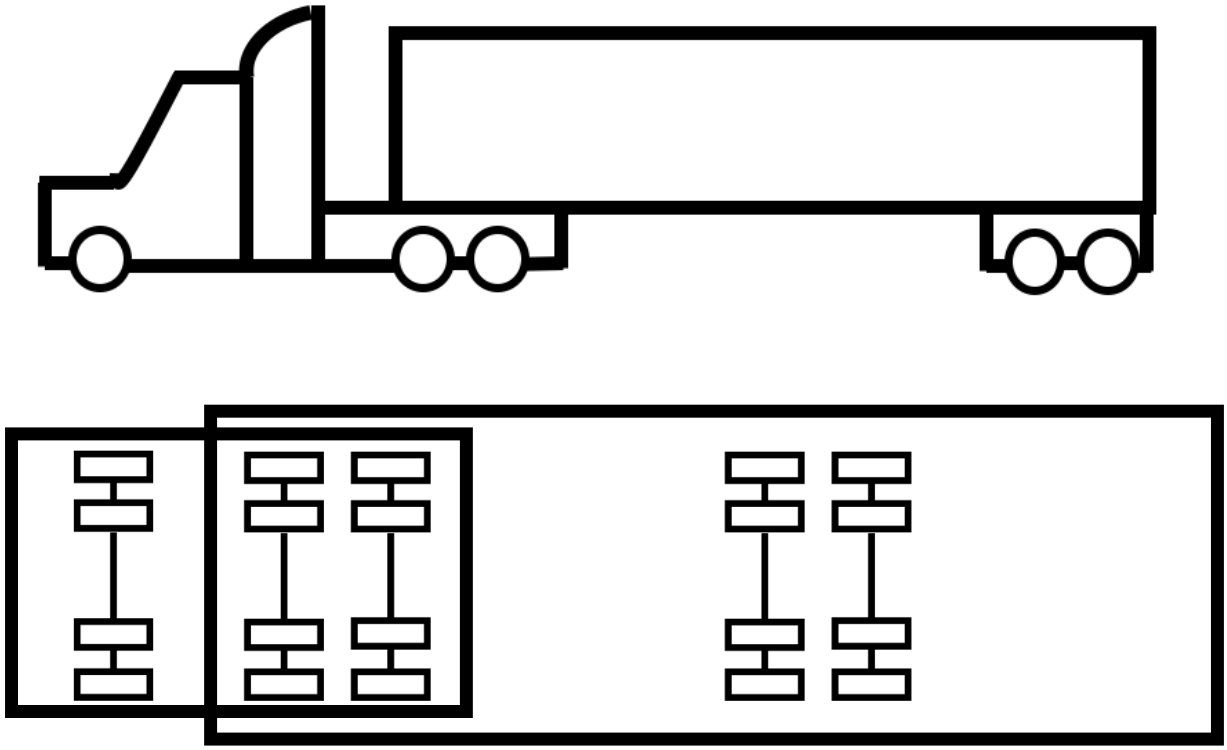

Fig. 3.1. Three-axle tractor-trailer model.

One of the causes of accidents in tractor-trailers is truck rollover that starts after the tire linked force on the inside wheels becomes zero (i.e., the tire lifts off of the roadway pavement). Rollover is usually triggered by elevated lateral forces produced by lateral acceleration. If the location of the COG is too high or the longitudinal velocity of the automobile is greater than permitted at a specified steer angle, the resultant lateral acceleration can be sufficiently high to result in a rollover accident [58]. As a general guide, large truck lateral acceleration should not exceed 0.50*g*.

There are many contributing factors that cause heavy-duty vehicles to lose control which can cause the yaw angle to become unstable or the truck to rollover. Hence, by applying an appropriate control scheme, the incidence of these crash scenarios listed below can be minimized [23, 69]:

- **High speed attempt a turn:** When the lateral acceleration of the automobile exceeds the yaw stability or the vehicles roll threshold during a maneuver situation then loss of the vehicle control would be initiated.
- **Abrupt maneuver steer to evade a collision:** When the motorist attempts a sudden steering operation, for example a single or a dual lane departure, this would create a lateral acceleration large enough to make the yaw angle unstable (oversteer phenomena).
- **Load condition in the Tractor-trailer:** When oversteering occurs the yaw angle becomes unstable and thus is more probable to happen when the truck is partially loaded as opposed to then the truck is fully loaded.
- **Surface condition in the roadway:** A truck attempting an evasive lane change in a large-friction roadway or a dry surface is less likely to have the yaw angle instability due to improved tire cornering stiffness.
- **Design shape of the roadway:** When a motorist under or overestimates the curvature radius of a highway ramp and does not sufficiently reduce vehicle speed. Thus, increased lateral acceleration might occur which could result in a rollover event.
- **Breaking maneuvers:** Applying the brakes improperly resulting in reduced vehicle maneuvering capability.
- **Vehicle factors:** Worn tires are more likely to contribute to vehicle yaw or under-steering in wet slippery circumstances.

3.2 Tractor-Trailer Modeling

The model and the derived equations for the tractor-trailer system are based on the coordinate definitions in Fig. 3.2.

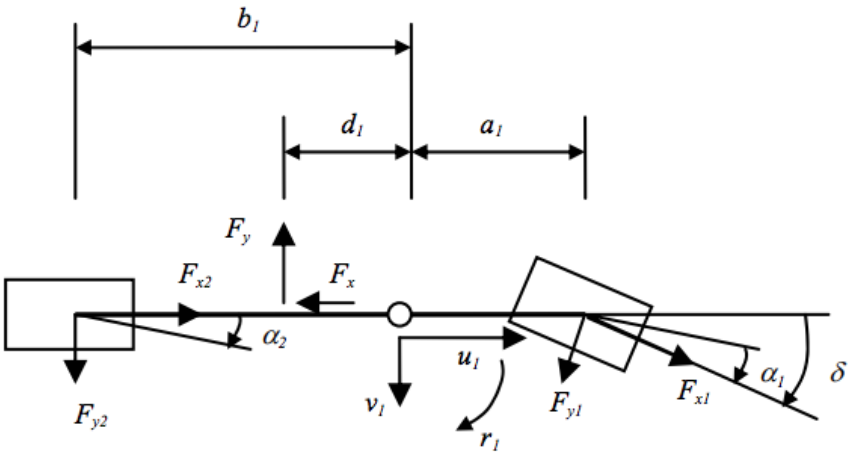

Fig. 3.2. Diagram of a single track model for tractor.

Fig. 3.3 indicates the dimensional parameters and forces of the trailer where the acceleration and velocity are defined in an inertial coordinate system that is fixed to the vehicle. The longitudinal velocities of the tractor and the trailer are u_1 and u_2, respectively. The lateral velocity of the tractor is v_1; the yaw rate of the tractor is r_1; the yaw rate of the trailer is r_2; the articulation angle is ψ. The input control variable is the front axle steering angle δ_f.

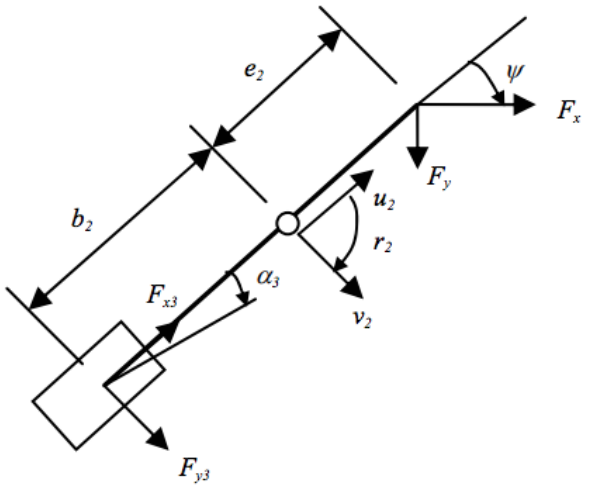

Fig. 3.3. Diagram of a trailer single-track model.

By applying Newton's second law, the dynamic model of the tractor-trailer can be derived. The equations for the torque and force acting on the tractor are as follows:

$$m_1 a_{x1} = F_{x1} cos\delta - F_{y1} sin\delta + F_{x2} - F_x - F_{a1}, \quad (3.1)$$

$$m_1 a_{y1} = F_{y1} cos\delta + F_{x1} sin\delta + F_{y2} - F_y, \quad (3.2)$$

$$I_{z1} \dot{r_1} = a_1 F_{y1} cos\delta + a_1 F_{x1} sin\delta - b_1 F_{y2} + d_1 F_y, \quad (3.3)$$

The equations for the torque and force acting on the trailer are given by

$$m_2 a_{x2} = F_x cos\psi + F_{x3} - F_y sin\psi - F_{a2}, \quad (3.4)$$

$$m_2 a_{y2} = F_{y3} + F_y cos\psi + F_x sin\psi\ , \quad (3.5)$$

$$I_{z2} \dot{r_2} = -b_2 . F_{y3} + e_2 \left(F_y . cos\psi + F_x . sin\psi\right), \quad (3.6)$$

The rate of change of the articulation angle in between the tractor and trailer is indicated by the following:

$$\dot{\psi} = r_1 - r_2. \quad (3.7)$$

The velocity and acceleration are defined in an inertial coordinate system that is fixed to the vehicle and is defined in Fig. 3.4. The relationships for the longitudinal and lateral velocities in the local coordinates can be obtained using Fig. 3.4. The longitudinal velocity is given by the following:

$$dV_x = (u + du).\cos(d\theta) - u - (v + dv).\sin(d\theta). \quad (3.8)$$

The lateral velocity variation is

$$dV_y = (v + dv).\cos(d\theta) - v + (u + du).\sin(d\theta). \quad (3.9)$$

Since the angle $d\theta$ is small and the time interval dt between the two points is small as well, (3.8) and (3.9) become

$$dV_x = du - v\, d\theta, \quad (3.10)$$

$$dV_y = dv - u\, d\theta. \quad (3.11)$$

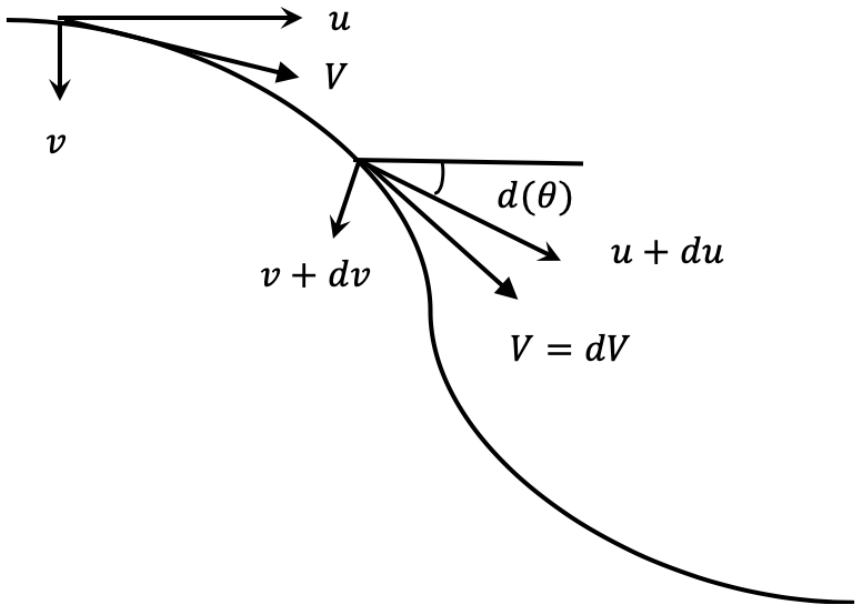

Fig. 3.4. Vehicle coordinate system velocity definitions.

The longitudinal and lateral acceleration is given as

$$a_x = \dot{u} - vr, \tag{3.12}$$

$$a_y = \dot{v} - ur. \tag{3.13}$$

The equations describing the motion of the tractor-trailer system can be adapted to the results of (3.10), (3.11), (3.12) and (3.13). The resulting equations representing the motion of the tractor and trailer are given as follows:

$$\dot{u_1} = v_1 r_1 + \frac{1}{m_1}\left(F_{x1}\, cos\delta - F_{y1}\, sin\delta + F_{x2} - F_{a1}\right), \tag{3.14}$$

$$\dot{v_1} = -u_1 r_1 + \frac{1}{m_1}\left(F_{y1}\, cos\delta + F_{x1}\, sin\delta + F_{y2} - F_y\right), \tag{3.15}$$

$$\dot{r_1} = \frac{1}{I_{z1}}\left(a_1 F_{y1}\, cos\delta + a_1 F_{x1}\, sin\delta - b_1 F_{y2} + d_1 F_y\right), \tag{3.16}$$

$$\dot{u_2} = v_2 r_2 + \frac{1}{m_2}\left(F_x\, cos\psi + F_{x3} - F_y\, sin\psi - F_{a2}\right), \tag{3.17}$$

$$\dot{v_2} = -u_2 r_2 + \frac{1}{m_2}\left(F_{y3} + F_y cos\psi + F_x sin\psi\right), \tag{3.18}$$

$$\dot{r}_2 = \frac{1}{I_{z2}}\left(-b_2 F_{y3} + e_2\left(F_y\, cos\psi + F_x\, sin\psi\right)\right), \tag{3.19}$$

where (3.14), (3.15) and (3.16) are the equations representing the tractor, and (3.17),(3.18) and (3.19) are the equations representing the trailer. The longitudinal speed is constant and thus the forward motion $u_1$is a constant. $\dot{\psi}$ remains the same as in (3.7).

The two interdependent states are constrained at the trailer pivot point as the following:

$$u_2 = u_1 \cos\psi - (v_1 - d_1 r_1)\sin\psi, \tag{3.20}$$

$$v_2 = u_1 \sin\psi + (v_1 - d_1 r_1)\cos\psi - e_2 r_2. \tag{3.21}$$

By back substituting and eliminating these constraints, the system order can be reduced. Thus one can find expressions for F_x and F_y as follows:

$$\begin{pmatrix} F_x \\ F_y \end{pmatrix} = \frac{1}{d_{11}d_{22} - d_{12}d_{21}} \begin{pmatrix} -d_{22} & d_{12} \\ d_{21} & -d_{11} \end{pmatrix} \begin{pmatrix} t_1 \\ t_2 \end{pmatrix}, \tag{3.22}$$

where,

$$d_{11} = \left(\frac{1}{m_1} + \frac{1}{m_2}\right)\cos\psi, \tag{3.23}$$

$$d_{12} = -\sin\psi\left(\frac{d_1^2}{I_{z1}} + \frac{1}{m_1} + \frac{1}{m_2}\right), \tag{3.24}$$

$$d_{21} = \left(\frac{1}{m_1} + \frac{1}{m_2} + \frac{e_2^2}{I_{z2}}\right)\sin\psi, \tag{3.25}$$

$$d_{22} = \left(\frac{e_2^2}{I_{z2}} + \frac{d_1^2}{I_{z1}} + \frac{1}{m_1} + \frac{1}{m_2}\right)\cos\psi, \tag{3.26}$$

$$d_0 = d_{11}d_{22} - d_{12}d_{21}. \tag{3.27}$$

$$t_1 = \sin\psi\left(F_{y2}\left(\frac{b_1 d_1}{I_{z1}} + \frac{1}{m_1}\right) - r_2 U_1\right) + \sin\delta\left(F_{x1}\sin\psi\left(\frac{1}{m_1} - \frac{a_1 d_1}{I_{z1}}\right) + \frac{F_{y1}}{m_1}\cos\psi\right) + \cos\psi\left(\frac{1}{m_1}(F_{a1} - F_{x2}) - (r_1 - r_2)(d_1 r_1) - r_2 V_1\right) + \cos\delta\left(F_{y1}\sin\psi\left(\frac{1}{m_1} - \frac{a_{1d_1}}{I_{z1}}\right) - \frac{F_{x1}}{m_1}\cos\psi\right) - \frac{1}{m_2}(F_{a2} - F_{x3}) + r_2 v_2, \tag{3.28}$$

$$t_2 = \sin\psi\left(\frac{1}{m_1}(F_{a1} - F_{x2}) - r_2V_1 + (-r_1 + r_2)(d_1r_1)\right) + \sin\delta\left(F_{x1}\cos\psi\left(\frac{a_1d_1}{I_{z1}} - \frac{1}{m_1}\right) + \frac{F_{y1}}{m_1}\sin\psi\right) + \cos\psi\left(-F_{y2}\left(\frac{b_1d_1}{I_{z1}} + \frac{1}{m_1}\right) + r_2U_1\right) + \cos\delta\left(F_{y1}\cos\psi\left(\frac{a_1d_1}{I_{z1}} - \frac{1}{m_1}\right) - \sin\psi\frac{F_{x1}}{m_1}\right) + F_{y3}\left(\frac{1}{m_2} - \frac{b_2e_2}{I_{z2}}\right) - r_2u_2. \quad (3.29)$$

The longitudinal forces that affect the system are

$$F_{x1} = F_{d1} + F_{b1}, F_{x2} = F_{d2} + F_{b2}, F_{x3} = F_{d3} + F_{b3}. \quad (3.30)$$

The side forces acting on the system tires are

$$F_{y1} = C_1\alpha_1, F_{y2} = C_2\alpha_2, F_{y3} = C_3\alpha_3. \quad (3.31)$$

C_1, C_2 and C_3 are the cornering stiffness of tires and are defined as

$$\alpha_1 = \delta - \frac{v_1 + a_1r_1}{u_1 + \varepsilon} \quad (3.32)$$

$$\alpha_2 = -\frac{v_1 - b_1r_1}{u_1 + \varepsilon} \quad (3.33)$$

$$\alpha_3 = -\frac{v_2 - b_2r_2}{u_2 + \varepsilon}, \quad (3.34)$$

where, ε is a small parameter to avoid a singularity at zero speed.

3.3 Linearized Model Development

With normal driving conditions, the steering angle and the articulation are small and thus result in the following approximation:

$$\cos\delta = 1, \sin\delta = \delta, \cos\psi = 1, \sin\psi = \psi. \quad (3.35)$$

Equations (3.32)-(3.34) can be reduced considering small angular excursions to

$$\alpha_1 = \delta - \frac{v_1 + a_1r_1}{u_1}, \quad (3.36)$$

$$\alpha_2 = -\frac{v_1 - b_1 r_1}{u_1}, \tag{3.37}$$

$$\alpha_3 = -\frac{v_2 - b_2 r_2}{u_2}. \tag{3.38}$$

With normal driving considerations the braking forces can assumed to be zero:

$$F_{b1} = F_{b2} = F_{d3} = 0,\ F_{x2} = F_{d2} \tag{3.39}$$

By applying (3.34)-(3.39) to the tractor-trailer equations (3.14)-(3.19), a simplified model can be obtained as the following

$$\dot{u}_1 = v_1 r_1 + \frac{1}{m_1}\left(F_{d2} - F_x - F_{y1}\delta - R_1\right), \tag{3.40}$$

$$\begin{pmatrix}\dot{v}_1 \\ \dot{r}_1\end{pmatrix} = A\begin{pmatrix}v_1 \\ r_1\end{pmatrix} + B\delta + DF_y, \tag{3.41}$$

$$\dot{u}_2 = v_2 r_2 + \frac{1}{m_2}\left(F_x - F_y\psi - R_2\right), \tag{3.42}$$

$$\begin{pmatrix}\dot{v}_2 \\ \dot{r}_2\end{pmatrix} = F\begin{pmatrix}v_2 \\ r_2\end{pmatrix} + GF_y + DF_x\psi\,, \tag{3.43}$$

where the matrices are defined as

$$A = \begin{pmatrix} -\frac{c_1+c_2}{m_1.u_1} & -U + \frac{-a_1c_1+b_1.c_2}{m_1.u_1} \\ -\frac{a_1c_1-b_1c_2}{I_{z1}u_1} & -\frac{a_1^2c_1+b_1^2c_2}{I_{z1}u_1} \end{pmatrix}, \tag{3.44}$$

$$B = \begin{pmatrix} \frac{c_1}{m_1} \\ \frac{a_1c_1}{I_{z1}} \end{pmatrix}, \tag{3.45}$$

$$D = \begin{pmatrix} -\frac{1}{m_1} \\ \frac{d_1}{I_{z1}} \end{pmatrix}, \tag{3.46}$$

$$F = \begin{pmatrix} -\frac{c_3}{m_2u_2} & -u_2 + \frac{b_2c_3}{m_2.u_2} \\ \frac{b_2c_3}{I_{z2}u_2} & -\frac{{b_2}^2c_3}{I_{z2}u_2} \end{pmatrix}, \tag{3.47}$$

$$G = \begin{pmatrix} \frac{1}{m_2} \\ \frac{e_2}{I_{z2}} \end{pmatrix}, \tag{3.48}$$

$$R_1 = F_{a1} + F_{r1} + F_{r2},\ R_2 = F_{a2} + F_{r3}. \tag{3.49}$$

Assuming that the articulation angle is small, the relationship between the velocities from (3.20)-(3.22) can be rewritten as

$$u_1 = u_2, v_2 = u_1\psi + (v_1 - d_1 r_1) - e_2 r_2. \tag{3.50}$$

Applying (3.50) to (3.40) and (3.42) one obtains the following relationship

$$v_1 r_1 + \frac{1}{m_1}(F_{d2} - F_x - R_1) = v_2 r_2 + \frac{1}{m_2}(F_x - R_2). \tag{3.51}$$

Under small angle operations the relationship for the 5th wheel force (trailer pivot point) in (3.22) can reduced to

$$\begin{pmatrix} F_x \\ F_y \end{pmatrix} = \frac{1}{d_0}\begin{pmatrix} -d_{22} & d_{12} \\ d_{21} & -d_{11} \end{pmatrix}\begin{pmatrix} t_1 \\ t_2 \end{pmatrix}, \tag{3.52}$$

where,

$$d_{11} = \left(\frac{1}{m_1} + \frac{1}{m_2}\right), \tag{3.53}$$

$$d_{12} = -\psi\left(\frac{d_1^2}{I_{z1}} + \frac{1}{m_1} + \frac{1}{m_2}\right), \tag{3.54}$$

$$d_{21} = \left(\frac{1}{m_1} + \frac{1}{m_2} + \frac{e_2^2}{I_{z2}}\right)\psi, \tag{3.55}$$

$$d_{22} = \left(\frac{e_2^2}{I_{z2}} + \frac{d_1^2}{I_{z1}} + \frac{1}{m_1} + \frac{1}{m_2}\right), \tag{3.56}$$

$$d_0 = d_{11}d_{22} - d_{12}d_{21}. \tag{3.57}$$

$$t_1 = \psi\left(F_{y2}\left(\frac{b_1 d_1}{I_{z1}} + \frac{1}{m_1}\right) - r_2 U_1\right) + \delta\left(F_{x1}\psi\left(\frac{1}{m_1} - \frac{a_1 d_1}{I_{z1}}\right) + \frac{F_{y1}}{m_1}\right) + \left(\frac{1}{m_1}(F_{a1} - F_{x2}) - (r_1 - r_2)(d_1 r_1) - r_2 V_1\right) + \left(F_{y1}\psi\left(\frac{1}{m_1} - \frac{a_1 d_1}{I_{z1}}\right) - \frac{F_{x1}}{m_1}\right) - \frac{1}{m_2}(F_{a2} - F_{x3}) + r_2 v_2, \tag{3.58}$$

$$t_2 = \psi\left(\frac{1}{m_1}(F_{a1} - F_{x2}) - r_2 V_1 + (-r_1 + r_2)(d_1 r_1)\right) + \delta\left(F_{x1}\left(\frac{a_1 d_1}{I_{z1}} - \frac{1}{m_1}\right) + \frac{F_{y1}}{m_1}\psi\right) + \left(-F_{y2}\left(\frac{b_1 d_1}{I_{z1}} + \frac{1}{m_1}\right) + r_2 U_1\right) + 1\left(F_{y1}\left(\frac{a_1 d_1}{I_{z1}} - \frac{1}{m_1}\right) - \psi\frac{F_{x1}}{m_1}\right) + F_{y3}\left(\frac{1}{m_2} - \frac{b_2 e_2}{I_{z2}}\right) - r_2 u_2. \tag{3.59}$$

Solving for F_x one can obtain the following

$$F_x = \frac{1}{d_{11}}\left(\frac{1}{m_1}F_{d2} - \frac{1}{m_1}R_1 + \frac{1}{m_2}R_2 - \frac{1}{m_1}F_{y1}\delta + \frac{1}{m_2}F_y\psi + v_1(r_1 - r_2) + d_1 r_1 r_2 + e_2 r_2^2 - u_1 r_2\psi\right). \tag{3.60}$$

The relationship between the nonlinear longitudinal state and lateral dynamics can be obtained as:

$$v_2 = \dot{u_1}\psi + (\dot{v_1} - d_1\dot{r_1}) - e_2\dot{r_2}, \tag{3.61}$$

$$\dot{u_1} = v_1 r_1 + \frac{1}{m_1 + m_2}\left(F_{d2} - F_{y1}\delta - (R_1 + R_2) - F_y\psi - m_2 R_x\right). \tag{3.62}$$

The state space equation of the tractor-trailer dynamics can be obtained from (3.41) and (3.43) with the expression for the forces F_x and F_y from (3.52) to be the following

$$\begin{pmatrix}\dot{v_1}\\ \dot{r_1}\\ \dot{r_2}\\ \dot{\psi}\end{pmatrix} = A\begin{pmatrix}v_1\\ r_1\\ r_2\\ \psi\end{pmatrix} + B\delta + DF_x\psi, \tag{3.63}$$

where $A = A_1 + A_2$,

$$A_1 = \begin{pmatrix} -\frac{c_1+c_2}{m_1u_1} & -u_1 + \frac{-a_1c_1+b_1c_2}{m_1u_1} & 0 & 0 \\ -\frac{a_1c_1-b_1c_2}{I_{z1}u_1} & -\frac{a_1^2c_1+b_1^2c_2}{I_{z1}u_1} & 0 & 0 \\ \frac{b_2c_3}{I_{z2}u_2} & -d_1\frac{b_2c_3}{I_{z2}u_2} & -\frac{b_2^2c_3}{I_{z2}u_2} - e2\frac{b_2c_3}{I_{z2}u_2} & \frac{b_2c_3}{I_{z2}u_2}u_1 \\ 0 & 1 & -1 & 0 \end{pmatrix}, \quad (3.64)$$

$$A_2 = \frac{1}{d_{22}}\begin{pmatrix} -\frac{1}{m_1} \\ \frac{d_1}{I_{z1}} \\ \frac{e_2}{I_{z2}} \\ 0 \end{pmatrix}(h_{11} \quad h_{12} \quad h_{13} \quad h_{14}), \quad (3.65)$$

$$h_{11} = \left(-\frac{c_1+c_2}{m_1u_1} - d_1 - \frac{a_1c_1-b_1c_2}{I_{z1}u_1}\right) - \left(-\frac{c_3}{m_2u_2} + e_2\frac{b_2c_3}{I_{z2}u_2}\right), \quad (3.66)$$

$$h_{12} = \left(-u_1 + \frac{-a_1c_1+b_1c_2}{m_1u_1} - d_1 - \frac{a_1^2c_1+b_1^2c_2}{I_{z1}u_1}\right) + d_1\left(-\frac{c_3}{m_2u_2} + e2\frac{b_2c_3}{I_{z2}u_2}\right) + u_1 \quad (3.67)$$

$$h_{13} = -\left(u_2 + \frac{b_2c_3}{m_2u_2} - e_2\frac{b_2^2c_3}{I_{z2}u_2}\right) + e_2\left(-\frac{c_3}{m_2u_2} + e_2\frac{b_2c_3}{I_{z2}u_2}\right) - u_1, \quad (3.68)$$

$$h_{14} = -\left(-\frac{c_3}{m_2u_2} + e_2\frac{b_2c_3}{I_{z2}u_2}\right)u_1. \quad (3.69)$$

$$B = \begin{pmatrix} \frac{c_1}{m_1} \\ \frac{a_1c_1}{I_{z1}} \\ 0 \\ 0 \end{pmatrix} + \begin{pmatrix} -\frac{1}{m_1} \\ \frac{d_1}{I_{z1}} \\ \frac{e_2}{I_{z2}} \\ 0 \end{pmatrix}, \quad (3.70)$$

$$D = \begin{pmatrix} -\frac{1}{m_1} \\ \frac{d_1}{I_{z1}} \\ \frac{e_2}{I_{z2}} \\ 0 \end{pmatrix}\frac{\frac{1}{m_2}+\frac{e_2^2}{I_{z2}}}{\left(\frac{e_2^2}{I_{z2}}+\frac{d_1^2}{I_{z1}}+\frac{1}{m_1}+\frac{1}{m_2}\right)} + \begin{pmatrix} 0 \\ 0 \\ \frac{e_2}{I_{z2}} \\ 0 \end{pmatrix}. \quad (3.71)$$

The equation representing the torque applied to the steering is the following

$$\dot{\delta}=\omega,\ \ \dot{\omega}=-B_s\omega - K_s\alpha_1+\tau_{hw}+\tau_{afs} \tag{3.72}$$

The side slip angle to front tire is

$$\alpha_1= \delta - \frac{v_1+a_1r_1}{u_1\varepsilon} \tag{3.73}$$

The previous mathematical model of the tractor-trailer system can be augmented to include earth-based coordinates for evaluating the lateral position in a manner similar to the passenger vehicle given by (2.4)-(2.6). A fifth state variable is added for the truck yaw-angle and a sixth state variable is added for the lateral position:

$$\dot{\varphi} = r \tag{3.74}$$

$$\dot{y} = u_1 \sin(\varphi) + v_1\cos(\varphi) \tag{3.75}$$

This results in a sixth-order system for the tractor-trailer system dynamics

$$\dot{x} = Ax + Bu\ ,\ y = Cx \tag{3.76}$$

The tractor-trailer modeling presented in this chapter does not explicitly consider the roll dynamics of the truck, however avoiding the tendency for rollover is usually accounted for by ensuring that the lateral acceleration is maintained less than $0.50g$.

3.3. Tractor-Trailer Platooning

There are two classes to form automated driving. The first is an individual vehicle maneuvering autonomously within traffic conditions of other vehicles. The second is platoon formation with coordination of adjacent vehicles. With platooning there is the capability for increased fuel economy from the aerodynamic drafting along with reduced highway congestion and safety improvements [2, 26]. Truck platooning is a technology for a coordinated highway operation of a group of two or more trucks equipped with a variety of sensors and communications

to inform each of the vehicles about surrounding traffic conditions and the status of partner vehicles. The leading truck wirelessly communicates to the following trucks and sends messages that controls the throttle and brakes as illustrated in Figs. 3.5 – 3.6.

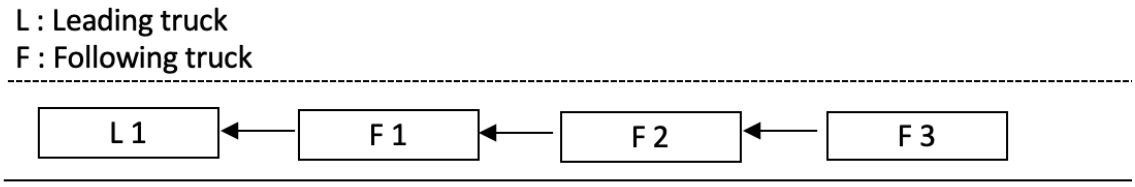

Fig. 3.5. Four trucks forming a platooning operation in a highway.

Fig. 3.6. Truck platooning demonstration (*source European truck platooning challenge* [59]).

A human driver is remains behind the wheel in the leading vehicle to steer for lateral control, while sensors that enable platooning operation of the truck lateral position control can be enhanced along with the reduction in aerodynamic drag is shown in Fig. 3.7. Platooning of tractor-trailers results in increased fuel economy and reduction in carbon dioxide emissions [60].

In a recent study, a group of two or more platooned trucks were examined where the fuel consumption was reduced in range of 5% to 7.6% [61]. Data from the federal highway

administration (FHWA) in 2016 indicates that large trucks in the U.S. consumed 29.6 billion gallons of fuel [60]. Consequently, a reduction of 5% or more of fuel consumption through truck platoons would be very beneficial for reducing greenhouse gas emissions.

Automated platooning operation would be more beneficial for heavy vehicle compared to passenger vehicles for the following reasons noted by Tsugawa [26]:

i. Utilization rate of trucks is much greater than of passenger vehicles which leads to more effective energy saving.
ii. Automated driving reduces driver workload.
iii. Reduced driving workload will result in safety improvements and accident reduction for heavy trucks which is more significant and costly than passenger cars.
iv. As professionally trained and supervised, heavy truck operators are better positioned to utilize the benefits of automated platoon operations.

One of the main objectives of this research is to provide control methods that enable heavy trucks to maintain lateral stability during a rapid lane change.

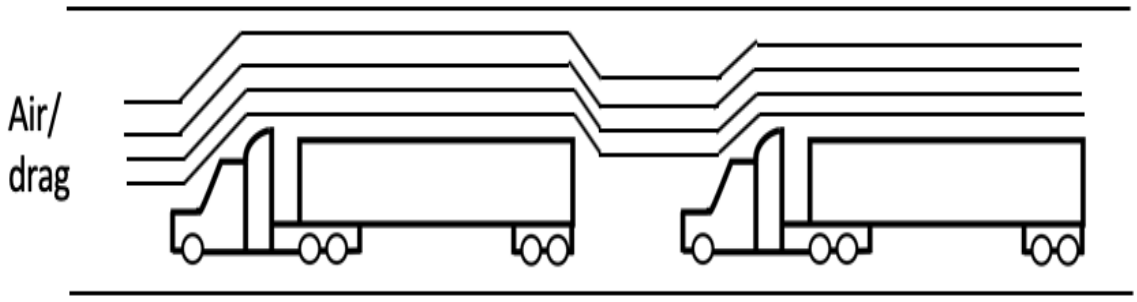

Fig. 3.7. Platooning leads to reduction in aerodynamic drag.

The functions of the platooning operation are obstacle avoidance, speed control, lane keeping and maintaining following distance. Automated platooning operation does not require additional infrastructure and roadway equipment. Technologies that would enable the platooning operation include sensors for longitudinal control for measuring the following truck distances and for obstacle detection. Sensors for lateral control are needed where sensors can detect divergence of the tractor from the roadway lane markings. In addition, a combination of communication technologies between the leading and following trucks is needed for real-time control functions. These capabilities are referred to as vehicle-to-vehicle (V2V) and vehicle-to-infrastructure (V2I) protocols. In most cases these are similar to IEEE 802.11 and provided for platooning operation as indicated in Fig. 3.8 [2, 62].

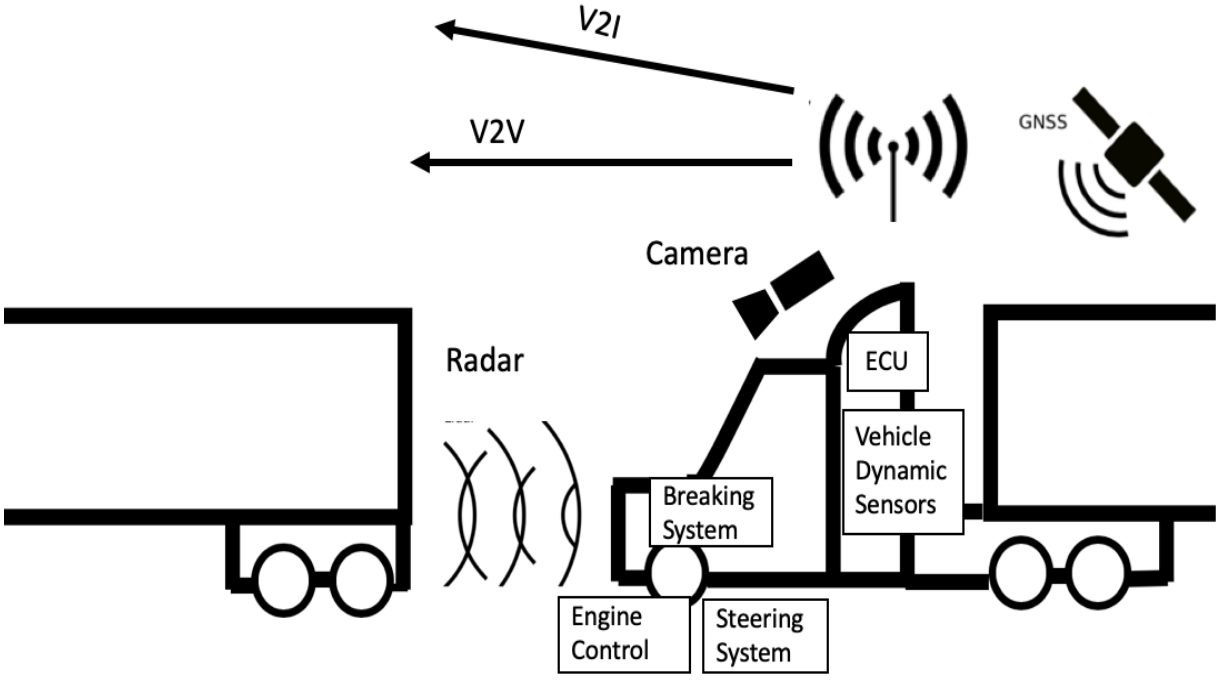

Fig. 3.8 Technologies that enable the platooning operation [62].

One of the concerns of V2V communication technologies are cybersecurity threats. There is ongoing research in overcoming concerns. For example, SIP-adus attempts to obtain security specifications by constructing joint modes based on risk analysis.

Human machine interfaces also present concerns regarding the effectiveness and safety of autonomous vehicles. There are three critical concerns that should be examined. The first is to examine the effects of previous data on driver reactions while using autonomous driving systems. The second is to evaluate methods for autonomous driving automobiles to interconnect with other roadway users under different traffic situations. The third is to examine the effect of driver reaction when attempting to transition from autonomous driving to manual driving as illustrated in Fig. 3.9 [63].

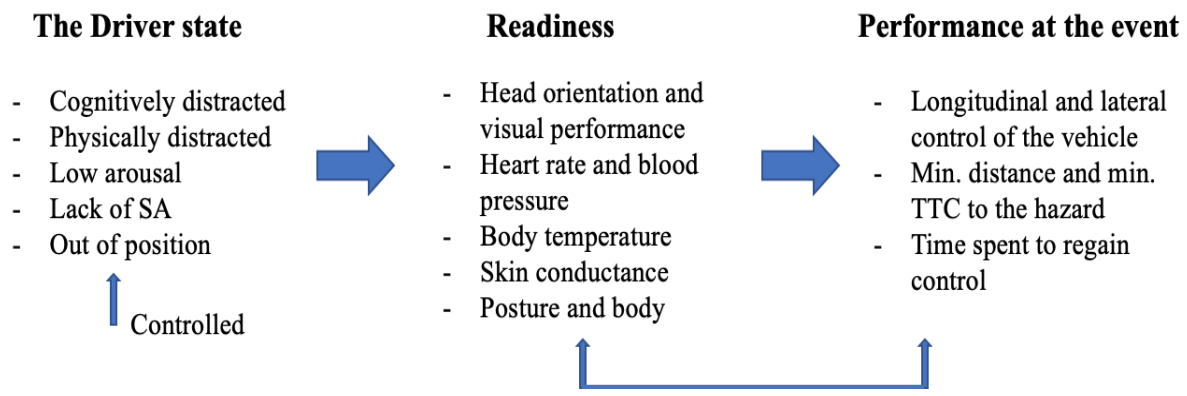

Fig. 3.9. Human machine interface [63].

Truck platooning levels can classified into six levels of automation based upon SAE standards presented earlier in Chapter 2 and Fig. 2.2. The first level of platooning would refer to systems that can only be automated based on forward truck speed such as autonomously maintaining a continuous time separation distance with respect to a leading truck. In this case a

motorist would remain in control over the lateral vehicle position. Several research efforts are ongoing for the development of Level 1 platooning such as the Auburn University EARP projects and the University of California at Berkley PATH project.

Several trucking manufacturing companies likewise have announced their intention in the near future to introduce to the market truck platoons in U.S. However it's not certain if these will be categorized as SAE level one or two. Concurrent developments in Singapore, Japan, Finland, Sweden, Germany, United Kingdom, Netherlands and Australia [64] have advanced autonomous vehicle operations. Fig. 3.10 shows the current level of platooning tests in these counties, with Japan and Singapore currently testing levels 1-4 [65].

The second level of platooning would include automated steering. Studies suggest it is critical to permit smaller forward distance separation between vehicles due to visibility restraints by the following truck at a smaller distances. This makes manual steering more challenging. Several studies have conducted testing on level two platoons. These studies include CHAUFFEUR, SARTRE, ENERY ITS, and Tesla Autopilot. Further in Texas, TTI is presently conducting trials of level two platoons in the surrounding region. Also other technology companies and truck manufactures are presently researching, developing and testing level two platoon on the public roadways. [11, 64].

The third level of platooning is where the motorist can divert his attention to additional tasks for a short period of time. However, the driver is expected to be ready to intervene when needed. The forth level of platooning assumes a capability that would guarantee achieving the least amount of hazard in any fault situation without any human intervention.

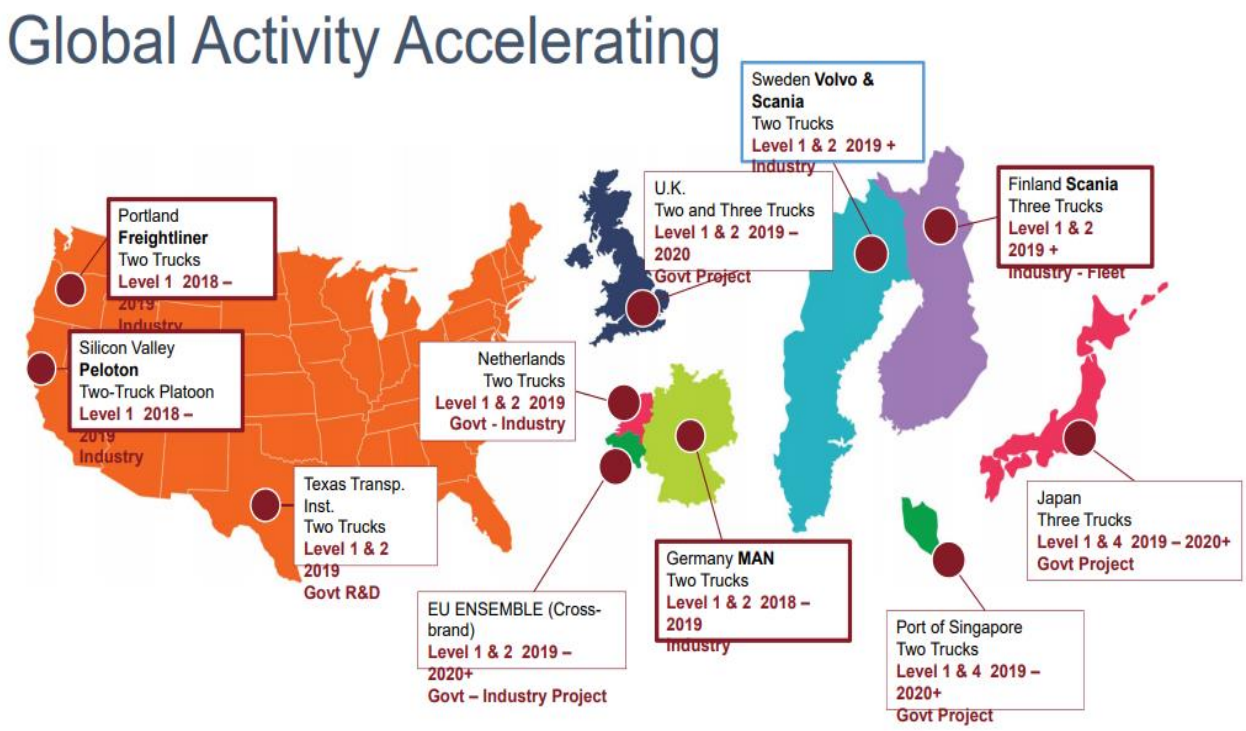

Fig. 3.10. Truck platooning levels in different countries *(source Peloton Technology*) [65].

Thus level three and four platooning truck operation could also be linked behind a leading truck at a lesser automated level. Hence these two levels at platooning initiate a high demand on safety assurance while many experts consider it as unsatisfactory to implement this level of automated trucks with the current state of the art for mixed highway speed and traffic operations. Hence, Levels 3-4 truck platooning might be exclusive to bounded closed locations such as ports or separated driveways in order to facilitate the operational design domain. However, Singapore announced in the near future they plan to adopt level four platooning in civil roadways [64].

Level five platooning corresponds to full automation where the truck can operate under all driving circumstances and the driver is merely a passenger and does not need to intervene or be involved in driving operations. This level of automation theoretically does not need a steering wheel or brake pedal, hence leaving the human driver out of all truck operations. This would serve

the business model of mobility services because driverless heavy-trucks would operate at increased labor efficiency [48]. The goal of this research is to reach level 2-3 of tractor-trailer platoons.

One of the impacts on autonomous trucks is the human driver. In reference to the Bureau of Labor Statistics (BLS), currently in the U.S. there is approximately 3 million truck drivers on national highways [66]. Automation creates a concern for drivers in the trucking business to lose their current jobs. A study made by the international transport forum (ITF) projected that in the U.S and Europe one million truck drivers are expected to lose their jobs by 2030 as result of the development of advanced autonomous trucks [67].

3.4. Highway Evasive Maneuver Scenario

Fig. 3.11 represents the scenario considered for an evasive maneuver situation for a tractor-trailer platoon to change lanes and avoid an obstacle in the highway. With the assumption that the truck is very close to the obstacle and does not have enough time to apply the brakes, it would be safer to depart the lane and be on the center of the lane after the maneuver is completed. It is also assumed that the technologies and sensors from the platooning operation are provided to the control algorithm.

Departing a lane safely is critical in an emergency situation especially when travelling at highway speeds and thus a fast time response is also important to avoid collisions. Furthermore, any improvement in the time response is crucial in the automotive industry.

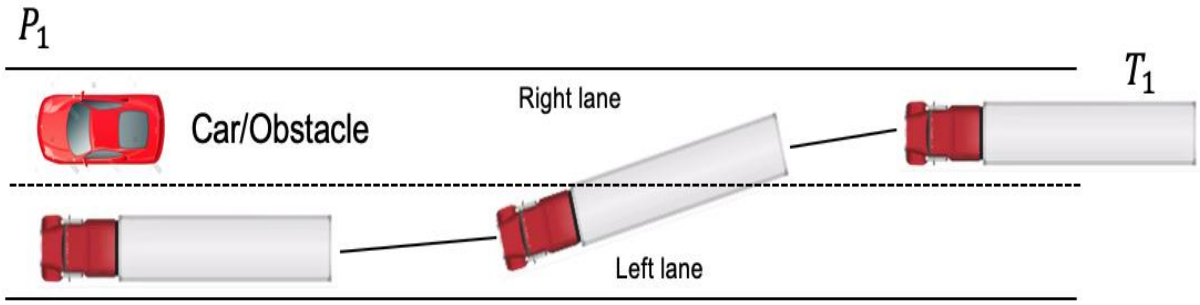

Fig. 3.11. Evasive maneuver scenario to avoid an obstacle.

The professional truck driver modeling is based on the study in [71] where 91 lane changes were observed. The average time for the tractor alone to depart a lane was 6.8 seconds and the fastest time was 4.04 seconds while the slowest time was 12 seconds. Furthermore, the average time for the tractor-trailer combined to depart a lane in the study was 7.7 seconds, with a fastest time of 4.7 seconds and the slowest time was 13.3 seconds. Providing an improvement over the skilled driver is one of goals of this research.

Chapter 4: Fractional Order Control

4.1 Introduction to Fractional Calculus

4.1.1 Fractional calculus background

Fractional calculus (FC) dates to the beginning stages of classical calculus. Newton and Leibniz applied symbols to represent different orders of derivatives to a function y(x). The notation by Netwon were $y'(x), y''(x), y'''(x)$, …, whereas, Leibniz presented the symbol $d^n \frac{y(x)}{dx^n}$ where n is a positive integer [74]. In 1695, a letter from the mathematician L'Hopital was sent to Leibniz questioning the meaning of $n = \frac{1}{2}$. Leibniz responded, "…thus it follows that $d^{\frac{1}{2}} x$ will be equal to $x\sqrt[2]{dx : x}$, an apparent paradox , from which one useful consequences will be drawn" [83]. This answer was reflected as the creation of fractional calculus [74].

The research community started concentrating on theoretical aspects in that past 60 years. Historic reviews on fractional calculus development can be obtained in [74, 83]. In the period after the 1960's the engineering fields started extending research on fractional calculus, where Pudlubny suggested applications of fractional order PID controller [74, 84]. Oustaloup introduced a fractional order robust controller scheme for automotive suspension applications. This was a significant step for the development of non-integer controllers for industry applications [85, 86].

Fractional calculus is being used in many academic and industrial fields such as digital signal processing [88], bioengineering [89], electronic circuits [90], physics [91], chemistry [92] and economic transactions [93]. Thus**,** the use of factional controllers in industry is likely to greatly improve the overall system performance by providing increased precision, performance and energy utilization [73, 78].

To demonstrate the concept of fractional calculus, Fig. 4.1 shows the concept of fractional differential and integrals. For classical integer calculus, a given function f can be integrated or differentiated for several times, but is limited to only the solid circular dots of the number line. For fractional order calculus, this idea can be extended to contain any of the points on the number line for differentiation and integration.

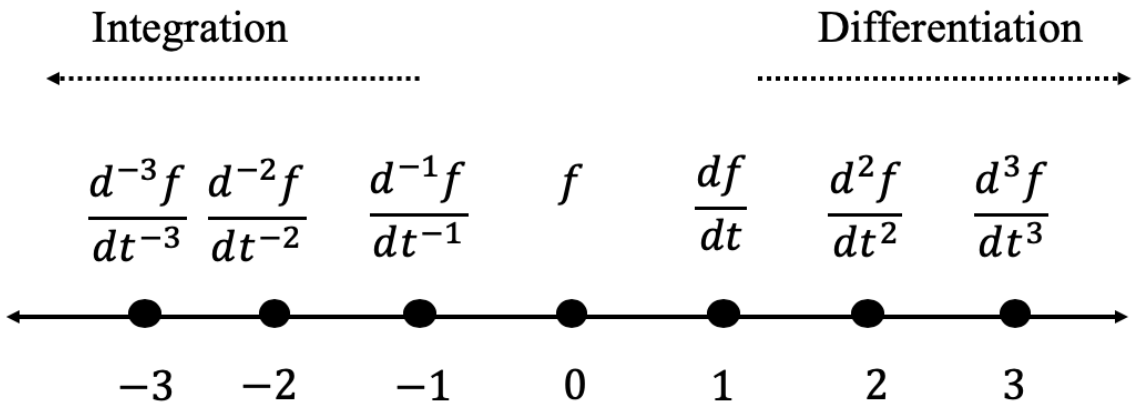

Fig. 4.1. Number line to demonstrate the concept of integral-differentials of fractional calculus.

4.1.2 Theoretical background and definitions

FC is a generalized concept to fractional (non-integer) order of integral and differential basic operator ${}_aD_t^\alpha$, where α denotes the fractional order, t and α are the limits of the opration as shown in the following unified definition in (4.1) [73, 74].

$$ {}_aD_t^\alpha = \begin{cases} \frac{d^\alpha}{dt^\alpha} & R(\alpha) > 0, \\ 1 & R(\alpha) = 0, \\ \int_a^t (dt)^{-\alpha} & R(\alpha) < 0. \end{cases} \tag{4.1} $$

Additionally, α is the operation order and it is generally assumed that α ϵ R, whereas α can also be a complex number.

A fractional order plant is a more realistic method to derive a mathematical model because most physical processes when examined in detail possess fractional order characteristics [75]. Several definitions of FO differentials and integrals can be found in the literature and further details can found in [89]. In the following section, three of the most commonly used definitions of a fractional differential and integral will be briefly described. Michele Caputos defines the derivative of a function $f(t)$ with respect to time as the following [74]:

I. Caputo definition for fractional differentiation

$$D_t^{\alpha} f(t) = \frac{1}{T(m-\alpha)} \int_0^t \frac{f^m(\tau)}{(t-\tau)^{\alpha+1-m}} d\tau. \tag{4.2}$$

Where m = α is an integer and Γ is the Gamma function.

II. Caputo fractional order integral definition

$$D_t^{-\alpha} f(t) = \frac{1}{T(\alpha)} \int_0^t \frac{f(\tau)}{(t-\tau)^{-\alpha+1}} d\tau \tag{4.3}$$

Aleksey Lenikov and Anton Grunwald, the Czech Republic and Russian mathematicians define fractional calculus integration and differentiation as the following

III. Grunwald-Lenikov fractional definition

$${}_aD_t^{\alpha} f(t) = \lim_{x \to 0} \frac{1}{x^{\alpha}} \sum_{i=0}^{\left[\frac{t-a}{x}\right]} (-1)^i \binom{\alpha}{i} f(t - ix). \tag{4.4}$$

Where [.] is the integer part and x is the step size

$$(-1)^j \binom{\alpha}{i} = \frac{(-1)^j \, \Gamma(\alpha+1)}{\Gamma(j+1)\Gamma(\alpha-j+1)}. \tag{4.5}$$

with the assumption that the function $y(t) = 0$, when $t \leq t_0$ and Γ is the Gamma function.

A somewhat different definition is used by Georg Riemann and Jospeh Liouville. They define fractional calculus integration with the assumption that $m - \alpha < \alpha \leq m$ as the following:

$${}_aD_t^{\alpha} f(t) = \frac{1}{\Gamma(m-\alpha)} \left(\frac{d}{dt}\right)^m \int_a^t \frac{f(\tau)}{(t-\tau)^{\alpha+1-m}} d\tau, \tag{4.6}$$

where Γ is the Gamma function, and the power for the term $(t-\tau)$ is ensured not to be less than the value -1.

IV. Riemann-Liouville fractional integral definition

$$D_t^{-\alpha} f(t) = \frac{1}{T(\alpha)} \int_0^t \frac{f(\tau)}{(t-\tau)^{-\alpha+1}} d\tau \tag{4.7}$$

Equation (4.7) can be simplified to $D_t^{-\alpha} f(t)$ when $0 < \alpha < 1$. It can be observed that the definition of fractional order integrals of Riemann-Liouville and Caputo are identical. The fractional differentiation of the R-L definition is based on the fractional integration.

V. Riemann-Liouville fractional differential definition

$$D_t^{\alpha} f(t) = \frac{d}{dt}[D_t^{-1+\alpha} f(t)]. \tag{4.8}$$

Some of the Fractional differentials and integrals critical properties are [82]

- If $f(t)$ is an analytical function of the variable$t$, then the fractional derivative of the operator $D_t^{\alpha} f(t)$ is also an analytical function of t and α.
- As $\alpha = m$, where m is of integer order, $D_t^{\alpha} f(t)$ provides an identical solution of the integer differential and integral.
- In the condition $\alpha = 0$, then $D_t^{\alpha} f(t)$ is the identity operator ($D_t^{\alpha} f(t) = f(t)$).
- The fractional differentials and integrals are linearly operated, thus this expression can be held: $D_t^{\alpha}\left(\lambda_1 f(t) + \lambda_2 g(t)\right) = \lambda_1 D_t^{\alpha} f(t) + \lambda_2 D_t^{\alpha} g(t)$. (4.9)
- The FO integration of an arbitrary order would hold the additive index law

$$D_t^{\alpha}\, D_t^{\beta} f(t) = \; D_t^{\beta} D_t^{\alpha} f(t) = D_t^{\alpha+\beta} f(t) \tag{4.10}$$

4.1.3 Critical functions of FC

1. Gamma Function

Γ(z) can be expressed as follows:

$$\Gamma(\mathrm{z}) = \int_0^\infty e^{-u} u^{z-1} du\,,\ \forall z \in \mathbb{R} \tag{4.11}$$

Thus, this function is an extension of the fractional non-integer numbers. Equation (4.9) converges in the right half plane$\mathbb{R}e(z) > 0$, then the following is given

$$\Gamma(\mathrm{x}+\mathrm{iy}) = \int_0^\infty e^{-t} t^{x-1+iy} dt = \int_0^\infty e^{-t} t^{x-1} e^{iy\log(t)} dt$$

$$= \int_0^\infty e^{-t} t^{x-1} [\cos(y\log(t)) + i\sin(y\log(t))] dt. \tag{4.12}$$

2. Beta Function

The definition of the beta function is expressed as follows:

$$B(p,q) = \int_0^1 (1-u)^{p-1} u^{q-1} du,\quad p,q \in \mathbb{R} \tag{4.13}$$

The gamma and beta functions can be related as follows

$$B(p,q) = \frac{\Gamma(\mathrm{p})\,\Gamma(\mathrm{q})}{\Gamma(\mathrm{p+q})} = B(q,p), \qquad p,q \in \mathbb{R} \tag{4.14}$$

3. Mittag-Leffler Function (ML)

The ML is commonly used to solve FO differential equations, the one parameter ML could be defined as:

$$E_\alpha(z) = \sum_{k=0}^\infty \frac{z^k}{\Gamma(\alpha\mathrm{k}+1)},\quad \alpha > 0 \tag{4.15}$$

ML function can be reduced to an exponential function for $\alpha = 0$. ML two parameter functions can be expressed as:

$$E_{\alpha,\beta}(z) = \sum_{k=0}^\infty \frac{z^k}{\Gamma(\alpha\mathrm{k}+\beta)},\quad \alpha > 0, \beta > 0. \tag{4.16}$$

The relation between (4.15) and (4.16) is

$$E_{\alpha,1}(z) = \sum_{k=0}^{\infty} \frac{z^k}{\Gamma(\alpha k+1)} = E_{\alpha}(z). \tag{4.17}$$

For variations in equation (4.16),

$$E_{1,1}(z) = \sum_{k=0}^{\infty} \frac{z^k}{\Gamma(k+1)} = \sum_{k=0}^{\infty} \frac{z^k}{k!} = e^z \tag{4.18}$$

$$E_{1,2}(z) = \sum_{k=0}^{\infty} \frac{z^k}{\Gamma(k+2)} = \sum_{k=0}^{\infty} \frac{z^k}{(k+1)!} = \frac{1}{z}\sum_{k=0}^{\infty} \frac{z^{k+1}}{(k+1)!} = \frac{e^z-1}{z}. \tag{4.19}$$

A general expression can be

$$E_{1,n}(z) = \frac{1}{z^{(-1+n)}}\left[e^z - \sum_{k=0}^{n-2} \frac{z^k}{k!}\right]. \tag{4.20}$$

4. Miller-Ross Function (MR)

The MR function is defined as

$$\xi_z(v,a) = \sum_{k=0}^{\infty} \frac{a^k z^{k+v}}{\Gamma(v+k+1)}. \tag{4.21}$$

The expression to relate (4.21) with the ML equation (4.16) is

$$\xi_z(v,a) = z^v E_{1,v+1}(az) \tag{4.22}$$

Several cases for MR functions and the relationship for the ML equivalence is given by

$$\xi_z(0,1) = E_1(z) = E_{1,1}(z) = e^z, \tag{4.23}$$

$$\xi_z(0,a) = E_1(az) = E_{1,1}(az) = e^{az}, \tag{4.23}$$

$$\xi_z(\beta-1,0) = z^{\beta-1}E_{1,\beta}(0) = \frac{z^{\beta-1}}{\Gamma(\beta)}. \tag{4.24}$$

4.1.4 Fractional order Laplace transformations

In feedback control applications, the Laplace integral transform is essential for most design methods. The Laplace transform is not only restricted to integer order functions, it also can be used for non-integer order functions. $F(s)$ a function of the complex variable s is the Laplace transform of the original function $f(t)$ given by [73, 74]

$$L\,[f(t)] = \int_0^{\infty} e^{-st} f(t)dt = F(s), \tag{4.25}$$

where $L\,[f(t)]$ denotes the Laplace transform of the function $f(t)$. Typically, the nth order differential can be retrieved from

$$L\left[\frac{d^n}{dt^n} f(t)\right] = s^n F(s) - F(s) - \sum_{k=1}^{n} s^{n-k}\ f^{(-1+k)}(0). \tag{4.26}$$

When all the differential values and the origin values of $f(t)$ are null, then (4.25) can be simplified to the following:

$$L\left[\frac{d^n}{dt^n} f(t)\right] = s^n F(s)\,. \tag{4.27}$$

The properties expressed above are necessary to formulate the ODE into algebraic equations. The integral equation when it is assumed that the initial conditions are zero is

$$L\left[\int_0^t f(\tau)d\tau\right] = \frac{F(s)}{s}\,. \tag{4.28}$$

For multiple integrals of $f(t)$ the Laplace transformation is

$$L\left[\int_0^t \ldots \int_0^t f(\tau)d\tau^n\right] = \frac{F(s)}{s^n}. \tag{4.29}$$

The function $f(t)$ could be retrieved from the Laplace transform through performing the inverse Laplace transformation of $F(s)$ as

$$f(t) = L^{-1}[F(s)] = \frac{1}{2\pi j}\int_{-j\infty+z}^{j\infty+z} e^{st}F(s)ds, \tag{4.30}$$

where *z* is larger than the real segment of the poles of the given by *F*(*s*).

With the assumption of zero initial conditions, the Laplace transformation of (4.4) can be expressed as:

$$L[D^{\alpha}] = s^{\alpha}F(s) \tag{4.31}$$

4.1.5 Fractional order calculus in the frequency and time domains

A FOTF can be presented in the following form

$$G(s) = \frac{b_m s^{\beta m} + b_{m-1} s^{\beta m-1} + \cdots + b_0 s^{\beta_0}}{a_n s^{\alpha n} + a_{n-1} s^{\alpha_{n-1}} + \cdots + a_0 s^{\alpha_0}} \; e^{-Ls} \tag{4.32}$$

The frequency domain can be acquired through substituting $s = jw$ in (4.32). The outcome for the frequency $\omega \in (0;\ \infty)$ can be calculated as

$$R(j\omega) = \frac{b_m (j\omega)^{\beta m} + b_{m-1} (j\omega)^{\beta m-1} + \cdots + b_0 (j\omega)^{\beta_0}}{a_n (j\omega)^{\alpha n} + a_{n-1} (j\omega)^{\alpha_{n-1}} + \cdots + a_0 (j\omega)^{\alpha_0}} \; e^{-L(j\omega)} \ , \tag{4.33}$$

Considering the relation for non-integer power $\alpha \in \mathbb{R}$ of the imaginary unit

$$j^{\alpha} = \cos\left(\tfrac{\alpha\pi}{2}\right) + j \sin\left(\tfrac{\alpha\pi}{2}\right) \tag{4.34}$$

For the time domain, another result with involves some numerical calculation of the FO derivatives which is from the revised G-L definition (4.4) and can be re-written as follows

$$_aD_t^{\alpha} f(t) = \lim_{x \to 0} \frac{1}{x^{\alpha}} \sum_{i=0}^{\left[\frac{t-a}{x}\right]} w_i^{(\alpha)} \, f(t - ix), \tag{4.35}$$

where x is the step size and $(-1)^j \binom{\alpha}{i}$ can be evaluated recursively from

$$w_0^{(\alpha)} = 1, w_i^{(\alpha)} = \left(1 - \frac{1+\alpha}{i}\right) w_{-1+i}^{(\alpha)} \ , \ i = 1, 2, \ldots \tag{4.36}$$

To acquire a numerical result, the signal $\bar{u}(t)$ should first be acquired by using the expression given in (4.30), where

$$\bar{u}(t) = \ b_m D^{\beta m} \, u(t) + \ b_{m-1} D^{\beta_{m-1}} \, u(t) + \cdots + \ b_0 \, D^{\beta_0} \, u(t) \tag{4.37}$$

The response time of the plant now could be found by applying:

$$y(t) = \frac{1}{\sum_{j=0}^{n} \frac{a_j}{x^{\alpha_j}}} \left[u(t) - \ \sum_{j=0}^{n} \frac{a_j}{x^{\alpha j}} \ \sum_{i=0}^{\left[\frac{t-a}{x}\right]} w_i^{(\alpha)} \, f(t - ix) \right]. \tag{4.38}$$

The technique presented here is a fixed step technique, where the precision of the simulation is dependent on the size of the step [73].

4.1.6. FO differential equations

The fractional order description would be a more realistic procedure to define and model systems since real processes are typically fractional in [75]. For example, a fractional order (non-integer) system corresponds to a lossy transmission line. Another example is heat conduction in a semi-infinite solid [77, 79].

FO dynamical system can be expressed in terms of a FODE as [78]

$$a_n D^{an}\, y(t) + \; a_{n-1} D^{a_{n-1}}\, y(t) + \cdots + a_0 D^{a_0} y(t)$$

$$= b_m\, D^{\beta m} u(t) + \; b_{m-1} D^{\beta_{m-1}} u(t) + \cdots + b_0 D^{\beta_0} u(t), \tag{4.39}$$

whereα^i, $\beta^j (i, j = 1,2, \dots)$ are arbitrary real numbers. The following equation is a fractional-order differential equation (FODE):

$$\frac{\mathrm{D}^{\frac{1}{2}}\mathrm{T(t)}}{\mathrm{Dt}^{1/2}} = \mathrm{Q(t)} \tag{4.40}$$

It can be clear that applying an IO differential equation (IODE) to model a system as in (4.30) would be less realistic from the actual system representation. Thus, a plant could be modelled as dynamical system by an FODE [79].

4.1.7. FO state-space representation

The FO operator can also be expressed in a state-space formation. A general FO LTI state-space model can be expressed as [82]:

$$_0D_t^{\alpha} x(t) = Ax(t) + Bu(t), \tag{4.41}$$

$$y(t) = Cx(t) + Du(t)\,, \tag{4.42}$$

where , α=[$\alpha_1, \alpha_2, \alpha_3, \dots, \alpha_n$] is the corresponding FO. Thus, one could also convert the fractional order state space form to a fractional order TF with the following relationship:

$$G(s) = C(s^{\alpha} I - A)^{-1} B + D \tag{4.43}$$

where $G(s)$, corresponds to the FOTF matrix with $px1$ dimension.

The FO continuous-time state space formation could also be discretized, which is expressed as [82]

$$x(k+1) = (AT^{\alpha} + I)x(k)BT^{\alpha}u(k), \text{ for } k = 0 \tag{4.44}$$

$$x(k+1) = (AT^{\alpha} + I)x(k) - \sum_{q=2}^{k+1}(-1)^{q}\binom{\alpha}{q}x(K+1-q) + BT^{\alpha}u(k), \text{for} k \geq 1 \tag{4.45}$$

$$y(k) = Cx(k) + Du(k) \tag{4.46}$$

With the consideration of the FO system infinite memory, (4.44, 4.45 and (4.46) can be represented in an extended formation as

$$\begin{bmatrix} x(k+1) \\ x(k) \\ x(k-1) \\ \vdots \end{bmatrix} = \bar{A}\begin{bmatrix} x(k) \\ x(k-1) \\ x(k-2) \\ \vdots \end{bmatrix}X + \bar{B}u(k) \tag{4.47}$$

$$y(k) = \bar{C}\begin{bmatrix} x(k) \\ x(k-1) \\ x(k-2) \\ \vdots \end{bmatrix} + Du(k), \tag{4.48}$$

where
$$\bar{A} = \begin{bmatrix} AT^{\alpha} + \alpha I & -I(-1)^{2}\binom{\alpha}{2} & -I(-1)^{3}\binom{\alpha}{3} & \cdots \\ I & 0 & 0 & \cdots \\ 0 & I & 0 & \cdots \\ \vdots & \vdots & \vdots & \ldots \end{bmatrix},\ \bar{B} = \begin{bmatrix} BT^{\alpha} \\ 0 \\ 0 \\ \vdots \end{bmatrix}, \tag{4.49}$$

$$\bar{C} = [C\ \ 0\ \ 0\ \ \ldots]. \tag{4.50}$$

4.2 Fractional Order Control (FOC)

4.2.1 Historical view

The first introduction of an FO in a feedback loop was proposed by Bode, Then Manabe presented the transient and frequency domain responses of an FO integration and the control systems applications associated with it. Then the TID control was suggested by Lurie. After that, Oustaloup presented the CRONE controller methodology. Podlubny introduced an FO control that is constructed by generalizing a typical PID controller in order to achieve an improved response

over the classical integer order PID method. The most commonly used FO controller in literature are the following [97, 98]:

- FOPID controller.
- CRONE controller.
- Tilted proportional and integral (TID) controller.

The TID control provides feedback using the classical IOPID controller where the proportional element of the IOPID controller is interchanged with a tilted element $s^{\frac{-1}{n}}$. This results in having a response more close to estimating an optimal response.

The CRONE controller was introduced by Oustaloup. The term comes from the French acronym meaning fractional order robust control. The CRONE controller includes the frequency domain characteristics to demonstrate the effectives of the FO controller. Systems with time variations, unstable and with minimum/non-minimum phase could also be controlled with this type of a controller. Some examples for real-life applications using the CRONE control method include, automobiles suspension control and hydraulic actuator control [98].

4.2.2 Fractional order PI/PID controller

The IOPID control, is one of the earliest developed control methods in control systems. Since the control structure and design techniques are straightforward and are simple to implement, this control strategy is very beneficial for industrial applications. Further, with the PID controller usually provides satisfactory results and the design technique don't necessarily need exact information of the plant model. Consequently, it has become the most widely used controller method in the process industry [74].

To demonstrate the control possibilities of using a fractional order $PI^{\lambda}D^{\mu}$ in a graphical way, Fig. 4.2, shows the four control points of a conventional PID range control points of the quarter-plane defined by selecting the fractional order values [74].

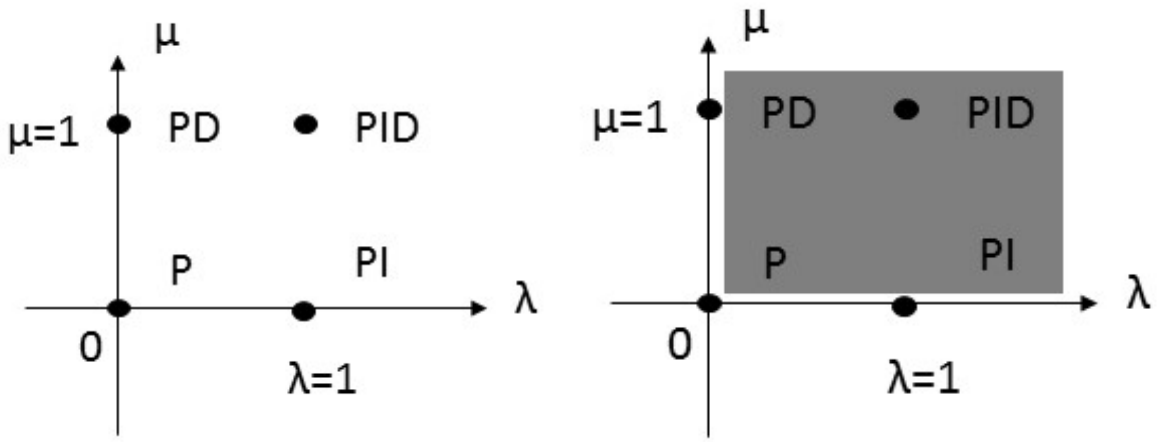

Fig. 4.2. Classical PID/FOPID.

The differential equation of the fractional order $PI^{\lambda}D^{\mu}$ control is given by

$$u(t) = K_p e(t) + \frac{K_i}{D^{-\lambda}} e(t) + K_d D^{\mu} e(t). \tag{4.51}$$

By applying a Laplace transformation to (4.51) with zero initial conditions, the TF of the fractional order version of this controller is $PI^{\lambda}D^{\mu}$,

$$G_c(s) = K_p + \frac{K_i}{s^{\lambda}} + K_d s^{\mu}. \tag{4.52}$$

As mentioned previously, these two additional two degrees of freedom λ and μ of the integrator and differentiator allow more flexibly to the designer to implement the controller and to meet the system requirements more accurately.

Using a fractional order PID controller allows the user up to five parameters to tune, while for a fractional order PI or PD the user have four parameters to design. With λ = 1 and μ = 1 a

classical PID controller would be obtained. Hence with λ = 1 and μ = 0, a PI controller is acquired, while a PD controller is obtained when λ = 0 and μ = 1.

Fig. 4.4 displays a block diagram of a typical FOPI^{λ} control for a SISO system. $G_c(s)$ is the fractional order controller given in terms of a transfer function as the following

$$G_c(s) = K_p + \frac{K_i}{s^{\lambda}}, \tag{4.53}$$

where the fractional order term is λ.

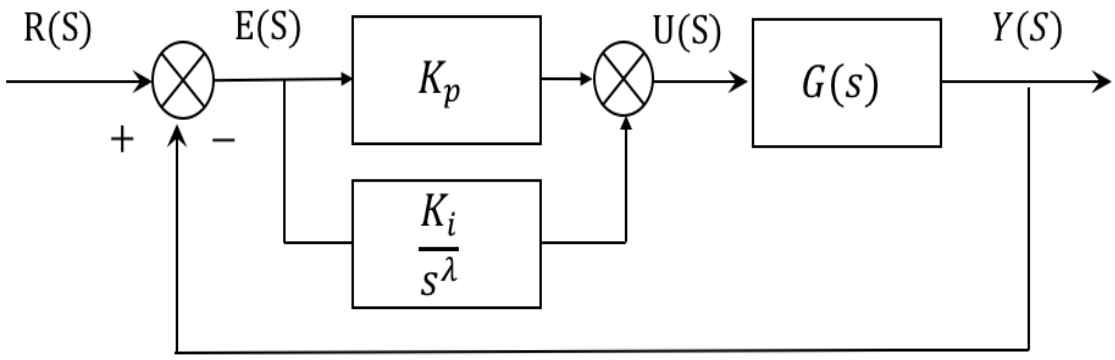

Fig. 4.3. Block diagram of a fractional order PI^{λ} control.

The additional adjustable parameter λ with the FOPI in contrast to the classical PI controller allows more flexibility to control the system and at the same time increases the control quality performance. As a comparison example, with FOPI, achieving closed-loop zero steady-state error and reducing the amplification of high-frequency disturbances can be accomplished. When using the classical IOPI controller there is a phase lag of 90 degrees. Thus, the FOPI structure provides a diminished constant phase lag of λ, which can introduce an improved transient dynamical response as opposed to the classical PI controller.

In regards to the large-frequency noise amplification, the magnitude Bode plot slope of the FOPI controller is smaller with 20 (1- λ) dB/decibel. Further in this manner the IOPI controller would be most suited as the associated slope in the case of high-frequencies can be 0 dB/ decibel [74].
In control system theory a plant can be controlled by either IO or FO controller, whereas the plant could also be derived as a fractional or integer order. There are four different combinations to apply an FO control scheme [78]:

a) IO plant with IO controller.
b) IO plant with fractional order (FO) controller.
c) FO plant with IO controller.
d) FO plant with FO controller.

In most cases the FO control would be applied to an ordinary linear or non-linear system to improve the system performance [96] .The focus of this research is to develop a linear FO controller applied to an IO plant corresponding to a semi-autonomous tractor-trailer with a FO controller. .

For loop-shaping control with an FO controller, the Bode magnitude would be 20λ dB/decibel and no longer limited to the 20dB/decibel slope as in the case for classical integer order control, which can provide the controller more robustness [79]. Fig. 4.3, shows a Bode plot comparison of a PID and FOPID in the frequency domain. With the integer order PID the slope is limited to 20 dB, while, with a fractional order with λ = 0.5, the slope order would be 10 dB and 5 dB with λ = 0.25, where K_p = K_i= K_d= 1.

In this example with additional tuning parameter λ and μ the controller can be better designed to meet the system specification and outperform the IO controller. When using the FO

controller it provides high robustness to gain and parameter variation. In contrast to IO controllers which require a more complex controller design to stabilize an uncertain system [80].

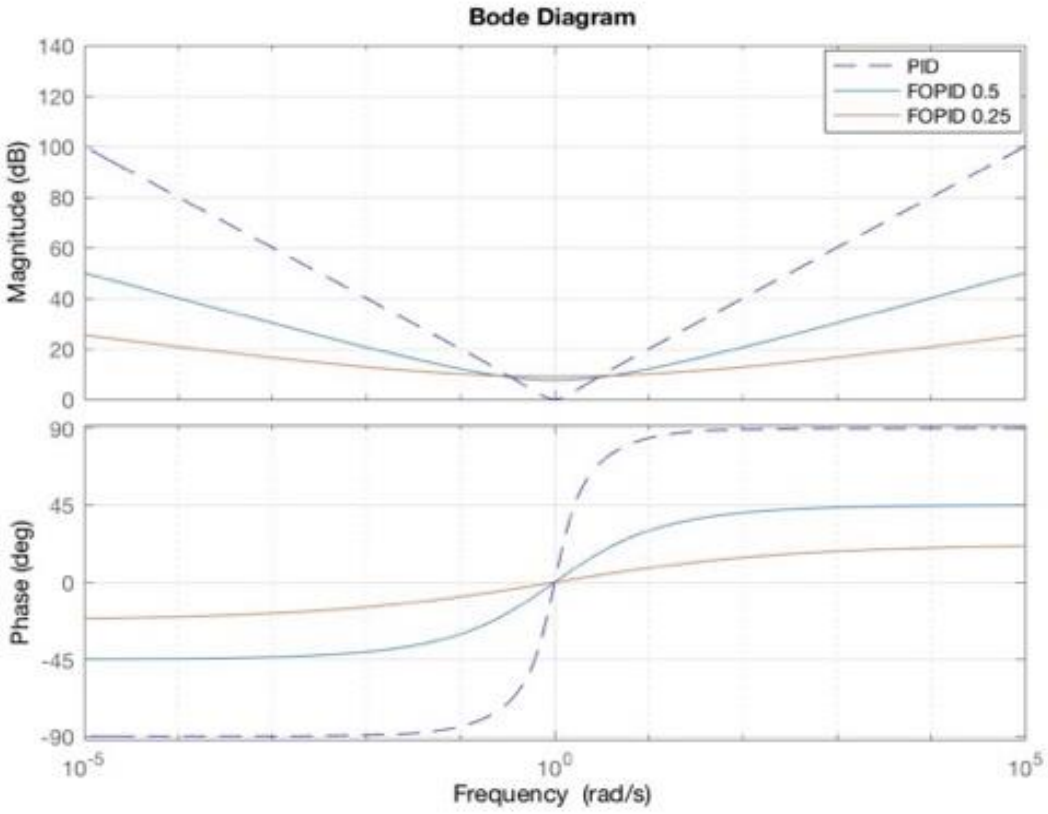

Fig. 4.4. Bode plot of a PID/FOPID controller.

For the FO controller the system can be robust against gain variation along with the iso-damping property related to the overshoot of the system being independent of the gains. Hence, for a given linear plant this would translate to an uncompensated (open loop) phase being nearly flat for the Bode plot. This would imply that, the derivative of the phase in respect to the frequency is null at a defined frequency range acknowledged as the tangent frequency w_c. Further, the Iso-damping property can be expressed in a mathematical term as [82]:

$$\frac{d\angle G(s)}{ds}\Big| = 0, \tag{4.54}$$

or otherwise as

$$\angle\frac{dG(s)}{ds}\Big| = \angle G(s)|. \tag{4.55}$$

where, $s = jw_c$. The Nyquist plot of the uncompensated (open-loop) plant would tangentially hit the sensitivity circle at the tangent frequency when this condition is guaranteed. With this condition, the Bode phase graph locally indicates that the plant provides robustness against changes occurring in the system gains [82].

4.2.3 Introductory example: FOC of passenger vehicles

As an initial investigation of fractional order control, this dissertation considers a $PI^{\lambda}D^{\mu}$ controller function. In Fig. 4.5 a block diagram of a fractional order $PI^{\lambda}D^{\mu}$ controller for a single input single output (SISO) system is presented. $\mathrm{G_c(s)}$ is the fractional order controller given in terms of a transfer function as the following:

$$G_c(s) = K_p + \frac{K_i}{s^{\lambda}} + K_d s^{\mu}. \tag{4.56}$$

With the additional adjustable parameters λ and μ (which are fractional powers) allows more flexibility to control the system and at the same time would increase the control quality. More demonstration of fractional calculus and FO control will be explained later in Chapter 4 of this dissertation.

Simulation results are presented in Figs. (4.6-4.8), which demonstrate the robustness of applying this control scheme as compared to a classical PID control. Thus, the vehicle position with different speed, mass and rear/front cornering stiffness is improved with the fractional order controller.

Table 1. Passenger vehicle parameters.

Symbol	Description	Value
m	Vehicle total mass	1480 kg
I_z	Yaw inertia moment	2350 kg m^2
l_f	Distance of CG from front axle	1.05 m
I_r	Distance of CG from rear axle	1.63 m
C_f	Front tire cornering stiffness	67500 N/rad
C_r	Rear tire cornering stiffness	47500 N/rad

The results for a passenger vehicle is implemented by applying a step response to the lateral position of the passenger vehicle model traveling at a speed of 55 mph and 80 mph. Results show meeting a specification of an overshoot of less than 5% and a settling time below 2 seconds. Hence, the IOPID control is established and then compared to the FOPID controller. Furthermore, the comparison is done in both time and frequency domain for the integer and non-integer control design.

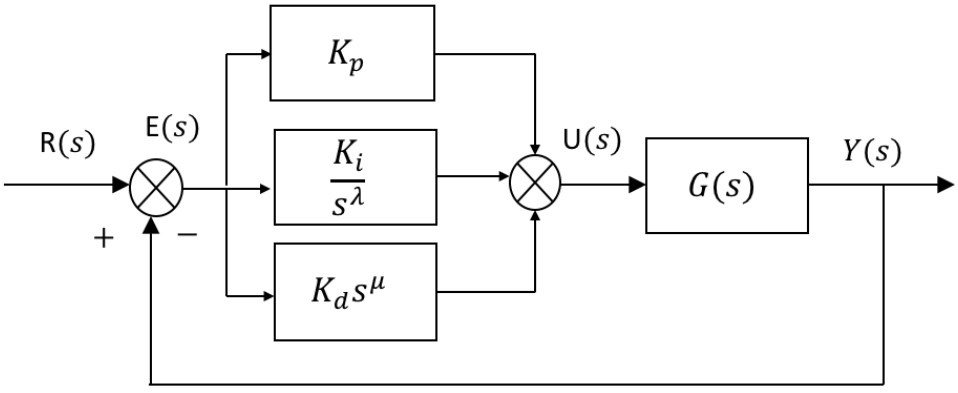

Fig. 4.5. Block diagram of a fractional order $PI^\lambda D^\mu$ control.

The passenger vehicle parameters are provided in Table 1. Fig. 4.6 and Fig. 4.7 shows the step response of lateral position of the vehicle while travelling at a speed of 55 mph and 80 mph of the linearized system. Fig. 4.8 shows the step response while doubling the vehicle mass of the linear system.

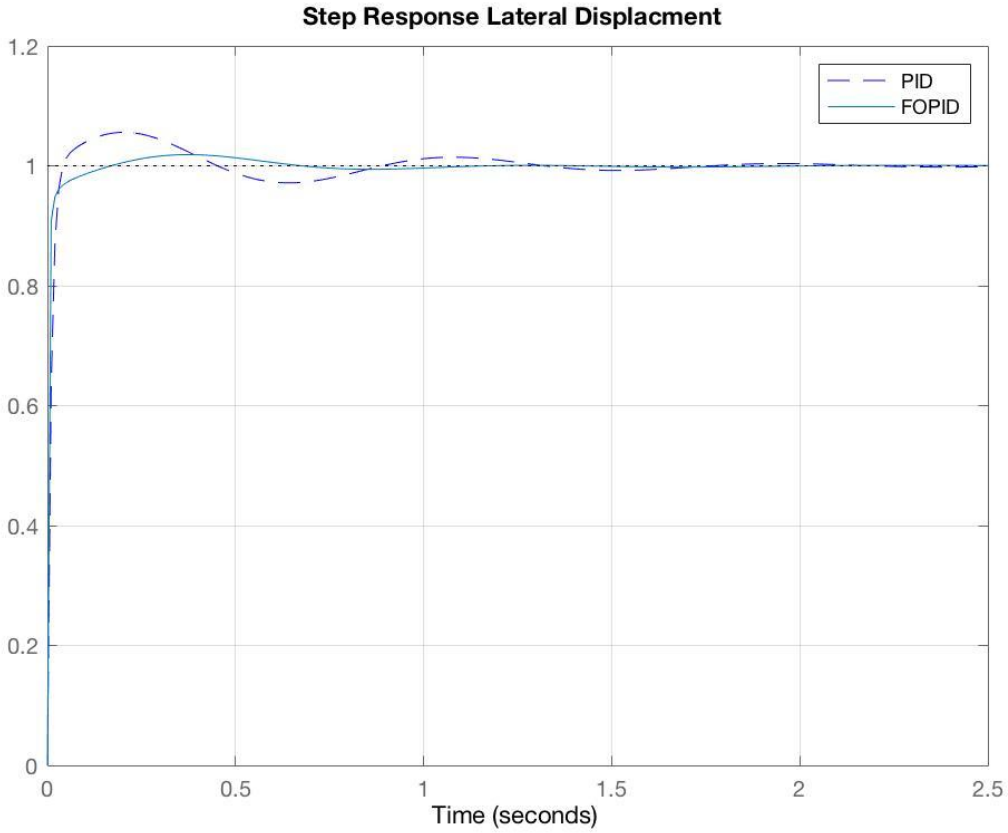

Fig. 4.6. Step response of the lateral displacement at 55 mph.

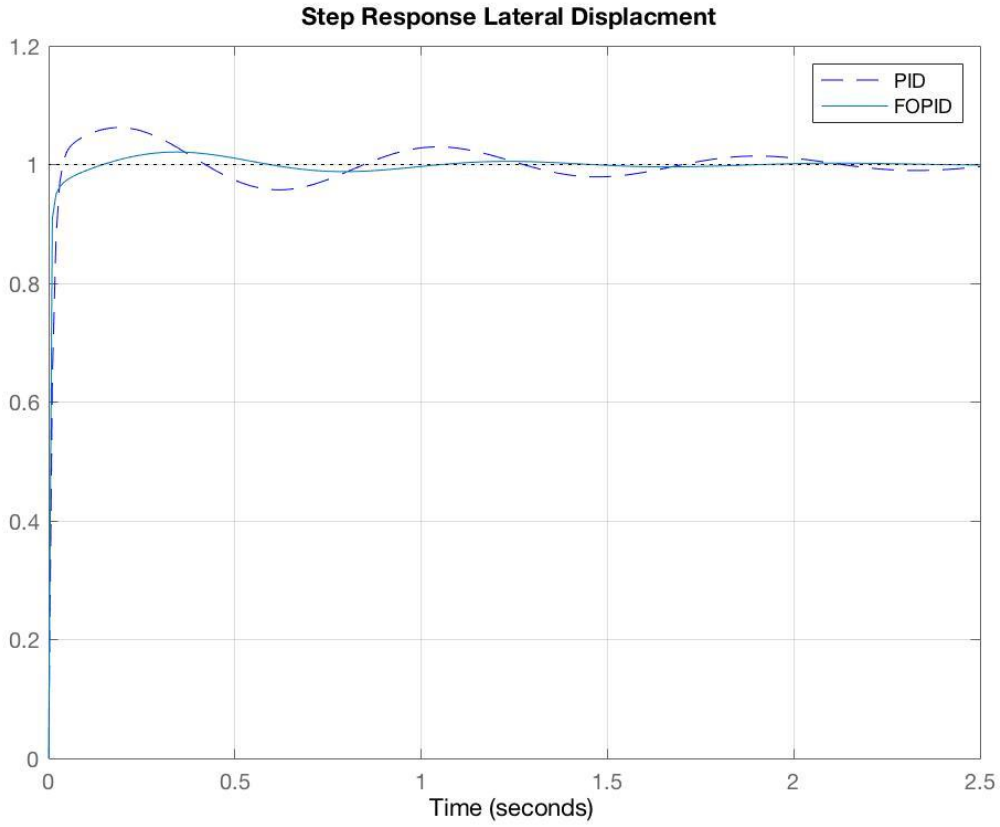

Fig. 4.7. Step response of the lateral displacement at 80 mph.

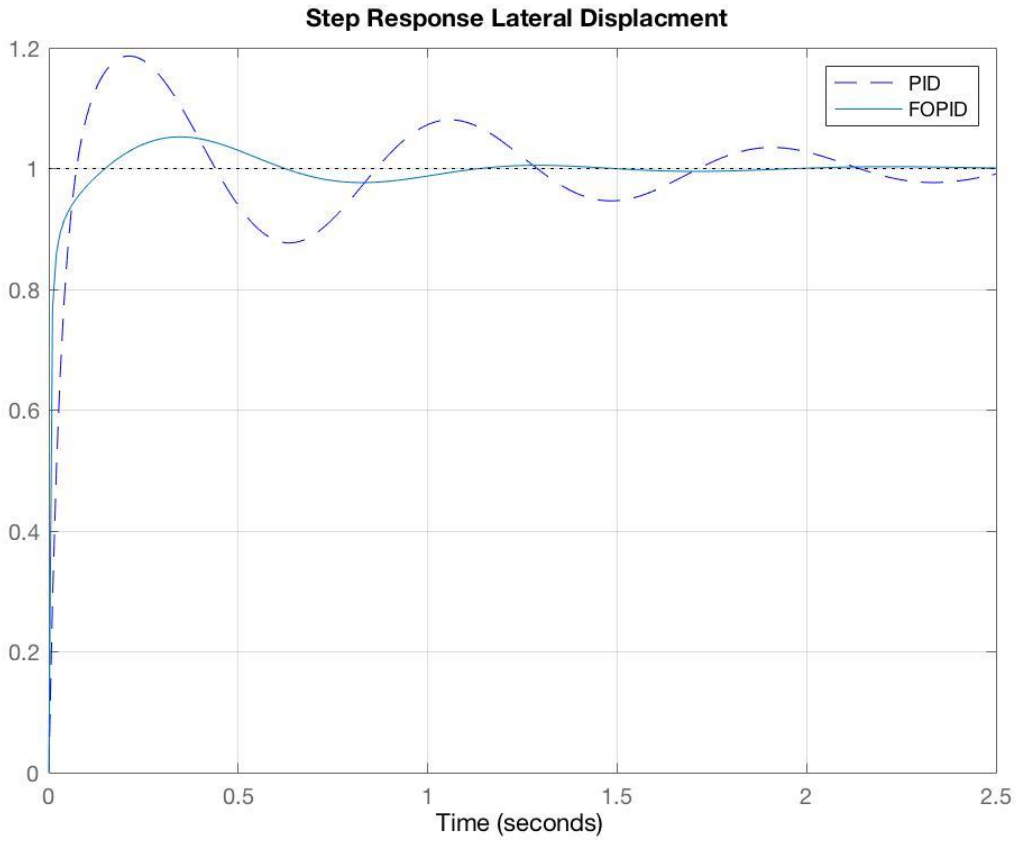

Fig. 4.8. Step response of the lateral displacement with varying the vehicle mass.

Also for verification of the passenger vehicle nonlinear model, the fractional order controller is implemented to the nonlinear model, Fig. 4.9 displays the lateral position of the vehicle while travelling at a speed of 80 mph. Fig. 4.10 and Fig. 4.11 shows the vehicle position while varying the vehicle mass and the vehicle front tire stiffness respectively.

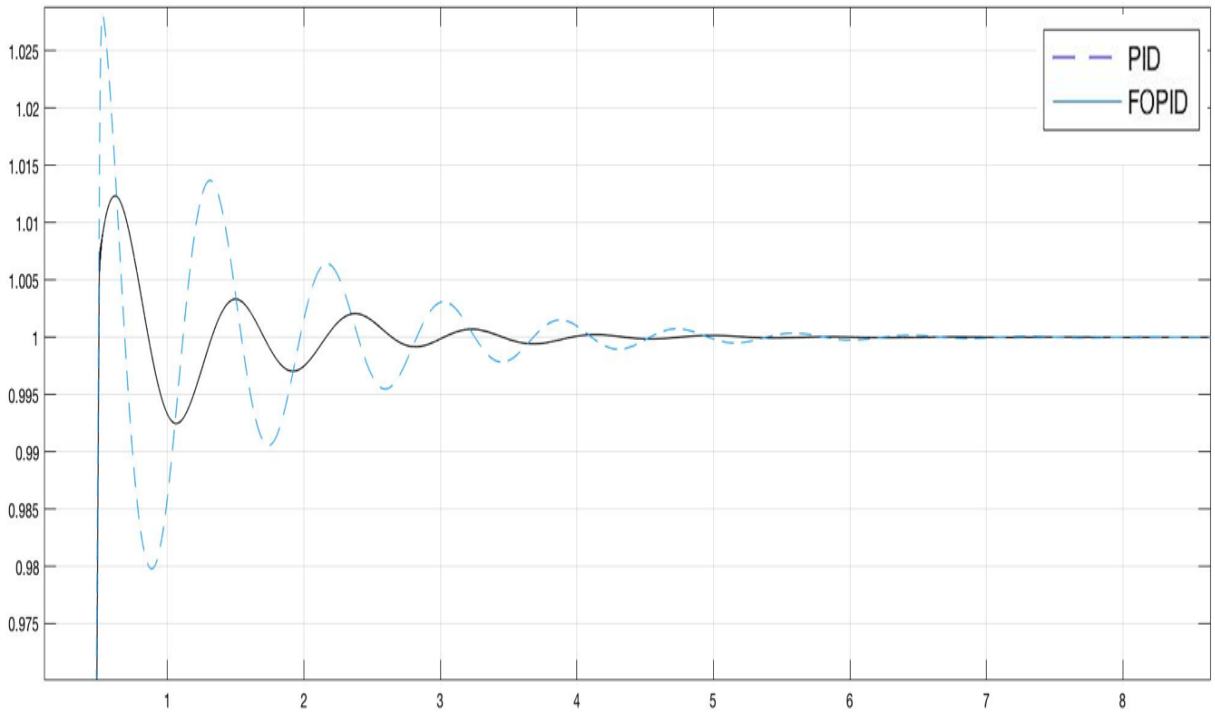

Fig. 4.9. Step response of the lateral displacement at 80 mph of nonlinear vehicle model.

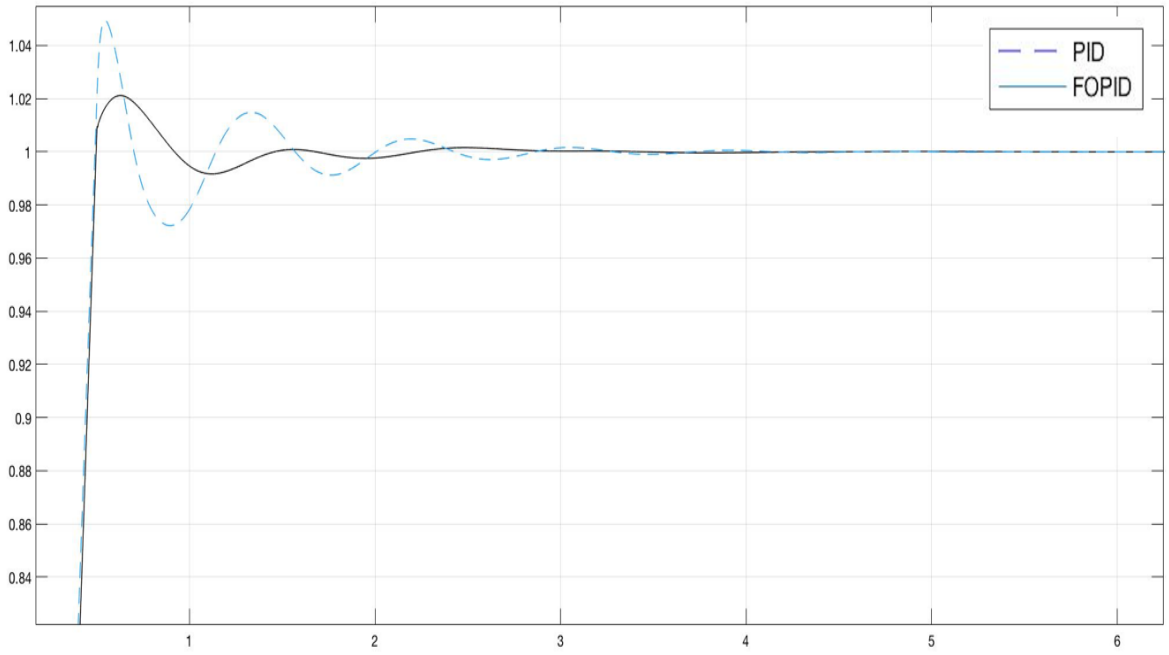

Fig. 4.10. Step response of the lateral displacement with mass variation of nonlinear model.

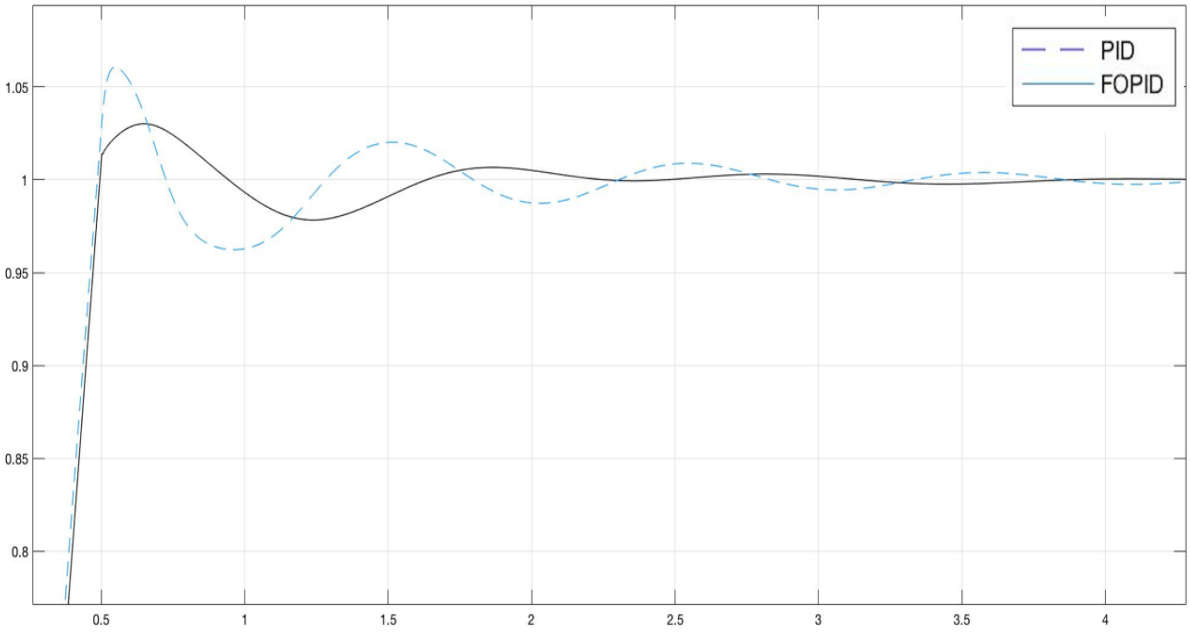

Fig. 4.11. Step response of the lateral displacement with varying C_r of nonlinear model.

Table 2 presents a summary of applying PID/FOPID to five different cases of varying the system parameters such as speed, mass, rear (C_r) and front (C_f) cornering stiffness. The frequency domain analysis demonstrates the robustness of applying a fractional order controller to a system with uncertainty. The stability margins of the system is improved as compared to the IOPID controller. Cases 4 and 5 are when the system becomes non-minimum phase. The controller was designed with the following parameters:

K_P = 7.68, K_i = 6.71, K_d = 2.2, λ = 0.5 and μ = 1.25.

Table 2. Passenger vehicle parameter variation.

Vehicle	Case 1	Case 2	Case 3	Case 4	Case 5
Mass	1480 Kg	1480 Kg	2960 Kg	1480 Kg	1480 Kg
Speed	24.6 m/s	35.7 m/s	24.6 m/s	24.6 m/s	24.6 m/s
C_r	47500 N/rad	47500 N/rad	47500 N/rad	32500 N/rad	32500 N/rad
C_f	67500 N/rad	67500 N/rad	67500 N/rad	67500 N/rad	70000 N/rad
Controller	---	---	---	---	---
PID phase margin	89.7°	89.1°	85.1°	89.8°	89.8°
FOPID phase margin $\lambda = 0.5, \mu = 1.25$	113°	113°	112°	113°	113°
FOPID phase margin. $\lambda = 0.5, \mu = 1.5$	135°	135°	135°	135°	135°

4.3 FO PI^{λ} Control Motivation

Control systems could contain the FO dynamical plant and a FO controller. Nevertheless, in control engineering it is more frequent in practice to regard only the FO controller which is owed to the fact that the system model could already have been acquired as a conventional IO model [79]. Further, FO control is being explored and investigated in many research fields such as electrical circuits, signal processing, chemical processes and bioengineering. Thus, FC has been discovered to be particularly beneficial in systems theory and automatic controls [73, 85, 87].

Little research exists for applying this control scheme for lateral stability of passenger vehicles [4, 12]. In particular no current research as of today exists for applying this control scheme for lateral stability for tractor-trailers system. FC would be highly beneficial for this application

since it has many advantages over integer control methods. FO control of nonlinear systems can alleviate the limitations of IO control algorithm [73].

FOPI^{λ} control could attain improved control performance compared to the IOPI controller and can be integrated into existing PI control loops [73-78]. It has been shown in previous studies that the extra degree of freedom introduced by the fractional integrator males it possible to further enhance the performance of the classical PI controller [79]. Also with the fractional integrator operator λ, the system can be robust against gain variation along with the iso-damping property that is related to the overshoot of the system being practically independent of the gains [82].

With an FO controller for IO plants there would be more flexibility in altering the gain and phase margin characteristics [78]. Furthermore, applying a fractional order PI^{λ} control for a dynamic system provides [73-74, 78]

- Fast time response and improved control quality of the dynamical system.
- Reduced percentage of overshoot and settling time.
- Improved output disturbance rejection to the system.
- Decreased steady state error.
- More flexibility to the designer with the additional degree of freedom λ.

For the tractor-trailer system with highway lane departures corresponding to tracking a ramp input requires an integrator with a higher power than one in order to provide accurate steady-state tracking. Thus with the integrator order between 1 and 2 one would expect that a fractional number can be found that provides minimized tracking errors for the steering system. This research develops a method to determine an optimal value for the FOPI controller leads to improved performance compared to an integer order PI controller.

4.4 Approximation to Fractional Order Operators

4.4.1 Oustaloups's recursive filer approximation

The Oustaloup recursive filter approximation method is well established in literature to approximate a fractional order differentiator [73, 79]. The filter can be written as the following:

$$G_f(s) = K \prod_{k=-N}^{N} \frac{s+wk}{s+wk} \tag{4.57}$$

where the gain, zero and pole can be determined from

$$w_k = w_b * w_u^{\frac{(\alpha-1+2*k)}{N}}, w_k' = w_b * w_u^{\frac{(-\alpha-1+2*k)}{N}}, \tag{4.58}$$

$$w_u = \sqrt{\frac{w_h}{w_b}},\ K = w_h^{\alpha}, \tag{4.59}$$

for k=1, 2…, N in the frequency range $(w_b; w_h)$

The Oustaloup filter can be implemented in the following procedure [97]:

a) Select the fractional value α, choose the order of approximation N, then select the upper and lower frequency range w_b, w_h respectively.
b) From equation (4.59) w_u and K can be computed, then from (4.58) w_k and w_k' can be obtained.
c) The Oustaloup filter $G_f(s)$ is then created from (4.57).

A bode plot comparison between different order of approximation for the Oustaloup filter is displayed in Fig. 4.12, where the fractional order operator $\frac{1}{s^{0.5}}$ is approximated with w_b=0.001 and w_h= 1000, for N=1,2 and 5. As can be seen in Fig. 4.12, the higher the order of approximation the more accurate the fractional order is approximated as the ripple is tends to be reduced as the order is increased.

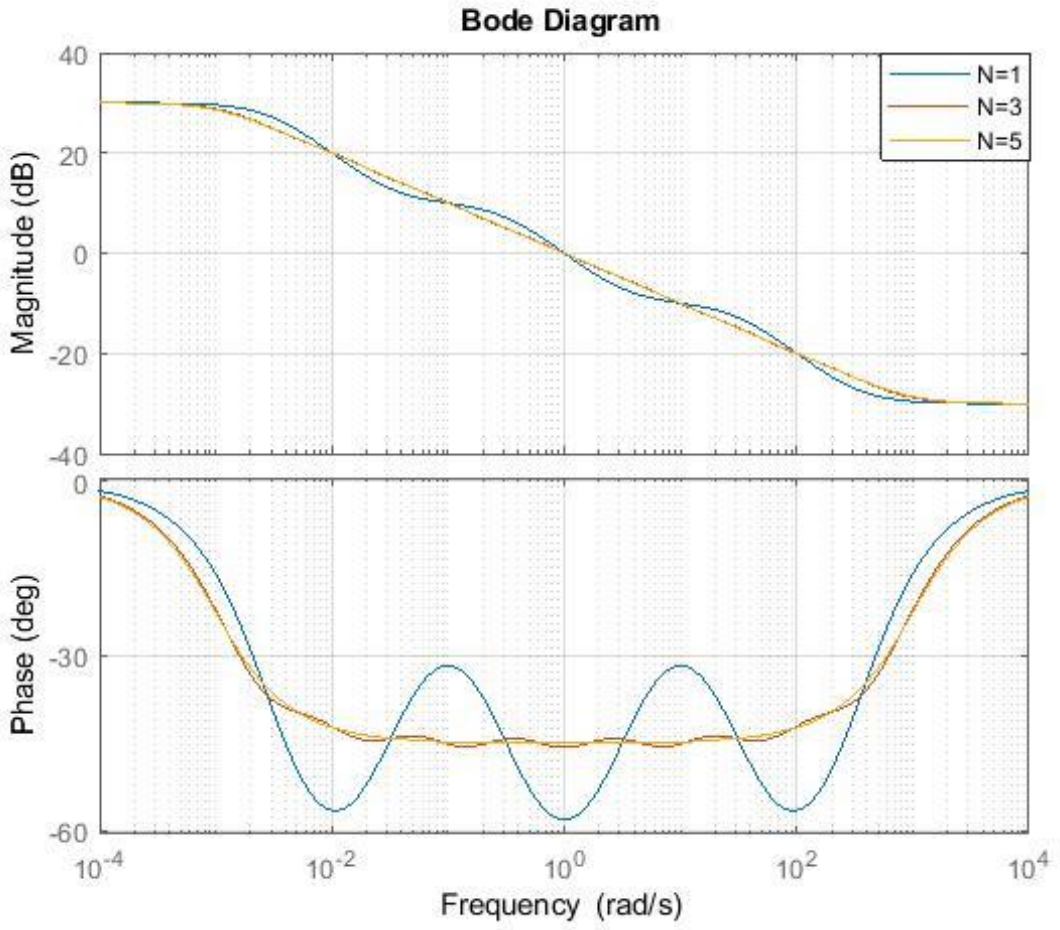

Fig. 4.12. Bode diagram for different orders of Oustaloup approximation for $\frac{1}{s^{0.5}}$.

4.4.2 Refined Oustaloup filter

The refined Oustaloup filter provides a better approximation and can be introduced by [81]:

$$s^{\alpha} \approx \left(\frac{dw_h}{b}\right)^{\alpha} \left(\frac{ds^2+bw_h s}{d(1-\alpha)s^2+bw_h s+d\alpha}\right) K \prod_{k=1}^{N} \frac{s+w\prime_k}{s+w_k}, \tag{4.60}$$

where

$$w'_k = w_b * w_u^{\frac{(\alpha-1+2*k)}{N}}, w_k = w_b * w_u^{\frac{(-\alpha-1+2*k)}{N}}, \quad K = w_h^{\alpha}. \tag{4.61}$$

Noting that α order should satisfy $\alpha \in (0,1)$ hence through experimental examination the weighting factors should be selected as b = 10 and d = 9 in order to obtain a good result for the

synthesis approximation [79]. A bode plot comparison between different order of approximation for the modified Oustaloup filter is presented in Fig. 4.13, where the fractional order operator $\frac{1}{s^{0.5}}$ is approximated with w_b=0.001 and w_h= 1000 for N=1,2 and 5. Also, similarly the higher the order of approximation the more accurate the fractional order is approximated as the ripple is reduced for the higher order approximation.

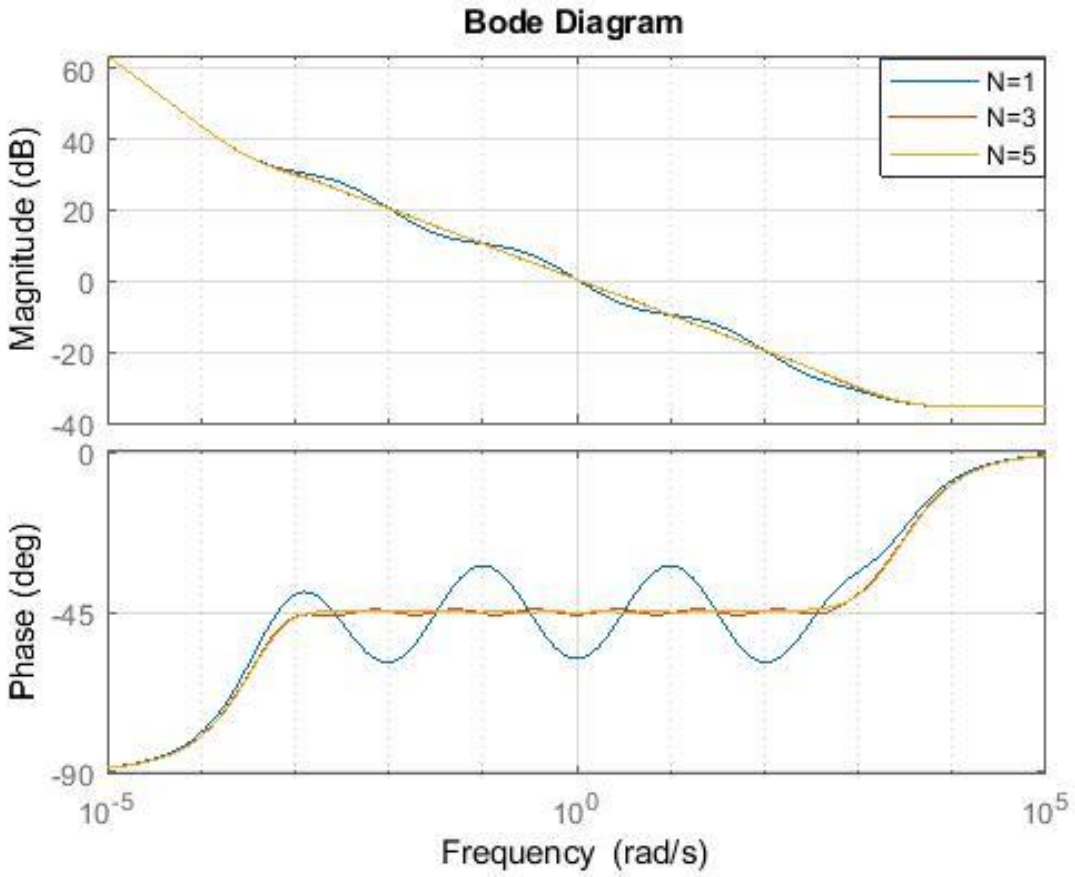

Fig. 4.13. Bode diagram for different orders of the refined Oustaloup approximation for $\frac{1}{s^{0.5}}$.

For this research the Oustaloup approximation method is applied to implement the integrator in FO controller for a tractor-trailer system.

4.5 Discrete Time Realization

The discrete-time realization is typically favoured over continues time, because it can be easily applied and updated using digital electronics. Two strategies are considered for discrete-time realization: direct and indirect. For indirect approaches, the frequency domain fit in the continuous-time case is achieved followed by the discretization of the transfer function s. There are additional frequency domain fitting techniques that could also be implemented, however, they lack a guarantee of stability for the minimum phase discretization.

Direct techniques attempts to provide a constant phase of the FO element directly in the frequency domain. Some of the approaches include Tustin operator fractional expansion, Euler operator power series expansion and numerical integral techniques.

These methods for discretizing the factional operator s^{α} are in infinite impulse response (IIR) form. Yet there are other techniques to acquire the FO differential in finite impulse response (FIR) form. Applying this technique might reduce the efficiency to approximate the FO operator s^{α} because of the large order of this type of filter. Further, a direct method is typically preferred over an indirect method for digital realization [82, 96].

4.5.1 Direct discretization techniques

For discretization, two stages should be considered in order to obtain the discretized function of an FO differential. First, selecting an appropriate producing function is critical as this defines the discrete FO differential$s = wz^{-1}$. The generalized form is typically considered [99]:

$$wz^{-1} = \frac{1-z^{-1}}{\beta T(\gamma+(1-\gamma)z^{-1})}, \tag{4.62}$$

where β is a tuned parameter of the gain, T is the period sample and γ is the phase parameter. The frequently applied methods to generate a function for discretizing are presented in Table 4. These

producing functions can be acquired from (4.62) in consideration of the gain and phase tuning parameters in Table 3.

Table 3 The tuning parameters β and γ.

Methods	F. Euler	Tustin	Al-Aaoui	B. Euler	Implicit Adams
β	1	---	---	---	---
γ	0	0.5	$^{7}/_{8}$	1	1.5

The second procedure is approximating the irrational formula with a finite order expression. To achieve this, two of the mathematical techniques, PSE and continuous fractional expansion (CFE), can be used. PSE and CFE can be expressed as follows [99]:

$$D^{\pm v}(z) \approx CFE[w(z^{-1})^{v}] \text{ or } D^{\pm v}(z) \approx PSE[w(z^{-1})^{v}] \tag{4.63}$$

Table 4 Discrete-time conversion rules.

Methods	$\boldsymbol{s \rightarrow z}$ conversion	Taylor series
Backward-difference (Euler)	$s^{v} \approx \left[\frac{1-z^{-1}}{T}\right]v$	$\left(\frac{1}{T}\right)\left[1 - vz^{-1} + \frac{v(v-1)}{2!}z^{-2} + \cdots\right]$
Trapezoidal (Tustin)	$s^{v} \approx \left[\frac{2(1-z^{-1})}{T(1+z^{-1})}\right]v$	$\left(\frac{2}{T}\right)[1 - 2vz^{-1} + 2v^{2}z^{-2} + \cdots]$
Al-Alaoui	$s^{v} \approx \left[\frac{8(1-z^{-1})}{7T(1+\frac{z^{-1}}{7})}\right]v$	---
Simpson	$s^{v} \approx \left[\frac{3(1-z^{-1})(1+z^{-1}}{T(1+4z^{-1}+z^{-2})}\right]v$	$\left(\frac{3}{T}\right)[1 - 4vz^{-1} + 2v(4v+3)z^{-2} + \cdots]$

4.5.2 Indirect discretization techniques

For indirect discretization, there are two steps. Step one, the TF s^v can be approximated by a rational TF using a continues approximation method. Next, by substituting s in the function, the discretized function can be acquired as:

$$s^v \approx \frac{P_n(s)}{Q_m(s)} \xrightarrow{s=wz^{-1}} s^v \approx G(z) \tag{4.64}$$

For example, in [100], s^v was approximated using the Oustaloup technique initially and then the discrete approximation was obtained by substituting s in the following:

$$s = \frac{(\alpha+1)(z-1)}{T(z+\alpha)}, \tag{4.65}$$

where the sample period is T and the weight element is within the closed interval $[0,1]$. For any irrational continuous TF, this procedure is typically used. The frequency response can be acquired by substituting$z = e^{jwt}$. Next, the impulse response can be acquired by applying an inverted FFT to the prior computed frequencies. From the impulse response the approximation for the TF is retrieved by applying a Steiglitz-McBride method, which can be expressed as:

$$Gz^{-1} = \frac{a_0+a_1z^{-1}+\cdots+a_nz^{-N}}{b_0+b_1z^{-1}+\cdots+b_nz^{-n}}. \tag{4.66}$$

where the approximation order is n.

4.5.3 Digital implementation

The procedure for implementing a digital FO TF is first to obtain the finite change relationship by the discretization technique presented in section above. Next, the FOTF can applied to a digital device such as an FPGA or DSP. Thus, implanting this controller scheme on an embedded devices, the following should be considered [73]:

- The memory size limits
- Computational abilities restrictions

- The performance limitations

A digital discrete-time implementation of an FOPI control can be given as the following:

$$H_{PI^{\lambda}}(z) = K_p + K_i {H_I}^{-\lambda}(z). \tag{4.67}$$

Where, ${H_I}^{-\lambda}(z)$ is the approximated discretization of the FO integral term of the order λ. K_p and K_i are the gains of the parallel formation of the control algorithm.

For digital realization, typically the controller technique could be based on the canonical form of an IIR filter defined as the following:

$$F(z^{-1}) = \frac{u(z^{-1})}{e(z^{-1})} = \frac{b_0 + b_1 z^{-1} + \cdots + b_M z^{-M}}{a_0 + a_1 z^{-1} + \cdots + a_N z^{-N}}. \tag{4.68}$$

The FO controller having the form of an IIR filter could likewise be implemented using an FPGA or DSP. Fig. 4.14 shows a block diagram of a canonical implementation of the direct form, where u(k) and e(k) are the output and input [78].

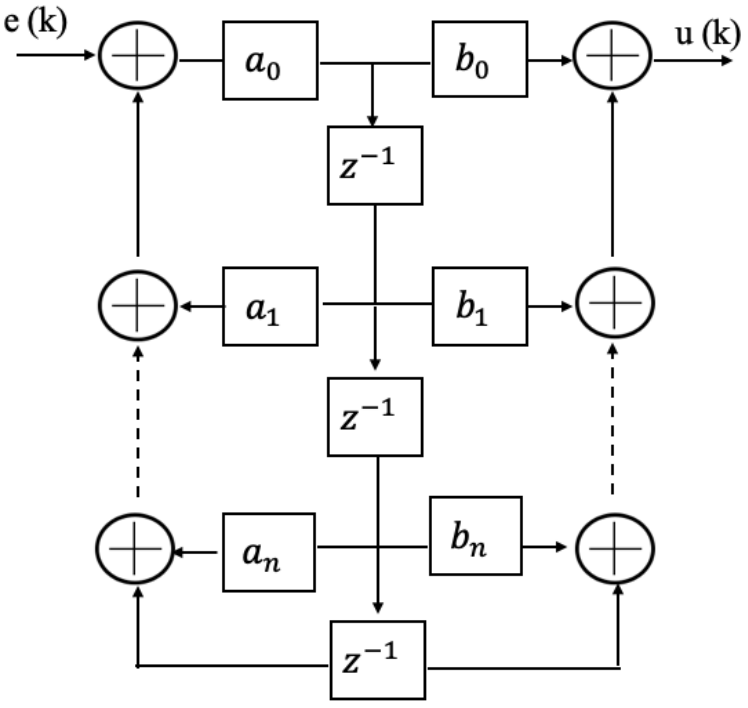

Fig. 4.14. Canonical IIR filter representation

For this research the FO controller would be approximated using the Oustaloup approximation method, and then discretized for real-time digital implantation for the tractor-trailer system. Choosing the order of approximation is critical in order to provide high accuracy for the fractional order controller approximation.

Chapter 5: FO State Feedback Control

5.1 State Feedback Control

Control system design is often expressed in terms of a reference signal $r(t)$ and system plant $G(t)$ are provided. The input $u(t)$ of the plant is a controlled actuator input that is configured by the system design and the output of the plant is $y(t)$. The objective is to design a feedback control system in order that the output of the plant $y(t)$ will track the reference signal $r(t)$ as closely as possible.

If the actuating signal $u(t)$ depends only on the reference signal and is independent of the system output, then the system is referred to as operating in open-loop control. If the actuating signal is dependent on both the reference signal and the plant output (i.e., employs feedback), then the system is defined to be operating in a closed-loop mode. Open-loop control is not able to compensate for parametric variability and external disturbances and therefore most control systems are operated in a closed-loop mode [96, 102].

A block diagram for a typical state feedback representation is displayed in Fig. 5.1. The feedback vector K_p, can improve the stability characteristics of the system. To select K_p several design methods exit in the literature that provide the designer number of options in meeting the design requirements.

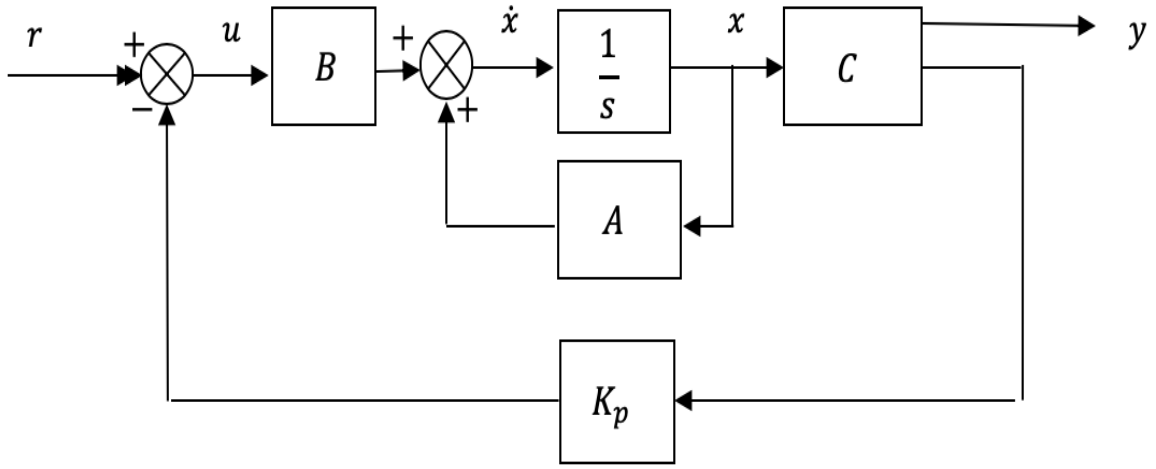

Fig. 5.1. State feedback system.

Consider the single variable state equation

$$\dot{x} = Ax + Bu,\ y = Cx \tag{5.1}$$

A system such as (5.1) is defined to be controllable if given any initial condition for the state vector x_0, then there exists an input $u(t)$ such that the systems state can be driven to zero in finite time. It can be shown that for linear time-invariant systems that controllability is equivalent to being able to use state-feedback to arbitrarily assign the closed-loop system poles [102]. The augmented tractor-trailer system in (3.76) can be shown to be completely controllable [68]. Consequently, the control input for the full state-feedback becomes:

$$u = r - kx = r - [k_{p1}\ \ k_{p2} \ldots k_{pn}]x = r - \sum_{j=1}^{n} k_{pj} x_j \tag{5.2}$$

where the elements of the feedback vector k are real-valued constants. By substituting equation (5.2) into equation (5.1)

$$\dot{x} = (A - Bk)x + Br, \quad y = Cx \tag{5.3}$$

With appropriate selection of k, then an asymptotically stable matrix can be acquired $(A - Bk)$ with eigenvalues that can be assigned by the control system designer.

5.1.1 State feedback with proportional gain

For the tractor-trailer system it is critical for the controller to track the desired lane position for an emergency lane departure in a highway. State feedback control with proportional gain is illustrated with a block diagram in Fig. 5.2, where, K_p is a scalar proportional gain and K is the feedback gain vector. With the tractor-trailer travelling at a constant highway speed 70 mph, the open-loop transfer function for the tractor trailer system used in this research can be expressed as [104]:

$$G_0(s) = \frac{110.4s^4+3174s^3+49960s^2+59800s+158700}{s^6+34.32s^5+395.8s^4+523.9s^3+1292s^2} \quad (5.4)$$

It is noted that (5.4) is a type 2 system, i.e., it contains a factor of $1/s^2$. A conventional state-feedback control law for the tractor-trailer system

$$u = \mathrm{r} - k_1 v_1 - k_2 r_1 - k_3 r_2 - k_4\, \psi - k_5 x_5 - k_p x_6. \quad (5.5)$$

where x_5, and $x_6$represent the yaw angle and the lateral position.

The system tracking will need to be adequate for performing the platooning operations described in Chapter 3. In particular, the type 2 as in (5.4) system with full-state feedback (5.5) will have a steady-state error to a ramp input command. This will create conditions where one of the following trucks may collide with an obstacle even though the lead vehicle may have properly responded in avoiding the object.

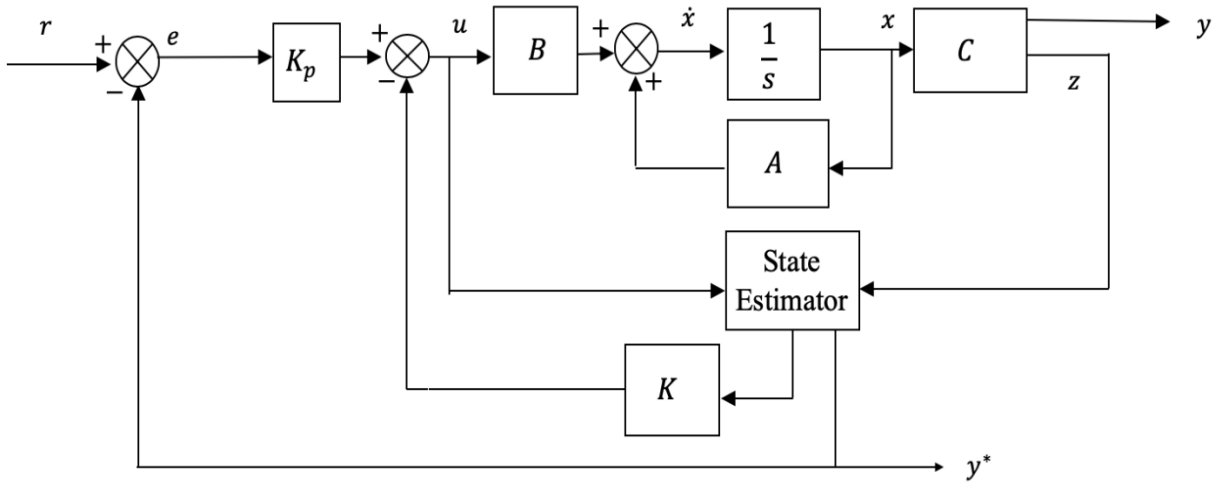

Fig. 5.2. Full state feedback with proportional gain.

As an initial assessment of the closed-loop system behavior, root locus analysis for the open-loop system with only output feedback was examined. In this case, $u = r - k_p y$ and the associated root locus is the set of solutions to $1 + k_p G_0(s) = 0$ for $k_p \geq 0$. The root locus plot is shown in Fig. 5.3. Of particular significance is that the tractor-trailer becomes unstable for small values of output feedback in the range of $0 < k_p < 8.2$. For larger values of $k_p$the tractor-trailer system is stable, however the real-component of the dominant poles asymptotically converge to -0.014 and thereby limit the decay rate of the closed-loop system to disturbances and input changes Consequently, the tractor-trailer system requires state-feedback to achieve adequate transient response during platooning operations.

Table 5 provides the eigen-values for the open-loop system (5.4) and the closed-loop system with the LQR control with a speed of 70 mph.

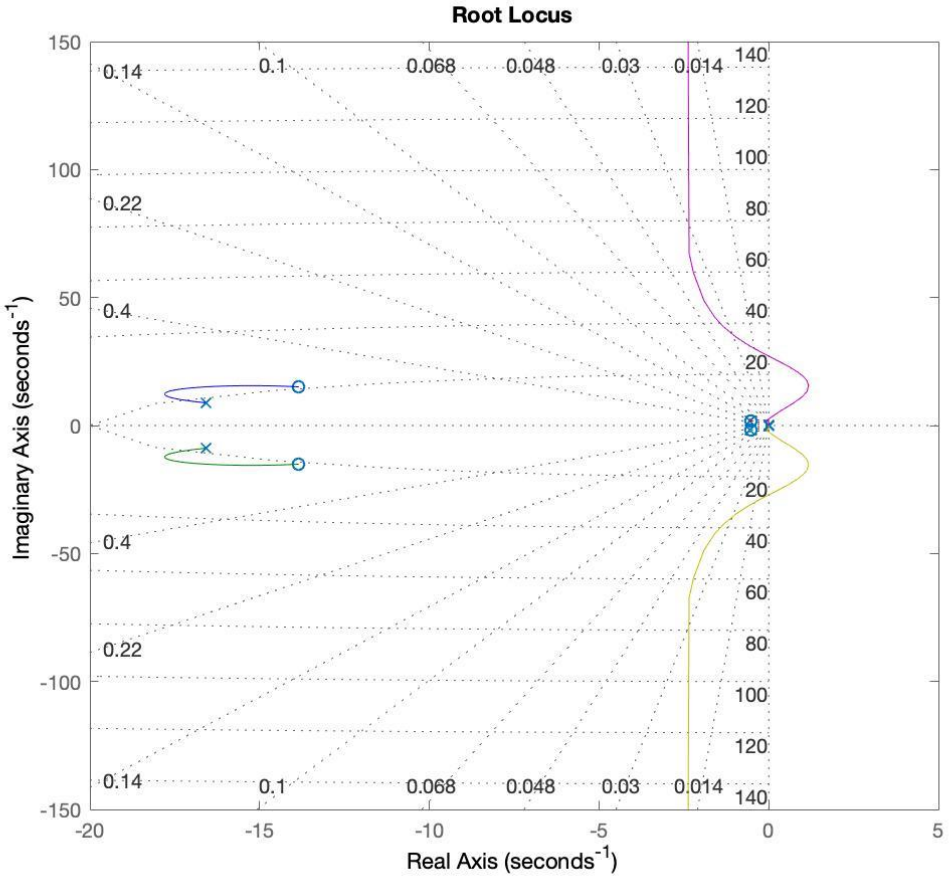

Fig. 5.3. Root-locus for the tractor-trailer system.

Table 5 Eigen-values for the system in (5.4).

Open-loop	**Closed loop**
0	-162.56
0	-10.17
-0.57 + 1.82i	-3.9 + j3.8
-0.57 – 1.82i	-3.9 - j3.8
-16.6 + 8.9i	-0.56 +j1.7
-16.6 – 8.9i	-0.56 -j1.7

It is noted that the open-loop system is type 2 and therefore the system is dominated by the two poles located at the origin of the s-plane. The use of pole placement for the remaining non-zero poles are needed primarily to shape the transient response by compensating for zeros in (5.4). Considerable insight can be obtained by considering a reduced-order model of the tractor-trailer system by only conserving the dominant poles. A Bode plot comparison between the full order truck dynamics (5.4) and a double integrator (reduced tractor-trailer model) is shown in Fig. 5.4. As can be seen the difference is mainly in the phase plot associated with the poles and zeros that are associated with the state equations derived in inertial reference frame coordinates in (3.63).

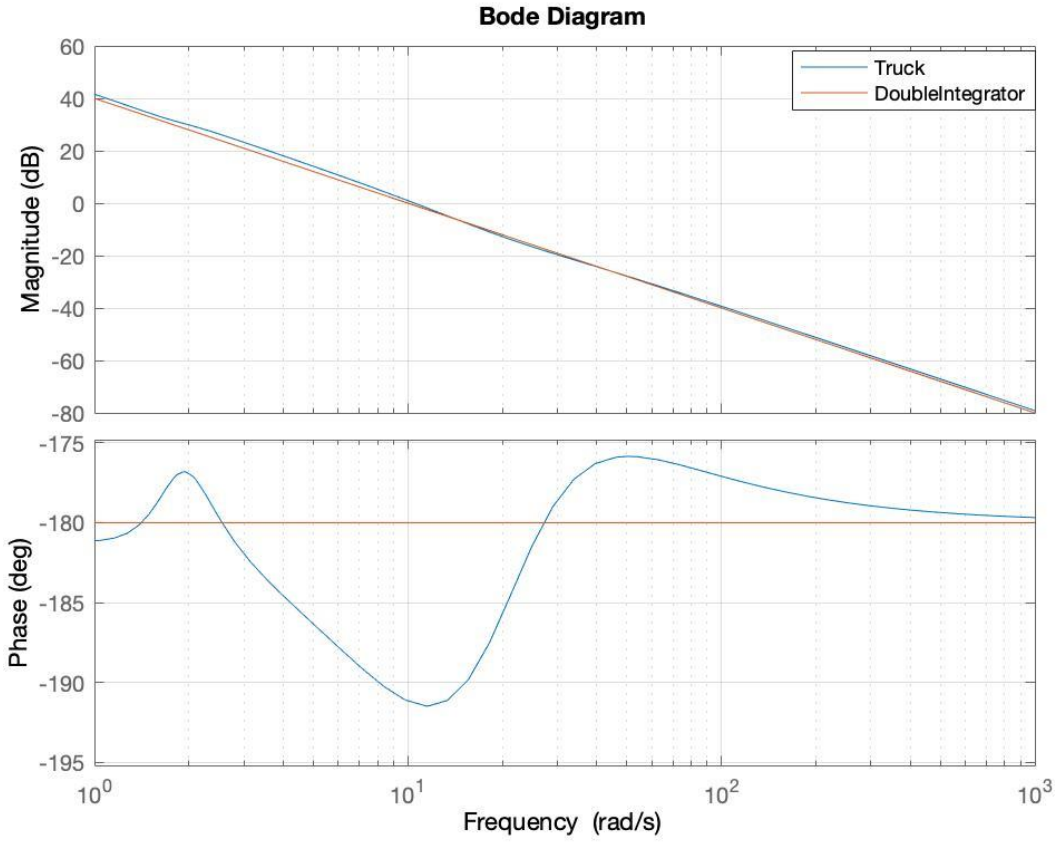

Fig. 5.4. Bode plot comparison for the truck TF and a double integrator TF.

To examine the system for the tractor-trailer for tracking, Fig. 5.5, shows a step response for the tractor-trailer system with state feedback, where the gains were obtained using the LQR method.

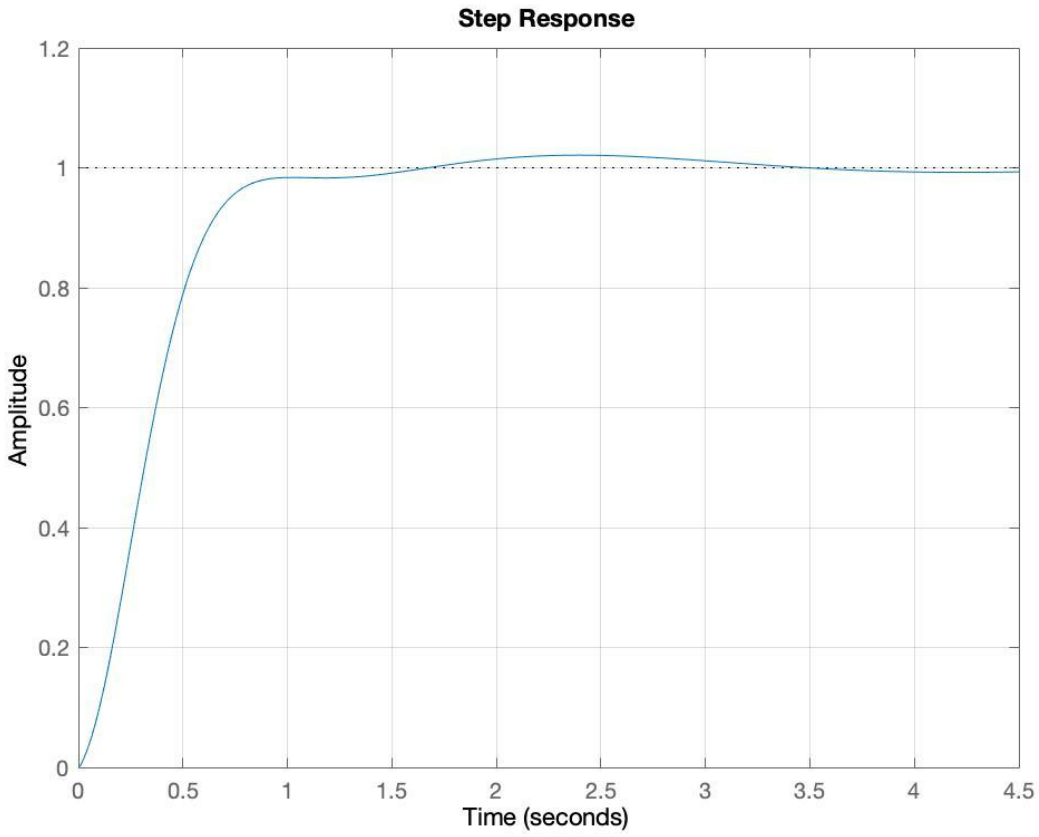

Fig. 5.5. Step response with state feedback with proportional gain for the tractor-trailer system.

To examine the system ramp input tracking for an evasive lane departure the response is compared to the desired lane change reference input shown in Fig. 5.6 for a constant highway speed of 70 mph. As can be seen in the in Fig. 5.6, it shows a steady-state constant ramp error that is unacceptable for platooning operations. As previously mentioned, this is a consequence of (5.4) being a type 2 system. The steady-state ramp error can be reduced by adding additional integrator

to the controller [102] to create a type 3 system. The mean squared error (MSE) for the lane change error is computed to be MSE=1.72. Fig. 5.7 displays lane error response for this system type. The effects of increasing the system type to greater than 3 will be examined in section 5.1.2, where it will be found that the MSE can reduced by increasing the system type to be greater than 3.

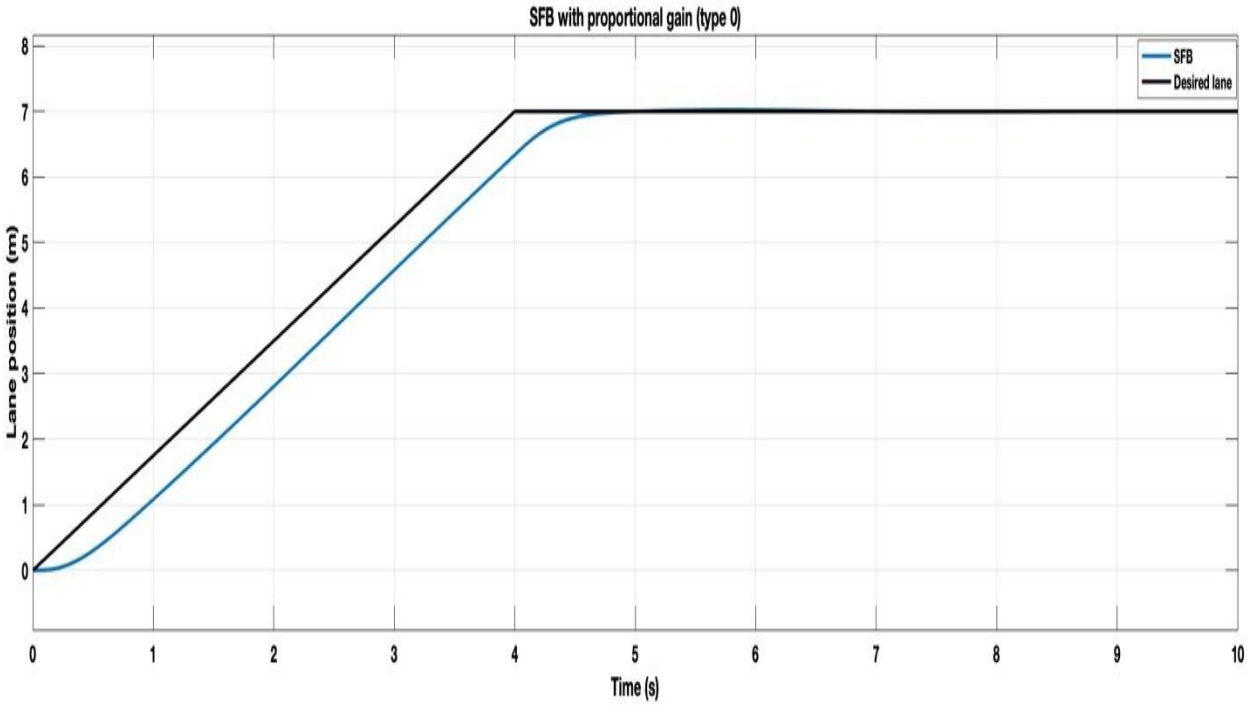

Fig. 5.6. Lane position with SFB with type 2 system.

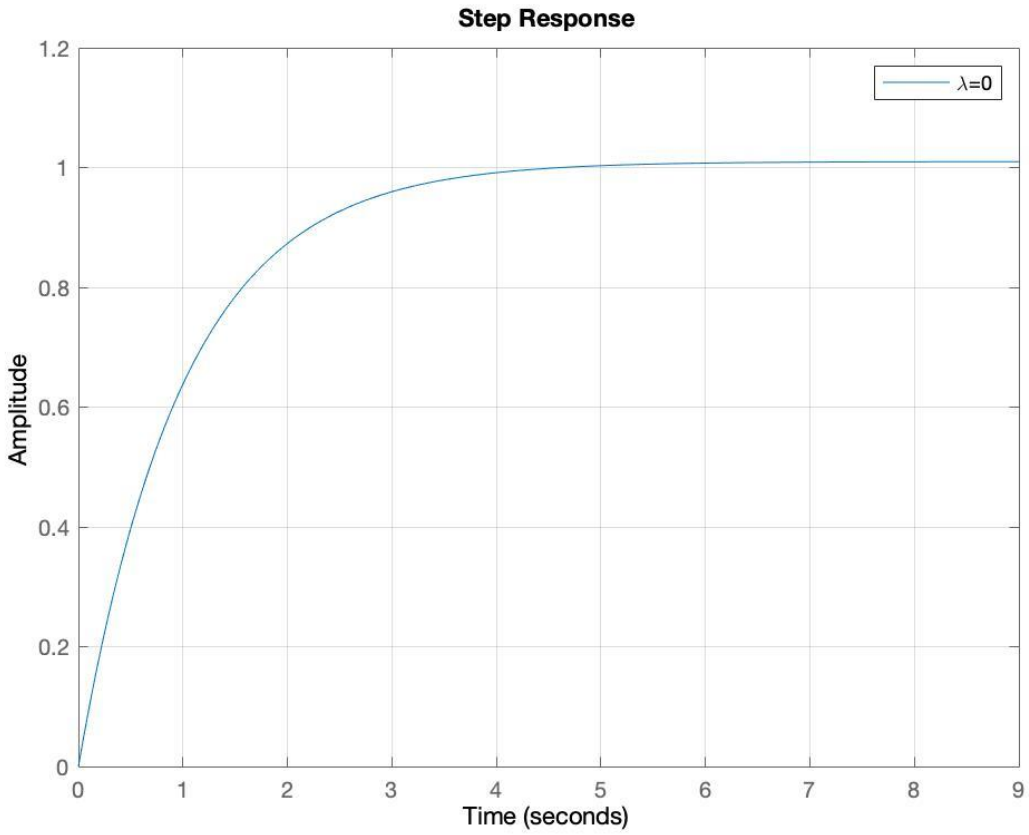

Fig. 5.7. Lane error with type 2 system.

5.1.2 State feedback with integer order integral action

The transfer function and state equation established for the tractor-trailer will vary for multiple reasons such as environment, aging or road variations. In order to provide robustness in tracking platooning commands and minimizing disturbances due to road and wind conditions, the controlled system integrator can be added to the state feedback in order to increase the system type as shown in Fig. 5.8. [94, 96].

Consider plant representing the tractor-trailer as

$$\dot{x} = Ax + Bu, y = Cx \tag{5.6}$$

With the plant being completely controllable. The TF of the system can be written as:

$$G_p(s) = C(sI - A)^{-1}B \tag{5.7}$$

Where s is the Laplace variable.

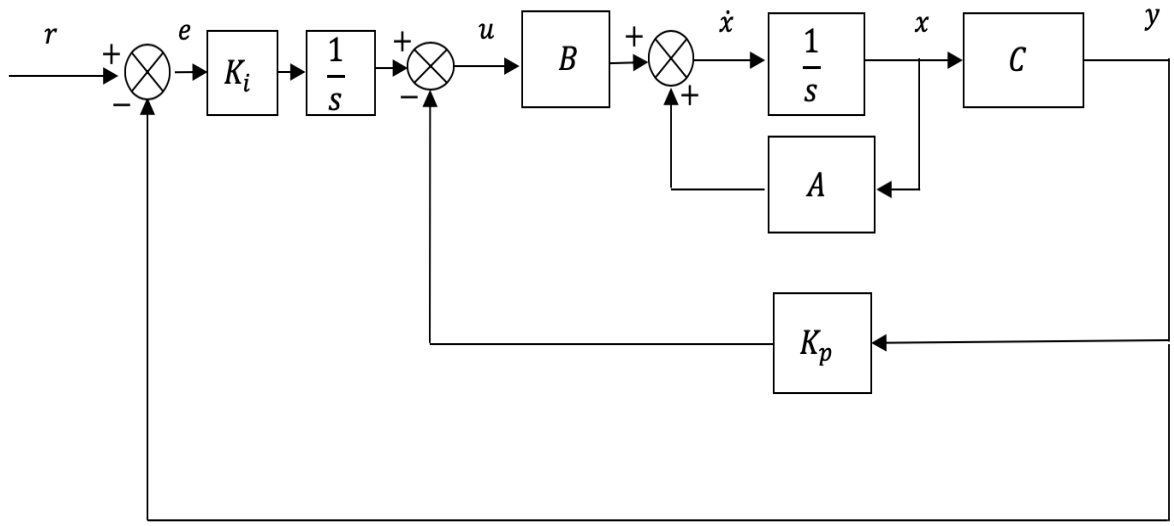

Fig. 5.8. Full state feedback with integral action.

The internal controller adds a state variable x_i, and the corresponding augmented state vector is $[x' x_i]'$. From Fig. 5.8, we have the following

$$\dot{x}_i = r - y = r - Cx, \tag{5.8}$$

Where the control law is

$$u = -K_p x - K_i\, x_i + r, \tag{5.9}$$

where x_i is the integral of the lane position error $e = r - y$.

The control law u is expressed as:

$$u = \begin{bmatrix} k_p & k_i \end{bmatrix} \begin{bmatrix} x \\ x_i \end{bmatrix} + r, \tag{5.10}$$

Now by combing equations (5.6) and (5.9) we have the following:

$$\begin{bmatrix}\dot{x}\\ \dot{x}_i\end{bmatrix}=\begin{bmatrix}A & 0\\ -C & 0\end{bmatrix}\begin{bmatrix}x\\ x_i\end{bmatrix}+\begin{bmatrix}B\\ 0\end{bmatrix}u(t)+\begin{bmatrix}0\\ 1\end{bmatrix}r(t). \tag{5.11}$$

The closed-loop system must be asymptotically stable such that $x(\infty), x_i(\infty)$ and $u(\infty)$ are bounded. In steady-state the system should achieve $\dot{x}_i(t)=0$ and have $y(\infty)=r$ for ramp input commands. For steady-state conditions the following can be given

$$\begin{bmatrix}\dot{x}(\infty)\\ \dot{x}_i(\infty)\end{bmatrix}=\begin{bmatrix}A & 0\\ -C & 0\end{bmatrix}\begin{bmatrix}x(\infty)\\ x_i(\infty)\end{bmatrix}+\begin{bmatrix}B\\ 0\end{bmatrix}u(\infty)+\begin{bmatrix}0\\ 1\end{bmatrix}r(\infty), \tag{5.12}$$

where $r(\infty)=r(t)=r$ for $t>0$. By subtracting (5.12) from (5.11) we have

$$\begin{bmatrix}\dot{x}-\dot{x}(\infty)\\ \dot{x}_i-\dot{x}_i(\infty)\end{bmatrix}=\begin{bmatrix}A & 0\\ -C & 0\end{bmatrix}\begin{bmatrix}x-x(\infty)\\ x_i-x_i(\infty)\end{bmatrix}+\begin{bmatrix}B\\ 0\end{bmatrix}[u(t)-u(\infty)], \tag{5.13}$$

By defining:

$$x-x(\infty)=x_e(t), \tag{5.14}$$

$$x_i-x_i(\infty)=x_{ie}(t), \tag{5.15}$$

$$u(t)-u(\infty)=u_e(t), \tag{5.16}$$

Then the expression above can be re-written as follows

$$\begin{bmatrix}\dot{x}_e(t)\\ \dot{x}_i(t)\end{bmatrix}=\begin{bmatrix}A & 0\\ -C & 0\end{bmatrix}\begin{bmatrix}x_e(t)\\ x_{ie}(t)\end{bmatrix}+\begin{bmatrix}B\\ 0\end{bmatrix}u_e(t), \tag{5.17}$$

where,
$$u_e(t)=-Kx_e(t)+K_i\,x_{ie}(t), \tag{5.18}$$

Defining the added $(n+1)$ error vector $e(t)$

$$e(t)=\begin{bmatrix}x_e(t)\\ x_{ie}(t)\end{bmatrix}=(n+1), \tag{5.19}$$

Then equation (5.17) can be re-written as

$$\dot{e}=\hat{A}e+\hat{B}u_e. \tag{5.20}$$

The state error equation can be retrieved by replacing (5.18) in (5.19) resulting in

$$\dot{e}=(\hat{A}e+\hat{B}\hat{K})e. \tag{5.21}$$

One of the techniques to obtain the state feedback gains along with the additional integral gain constant term, is using a pole placement method if the desired eigen-values for the closed loop system are specified [93, 95]. In situations where the state variables cannot be measured directly, then a state estimator (observer) is needed to obtain these measurements for feedback.

We can assume that a constant disturbance w with unknown magnitude is added to the input of the plant. By modifying equation (5.6) the state equation becomes:

$$\dot{x} = Ax + Bu + Fw,\ y = Cx \tag{5.22}$$

where, $\in\ \mathbb{R}^{nxn}$, $B\ \in\ \mathbb{R}^{nx1}$, $F\ \in\ \mathbb{R}^{nx1}$ and $C\ \in\ \mathbb{R}^{1xn}$ are the given plant matrices.

$x\ \in\ \mathbb{R}^n$ is the state vector, $u\ \in\ \mathbb{R}$ is the control input, $w \in\ \mathbb{R}$ is the disturbance input and

$y \in \mathbb{R}$ is the output.

The closed-loop response can be written as:

$$\begin{bmatrix}\dot{x}\\ \dot{x}_i\end{bmatrix} = \begin{bmatrix}A - BK_p & BK_i\\ -C & 0\end{bmatrix}\begin{bmatrix}x\\ x_i\end{bmatrix} + \begin{bmatrix}0\\ 1\end{bmatrix} \mathrm{r} + \begin{bmatrix}F\\ 0\end{bmatrix} w \tag{5.23}$$

$$y = [C\ 0]\ \begin{bmatrix}x\\ x_i\end{bmatrix} \tag{5.24}$$

Which illustrates the system in Fig. 5.9.

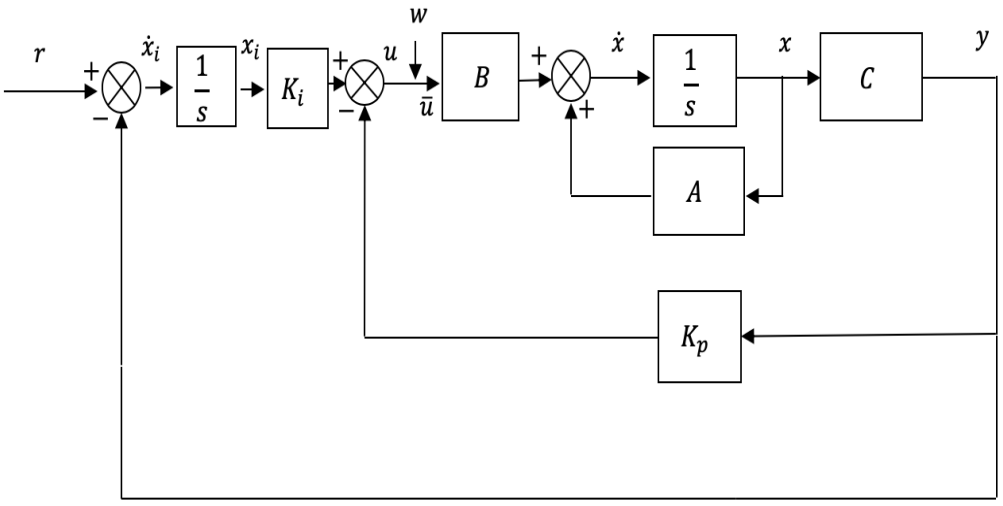

Fig. 5.9. State feedback with disturbance and integral action.

Thus, by increasing the system order to type 3, as shown in Fig. 5.9, the tractor-trailer ramp tracking can be improved for the lane changes. With the tractor-trailer travelling at a constant highway speed of 70 mph, the closed-loop tractor-trailer system transfer function with the added integrator can be expressed as:

$$G_1(s) = \frac{110.4s^5+3174s^4+49960s^3+59800s^2+158700s}{s^7+182.6s^6+3400s^5+24980s^4+99890s^3+158700s^2+270300s+158700} \quad (5.25)$$

With the additional integrator, the control law for the tractor-trailer system becomes as follows:

$$u = \mathrm{r} - k_1 v_1 - k_2 r_1 - k_3 r_2 - k_4\,\psi - k_5 \varphi + k_i\,\mathrm{y} + \frac{k_7}{s} x_7. \quad (5.26)$$

The step response using (5.26) is shown in Fig. 5.10. To compare the ramp tracking for a double lane change, Fig. 5.11 displays a comparison between the desired lane reference input and the state feedback with integral action. As can be seen in Fig. 5.11, the system tracking is improved compared to the previous state-feedback system (5.4) without the added integrator. The MSE for the lane error is computed to MSE= 0.3719, which is significantly reduced from the MSE = 1.72 found for the controller in (5.4).

The tracking can also be further improved by adding higher order integrals in order to further increase the system type. However, there are some tradeoffs to consider when designing for a tractor-trailer system. For example, the system lateral acceleration tends to increase for higher orders of the integral term. This leads to concerns that the tractor-trailer may reach a rollover condition if the system type is increased beyond a certain point. These trade-offs will be explored in Section 5.2.2, where it is found that an optimal system type can be obtained which provides an optimal trade-off between path tracking error verses a safety margin to avoid a rollover condition. Table 6 shows the eigen-values for the open-loop system and the closed-loop system with the truck

travelling at a speed of 70 mph for a type 3 system. Fig. 5.12 shows the lane error response for the type 3 system response.

Table 6 Eigen-values with type 3 system.

Open-loop	**Closed loop**
0	-162.56
0	-10.17
-0.57 + 1.82i	-3.9 + j3.8
-0.57 – 1.82i	-3.9 - j3.8
-16.6 + 8.9i	-0.56 +j1.7
-16.6 – 8.9i	-0.56 -j1.7j
0	-10

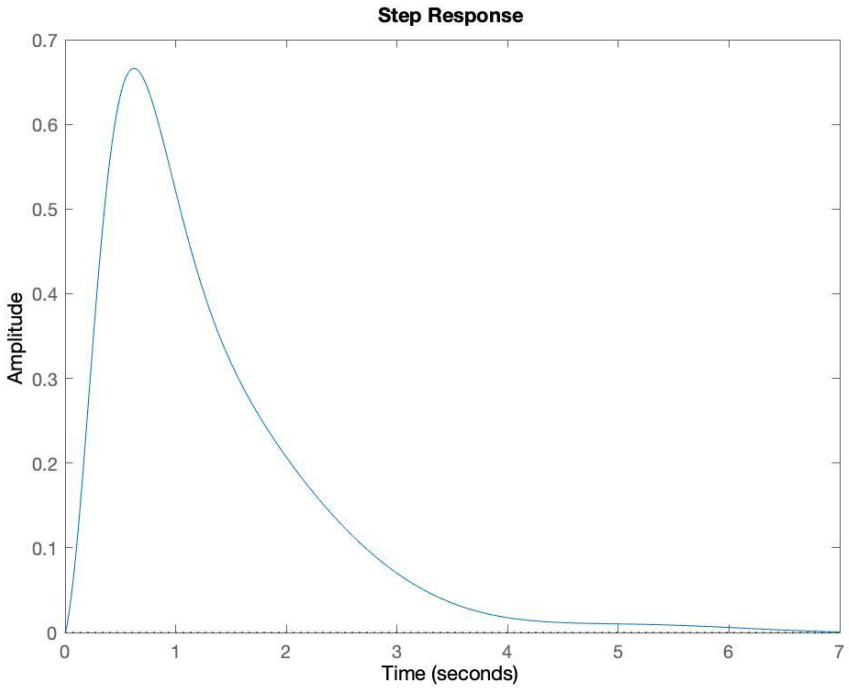

Fig. 5.10. Step response with SFB with integral action for the tractor-trailer system.

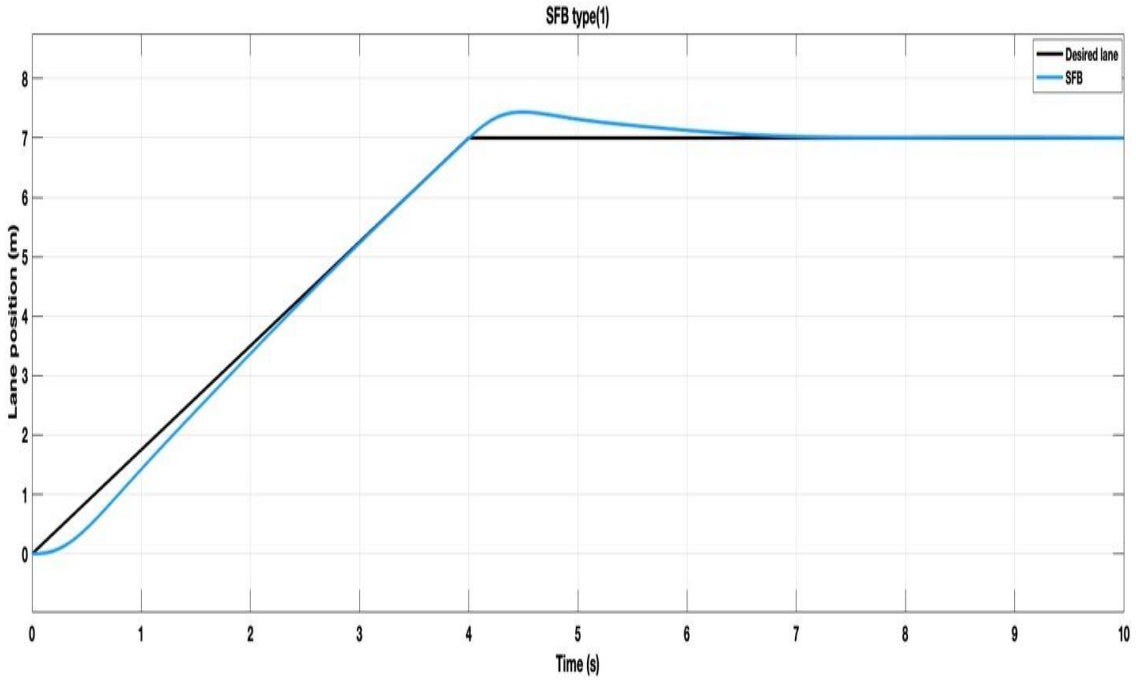

Fig. 5.11. Lane position with SFB with single integral controller.

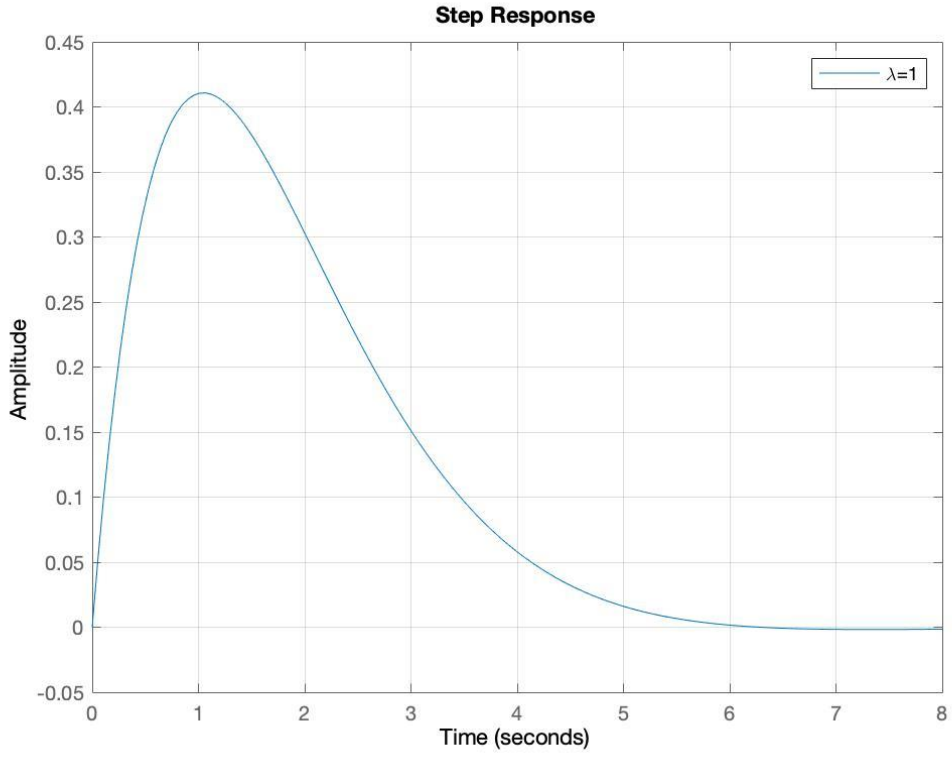

Fig. 5.12. Lane error with integral controller.

5.1.3 State feedback with integer order double integrator action

To examine the tractor-trailer system ramp input tracking for higher order controller integrals, the system is further modified with a second controller integrator. With the tractor-trailer travelling at a constant highway speed of 70 mph, the closed-loop tractor-trailer system transfer function with the added double integrator can be expressed as:

$$G_2(s) = \frac{110.4s^6+3174s^5+49960s^4+59800s^3+158700s^2}{s^8+183.6s^7+3533s^6+27490s^5+11890s^4+268100s^3+429500s^2+386200s+158700} \quad (5.27)$$

thus with this system type the control law for the tractor-trailer now can be represented as:

$$u = \mathrm{r} - k_1 v_1 - k_2 r_1 - k_3 r_2 - k_4\,\psi - k_5 x_5 + k_p x_6 + \frac{k_7}{s} x_7 + \frac{k_8}{s^2} x_8. \quad (5.28)$$

Table 7, presents the eigen-value comparison for the open-loop and closed-loop tractor-trailer system with the second order integral controller.

Table 7 Eigen-value comparison with a double integrator.

Open-loop	**Closed loop**
0	-162.56
0	-10.17
-0.57 + 1.82i	-3.9 + 3.8i
-0.57 – 1.82i	-3.9 - 3.8i
-16.6 + 8.9i	-0.87 + 0.5i
-16.6 – 8.9i	-0.87 - 0.5i
0	-0.54 + 1.7i
0	-0.54 - 1.7i

A step response with the double integrator added is displayed in Fig. 5.13. As can be seen with the higher order integral controller the overshoot and settling time is improved as compared to the system with a single integrator.

The tracking for the tractor-trailer ramp input with the integral controller of order 2 is compared to the desired reference lane change as shown in Fig. 5.14, the tracking has improved for the system as compared to the lower order of the integral term as demonstrated earlier for (5.4) and (5.25) . Hence, the system with the double integrator controller has MSE= 0.19, which continues the trend in reducing the ramp error as the controller integral terms are increased. Fig. 5.15 displays the lane error the ramp input. It is also noted that the rapid rise and decrease in the ramp error is also indicative of increasing instantaneous lateral accelerations, thereby indicating that there may be an optimal value of the controller integral order that yields reduced tracking errors but maintains adequate margin to avoid a rollover condition (i.e., maintain peak lateral acceleration to be less than 0.50 g).

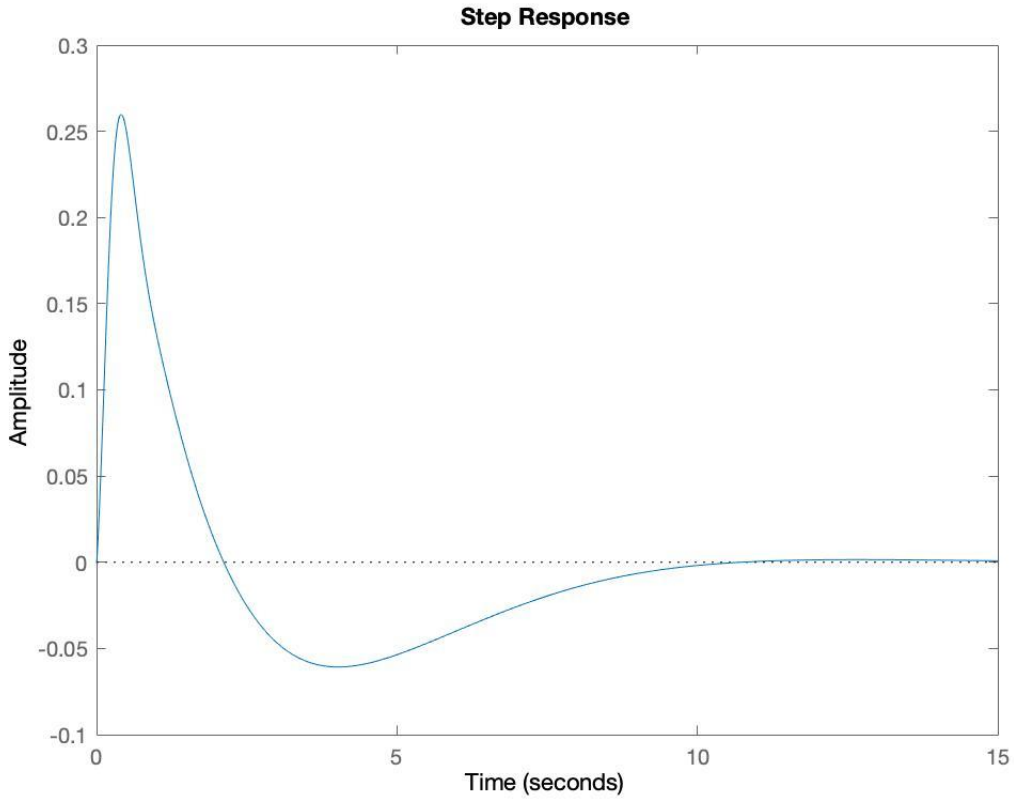

Fig. 5.13. Ramp response with state feedback with double integral action.

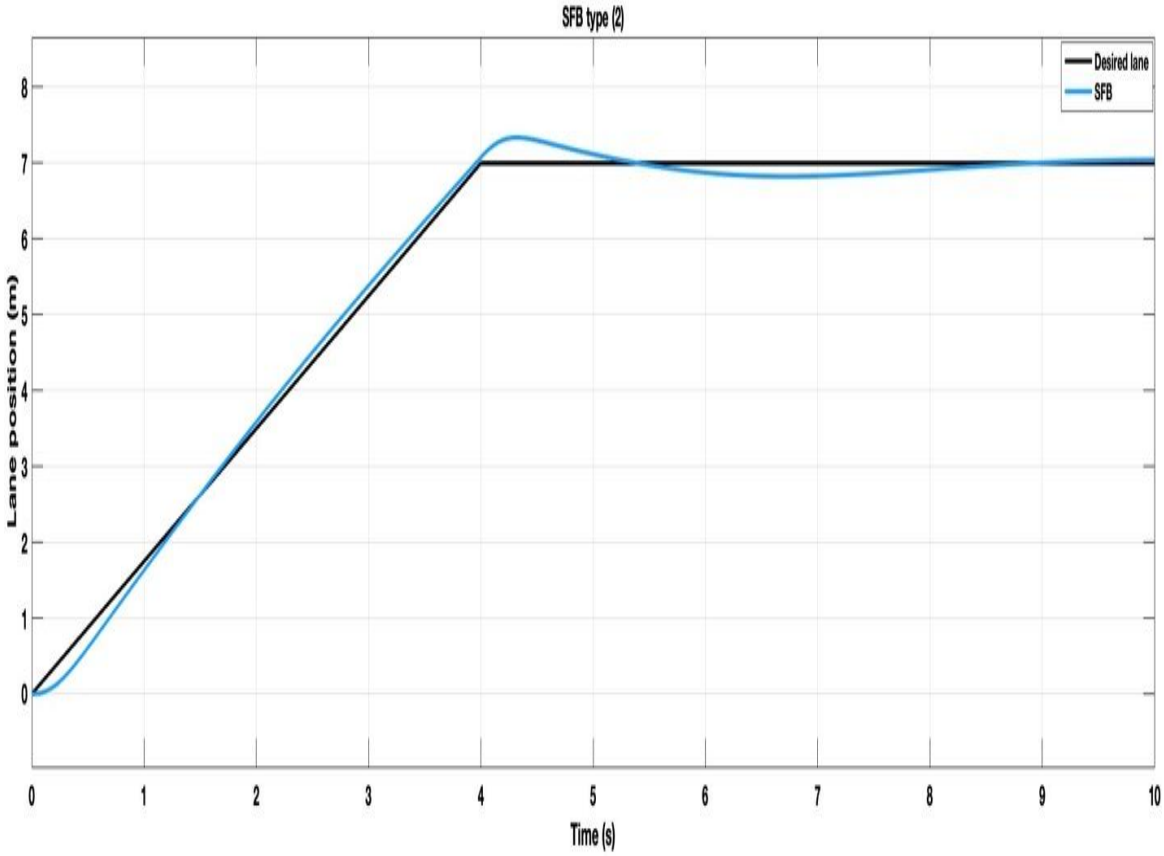

Fig. 5.14. Lane position with SFB with a double integrator.

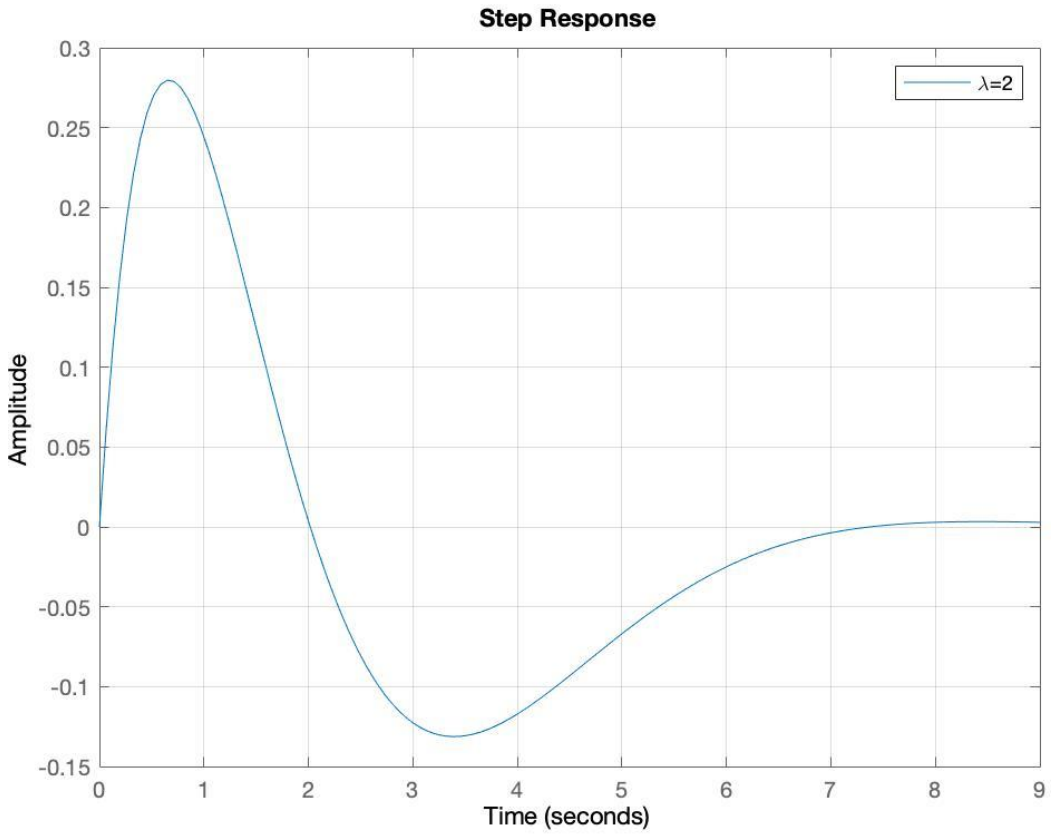

Fig. 5.15. Lane error response with a double integral controller.

To summarize the effects of the order of the controller integer terms on the tracking error, Fig. 5.16 shows a comparison for a step response for controller integrator orders from 0-5. Selecting the order of the controller integration should account for the associated lateral accelerations that are indicative of a rollover as well as excessive articulation angles that are a precursor to a jackknife event. This research considers the question that an optimal controller integration order may lie between discrete integer values. This would then necessitate the use of a fractional order integrator. Methods to determine the optimal and possible fractional order integer controller is investigated in Section 5.2.

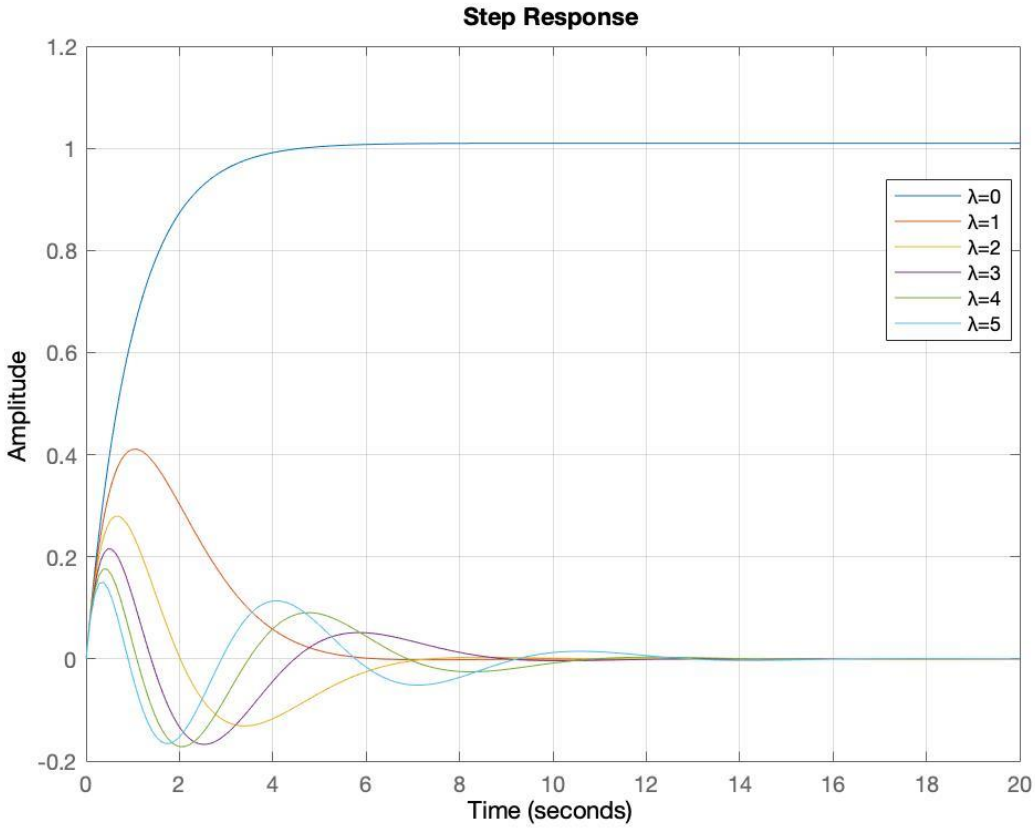

Fig. 5.16. Lane error comparison between different integrator orders from 1 to 5.

5.1.4 Linear quadratic regulators

The feedback controller gain of a given system can be obtained by optimizing a quadratic cost function as an alternative approach of selecting the closed loop eigenvalue locations of the system in order to achieve closed-loop performance requirements. In mechanical and electrical systems, quadratic cost functions account for the energy associated with the state variables. Thus minimizing a quadratic cost function defined in terms of errors in state variable such as velocity, forces, voltages and currents translates into an energy and power constraint on the system. Consequently, linear quadratic regulator (LQR) design is often used in electrical and mechanical

systems by providing a method of designing closed-loop control system that are specified based on physical constraints [94,95]. However, the solution to LQR design problems can be numerically challenging. In this research, well-established numerical methods employed by the Mathworks Corp, In Matlab is used to solve the LQR problems. Fig. 5.17 presents a block diagram of an optimal regulator system. Given a multi-input linear system

$$\dot{x} = Ax + Bu, \text{ where, } x \in \mathbb{R}^{nxnn}, u \in \mathbb{R}^{m} \tag{5.29}$$

The matrix K of the optimal controller

$$u(t) = -Kx(t). \tag{5.30}$$

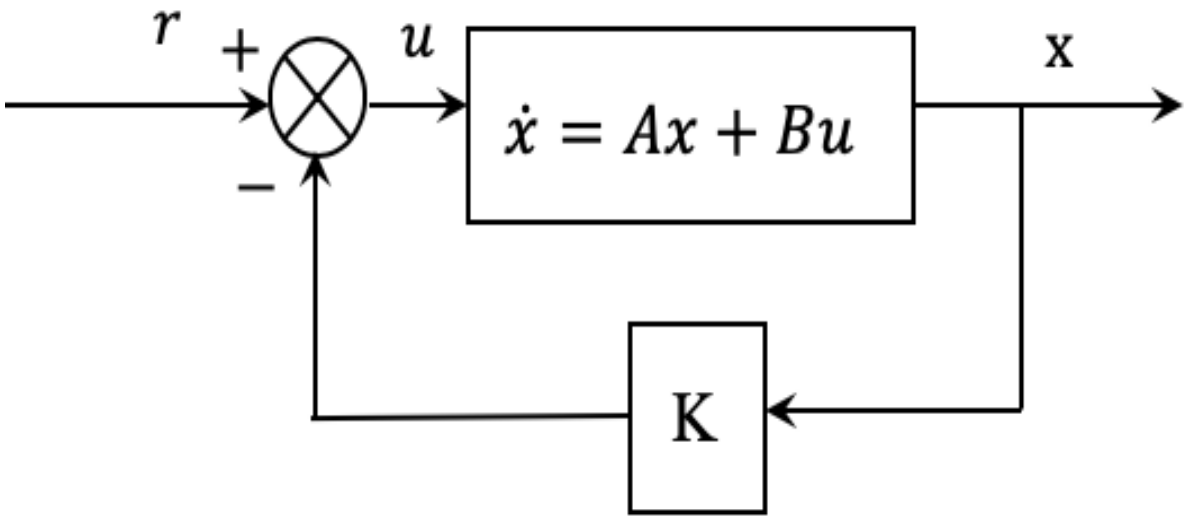

Fig. 5.17. Optimal regulator system.

The problem of minimizing the quadric performance index

$$\mathrm{J} = \int_{t_s}^{\infty} (x^T \mathrm{Q_x}\, \mathrm{x} + u^T \mathrm{Q_r}\, \mathrm{u})\, \mathrm{dt}. \tag{5.31}$$

Where $\mathrm{Q_r} > 0$ and $\mathrm{Q_x} \geq 0$ are both symmetric and positive (semi-definite) with appropriate dimension matrices. Hence, choosing the weights Q_x and $\mathrm{Q_r}$ of the LQR problem is critical for the design process, thus by ensuring $\mathrm{Q_r} > 0$ and $\mathrm{Q_x} \geq 0$ this would guarantee that a solution exists. If the undetermined element of K is known by minimizing the performance index, then $u(t) = -Kx(t)$ is an optimal approach for any initial state $x(0)$. In order to obtain a solution to the LQR problem, the control law is given in the following form

$$u = Q_r^{-1} B^T P x. \tag{5.32}$$

Where $\mathrm{P} \in \mathbb{R}^{nxn}$ is a positive definite, symmetric matrix which satisfies the following equation:

$$PA + A^T P - PBQ_r^{-1}B^T P + Q_x = 0. \tag{5.33}$$

Equation (5.33) is called the Algebraic Riccati Equation (ARE). To obtain a solution for ARE, the design procedure can be listed as [94]

a) Compute (5.33) for P(positive definite). Then the system should have all the Eigen-values in the LHP with (A-BK) having negative real parts so that the system is stable.

b) Set $K = T^{-1}(T^{*})^{-1}BP = \mathrm{Q_r}^{-1}BP$. The result is a value for K that is the optimal solution to (5.31).

The state-feedback control law for a closed loop system becomes

$$\dot{x} = (\mathrm{A} - \mathrm{BK})\mathrm{x}. \tag{5.34}$$

5.2 Proposed Controller Scheme

The proposed controller method for this research; is a fractional order PI^{λ} with full state feedback with integral action control. This scheme would allow eliminating the steady state errors associated with plant, and to meet the system specification more accurately with the fractional integral term as opposed to the classical integer integral. Thus, determining the suitable integrator

and proportional state feedback gains can be quite complicated, especially for the tractor-trailer system. Hence, the feedback law is added in order to compensate for the deviations and disturbance occurring in the system.

A block diagram of the proposed full state feedback with a FOPI controller, is provided in Fig. 5.18. This typology would be applied the tractor-trailer non-linear model, where the fractional term (λ) is added to the state feedback controller.

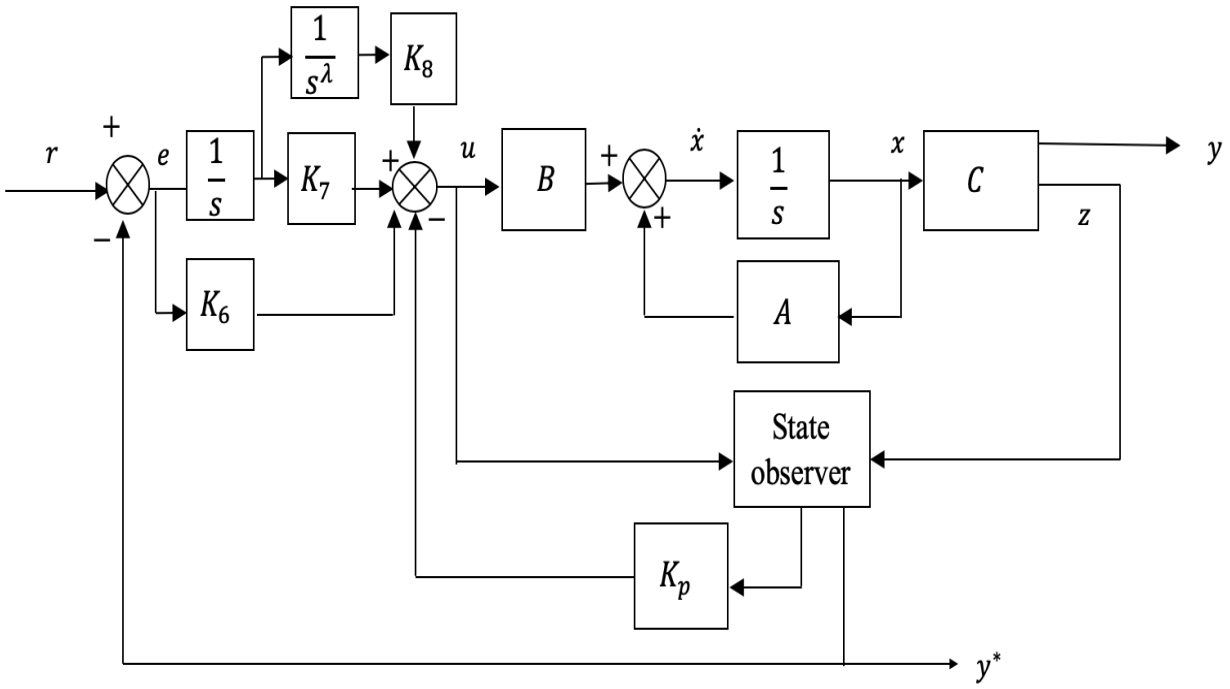

Fig. 5.18. Closed loop scheme with a fractional order PI and state feedback controllers.

From the state feedback diagram presented in Fig. 5.18, the states are assumed to be available to the control algorithm and would be measured from currently available commercial sensors on trucks, thus the lateral position (y^*) would be measured from an image sensor and GPS, while $\dot{v}_1, r_1$ and r_2 would be measured from an accelerometer and a gyroscope sensors respectively (z). The articulation angle $\dot{\psi}$ is the difference in the yaw rates of the tractor and trailer ($r_1 - r_2$).

As an alternative of adding a classical IO integral $\left(1/s\right)$, a FO integrator$\left(1/s^{\lambda}\right)$ is considered, which would eliminate the system steady-state error by providing lane position tracking control..

In Fig. 5.16 a comparison between different integer orders from 0 to 5, is shown. It can be seen that choosing a λ order less than 1, would not provide enough tracking for a ramp input for the tractor-trailer system, while selecting a λ value higher than 1 and lower than 2 (in between with a fractional order), would be a preferred choice since, λ with order equal to 2 would provide slight improved tracking, but at the same time degrade the truck performance in terms of the lateral acceleration and articulation angle.

With λ=1, there would be good tracking as compared to λ less than 1, and also when λ=1 the truck performance does not degrade in terms of the lateral acceleration and the articulation angle for an evasive maneuver situation.

By choosing a fractional order value for the integrator between 1 and 2, this would provide an improved solution for tracking a ramp input for the tractor-trailer system and at the same time not degrade the system performance for the articulation angle and the lateral acceleration for the truck in case of an emergency lane departure during platoon operation on a highway.

The controller is designed first for the tractor-trailer linear system and then the linear controller is evaluated on the non-linear dynamics presented in equations (3.10)-(3.15). The controller was designed with a constant forward speed of 70 mph, in accordance with the average maximum highway speeds in the U.S.

Tables 8 and 9 present an eigen-value analysis for the open-loop and closed-loop tractor trailer system with an LQR controller for various highway speeds of 60, 70 and 80 mph. As the tractor-trailer system eigen-values are shifted more toward the LHP during low speeds and shifted more

toward the right for higher speeds, this indicates the tractor-trailer stability margins are reduced as the vehicle speed is increased.

Table 8 System eigen-values without control for different speeds.

60 mph	**70 mph**	**80 mph**
0	0	0
0	0	0
-0.66 + j1.8	-0.57 + j1.8	-0.5 + j1.8
-0.66 – j1.8	-0.57 – j1.8	-0.5 – j1.8
-19.38 + j6.64	-16.6 + j8.9	-14.5 + j10.07
-19.38 – j6.64	-16.6 – j8.9	-14.5 – j10.07
0	0	0
0	0	0

Table 9 System eigen-values with LQR control for different speeds.

60 mph	**70 mph**	**80 mph**
-163.32	-162.56	-161.8
-10.93	-10.17	-12.6
-3.92 + j3.4	-3.9 + j3.8	-3.3 + j3.5
-23.9 - j3.4	-3.9 - j3.8	-3.3 - j3.5
-0.62 + j1.7	-0.87 + j0.5	-0.87 + j0.5
-062 – j1.7	-0.87 - j0.5	-0.87 - j0.5
-0.87 + j0.5	-0.54 + j1.7	-0.5 + j1.7
-0.87 - j5	-0.54 - j1.7	-0.5 - j1.7

5.2.1 State feedback with fractional higher order integral action

The benefits of including the fractional integrator in the feedback system is primarily for providing improved ramp input tacking performance by eliminating the steady state error for the tractor-trailer system for an evasive manoeuvring situation. With a fractional order integral an optimal value can be obtained, which can provide the optimal tracking performance and at the same time minimize the affect occurring on other aspects of the tractor-trailer stability such as, the articulation angle deflection and lateral acceleration increases.

The block diagram for the proposed controller method displayed in Fig. 5.18 can be represented given an LTI system as:

$$\dot{x} = Ax + Bu,\ y = Cx \tag{5.35}$$

where the control law can be formed as

$$u = -K_p x + K_i x_i \tag{5.36}$$

where

$$\dot{x}_i = r - Cx_i \tag{5.37}$$

$\dot{x}_i$ is the tacking error integral and r is the reference input signal, which is trackable by y. The control law can be expressed with introducing the state vector $X = \begin{bmatrix} x \\ x_i \end{bmatrix}$

$$u = \begin{bmatrix} -K_p & K_i \end{bmatrix} X \tag{5.37}$$

For active stability control of the tractor-trailer representation, the system matrix can be expressed as

$$\dot{x} = \left(\mathrm{A} - \mathrm{B}\widehat{K}\right) \mathrm{x} \tag{5.38}$$

The state-space matrices A and B representing the tractor-trailer are given in Chapter 3. With the additional added state matrix (below) are completely controllable

$$\begin{bmatrix} A & B \\ -C & 0 \end{bmatrix} \tag{5.39}$$

The state error equation is

$$\dot{e} = \hat{A}e + \hat{B}u_e \tag{5.40}$$

With the tractor-trailer travelling at a constant highway speed of 70 mph, the tractor trailer open-loop system with the system parameters given in Table 10 and the added yaw angle and lateral position described in Chapter 3 (3.76), thus the is system is given as

$$A = \begin{bmatrix} -6.95 & -29.98 & -3.12 & 10.04 & 0 & 0 \\ 5.42 & -25.77 & 1.54 & -4.96 & 0 & 0 \\ = 1.29 & 2.73 & -1.61 & 5.16 & 0 & 0 \\ 0 & 1 & -1 & 0 & 0 & 0 \\ 0 & 1 & 0 & 0 & 0 & 0 \\ 1 & 0 & 0 & 0 & 31.3 & 0 \end{bmatrix}, \tag{5.41}$$

$$B = \begin{bmatrix} 110.39 \\ 118.12 \\ 1.042 \\ 0 \\ 0 \\ 0 \end{bmatrix}, \tag{5.42}$$

$$C = [0 \quad 0 \quad 0 \quad 0 \quad 0 \quad 1]. \tag{5.43}$$

5.2.2 Optimal fractional order integrator selection

The previous section has shown that adding an integrator term to the state feedback control algorithm would provide increased lane position tracking for the tractor-trailer system for a ramp input (lane change). Selecting a fractional integrator order value in between type 1 and type 2 controller can provide improved lane position tracking and at the same time degraded lateral acceleration and articulation angle performance for the tractor-trailer system.

Having a fractional order integral term, in between the integral order type1 and type 2 would provide optimal performance for the tractor-trailer stability margin for an evasive maneuver. Fig.

19, displays a comparison between different integrator orders for the lane position error corresponding to a ramp input for the tractor-trailer system.

Finding an optimal fractional integrator value is obtained in this research, by minimizing the performance index in terms of the lane position with the tractor lateral acceleration and the lane position with the articulation stability. Fig. 5.20 shows the performance index relationship between the lane position error and the tractor lateral acceleration. This relationship indicates that the optimal value for the fractional order integrator is near λ=1.4 can provide the best lane tracking for a ramp input, while also indicating that increasing the order of the fractional integrator tends to increase the lateral acceleration of the tractor.

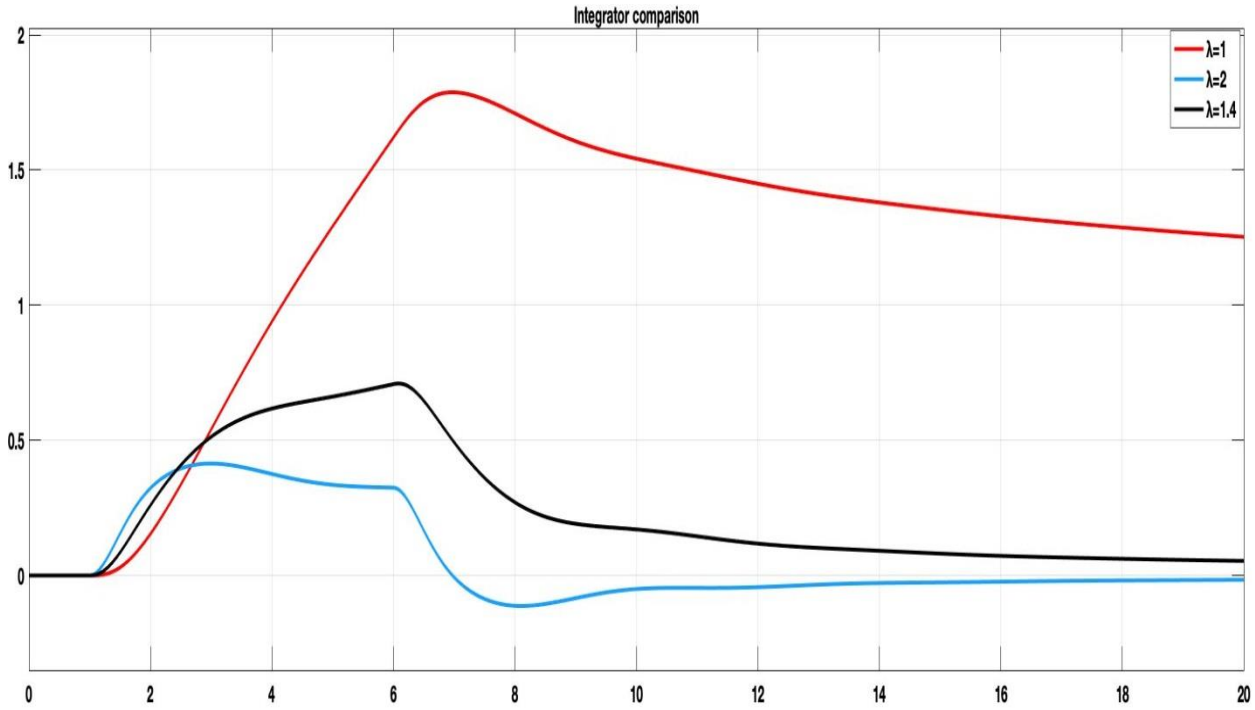

Fig. 5.19. Lane position error comparison for different integrator order.

Fig. 5.21, show the performance index relationship between the lane position error and the articulation angle degree, as indicated in the relationship graph the optimal value for the fractional order value that provides the good lane tracking and articulation stability is near λ=1.4, and similarly to the relationship in Fig. 5.21. It is observed that increasing the fractional order value would decrease the stability margin of the articulation angle and improve the lane tracking.

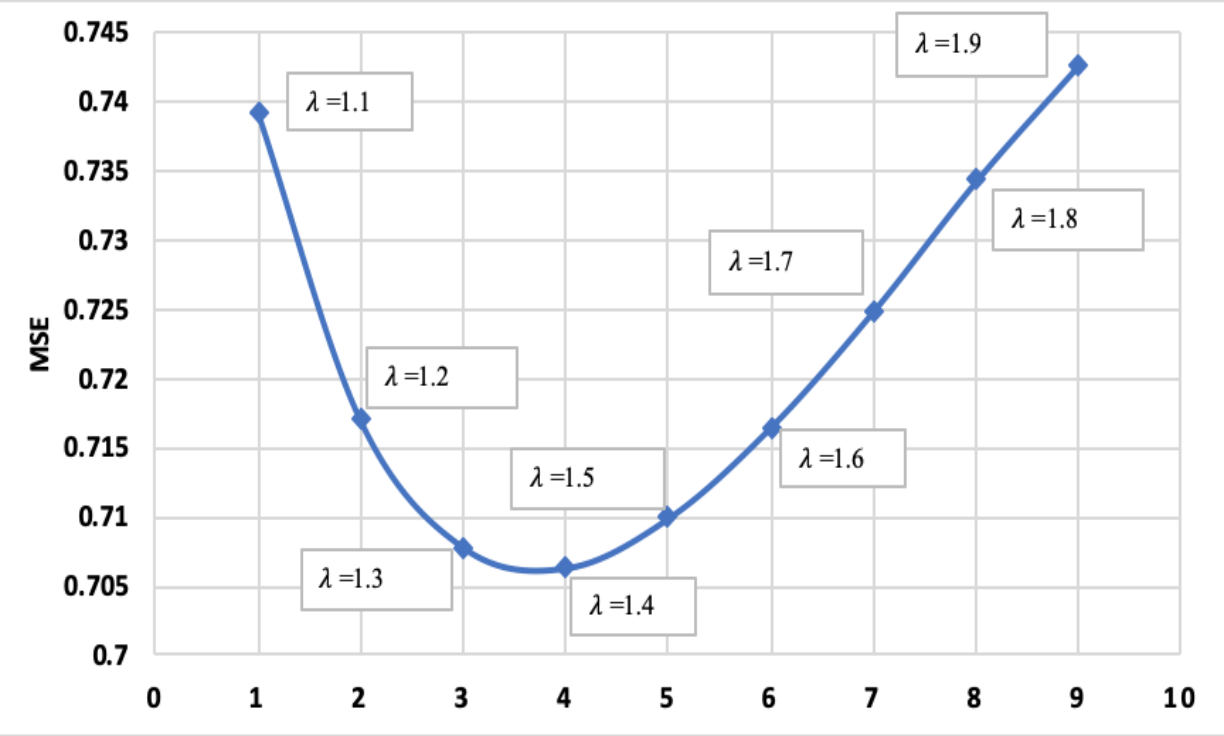

Fig. 5.20. Performance index relationship for lane position error with tractor lateral acceleration.

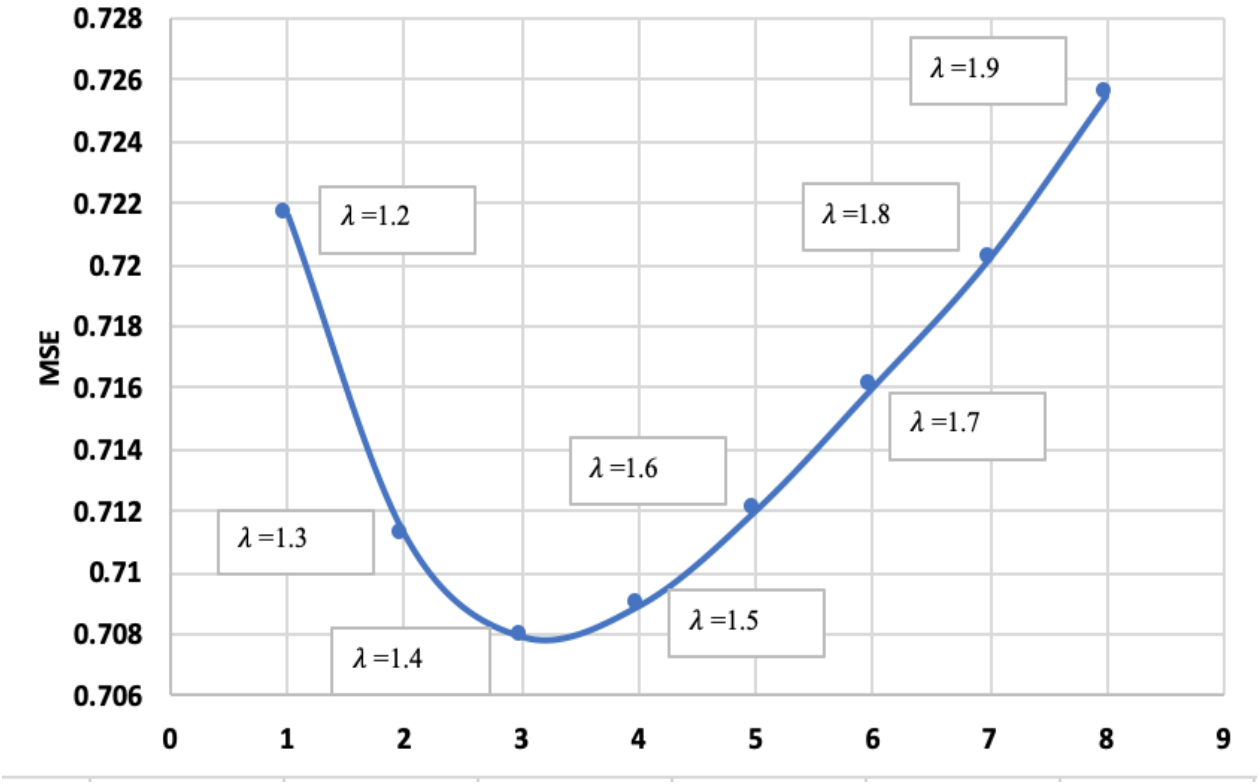

Fig. 5.21. Performance index relationship for lane position error with the articulation angle.

For the tractor-trailer system, providing a reduced lane tracking errors for a ramp input (i.e., lane change) and also increased stability margin in terms of the articulation angle and the lateral acceleration of tractor is critical for safety design. This is based on the situation for a highway evasive maneuver where the truck should complete rapid lane change departure and be in the center of the adjacent lane after the maneuver is completed. Thus, selecting a λ=1.4 value, for the particular truck parameters considered in the research provides a solution for this requirement. For a different set of tractor-trailer parameters then the particular ramp following and acceleration responses will be different. However, all articulated vehicles have similar structural characteristics such that one would expect that the optimal value λ would still fall into a similar range.

5.2.3 FO controller approximation

The fractional order controller term $\left(1/_{s^{0.4}}\right)$, is first approximated using the Oustaloup method presented earlier in Section 4.4. This approximation is done in order to implement the controller for a real-time embedded system for the tractor-trailer system. Choosing the order of the approximation that provides the best accuracy for the fractional controller is based on the frequency response analysis for different orders of the Oustaloup approximation shown in Fig. 4.12. The order selected for the approximation is N=5, with the fractional order integral α = -0.4, the lower approximation frequency w_b= 10^{-3} rad/sec, and the lower approximation frequency w_h=10^2 rad/sec, $w_u = \sqrt{\frac{w_h}{w_b}}$ = 316.23 and $K = w_h^{\alpha}$= 0.16. The gain, zero and pole determined then to be

$$w_k = w_b * w_u^{\frac{(\alpha-1+2*k)}{N}}, w_k' = w_b * w_u^{\frac{(-\alpha-1+2*k)}{N}}. \quad (5.44)$$

The continuous Oustaloup filter TF can be found from

$$\hat{G}(s) = w_h^{\alpha} \frac{(s-\omega'_{-q})(s-\omega'_{-q+1})\ldots(s-\omega'_{q})}{(s-\omega_{-q})(s-\omega_{-q+1})\ldots(s-\omega_{q})}. \quad (5.45)$$

where $k = \{-q, -q+1, \ldots, 0, \ldots, q-1, 1\}$.

The filter would approximate the FO order $s^{\alpha} \approx \hat{G}(s)$, and hence the TF approximation of the FO controller $\left(1/_{s^{0.4}}\right)$, is computed as:

$$\hat{G}(s) = \frac{0.16s^5+8.83s^4+44.68s^3+22.4s^2+1.1s+0.005}{s^5+22.17s^4+44.68s^3+8.9s^2+0.18s+0.0003}, \quad (5.46)$$

where,

$$\hat{G}(s) = KG_1(s)G_2(s)G_3(s)G_4(s)G_5(s). \quad (5.47)$$

$$G_1(s) = \frac{s+0.5}{s+0.199}, \quad (5.48)$$

$$G_2(s) = \frac{s+5.01}{s+1.99}, \quad (5.49)$$

$$G_3(s) = \frac{s+50.12}{s+19.95}, \tag{5.50}$$

$$G_4(s) = \frac{s+501.2}{s+199.5}, \tag{5.51}$$

$$G_5(s) = \frac{s+5012}{s+1995}. \tag{5.52}$$

The Bode plot of the approximated FO controller is displayed in Fig. 5.22.

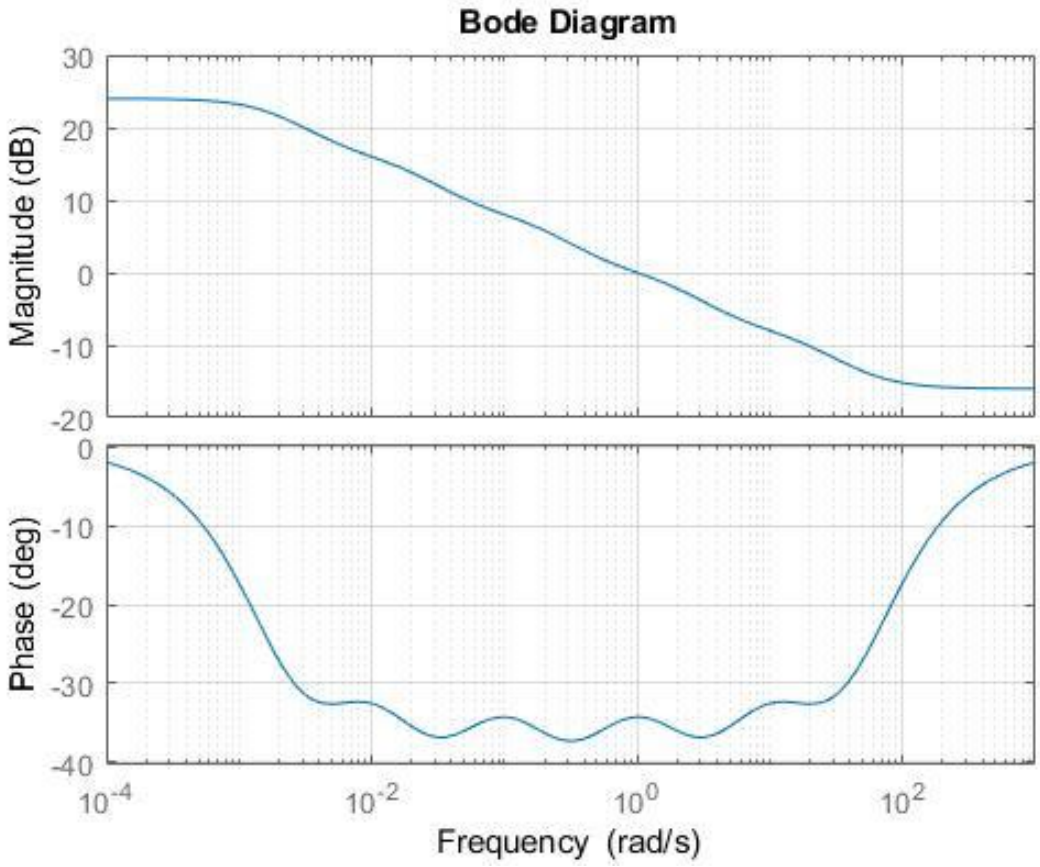

Fig. 5.22. Bode plot of the approximated FO controller $\hat{G}(s)$.

The state space realization of the factional order controller can also be approximated to an integer order space representation. With order of approximation order N = 5, by applying the following algorithm [73,74]

$$\left.\begin{array}{c} For\ n = 1{:}5 \\ \mathrm{a(n)} = \mathrm{z(n)} - \mathrm{p(n)} \\ \mathrm{b(n)} = \mathrm{z(n)} - \mathrm{p(n)} \\ c(n) = 1 \\ d(n) = 1 \end{array}\right\} \tag{5.53}$$

where z and p are the zeros and poles of the system. The state space realization can be obtained from the following:

$$\mathrm{A} = \begin{bmatrix} \mathrm{a(1)} & 0 & 0 & 0 & 0 \\ \mathrm{b(2)} & \mathrm{a(2)} & 0 & 0 & 0 \\ \mathrm{b(3)} & \mathrm{b(3)} & \mathrm{a(3)} & 0 & 0 \\ \mathrm{b(4)} & \mathrm{b(4)} & \mathrm{b(4)} & \mathrm{a(4)} & 0 \\ b(5) & b(5) & b(5) & b(5) & a(5) \end{bmatrix}, \tag{5.54}$$

$$B = K \begin{bmatrix} b(1) \\ b(2) \\ b(3) \\ b(4) \\ b(5) \end{bmatrix}, \tag{5.55}$$

$$C = [1 \quad 1 \quad 1 \quad 1 \quad 1],\ D = [K]. \tag{5.56}$$

with $\alpha = -0.4$, and $K = w_h^{\alpha} = 0.16$, the state space approximation can be obtained as

$$\mathrm{A} = \begin{bmatrix} -0.002 & 0 & 0 & 0 & 0 \\ 0.03 & -0.02 & 0 & 0 & 0 \\ 0.31 & 0.31 & -0.2 & 0 & 0 \\ 3.1 & 3.02 & 3.02 & -2 & 0 \\ 30.17 & 30.17 & 30.17 & 30.17 & -20 \end{bmatrix}, \tag{5.57}$$

$$B = \begin{bmatrix} 0.00048 \\ 0.0048 \\ 0.048 \\ 0.48 \\ 4.78 \end{bmatrix}, \tag{5.58}$$

$$C = [1 \quad 1 \quad 1 \quad 1 \quad 1],\ D = [0.16]. \tag{5.59}$$

The Bode plot for the approximated FO controller in in state space is shown in Fig. 5.23. where selecting N=5 provides a good approximation of the fractional order controller, while maintaining a low order of the controller approximation as opposed to selecting a higher order

approximation, which would make the system difficult to implement with an automotive digital device such as an FPGA or DSP. It was demonstrated previously that a low order such as, N=1, would provide more ripple as illustrated in the bode plot in Fig. 4. 12.

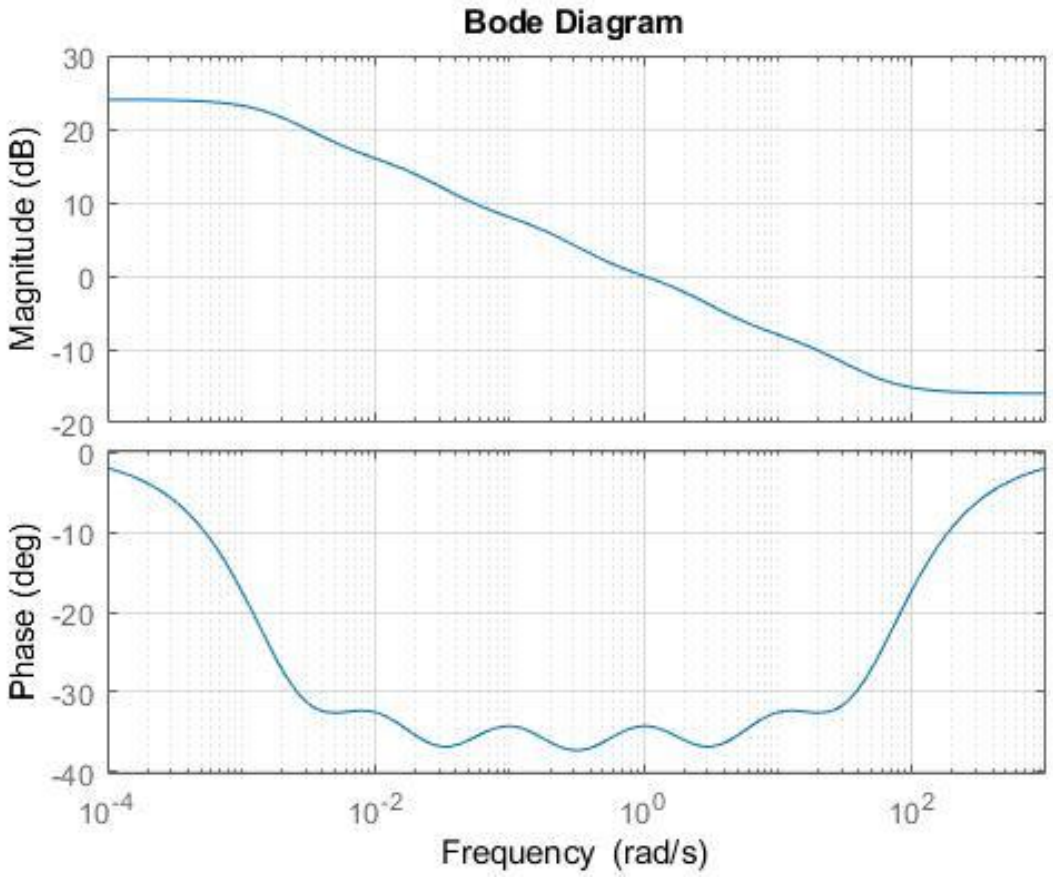

Fig. 5.23. Bode plot of the approximated FO controller in state space.

With FO controller in the specified frequency range, the ripple amount in the phase response could as well be obtained [73]. Thus, the approximated FO controller could also be discretized in order to be applied on embedded devices. The state space approximation can discretized since$\dot{x}(t) = \lim_{T \to 0} \frac{x(t+T)-x(t)}{T}$.

Hence the continuous time can be approximated as [96]:

$$x(t+T) = x(t) + Ax(t)T + Bu(t)T, \tag{5.60}$$

then,

$$x[K+1] = A_d x[k] + B_d u[k], \tag{5.61}$$

$$\text{y[k]}=C_d x[k] + D_d u[k]. \tag{5.62}$$

with

$$A_d = e^{AT},\ B_d = A^{-1}(A_d - I)B,\ C_d = C,\ D_d = D. \tag{5.63}$$

The continuous system can be discretized with T=0.01 as follows:

$$A_d = \begin{bmatrix} 1 & 0 & 0 & 0 & 0 \\ 0.0003 & 0.1 & 0 & 0 & 0 \\ 0.003 & 0.003 & 0.1 & 0 & 0 \\ 0.03 & 0.03 & 0.03 & 0.98 & 0 \\ 0.28 & 0.28 & 0.28 & 0.27 & 0.82 \end{bmatrix}, \tag{5.64}$$

$$B_d = \begin{bmatrix} 0 \\ 0 \\ 0.0005 \\ 0.0047 \\ 0.04 \end{bmatrix}, \tag{5.65}$$

$$C_d = [1 \quad 1 \quad 1 \quad 1 \quad 1],\ D_d = [0.16]. \tag{5.66}$$

The approximated FO controller $s^\alpha \approx \hat{G}(s)$, in equation (5.46), discrete-time equivalent can also be obtained for embedded devices implementation. With the sampling interval T_s provided, then the high frequency w_h can be set as $w_h = \frac{2}{T_s}$. By considering the zero-pole equivalent match technique for discretizing the continuous time TF , as the follows is used for mapping the poles a and zeros [73, 103]:

$$z = e^{sT_s}, \tag{5.67}$$

where s referes to the poles and zeros, thus, for each k in equation (5.44)

$$\theta'_k = e^{-T_s\omega'_k},\ \theta_k = e^{-T_s\omega_k}, \tag{5.68}$$

The approximated FO controller in equation (5.46), can be discretized and thus expressed as:

$$H(z) = k_z \frac{(z-\theta'_{-q})(z-\theta'_{-q+1})\ldots(z-\theta'_{q})}{(z-\theta_{-q})(z-\theta_{-q+1})(z-\theta_{q})}, \tag{5.69}$$

where

$$k_z = \frac{w_h^{\alpha}}{|H(e^{j\omega_u T_s})|}, \tag{5.70}$$

The discrete-time realization of the fractional order controller with a sampling time equal to 0.01 seconds, can be computed as:

$$\mathrm{H(z)} = \frac{0.19z^5-0.84z^4+1.53z^3-1.34z^2+0.62z+0.11}{z^5-4.8z^4+9.2z^3-8.8z^2+4.2z-0.8}. \tag{5.71}$$

For digital realization the controller technique could be based on the canonical form of an IIR filter as presented earlier in Section 4.5.3.

5.2.4 Controller design for tractor-trailer dynamics

The fractional order linear controller was designed for the tractor-trailer small angle approximation, and then implemented on the truck nonlinear dynamics. The fractional order integrator order was selected based on the optimal value for tracking a ramp input for the tractor-trailer for a lane departure. Thus a performance index was evaluated to acquire the optimal FO value, where the lane position error with the truck lateral acceleration and the articulation angle were considered for the selection optimal design presented in Section 5.2.2.

The value of the factional order equal to 1.4 was selected, since it was found that this value can provide the optimal tracking performance for a lane change and at the same time the stability margin for the truck is increased in terms of the lateral acceleration and the articulation angle. Then fractional order controller is approximated as presented in the previous section.

The tractor-trailer open-loop system with a double integrator is given as follows:

$$\hat{A} = \begin{bmatrix} A & 0 \\ -C & 0 \end{bmatrix} = \begin{bmatrix} -6.95 & -29.98 & -3.12 & 10.04 & 0 & 0 & 0 & 0 \\ 5.42 & -25.77 & 1.54 & -4.96 & 0 & 0 & 0 & 0 \\ 1.29 & 2.73 & -1.61 & 5.16 & 0 & 0 & 0 & 0 \\ 0 & 1 & -1 & 0 & 0 & 0 & 0 & 0 \\ 0 & 1 & 0 & 0 & 0 & 0 & 0 & 0 \\ 1 & 0 & 0 & 0 & 31.3 & 0 & 0 & 0 \\ 0 & 0 & 0 & 0 & 0 & 1 & 0 & 0 \\ 0 & 0 & 0 & 0 & 0 & 0 & 1 & 0 \end{bmatrix}, \quad (5.71)$$

`

$$\hat{B} = \begin{bmatrix} B \\ 0 \end{bmatrix} = \begin{bmatrix} 110.39 \\ 118.12 \\ 1.042 \\ 0 \\ 0 \\ 0 \\ 0 \\ 0 \end{bmatrix}, \quad (5.72)$$

The control signal

$$u = r - K_p x + k_6 e + \frac{K7}{s^1} e + \frac{K8}{s^\lambda} e. \quad (5.73)$$

where

$$K_p = [k_1\ k_2\ k_3\ k_4\ k_5\ ]. \quad (5.74)$$

The system should be examined for controllability as the rank of matrix M is full rank and is equal to 8.

$$M = \begin{bmatrix} A & B \\ -C & 0 \end{bmatrix}. \quad (5.75)$$

The gain K_p can be obtained by a linear quadric minimization method LQR, which minimizes the objective performance index in (5.31) is the solution to the algebraic Riccati equation

$$P\hat{A} + \hat{A}^T P - PBQ_r^{-1}\hat{B}^T P + Q_x = 0. \quad (5.76)$$

This can be solved for P, and thus the control feedback matrix $\widehat{K}$ is obtained by

$$\widehat{K} = \mathrm{Q_r}^{-1}\, \hat{B}' P. \quad (5.77)$$

The weighting matrices Q_x and Q_r in (5.76) are selected in order to ensure the system behaves with high stability margin

$$Q_x = \begin{bmatrix} 1 & 0 & 0 & 0 & 0 & 0 & 0 & 0 \\ 0 & 1 & 0 & 0 & 0 & 0 & 0 & 0 \\ 0 & 0 & 1 & 0 & 0 & 0 & 0 & 0 \\ 0 & 0 & 0 & 1 & 0 & 0 & 0 & 0 \\ 0 & 0 & 0 & 0 & 1 & 0 & 0 & 0 \\ 0 & 0 & 0 & 0 & 0 & 1 & 0 & 0 \\ 0 & 0 & 0 & 0 & 0 & 0 & 1 & 0 \\ 0 & 0 & 0 & 0 & 0 & 0 & 0 & 1 \end{bmatrix}, Q_r = 1. \quad (5.78)$$

The weights are designed by considering the overall performance of the tractor-trailer system response through its operation for a high speed evasive manoeuvring. Eigen-values assessment is done for three different speed levels 60, 70 and 80 mph and the comparison is provided in Table 8-9 before applying the LQR controller and after the controller is implemented.

To implement the LQR controller for the tractor-trailer system, the system states should be available for the control algorithm with measurement devices. Thus, these devices (sensor) are commercially available sensor on board for tractor-trailer in platooning operation, which include an image (optical) sensor, GPS, gyroscope and accelerometer sensors. These sensors can provide the measurements for the lateral position, yaw rates for the tractor and trailer.

In circumstances these sensor can't provide these measurements, other methods can be applied to obtain them such as, having an observer/Kalman filter. In the research, it is assumed that all the states area available to the control algorithm with suitable accuracy without the need of a state estimator (observer) to be included in the control design.

After approximating the FO integrator, the LQR method is used to determine the feedback gains for the system, thus, using a convex incremental linear interpolation strategy with respect to the fractional order integrator value λ. The convex method that was used can be expressed as:

$$C_{(n)} = (1 - \lambda)C_0 + \lambda C_1. \quad (5.79)$$

where λ, is the fractional order term. Further, by applying the LQR controller between the controller type 1 and type 2 systems, the feedback gains for the system using the convex incremental equation in (5.79) are determined by the following equation:

$$K_{FO} = [(1 - |\lambda|)(K_{LQR1}) + (|\lambda|)(K_{LQR2})]. \quad (5.80)$$

Where λ is the fractional order integrator, $KLQR_1$ corresponds to the LQR for the 7th order system, and $KLQR_1$ corresponds to the LQR for the 8th order system. K_{FO} is the resulting convex-weighted interpolated feedback gain using (5.79).

The control law for the active front steering then becomes:

$$\tau_{afs} = k_1 v_1 + k_2 r_1 + k_3 r_2 + k_4\, \psi + k_5 x_5 - k_6 x_6 - \frac{k_7}{s} x_7 - \frac{k_8}{s^{\lambda}} x_8. \quad (5.81)$$

The feedback gains $[k_1, k_2, k_3, k_4, k_5, k_6, k_{7,}\, k_8]$ are computed to be:

$$k_1 = 0.26, k_2 = 1.02, k_3 = -0.18, k_4 = -0.15, k_5 = 12.42, k_6 = 1.48, k_7 = 1.53, k_8 = 0.4.$$

The feedback gain matrix k_{p} would change the pole location of the system and k_6, k_7 and k_8 provides the lane position tracking by eliminating the steady state error of the tractor-trailer system. With the feedback gains determined, the closed loop system with the higher order integral action can be represented as:

$$\begin{bmatrix} \dot{x} \\ \dot{x}_i \end{bmatrix} = \begin{bmatrix} A - BK_p & BK_i \\ -C & 0 \end{bmatrix} \begin{bmatrix} x \\ x_i \end{bmatrix} + \begin{bmatrix} 0 \\ 1 \end{bmatrix} \mathrm{r}, \quad (5.82)$$

$$y = [C\ 0] \begin{bmatrix} x \\ x_i \end{bmatrix} + [0]r. \quad (5.83)$$

5.3 Linear Model Simulation

Simulation results are presented for the tractor-trailer linear model using Matlab/Simulink. An evasive highway maneuvering scenario for tractor-trailer platoons is considered as shown in Fig 3.11. To achieve lateral stability the effectiveness of the proposed new FOSFB controller

scheme is evaluated. Hence, it is assumed that the tractor-trailer is travelling in a straight path before the evasive maneuver happens. In evaluating the dynamical performance of the system, the maximum settling time and overshoot are critical evaluation measurements.

The equations considered for the high speed emergency evasive maneuver while the tractor-trailer is travelling at a constant speed of 70 mph are the following

$$m_1 a_{y1} = F_{y1} cos\delta + F_{x1} sin\delta + F_{y2} - F_y, \tag{5.84}$$

$$I_{z1} \dot{r_1} = a_1 F_{y1} cos\delta + a_1 F_{x1} sin\delta - b_1 F_{y2} + d_1 F_y, \tag{5.85}$$

$$m_2 a_{y2} = F_{y3} + F_y cos\psi + F_x sin\psi, \tag{5.86}$$

$$I_{z2} \dot{r_2} = -b_2 . F_{y3} + e_2 \left(F_y . cos\psi + F_x . sin\psi \right). \tag{5.87}$$

where the articulation joint angle is the change rate of the yaw angle for the tractor and trailer respectively. Table 10 shows the parameters of the tractor-trailer system.

The proposed FOSFB controller was designed first for the linear model of the tractor-trailer, then the linear controller is implemented to the nonlinear system model for verification and validation of the proposed control scheme. The controller was designed with the truck travelling at a constant speed of 70 mph in a highway in order to avoid a collision. The steering angle torque signal (τ_{afs}) is controlled to provide the lateral stability. The Simulink model used to implement the proposed control for the tractor-trailer linear model is given in .

The fractional order state feedback controller block diagram shown in Fig. 5.27. The fractional order controller gains were selected, as explained in Section 5.2. To summarize, the gains are computed to be:

$$k_1 = 0.26, k_2 = 1.02, k_3 = -0.18, k_4 = -0.15, k_5 = 12.42, k_6 = 1.48, k_7 = 1.53, k_8 = 0.4.$$

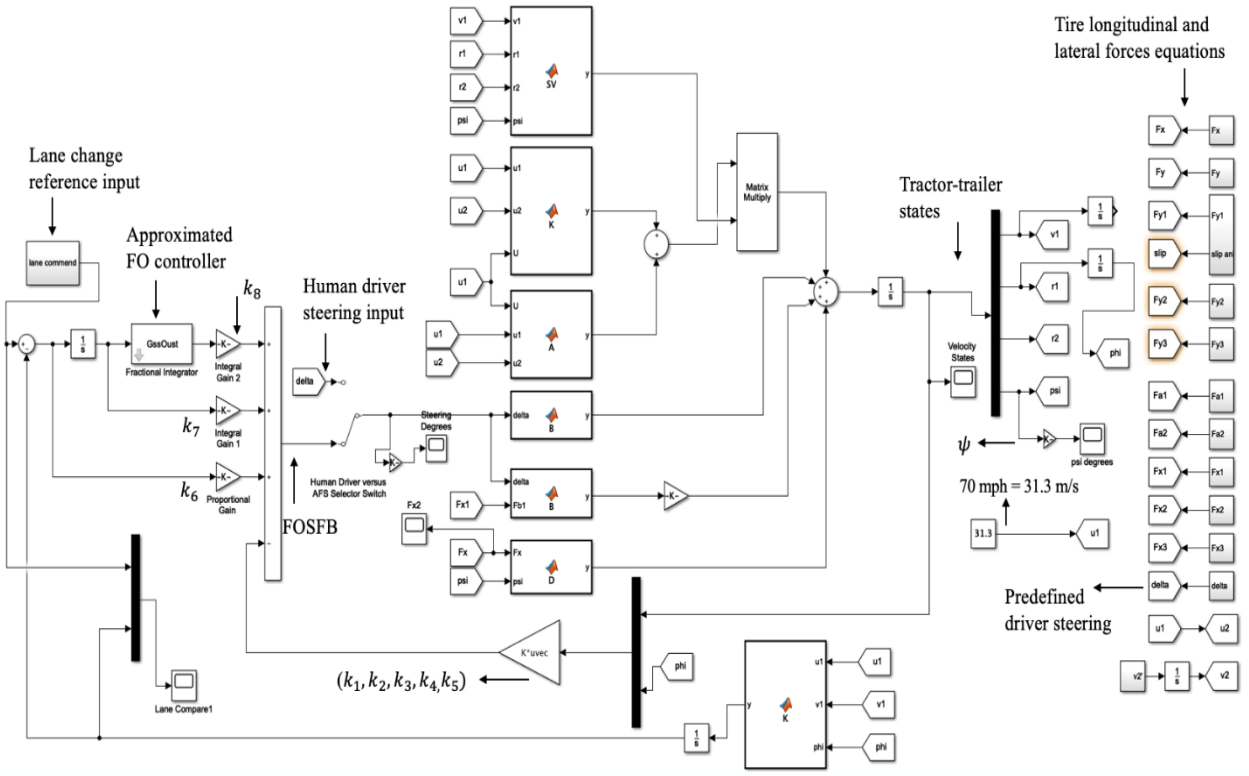

Fig. 5.24. Simulink for the linear tractor-trailer with FO state feedback.

Fig. 5.25 displays the ramp-step desired lane change reference input. Where the goal of the controller is provide accurate lane position tracking for a ramp input (lane change maneuver) in order for the tractor-tractor to complete the evasive maneuver safely. Adding in integrator term to the system shows that the tracking is improved, and at the same time does not degrade the stability aspects for the tractor-trailer in terms of the articulation and the tractor velocity.

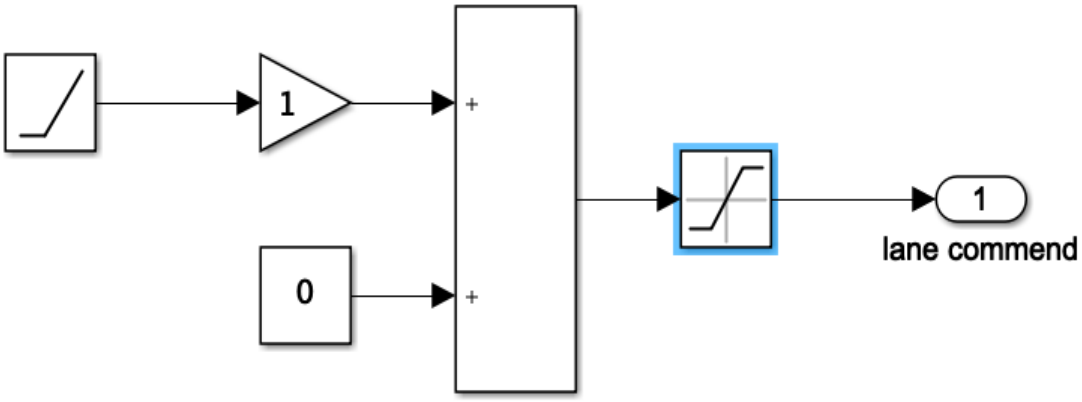

Fig. 5.25. Desired lane change reference input.

Fig. 5.26 shows the driver predefined generated steering command, which emulates a human driver steering behavior.

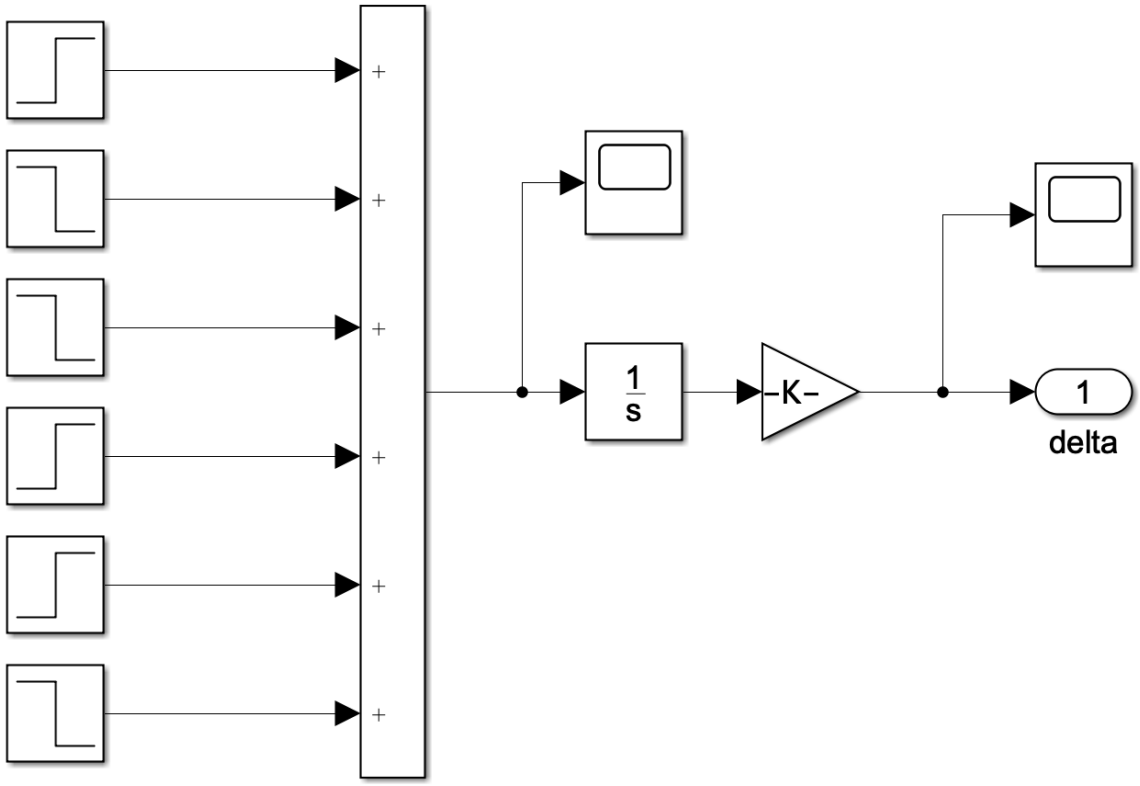

Fig. 5.26. Driver steering input command.

Table 10 Tractor-trailer parameters.

m_1	5450	kg	C_1	630000	N/rad	b_1	2.0676 m
m_2	27800	kg	C_2	$1.84x10^8$	N/rad	b_2	2.3886 m
Iz_1	9500	kg-m^2	C_3	600000	N/rad	d_1	0.8611 m
Iz_2	200000	kg-m^2	B_σ	31.85	N-m-s/rad	e_2	7.3396 m
J_s	0.32	kg-m^2	a_1	1.7424	m	ε	0.92 m/s

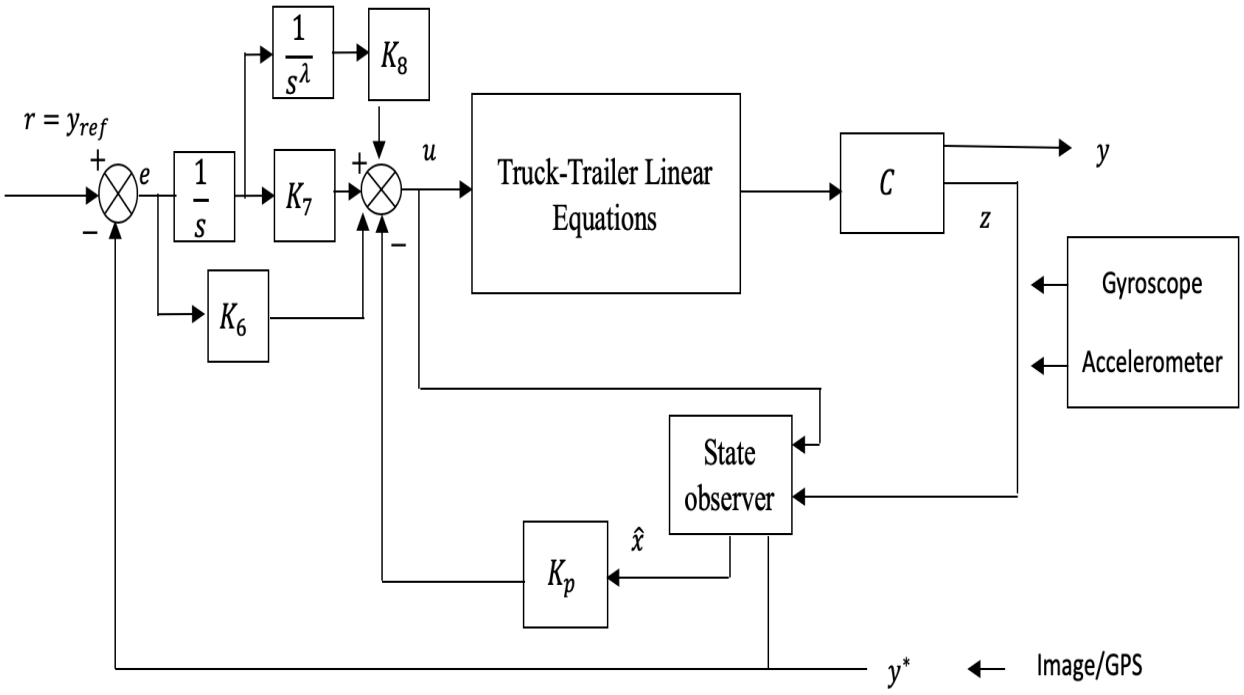

Fig. 5.27. FOPI state-feedback controller typology applied to the linear system.

5.3.1 Linear model response for evasive single lane maneuver scenario

This section provides the simulation results for a single lane change maneuver situation in a highway with 3.5 m lane change. To evaluate the steering response with the FO state feedback controller and a human driver. Fig. 5.28 displays the predefined truck driver steering angle, where the steering input is designed in order to emulate a human driver without any compensation in the

system in a manner to the study in [71]. In that study, 91 lane changes were conducted for truck drivers, and they averaged 7.6 sec. to finish the lane departure in the highway. Fig. 5.29 presents the steering angle input with the applied FOSFB controller scheme, noting that the steering response becomes faster with the fractional controller as compared to the human driver.

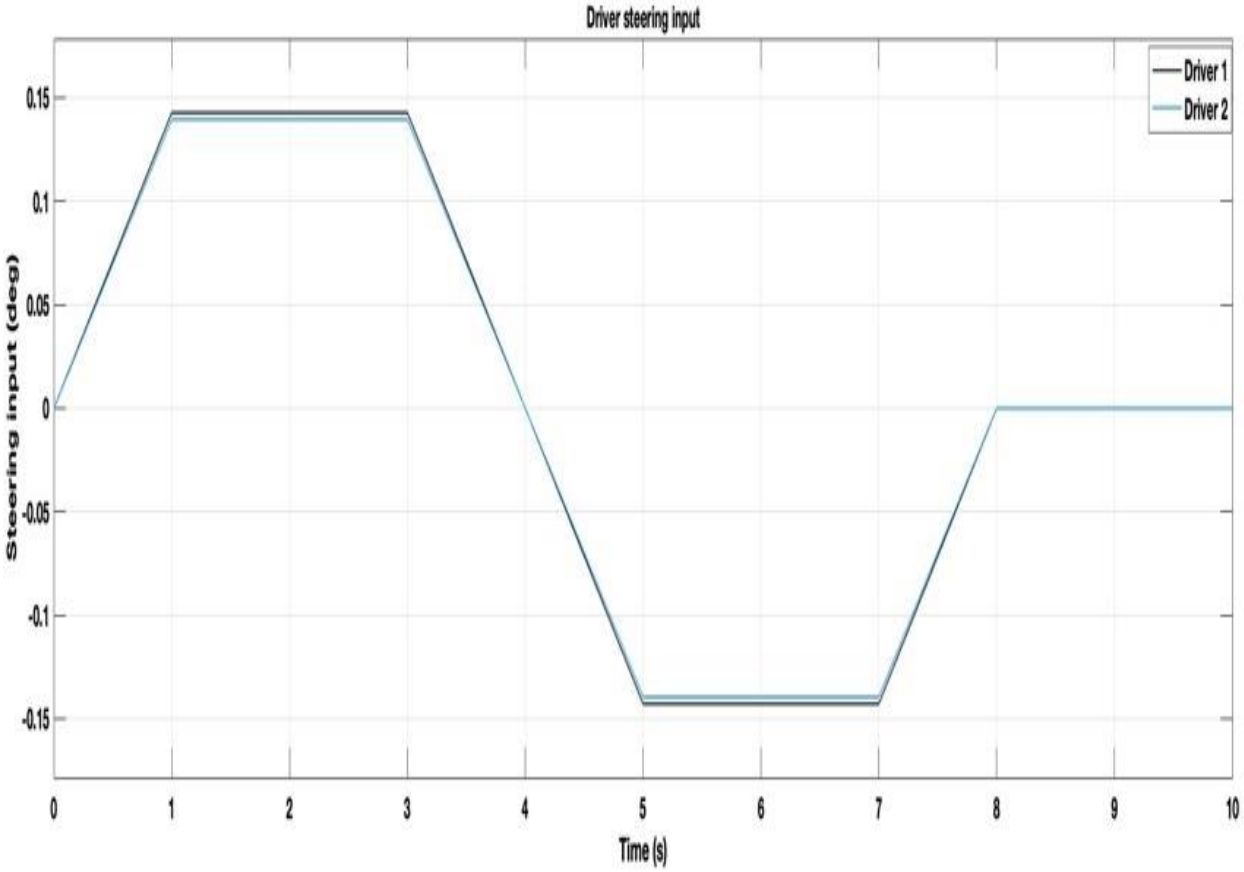

Fig. 5.28. Steering angle input for the driver.

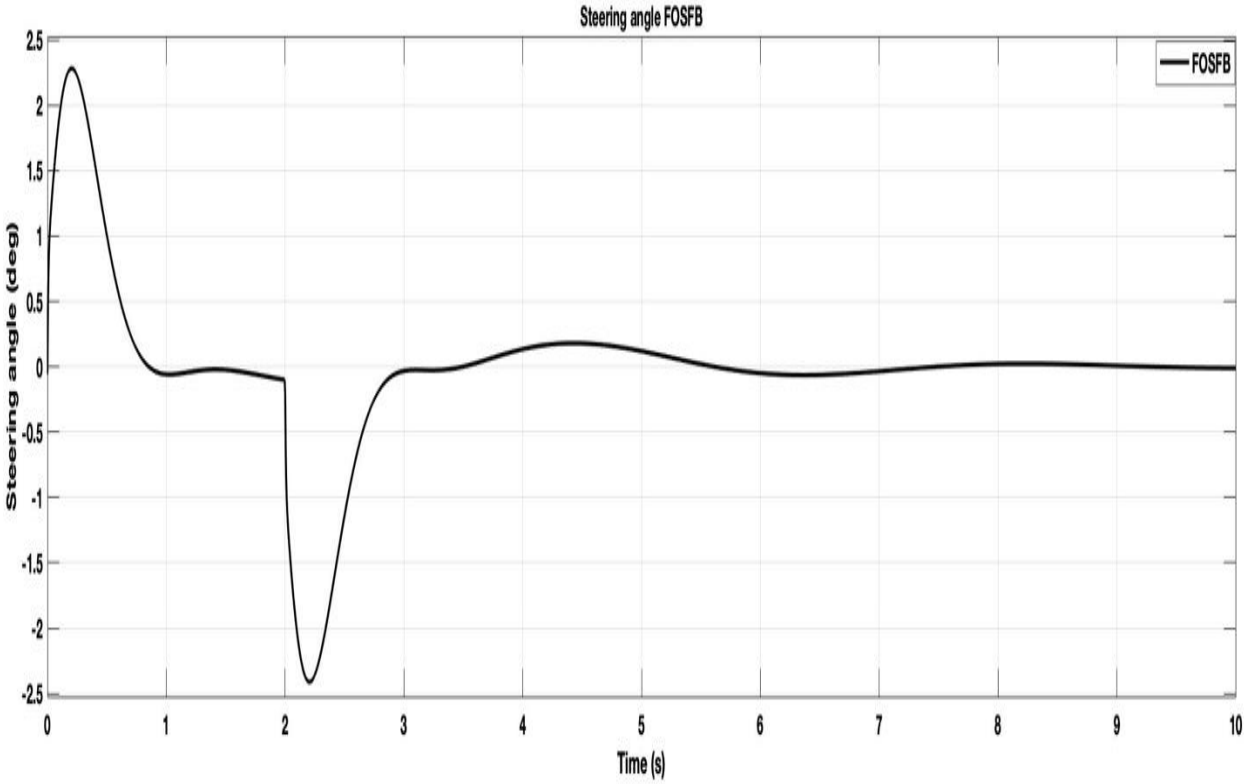

Fig. 5.29. Steering angle input with FOPI state feedback.

Fig. 5.30 displays the tractor-trailer response for a single lane change in an evasive maneuver situation to avoid an obstacle, while travelling at a highway speed of 70 mph. A comparison is shown between the professional truck driver responses, the FOSFB response and the desired change lane response. It can be observed that with the proposed FO controller the lane tracking is significantly improved and that the response time is also improved by 20% compared to skilled truck driver.

With a the fractional order integrator $\lambda = 1.4$, it is shown that it provides an optimal response for the tractor-trailer performance to complete the lane change safely and being in the center of the lane once the lane maneuver is completed in a prompt manner compared to a professional human driver.

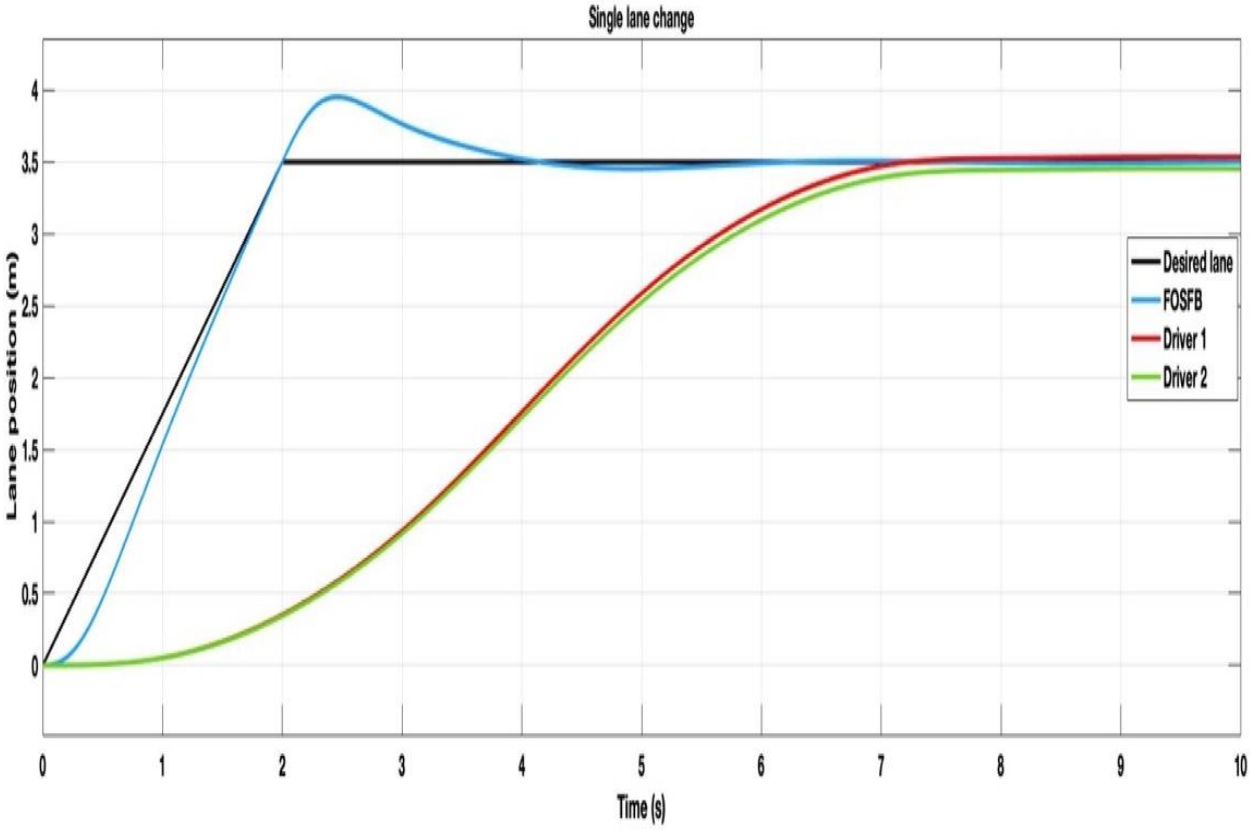

Fig. 5.30. Lane position with truck travelling at 70 mph speed compared to the driver.

5.3.2 Linear model response for evasive double lane maneuver scenario

The FOSFB controller is compared for the professional truck driver in the case that requires a double lane change at a highway speed of 70 mph. Fig. 5.31 shows the predefined steering angle input for the truck driver, which is designed to emulate a human driver steering behavior. Fig. 5.32 demonstrations the steering angle input with the FOSFB controller, as can be seen the response is faster than the human truck driver. The amplitude for the steering input is increased with FOSFB, which is expected for achieving the fast time response for the tractor-trailer to change lanes during an emergency situation.

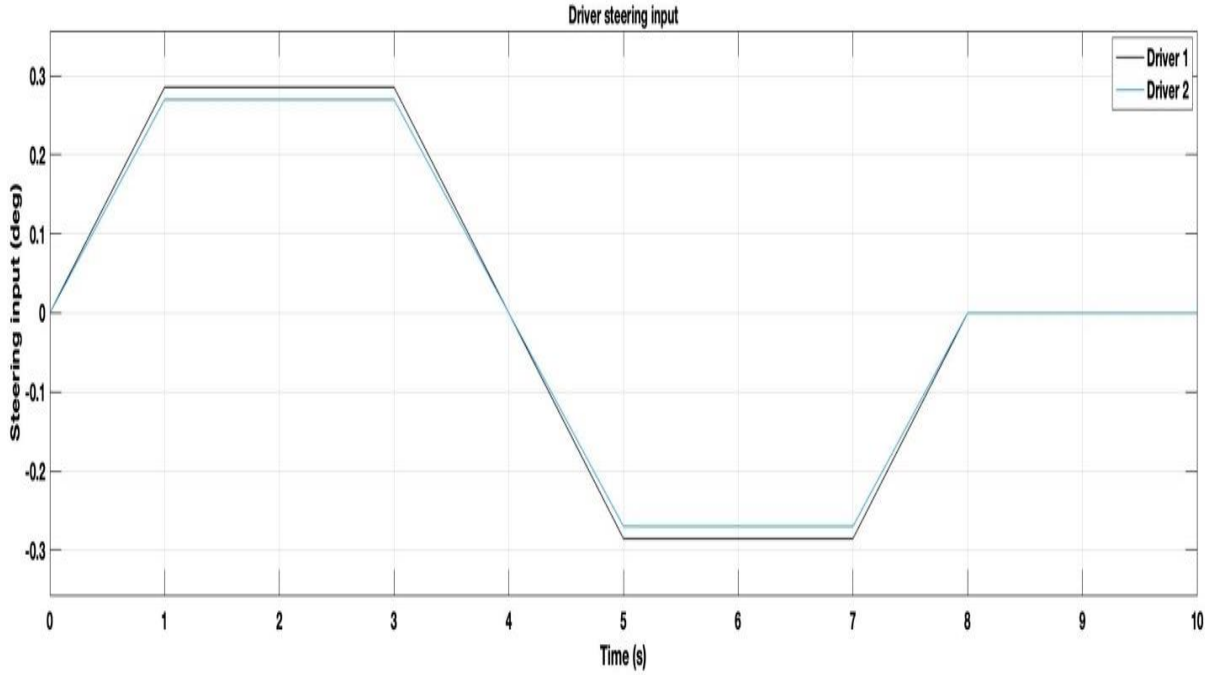

Fig. 5.31. Steering angle input for the driver.

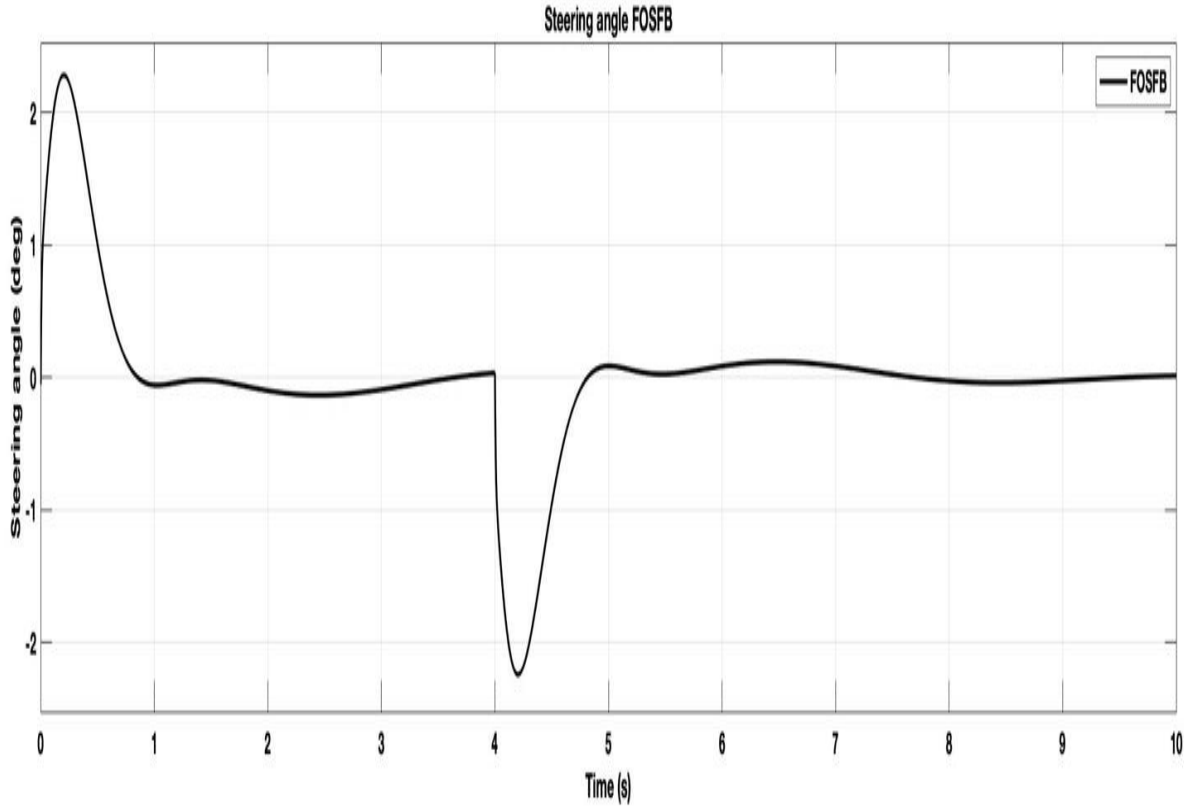

Fig. 5.32. Steering angle input with FOPI state feedback.

Fig. 5.33 presents the tractor-trailer response for a double lane change in an evasive maneuver situation to avoid an obstacle, while travelling at a highway speed of 70 mph. A comparison is shown between the professional truck driver and the response with the FOSFB. With the proposed FO controller the lane position tracking is improved and the response time is also enhanced compared to truck driver for the 7 meter highway lane change situation.

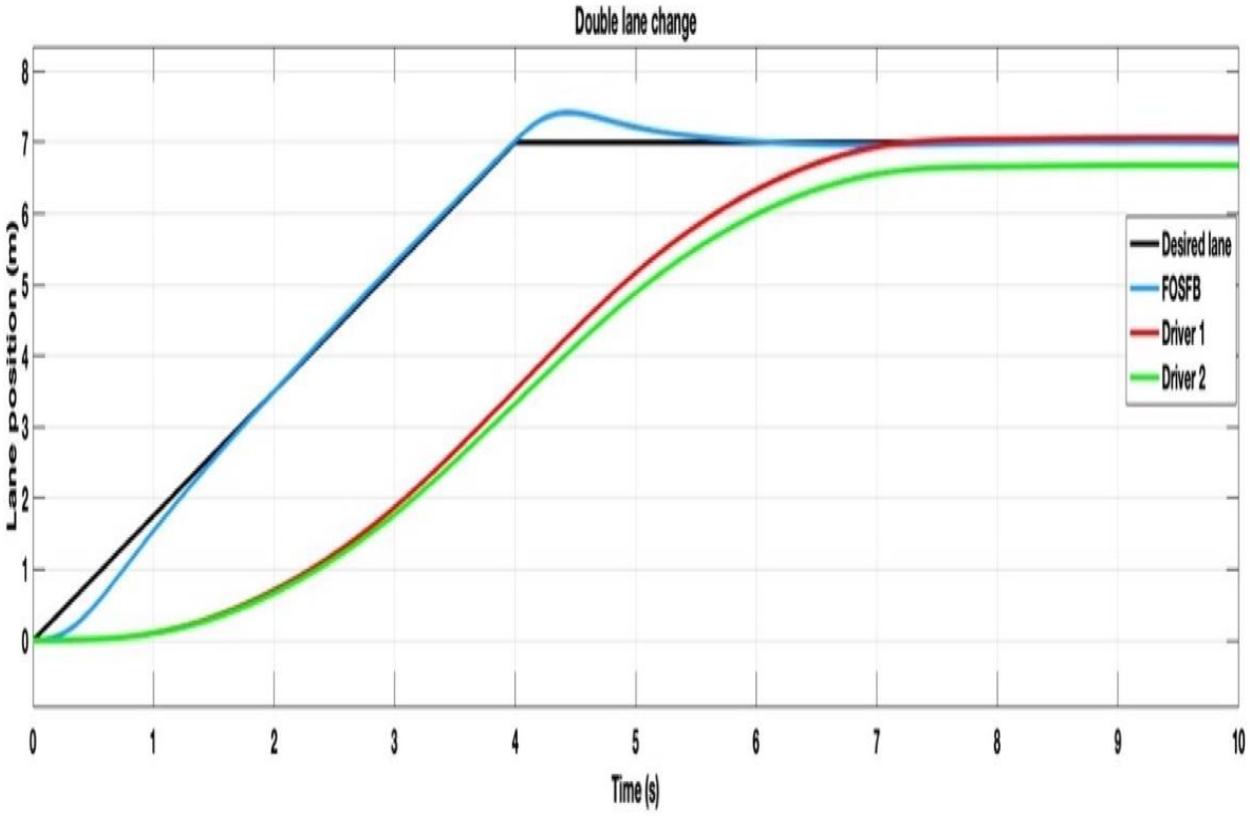

Fig. 5.33. Lane position with truck travelling at 70 mph speed compared to the driver.

5.3.3 Linear model response for an evasive maneuver scenario with different speeds

The controller is also evaluated for the case when the truck is travelling at different highways speeds. Fig. 5.34, displays the tractor-trailer travelling at three different highway speeds 60 mph, 70 mph and 80 mph.

With the FOSFB controller the response time is marginally improved at higher speeds. At lower speeds the time response for the single lane change is slightly degraded. Fig. 5.35 shows the steering angle input for these three different highway speeds with the FOSFB as the steering angle is a little increase for the low speed. Figs. 5.36-38 displays the tractor lateral position, articulation angle and the trailer yaw rate for the different highway speeds, as can be observed from the articulation angle response, the tractor-trailer stability would marginally start to improve with the lower speed as opposed to the higher speed.

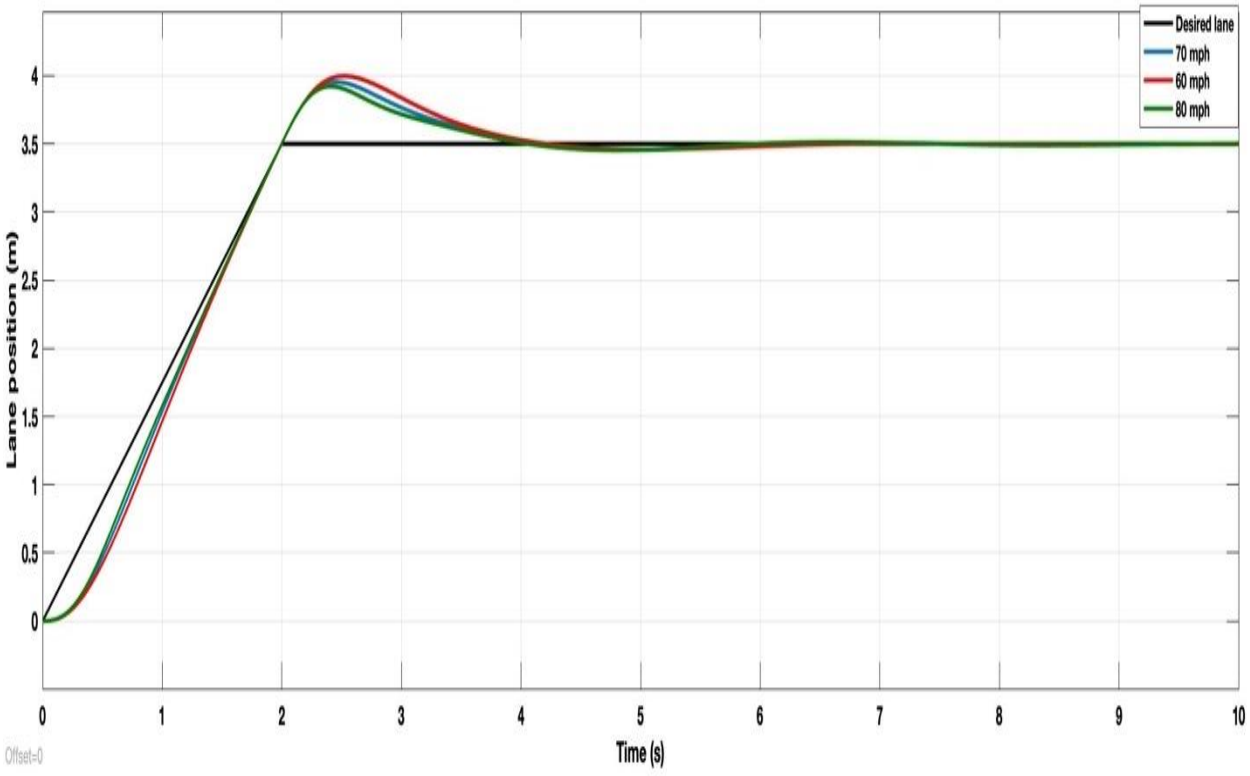

Fig. 5.34. Lane position response for different highway speeds.

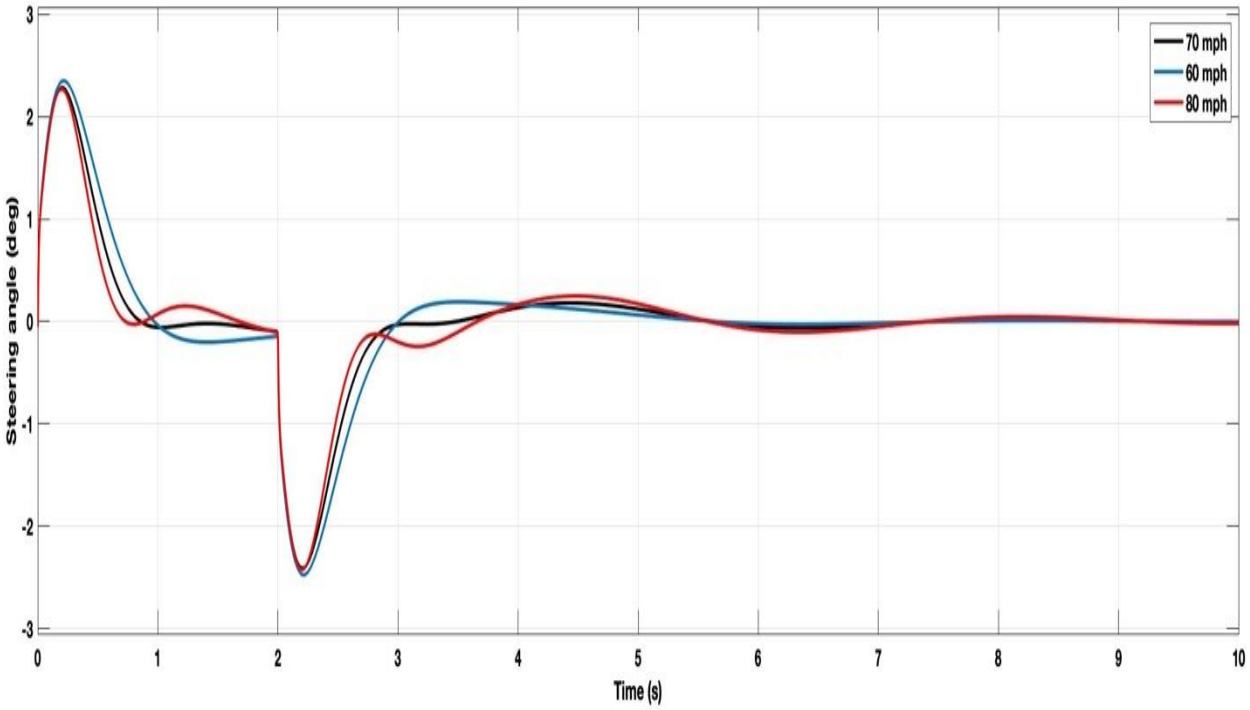

Fig. 5.35. Steering angle input with FOPI state feedback with different highway speeds.

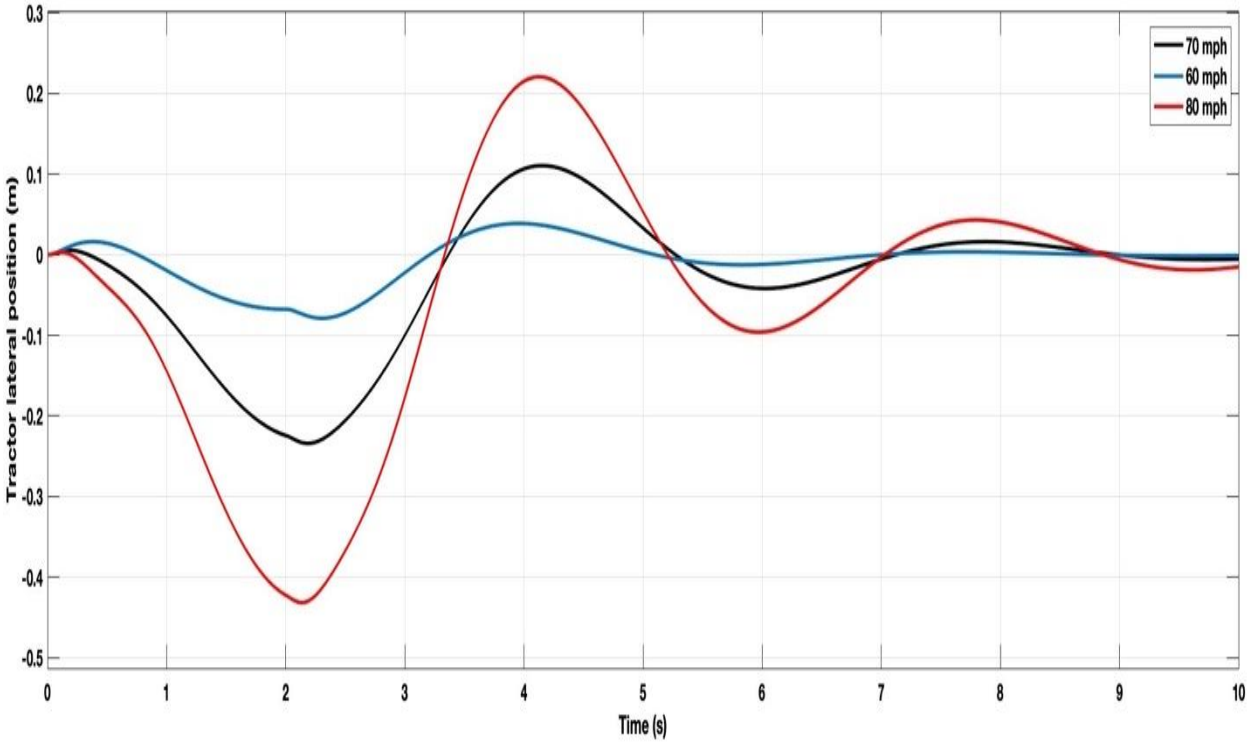

Fig. 5.36. Tractor lateral position with FOPI state feedback.

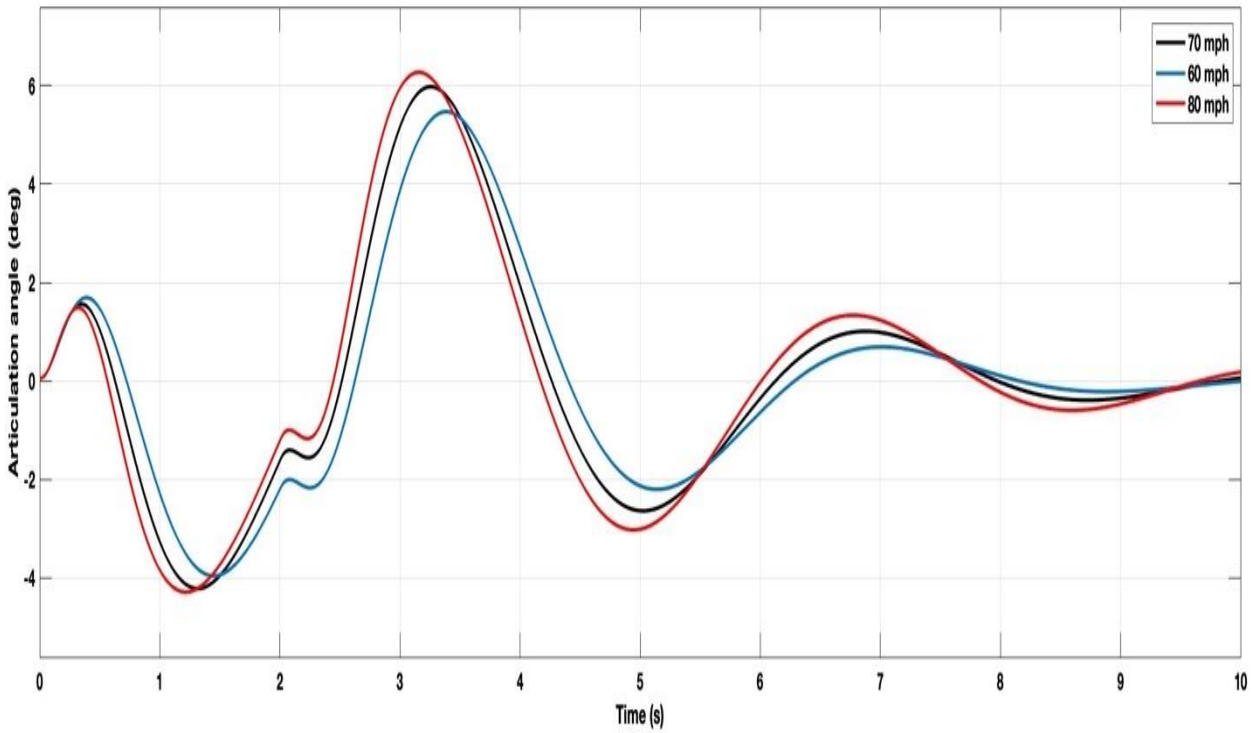

Fig. 5.37. Articulation angle for different speeds.

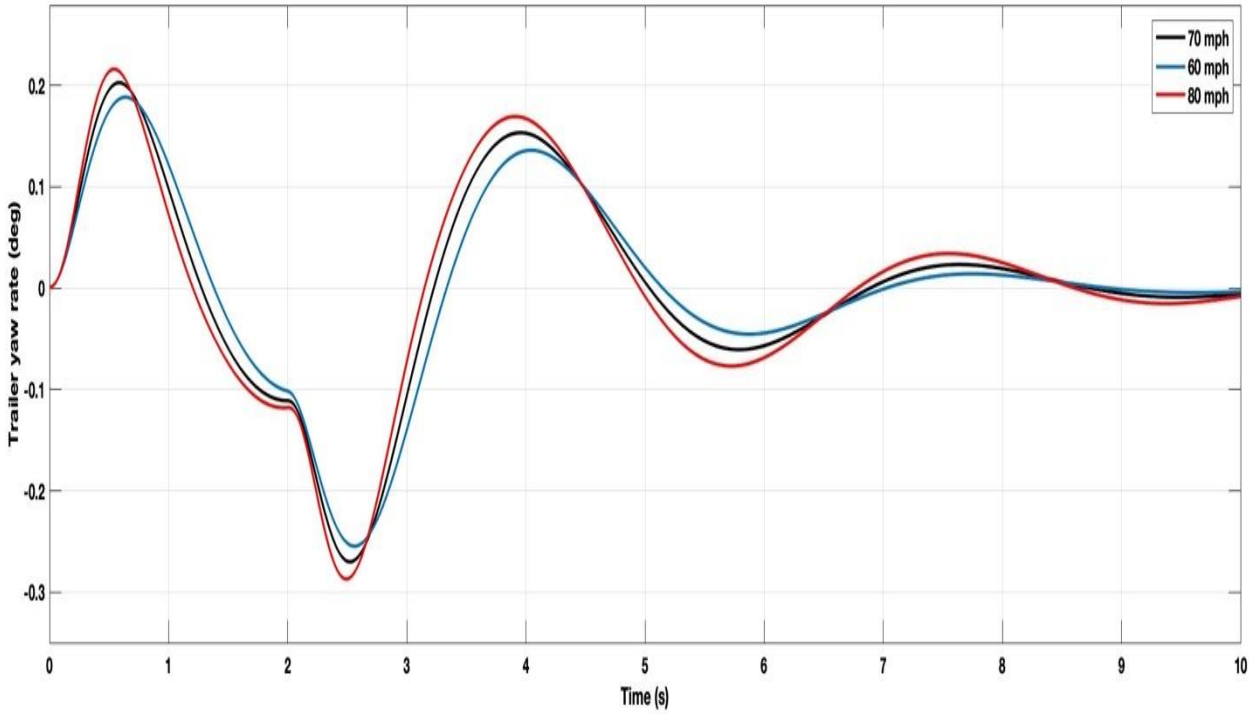

Fig. 5.38. Trailer yaw rate for different speeds.

5.3.4 Linear model response for the trailer partial load and over-load by 50%

To evaluate the controller with different loading conditions while attempting a single lane evasive maneuver scenario, the trailer cargo load is decreased by 50% ($m_2 = 13900$ kg) and also an over-load case is examined when the trailer load is increased by 50% ($m_2 = 41700$ kg). Fig. 5.39 and Fig. 5.40 shows lane position response the articulation angle for the varying load conditions. As can be seen, when the trailer is partially loaded, the tractor-trailer performance would marginally decrease in terms of the articulation angle stability and the lane position tracking.

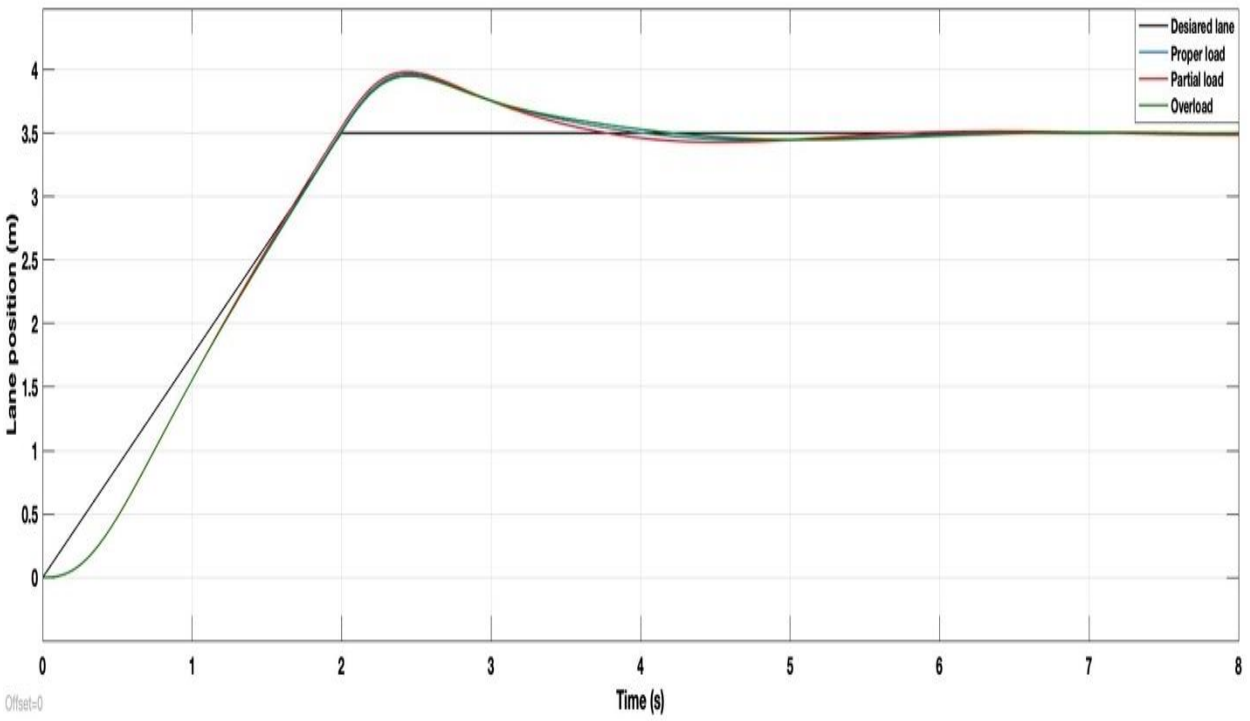

Fig. 5.39. Lane position for a single lane change with different loading conditions.

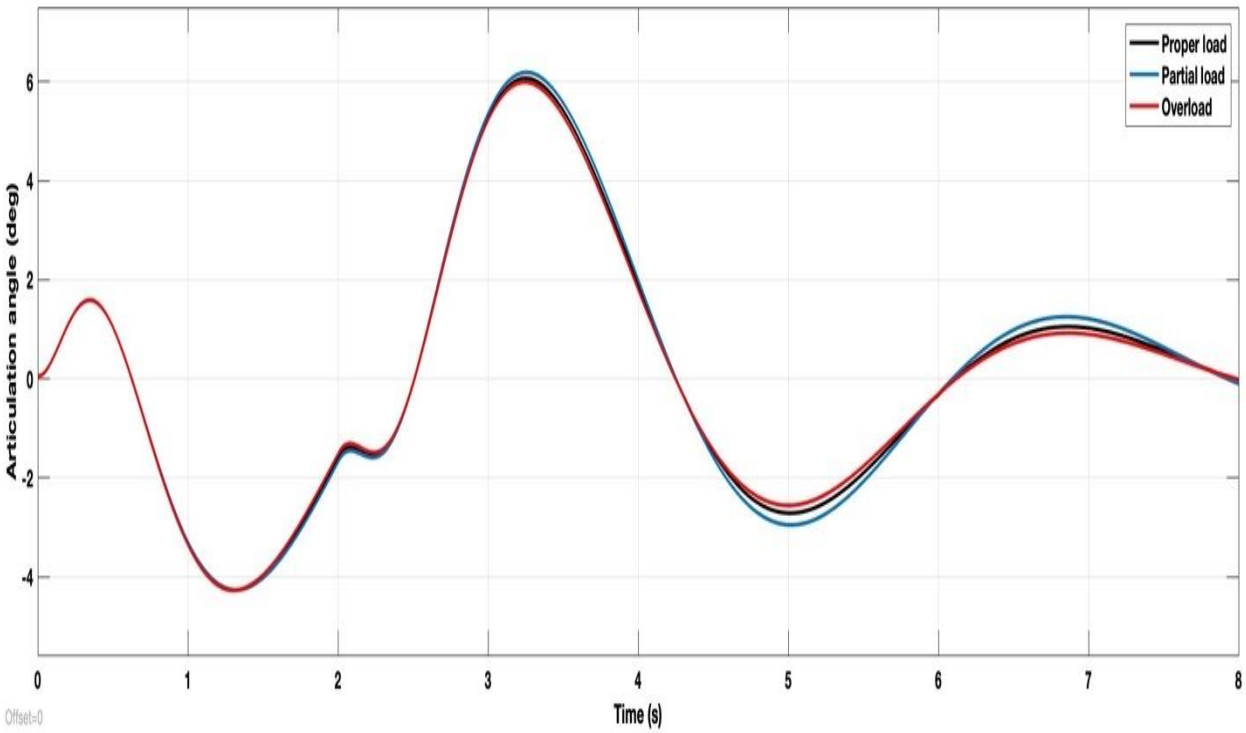

Fig. 5.40. Articulation angle for a single lane change with different loading conditions.

5.3.5 Linear model response for tire stiffness variation

The FOSFB is evaluated under tire stiffness variation for the tractor-trailer system. Fig. 5.41 shows the lane position response with varying the truck tire cornering stiffness parameter c_1, by a 50% increase and decrease, Fig. 5.41 demonstrates the controller effectiveness to the tire stiffness variation, where the lane position response is quite the same for the three cases.

As Fig. 5.42 displays the articulation angle response with the tire stiffness variation of 50%. As the results also confirms the controller robustness to the tire stiffness parameter variation as there nearly no change in the articulation angle response for the three different cases.

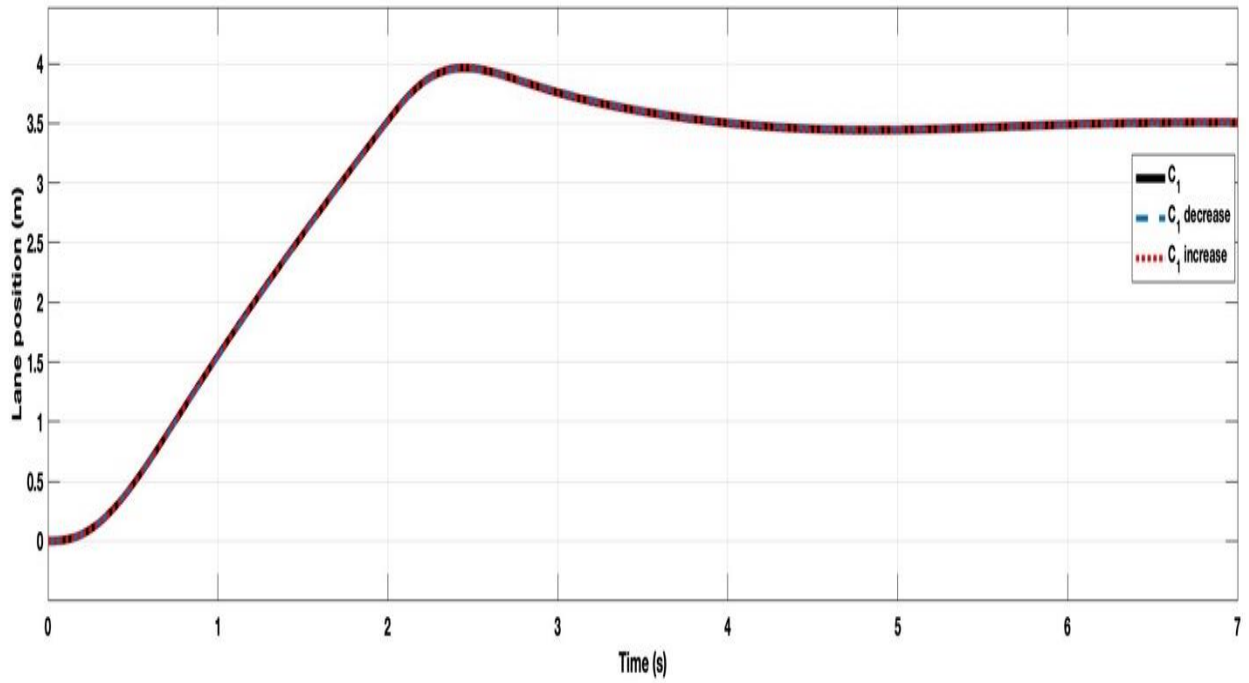

Fig. 5.41. Lane position for a single lane change with varying c_1.

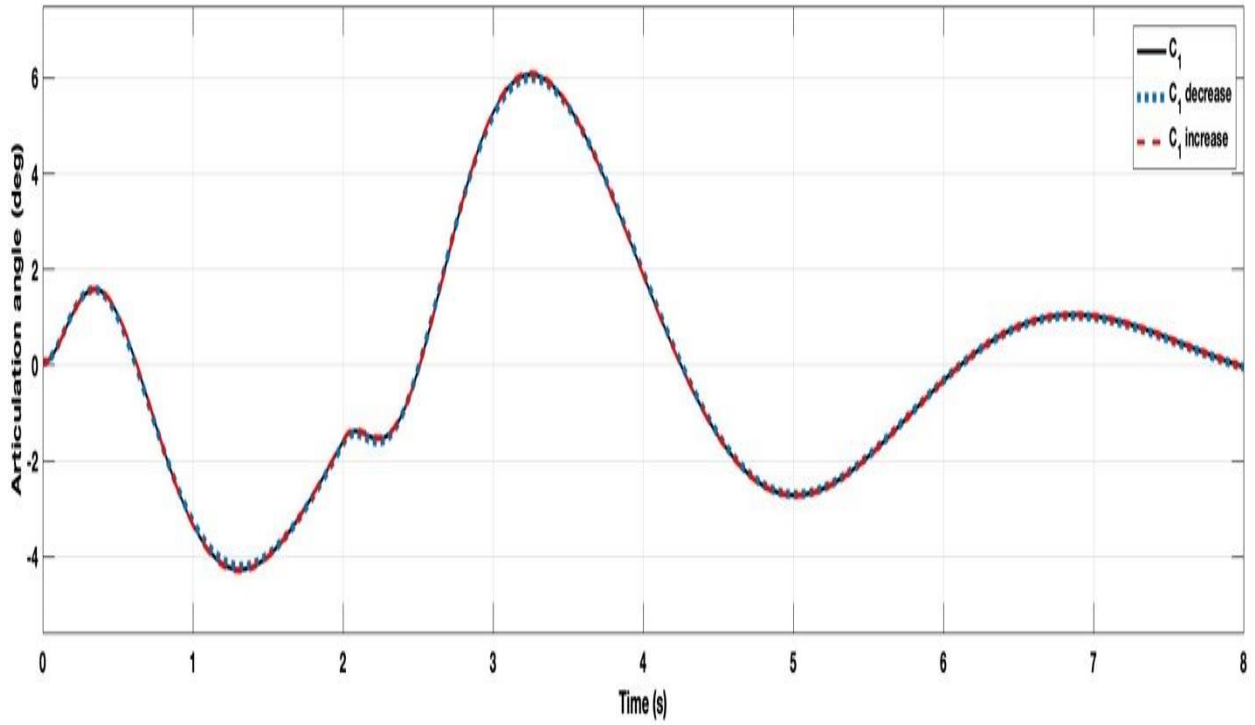

Fig. 5.42. Articulation angel of tractor-trailer with varying c_1.

This Chapter presented the tractor-trailer linear model response with the applied fractional order state feedback controller. It demonstrated that the controller improved performance for tracking the lane position while attempting an evasive maneuver scenario and providing a fast lane change time response as compared a professional truck driver. The controller was also evaluated for different cases, such as, varying the speed, load and tire stiffness for the tractor-trailer, while attempting the evasive lane change.

In Chapter 6, for verification of the designed fractional order controller, the tractor-trailer nonlinear system is examined, with the proposed FO controller.

Chapter 6: Nonlinear Model Simulation Results

6.1 Nonlinear Model Simulation

In this Chapter, to verify the linear controller for the tractor-trailer system, simulation results using Matlab/Simulink are provided. As mentioned previously the proposed fractional order state feedback controller was designed first with the small angle approximation and applied to the linear tractor-trailer system and then implemented to the highly nonlinear tractor-trailer model. Thus, the pre-defined steering inputs for the professional truck drivers are measured in an open-loop means without any correction by the driver, and thus agreeing to the study presented in [71], which examined real road testing for a trained truck driver attempting a lane change departure.

Furthermore, the professional truck driver time response to change lanes for an emergency evasive maneuver scenario is compared to the proposed fractional order control strategy. The controller is also evaluated for the nonlinear dynamics for different circumstances, such as, load, speed, tire stiffness variation to the tractor-trailer parameters, also including a case for wind disturbance rejection by applying a wind side force acting on the trailer.

The equations considered for the high speed emergency evasive maneuver while tractor-trailer is travelling at a constant speed of 70 mph are the following:

$$\dot{v_1} = -u_1 r_1 + \frac{1}{m_1}\left(F_{y1}\cos\delta + F_{x1}\sin\delta + F_{y2} - F_y\right), \tag{6.1}$$

$$\dot{r_1} = \frac{1}{I_{z1}}\left(a_1 F_{y1}\cos\delta + a_1 F_{x1}\sin\delta - b_1 F_{y2} + d_1 F_y\right), \tag{6.2}$$

$$\dot{v_2} = -u_2 r_2 + \frac{1}{m_2}\left(F_{y3} + F_y\cos\psi + F_x\sin\psi\right), \tag{6.3}$$

$$\dot{r_2} = \frac{1}{I_{z2}}\left(-b_2 F_{y3} + e_2\left(F_y\cos\psi + F_x\sin\psi\right)\right). \tag{6.4}$$

Where the articulation angle is the change rate of the yaw angle for the tractor and trailer respectively. The steering equation of the system can expressed as:

$$J_s\ddot{\delta}=-B_s\dot{\delta}-K_s\alpha_1+\tau_{hw}+\tau_{afs} \tag{6.5}$$

Where,

$$\alpha_1=\delta-\frac{v_1+a_1r_1}{u_1} \tag{6.6}$$

With the small angle approximation to the tractor-trailer nonlinear equations, the system was linearized and the FOPI state-feedback controller was developed, thus, then the linear controller was applied to the highly non-linear system, as demonstrated in Fig. 6.1, where the proposed controller typology is illustrated in the block diagram. The description of the controller design and gain selection including the method to choose the fractional order integral are provided in the previous Chapter.

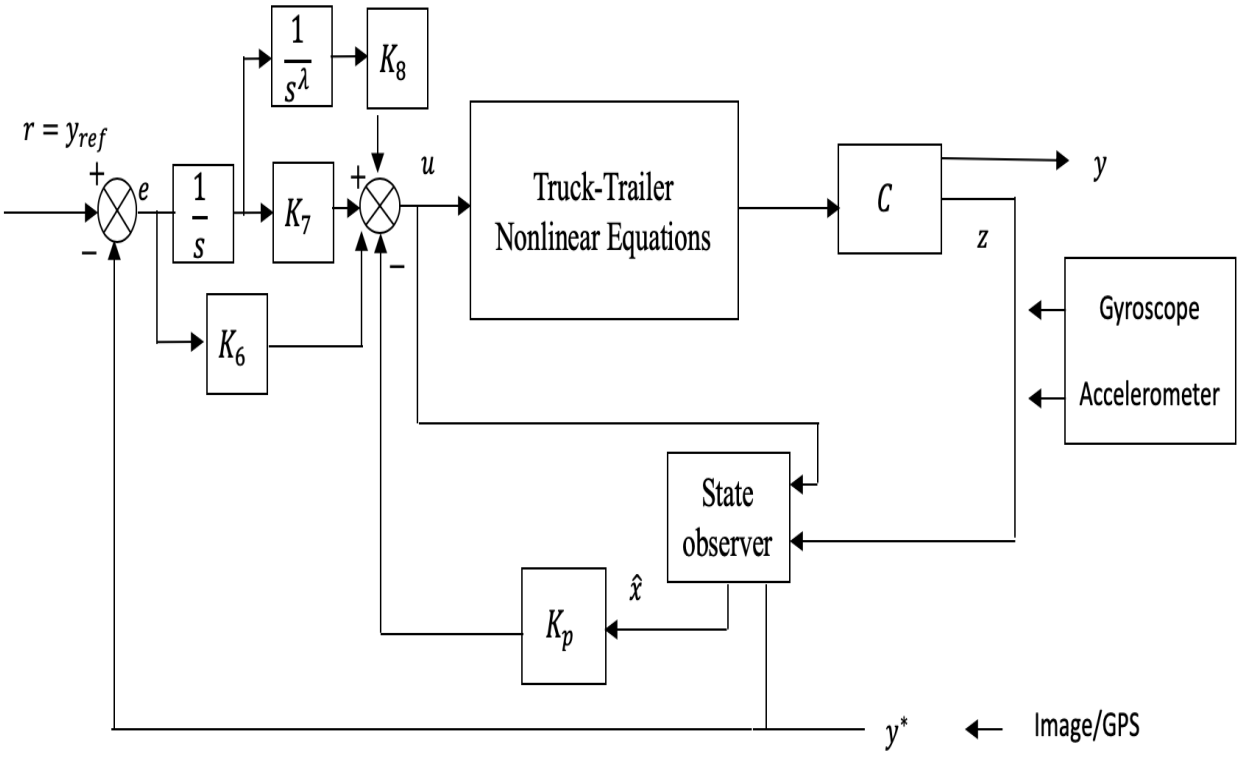

Fig. 6.1. Proposed control scheme for nonlinear tractor-trailer model.

The nonlinear model system equations were implemented in Simulink in order to confirm and validated the FO state feedback controller, the tractor-trailer nonlinear model with FOSFB (C. code) version can be found in the Appendix.

6.1.1 Tractor-trailer with FOSFB control for different highway speeds

Fig. 6.2, displays the steering angle of truck with the applied FO state feedback control for different speed levels of 60, 70, and 80 mph. Fig. 6.3 shows the lane position response for a single lane change for these three different speeds, thus as the controller was designed with a constant highway speed of 70 mph. For a lower speed of 60 mph the response would slightly degrade, as the response time would slightly improve for a higher speed of 80 mph. Figs. 6.4-6.6 displays the tractor lateral position, lateral velocity and yaw rate for these three different speeds for the lane change of 3.5 meters.

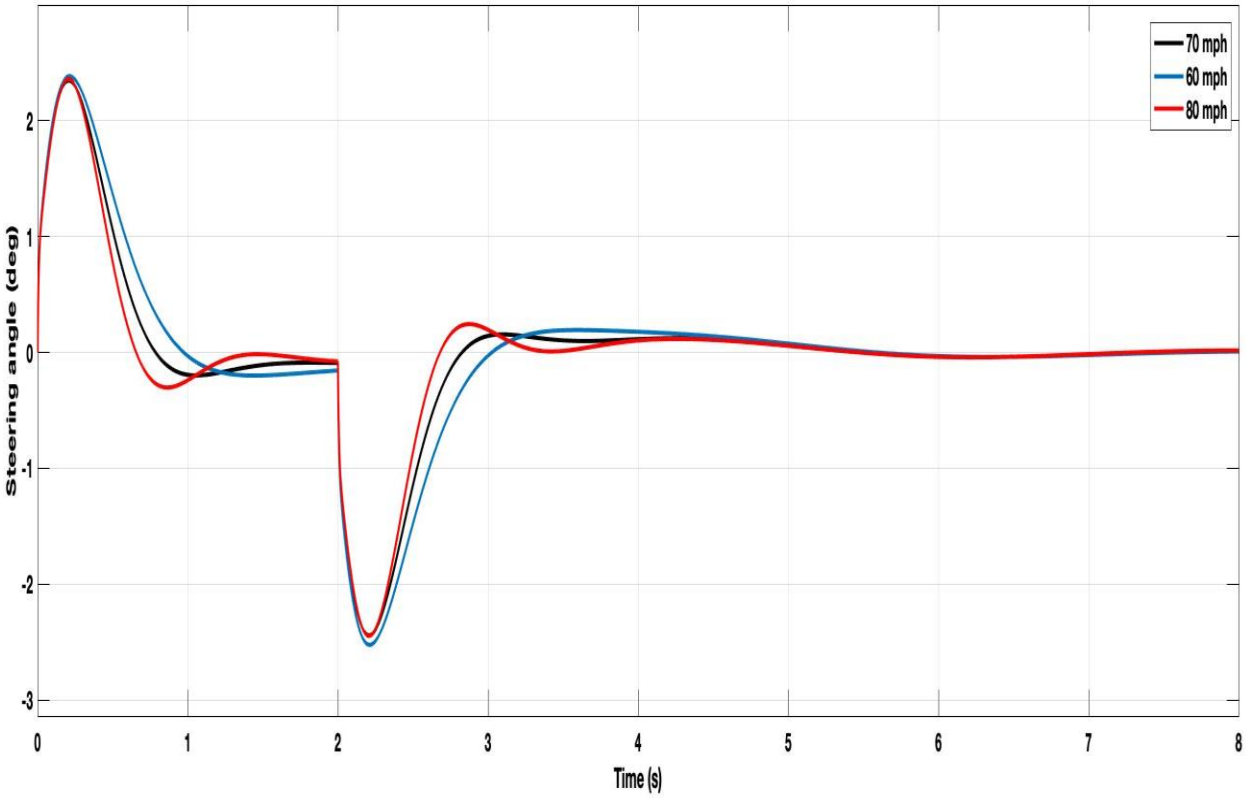

Fig. 6.2. Steering angle with different speeds with FO control.

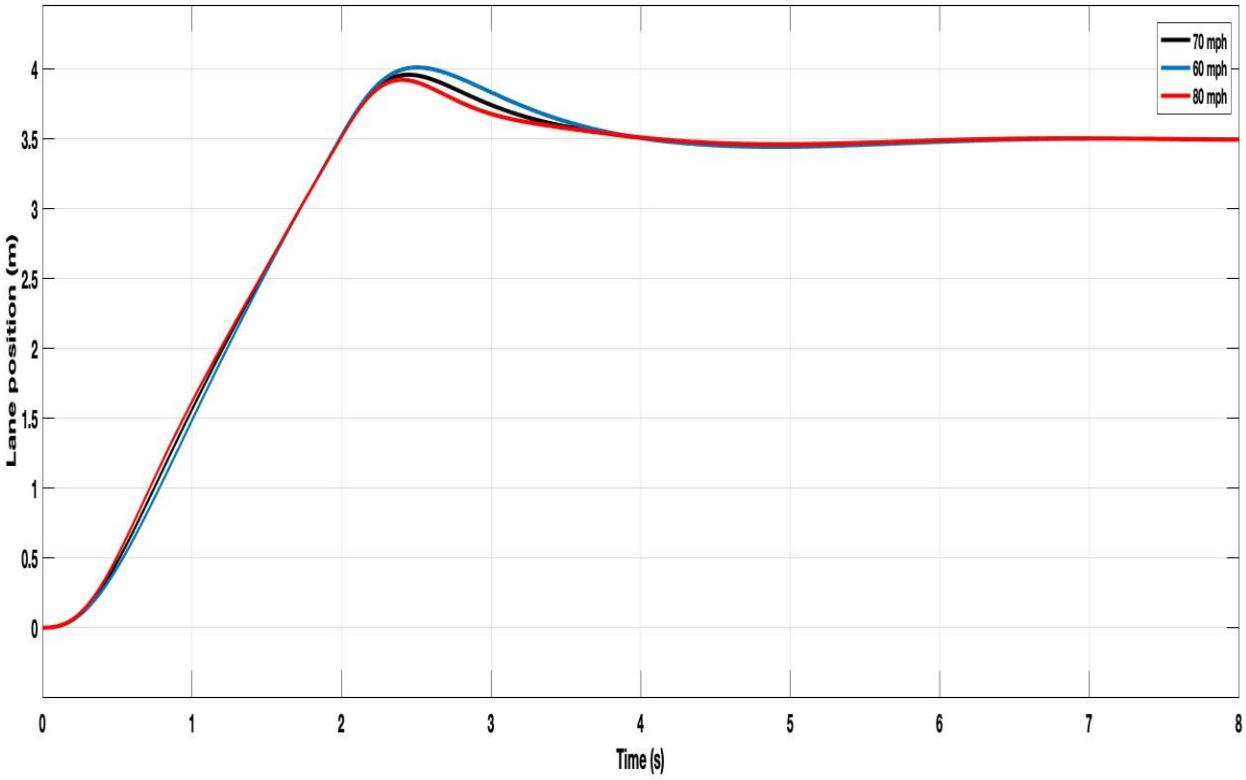

Fig. 6.3. Lane position for different highways speeds for a single lane change.

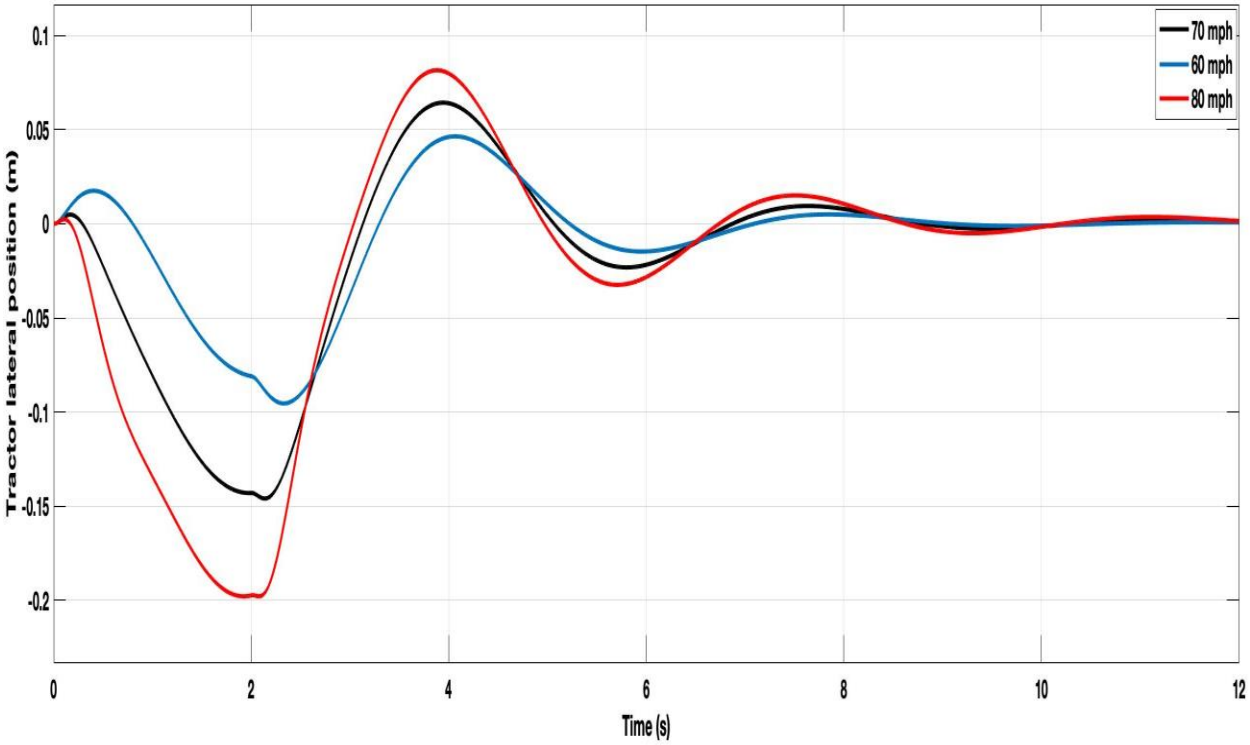

Fig. 6.4. Truck lateral position with different velocities for a single lane change.

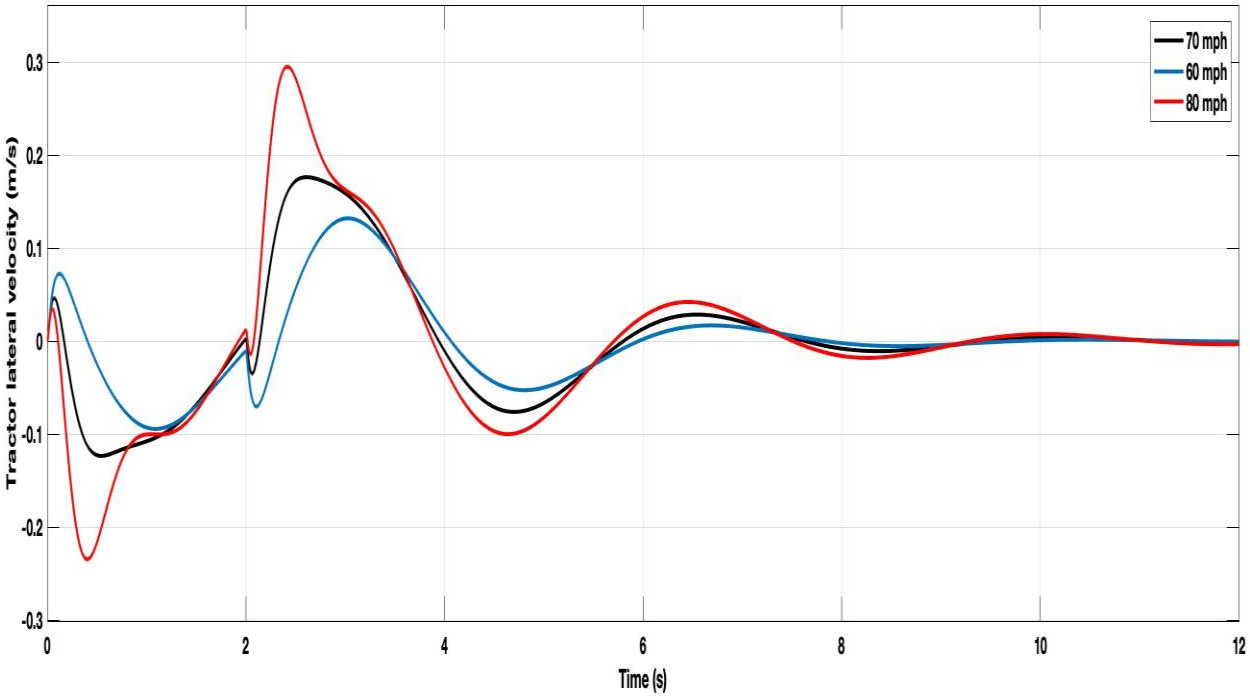

Fig. 6.5. Tractor lateral velocity with different speeds for a single lane change.

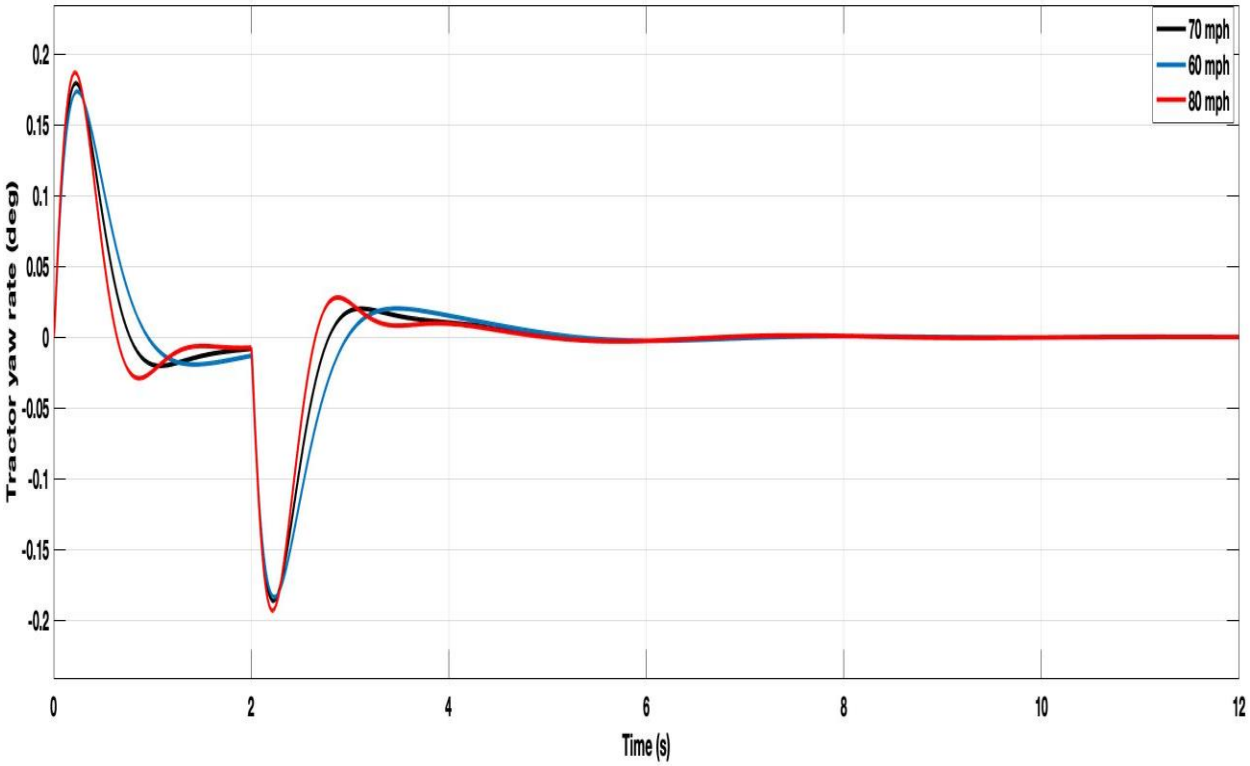

Fig. 6.6. Tractor yaw rate with different velocities for a single lane change.

The trailer yaw for different highways is presented in Fig. 6.7 as the yaw would increase as the speed goes up and would decrease as the speed goes down. Fig. 6.8 shows the articulation angle for the different speeds, hence as the speed goes down for example at 60 mph the articulation angle stability would tend to increase as opposite to when the speed is increased for example at 80 mph, where the stability would decrease for the articulation angle for single highway lane change.

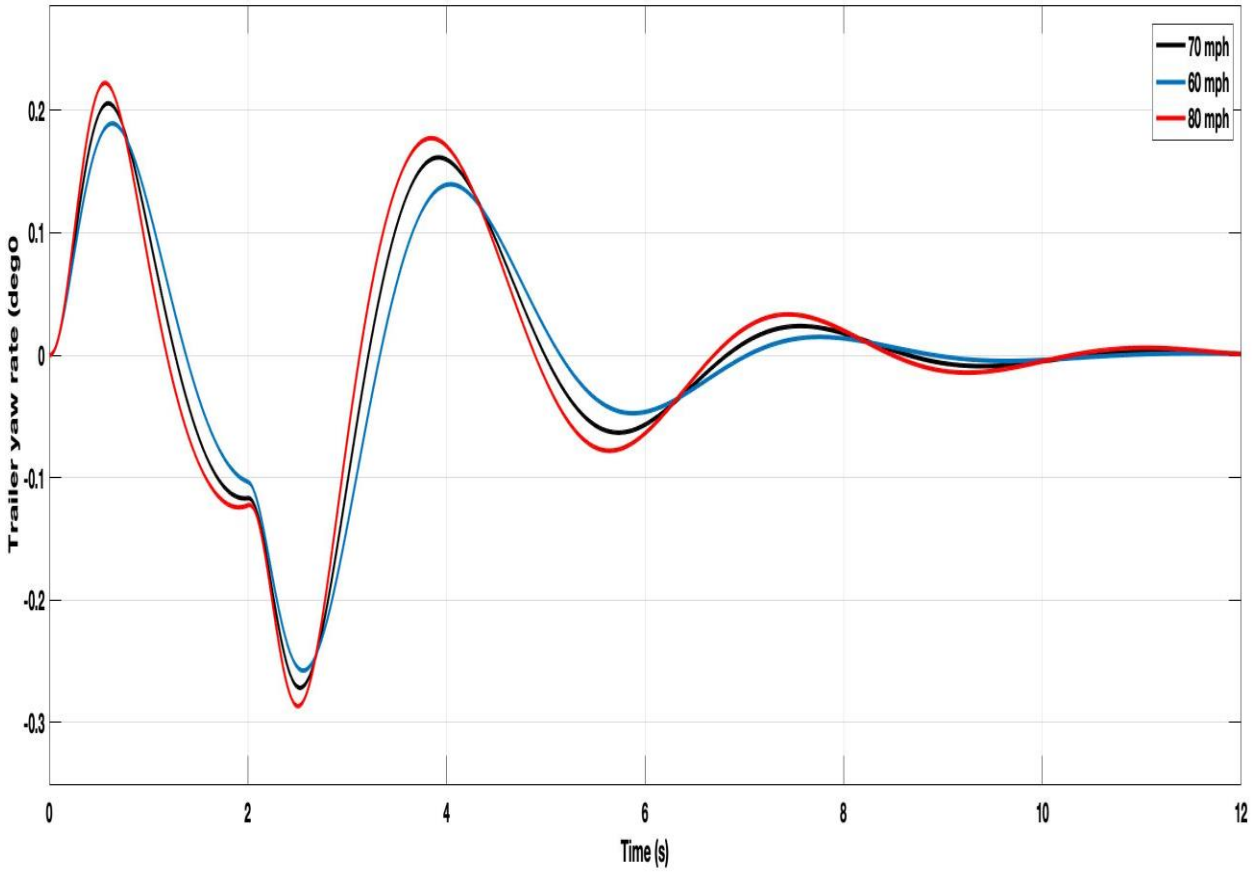

Fig. 6.7. Trailer yaw rate with different velocities for a single lane change.

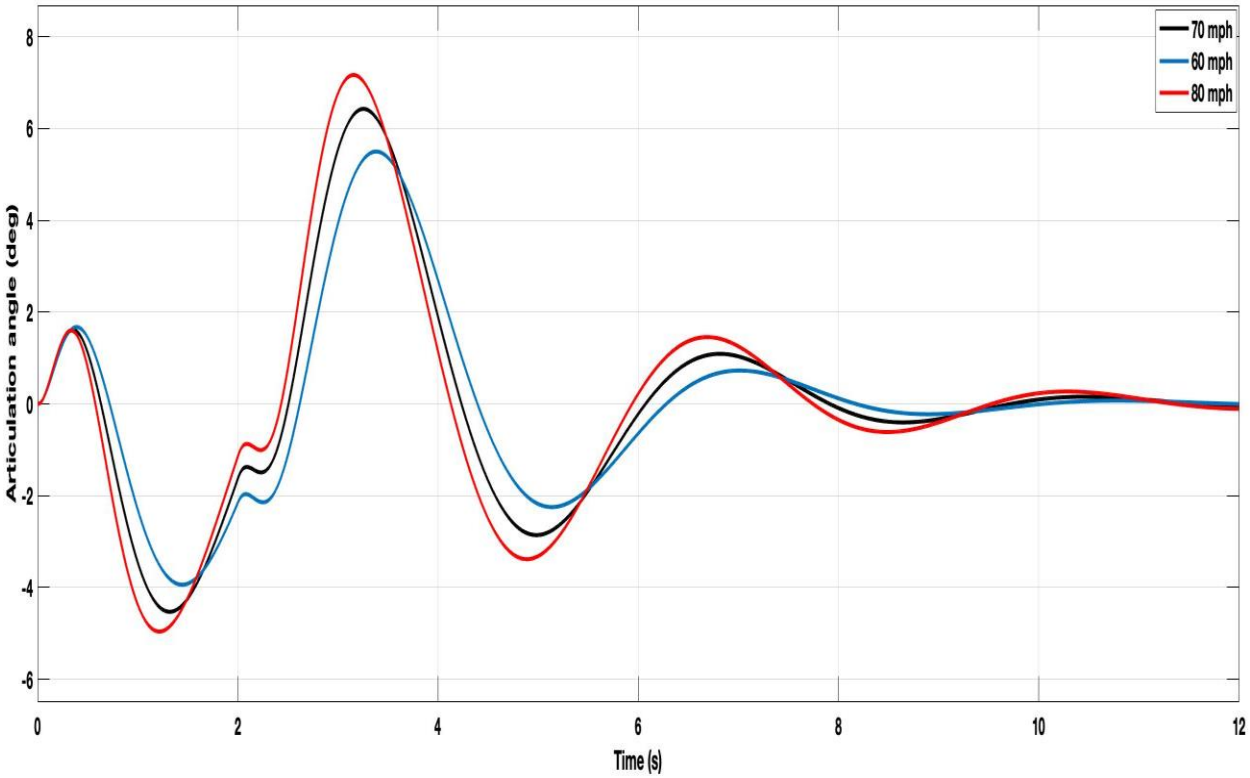

Fig. 6.8. Articulation angle for different velocities for a single lane change.

6.1.2 Evasive maneuver scenario comparison between the driver and FOSFB control for a single lane change

In Fig. 6.9, the steering angle input for the professional truck driver, which is predefined and obtained without any compensation (open-loop) in order emulate a human driver steering input. While Fig. 6.10, shows the steering angle with the applied FOSFB controller, thus it can been seen that the response time with the FOSFB controller is faster as compared to the skilled driver response.

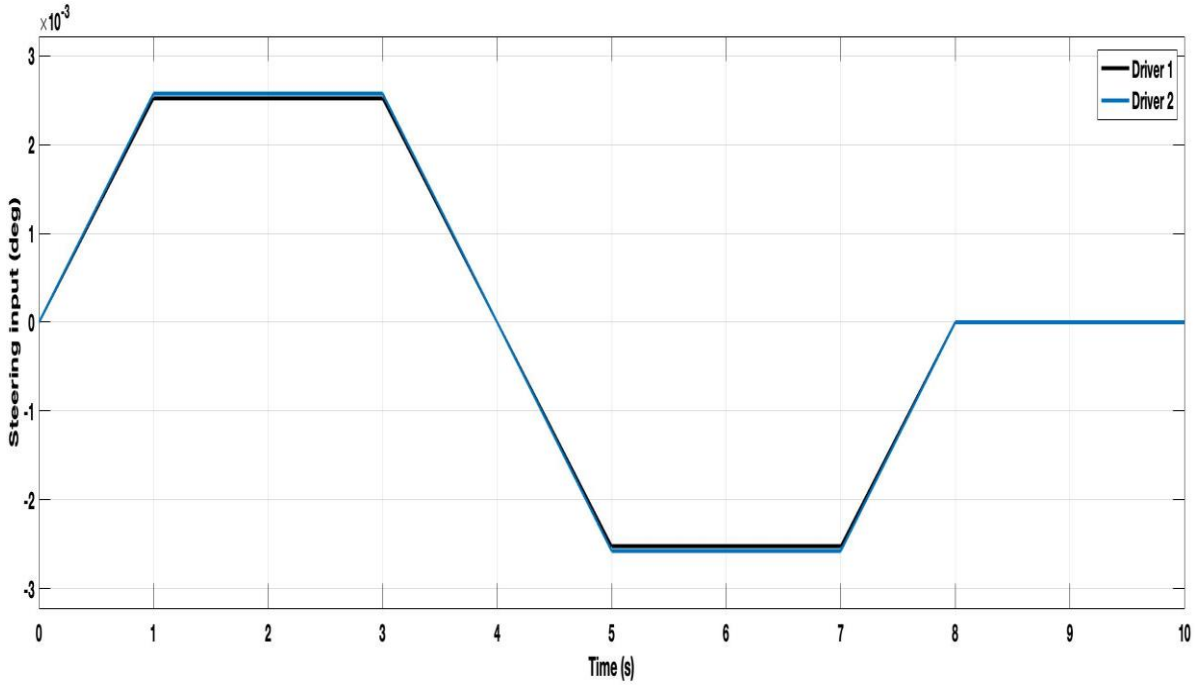

Fig. 6.9. Steering angle input for the driver for a single lane change.

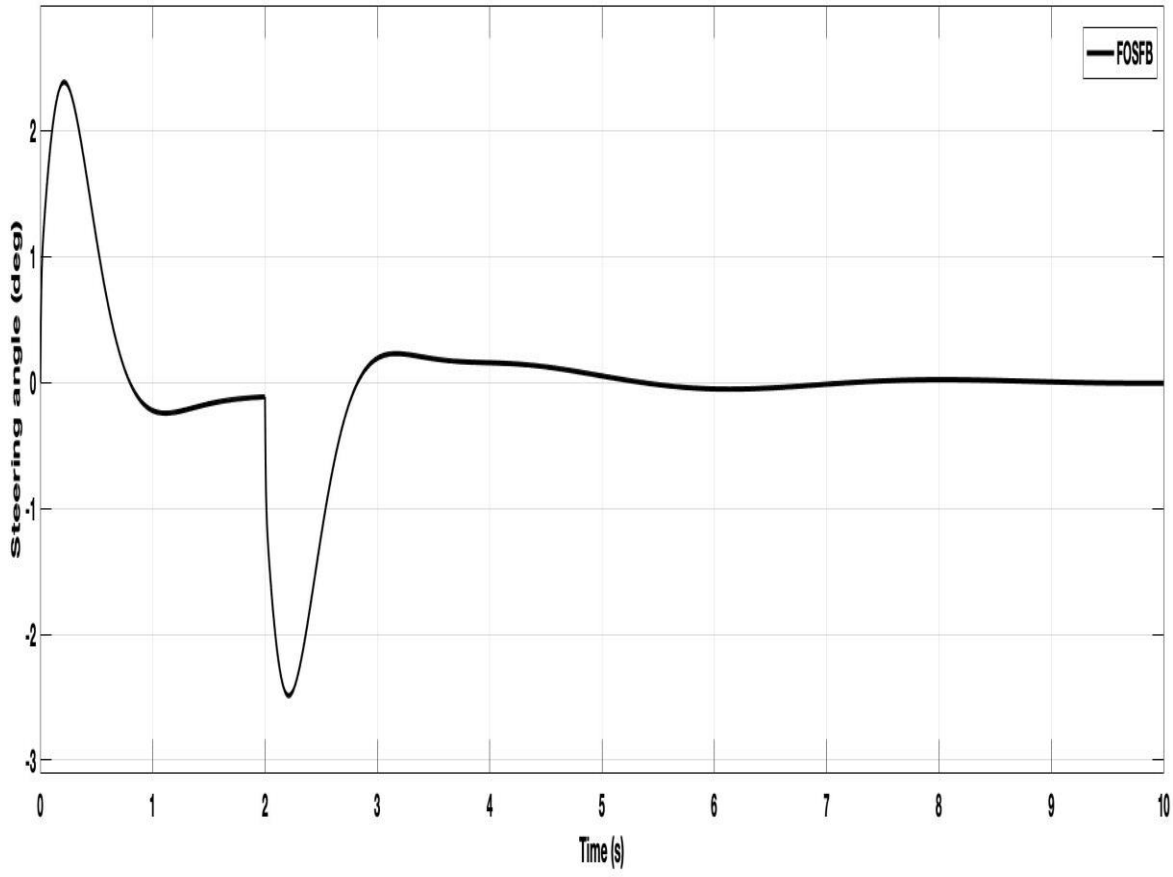

Fig. 6.10. Steering angle with FO state feedback for a single lane change.

With the truck travelling at a highway speed of 70 mph the response time for single lane change is compared to two different professional drivers and the proposed fractional order controller with the desired lane change position as displayed in Fig. 6.11, thus the results confirm that with the FOSFB controller the lane position is improved with faster time response and the tracking for the desired lane is also improved as compared to the professional truck driver.

Furthermore, Fig. 6.11, shows that the professional truck driver takes about 7.5 sec. in order to finish the lane departure, while with the proposed fractional order controller it would take 6 sec. to complete the lane departure. Hence this result confirm one of the objectives of this research to outperform a professional truck driver for an evasive highway maneuver scenario to avoid an obstacle with a 20% time response improvement to change lanes safely. Thus the time response improvement is critical for avoiding a collision quickly and provides improved safety operation for the tractor-trailer in the highways.

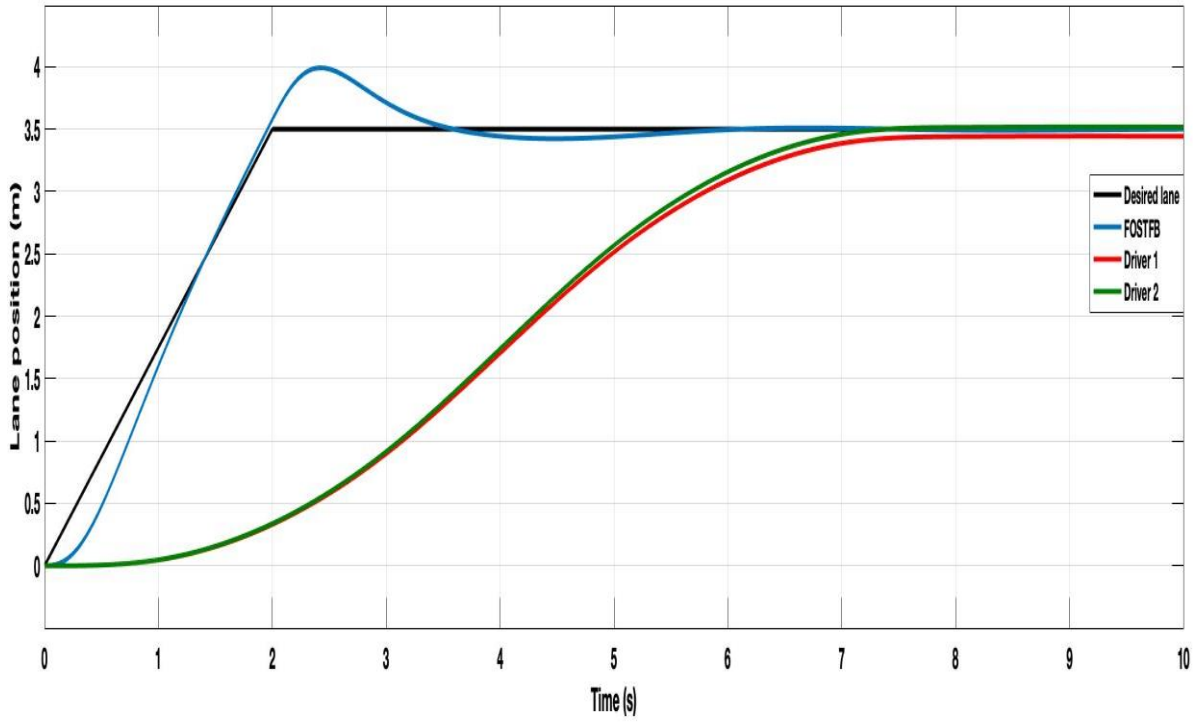

Fig. 6.11. Lane position comparison between the driver and FOSFB for a single lane change.

6.1.3 Evasive maneuver scenario comparison between the driver and FOSFB for a double lane change

The tractor-trailer system is simulated for a double lane change case, where similarly to single lane change the professional driver steering input is pre-defined and is designed based on the uncompensated system in order to emulate a human driver, Figs. 12-13 demonstrations the steering input for the driver and with FOSFB respectively.

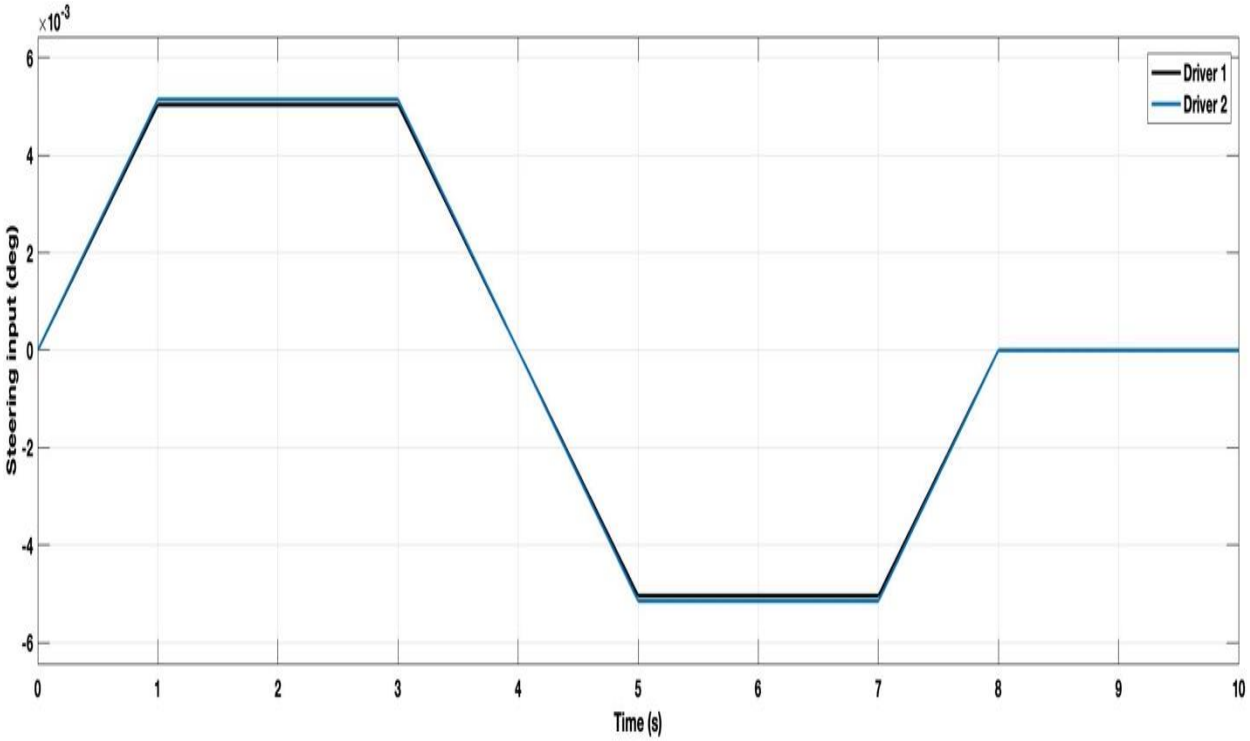

Fig. 6.12. Steering angle input for the driver for a double lane change.

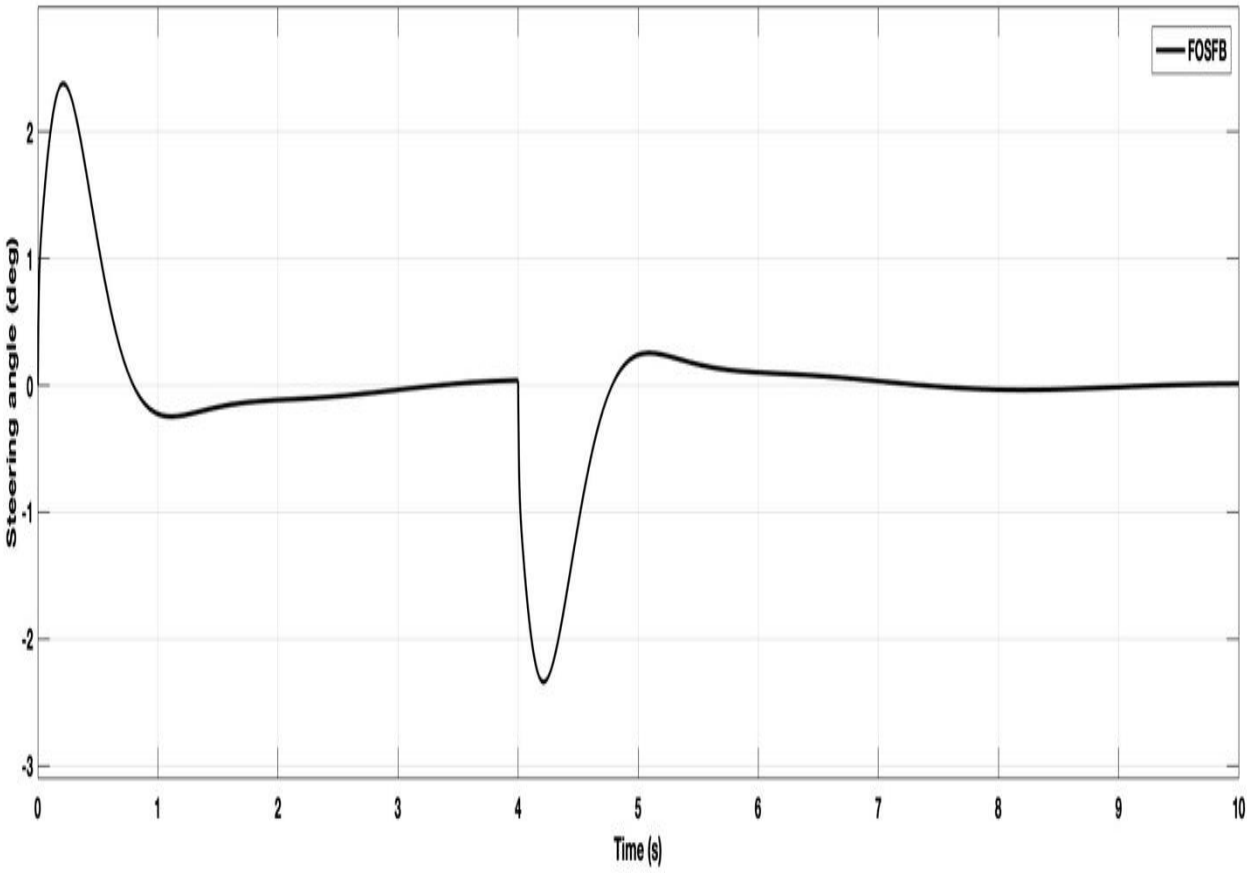

Fig. 6.13. Steering angle with FO state feedback.

Fig. 6.14 shows the double lane position response for the driver and with the FOSFB, thus as can been the tracking for the desired lane position and the time response is improved with the proposed controller to complete the double lane change as compared to driver one and two in Fig. 6.14.

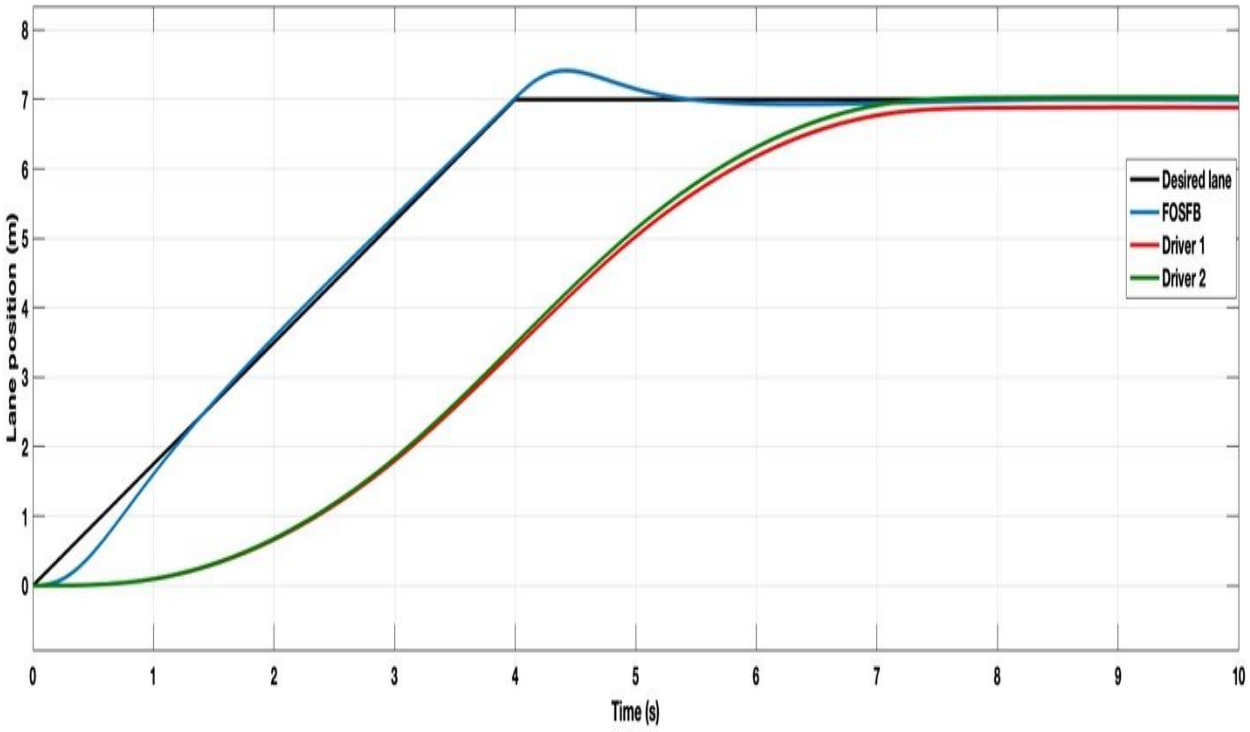

Fig. 6.14. Lane position comparison between the driver and FOSFB for a double lane change.

6.1.4 Evasive maneuver scenario with the trailer partially loaded and over-loaded

The controller is also examined under different loading conditions. This section shows the tractor-trailer response when the trailer is properly loaded, partially loaded and overloaded by a variation of 50%. Fig. 6.15, displays the steering input for these different loading condition. Fig. 6.16 displays the lane position for different loading conditions on the trailer, thus as can been with the FOSFB controller the truck can perform the single lane change safely. Figs. 6.17-6.18 below, presented the trailer yaw and the articulation angle for different loading condition for a single lane change, as can observed the trailer yaw rate would tend decrease when the trailer is partially loaded and increased at the time the trailer is overloaded properly load, also the articulation angle satiability would tend to decrease when the trailer is overload and increase at the time the trailer is partially loaded.

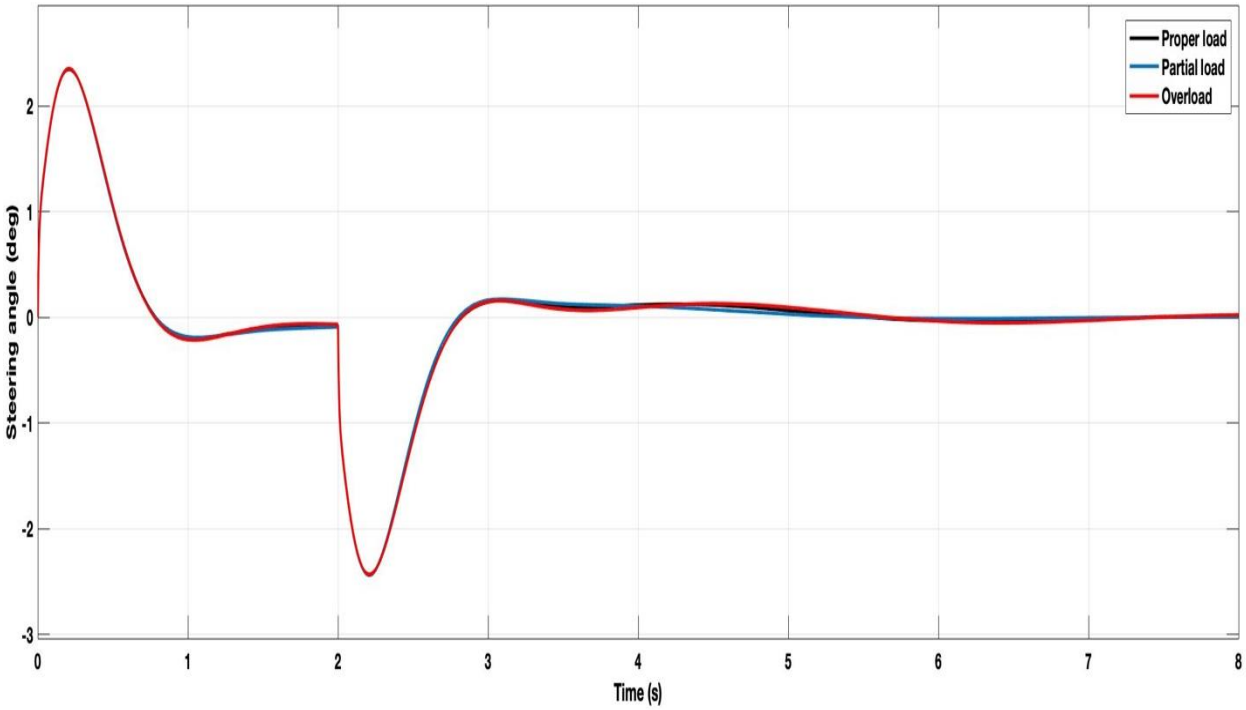

Fig. 6.15. Steering angle for different loading condition of the trailer.

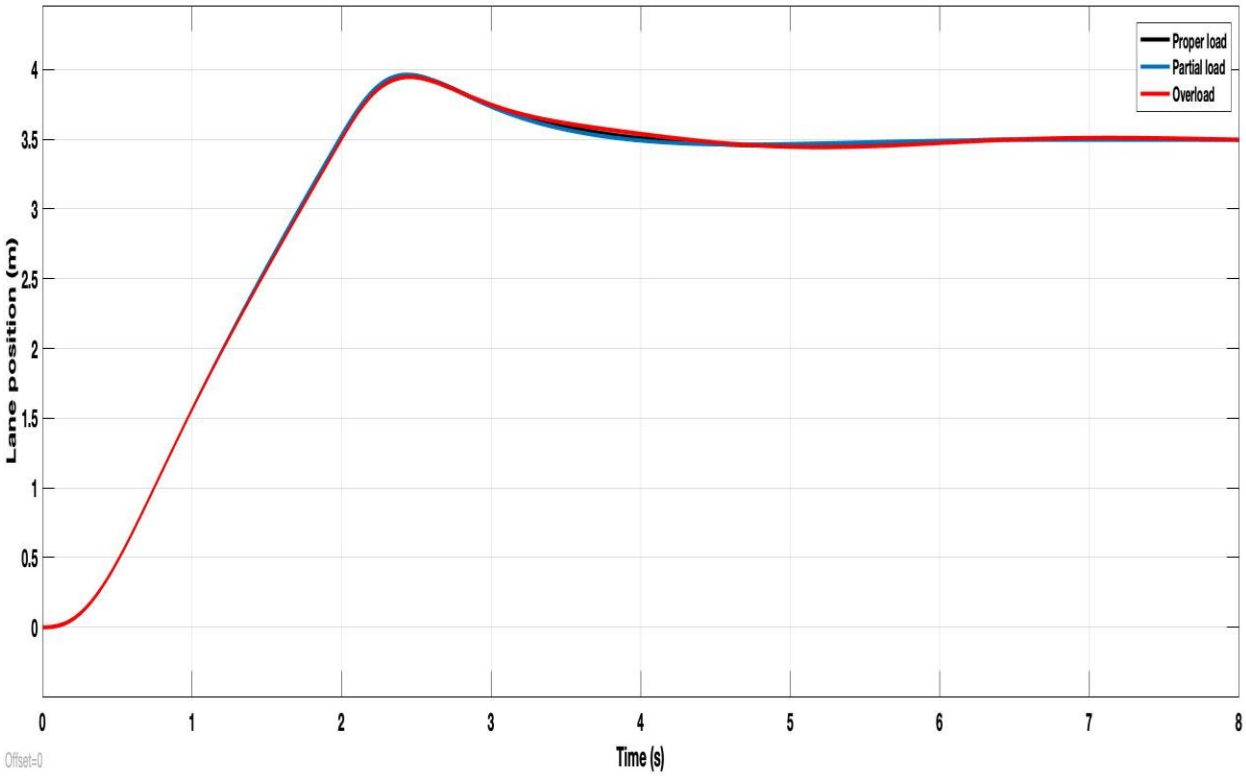

Fig. 6.16. Lane position of the tractor with different loading condition of the trailer.

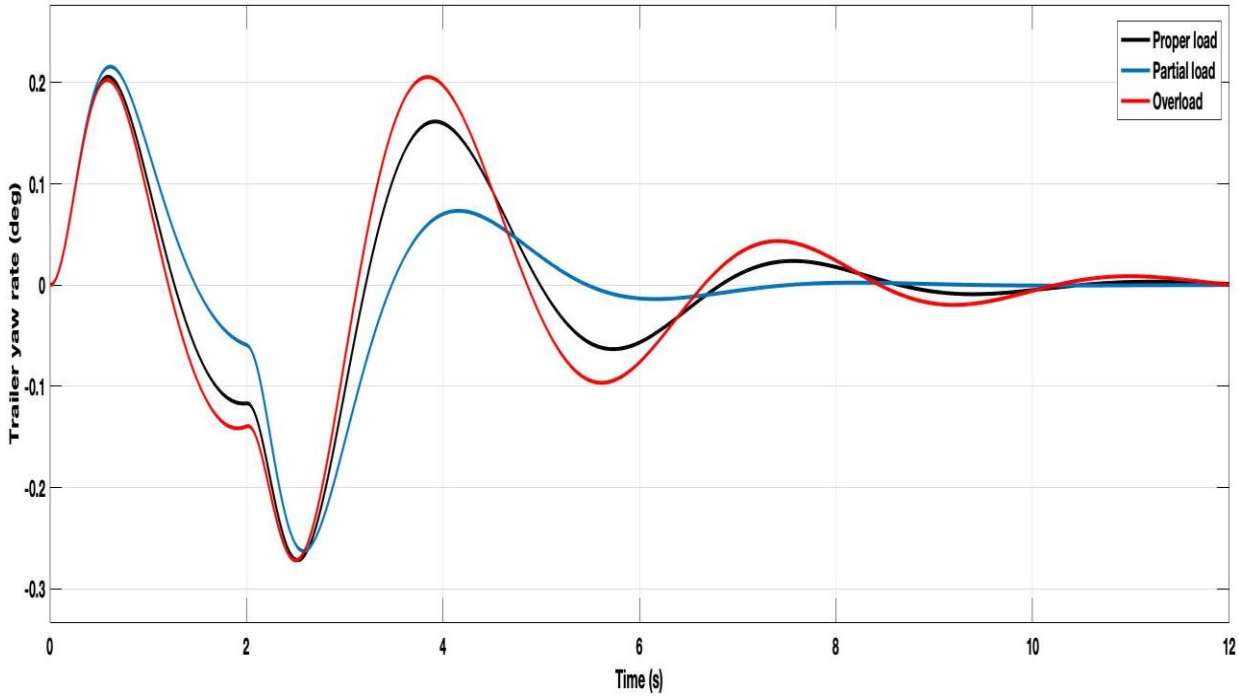

Fig. 6.17. Trailer yaw rate for different loading conditions.

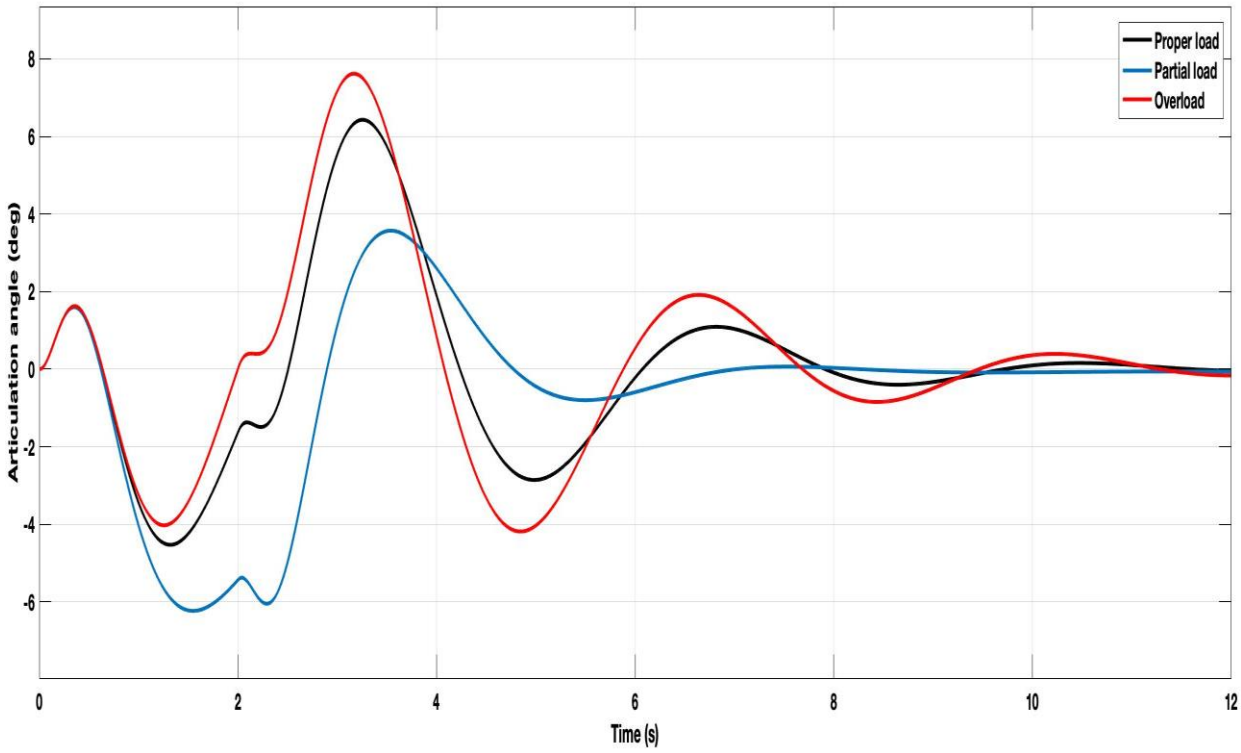

Fig. 6.18. Articulation angle for different loading conditions.

6.1.5 FOSFB control with tire stiffness variation

To show the robustness of the controller, the front tire cornering stiffness c_1 is varied for the truck by an increase and decrease of 50% from the initial value. Fig. 6.19, presents two different cases of the lateral position of the truck while increasing and decreasing the tire stiffness. The results show very similar response to converge at 6 seconds, which confirm the robustness against tire stiffness variation. Fig. 6.20, shows the articulation response for varying the tire stiffness, which also demonstrated the controller robustness.

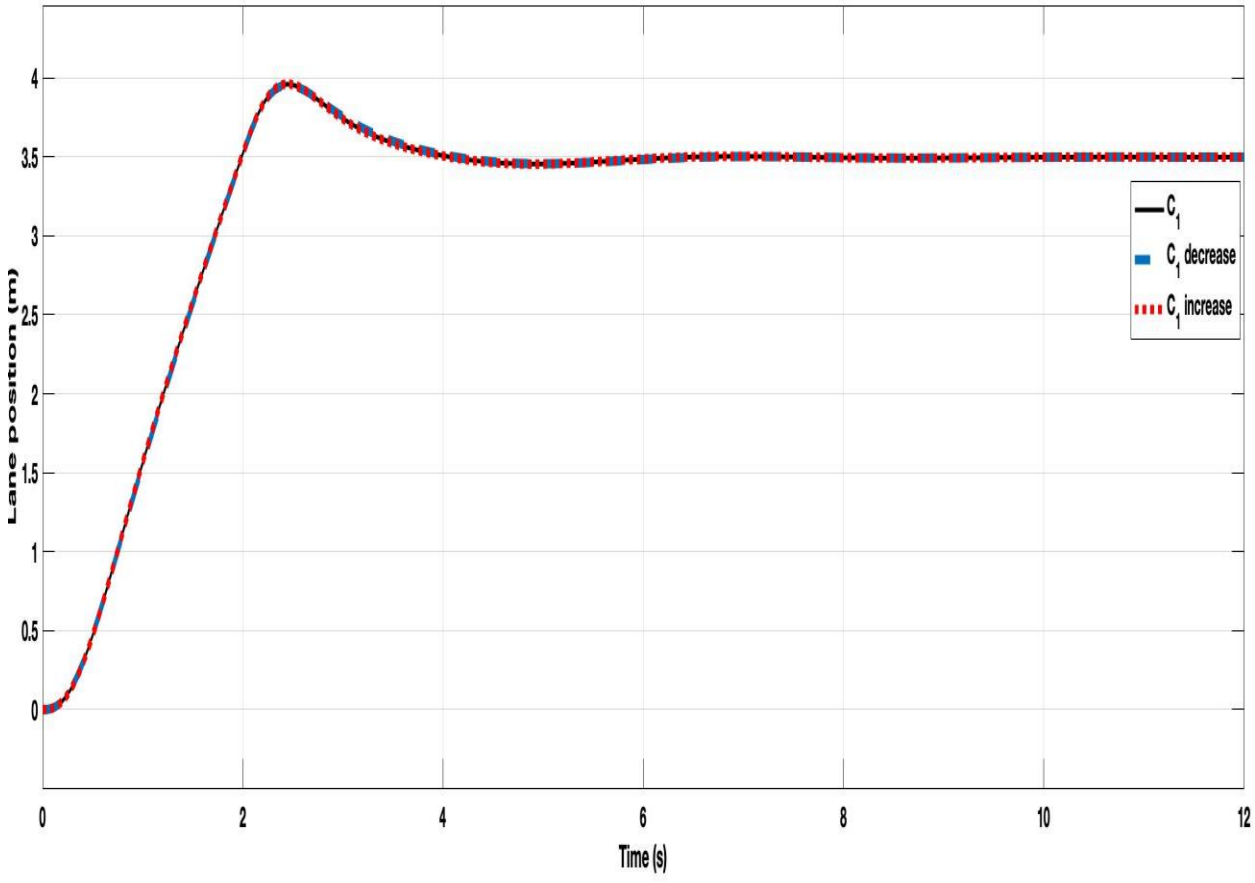

Fig. 6.19. Lateral position of tractor-trailer with varying c_1.

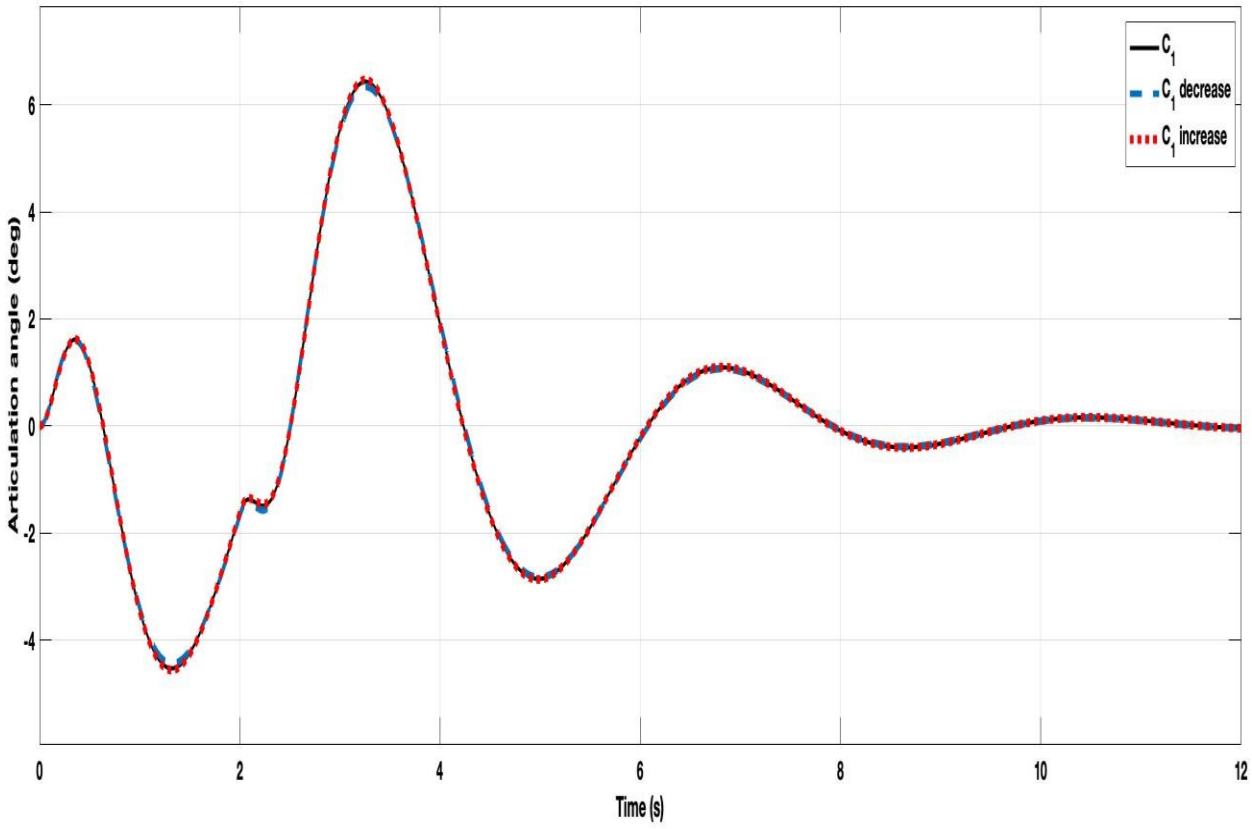

Fig. 6.20. Articulation angel of tractor-trailer with varying c_1.

6.1.6 Wind disturbance rejection (in the same direction) with FOSFB

While effects of the lateral wind disturbances have been also examined under different conditions. As the effects of a side-wind guest acting on the same direction of the trailer while travelling at a speed of 70 mph is examined, thus by adding a positive step disturbance input to equation (6.3). Fig. 6.21 and Fig. 6.22 displays the steering input and the lane position response for the tractor-trailer, as can be seen the truck would have a similar response for completing the lane change successfully with wind disturbance (in the same direction of the trailer) and without the wind-side disturbance.

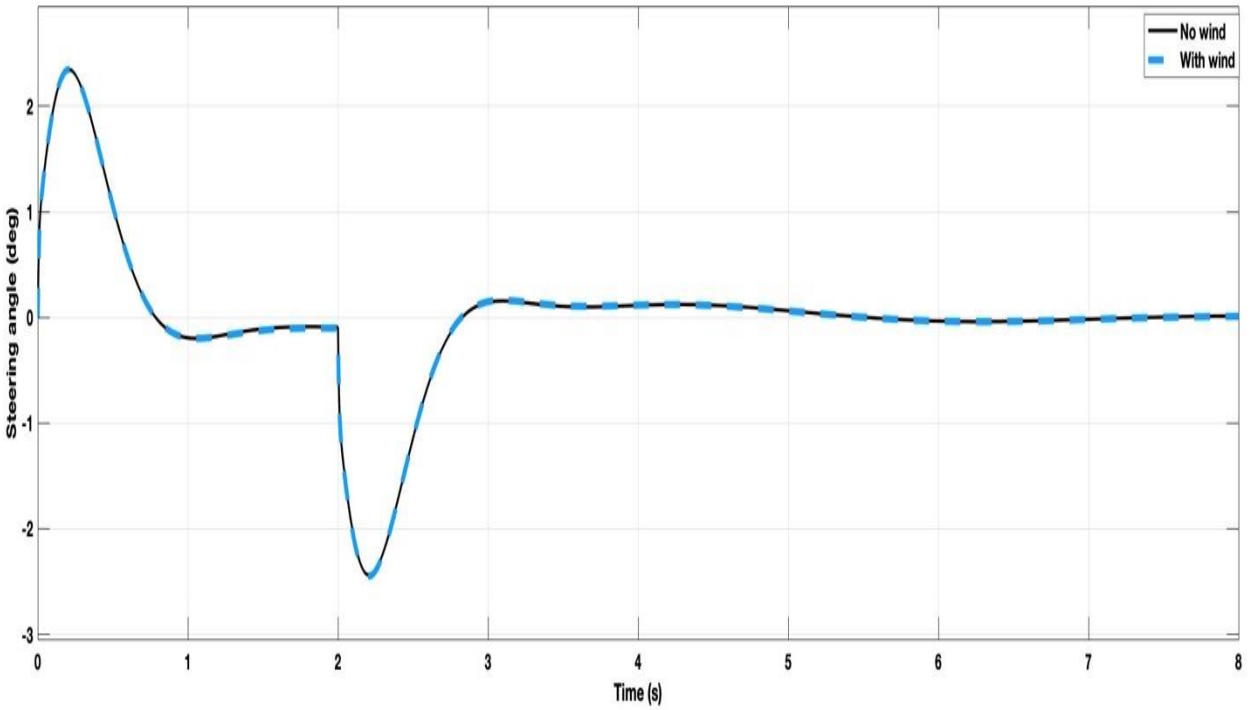

Fig. 6.21. Steering angle with/without wind disturbance at 70 mph.

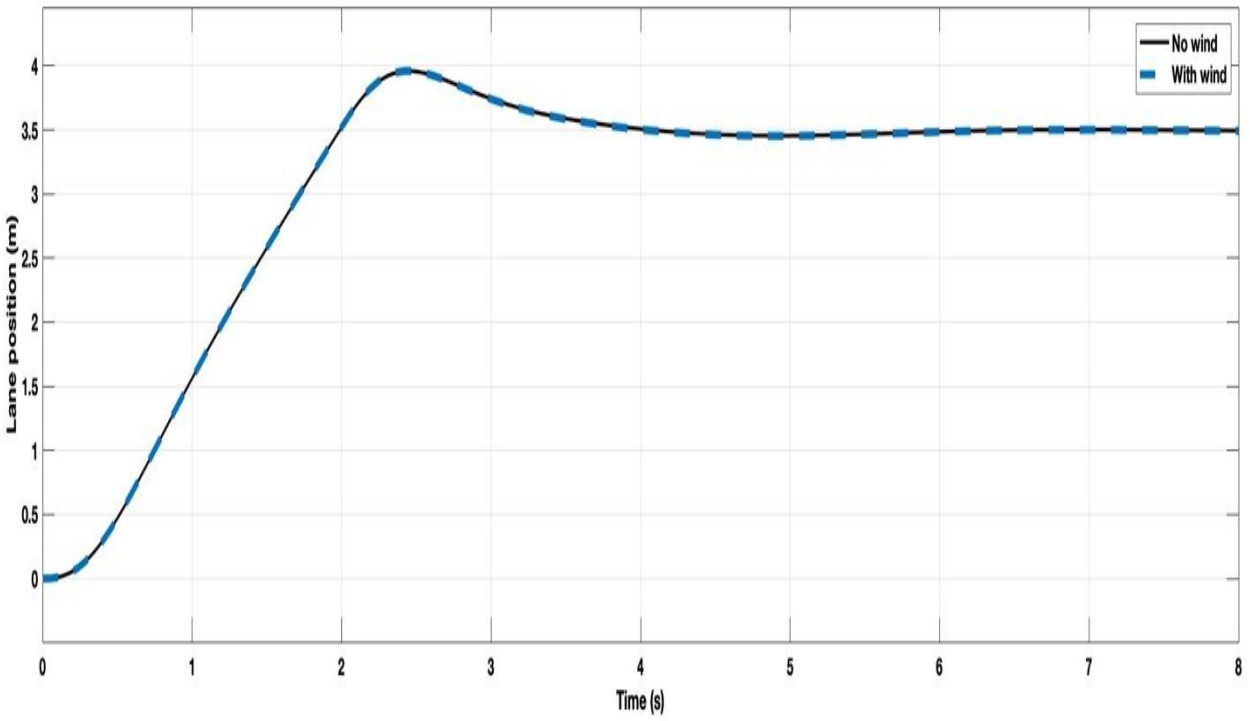

Fig. 6.22. Lane position with/without wind disturbance for a single lane change.

The yaw rates for both tractor and trailer are displayed in Fig. 6.23 and Fig. 6.24, as the simulation results demonstrate the effect of the FOPI state feedback for minimizing the effect of wind guest acting on the trailer, as the trailer yaw rate is slightly increased with the wind acting on the same direction while attempting the single lane change.

The tractor and trailer lateral velocity with wind side disturbance and without the wind disturbance are presented in Fig. 6.25 and Fig. 6.26, as the simulation results show nearly similar response for the lateral velocities, which, conforms the controller performance under side-wind disturbance acting on the same direction of the trailer, while performing a lane departure at a highway speed.

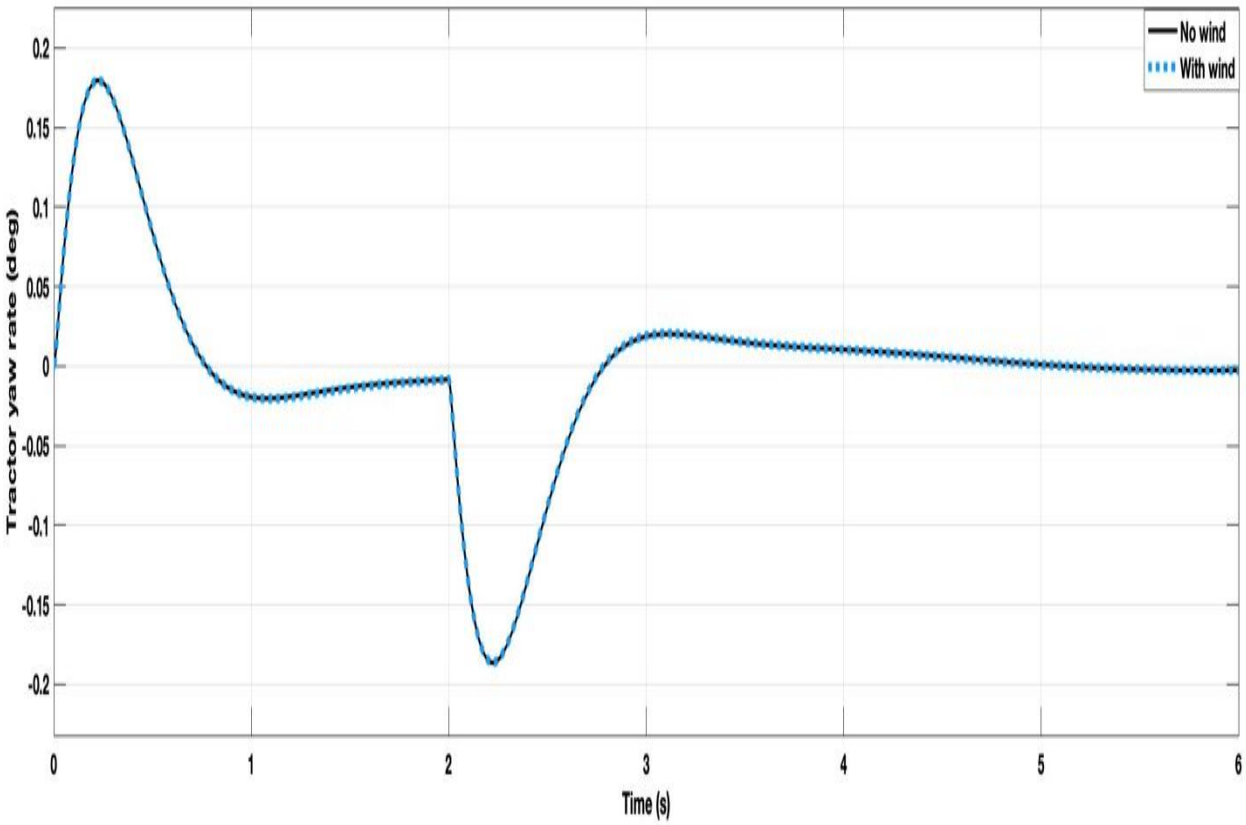

Fig. 6.23. Yaw rate of tractor with/without wind disturbance for a single lane change.

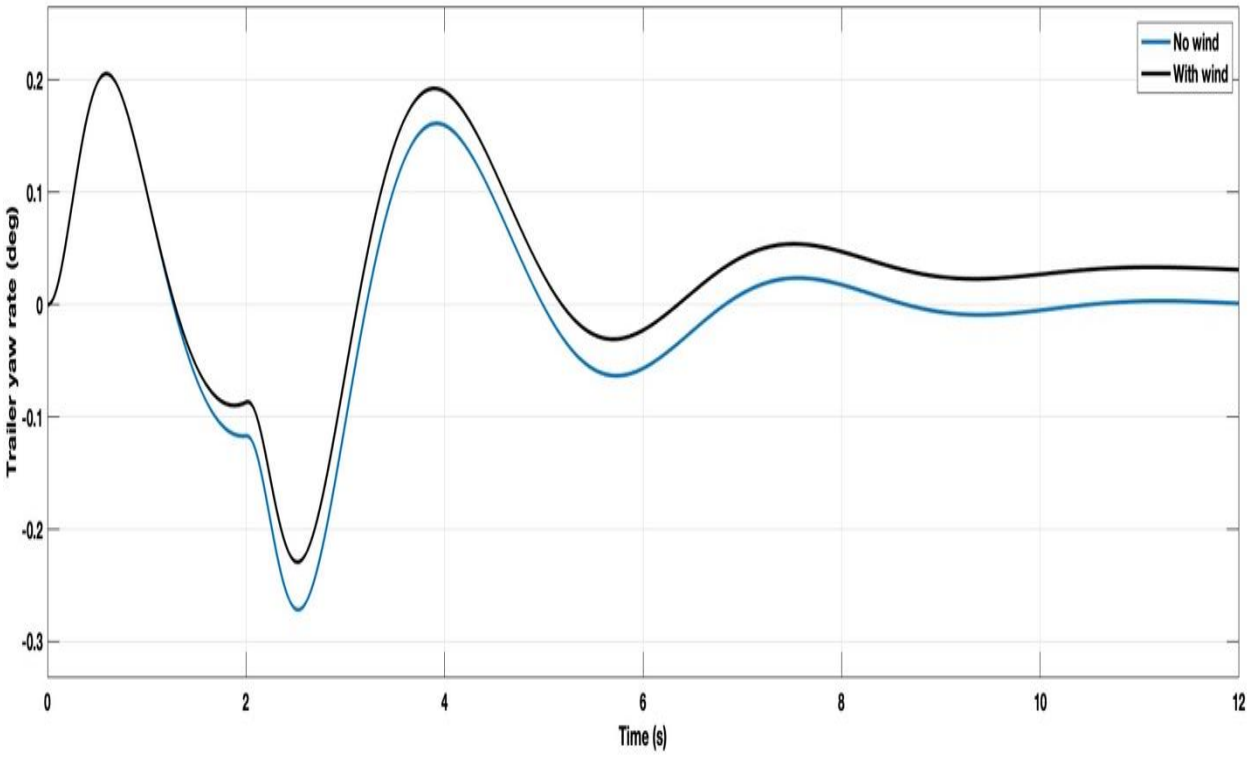

Fig. 6.24. Yaw rate of trailer with/without wind disturbance for a single lane change.

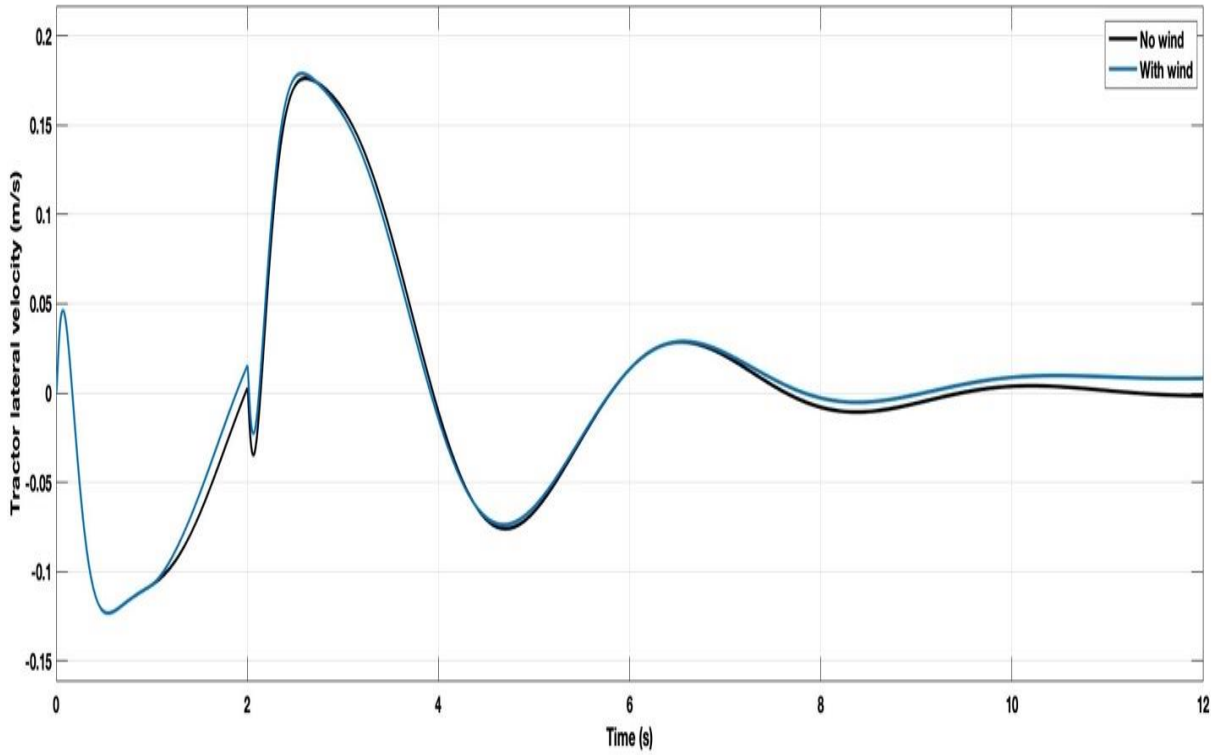

Fig. 6.25. Tractor lateral velocity with/without wind disturbance for a single lane change.

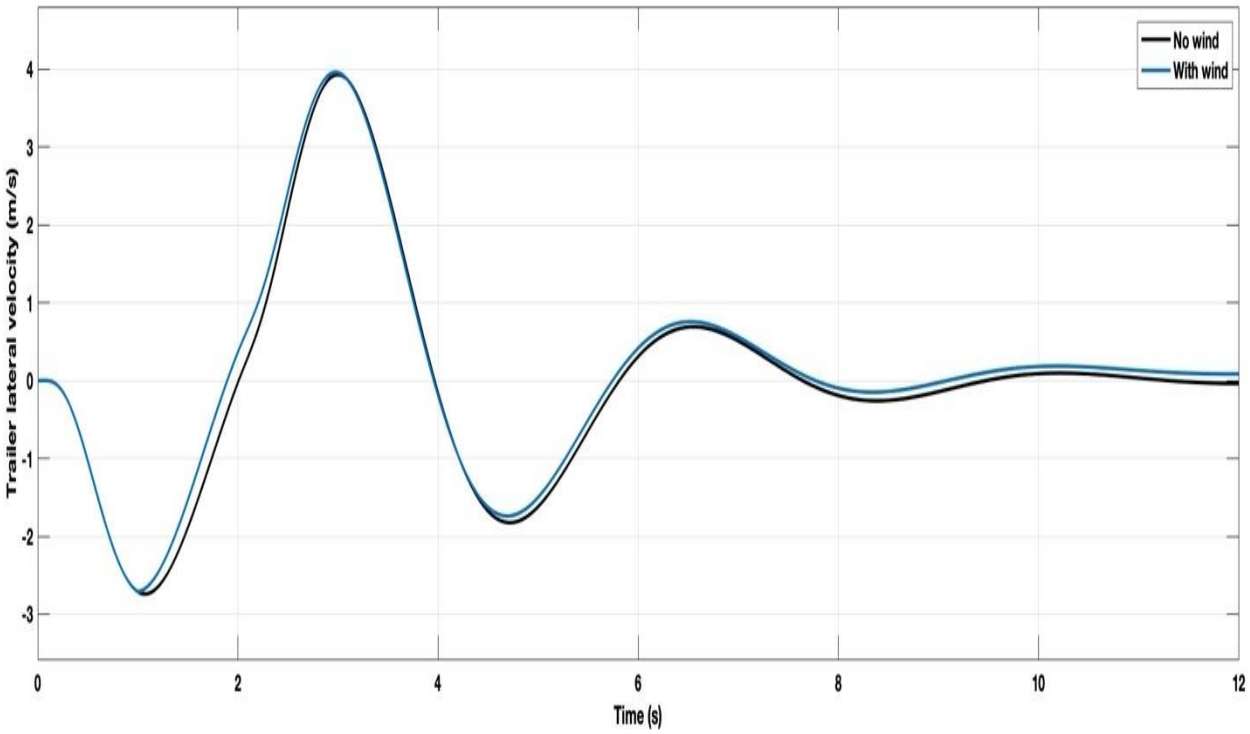

Fig. 6.26. Lateral velocity of the trailer with/without wind disturbance for a single lane change.

6.1.7 Wind disturbance rejection (in the opposite direction) with FOSFB control

To further examine the case when a side-wind disturbance is occurring in the opposite direction of the trailer while attempting the evasive maneuver scenario for a single lane change, consequently by including a negative step input added to equation (6.3) for the trailer. Fig. 6.27 and Fig. 6.28 shows the comparison on the steering angle and the lane position response for the tractor-trailer with the opposite side-wind disturbance and without the wind disturbance. Fig. 6.29-6.30 displays the tractor and trailer yaw rates, hence as the yaw rate of the trailer is marginally increased when there is the wind disturbance acting in the opposing direction of the trailer.

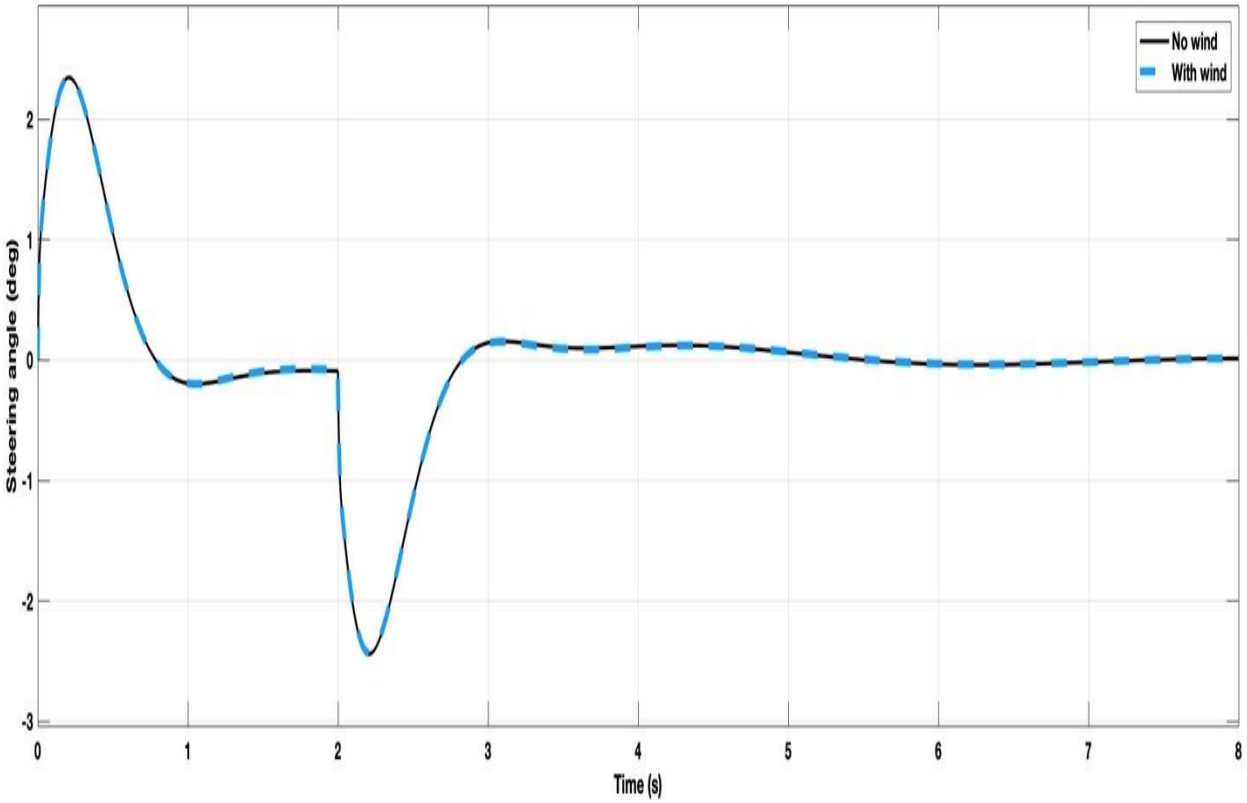

Fig. 6.27. Steering angle with/without wind disturbance in the opposite direction.

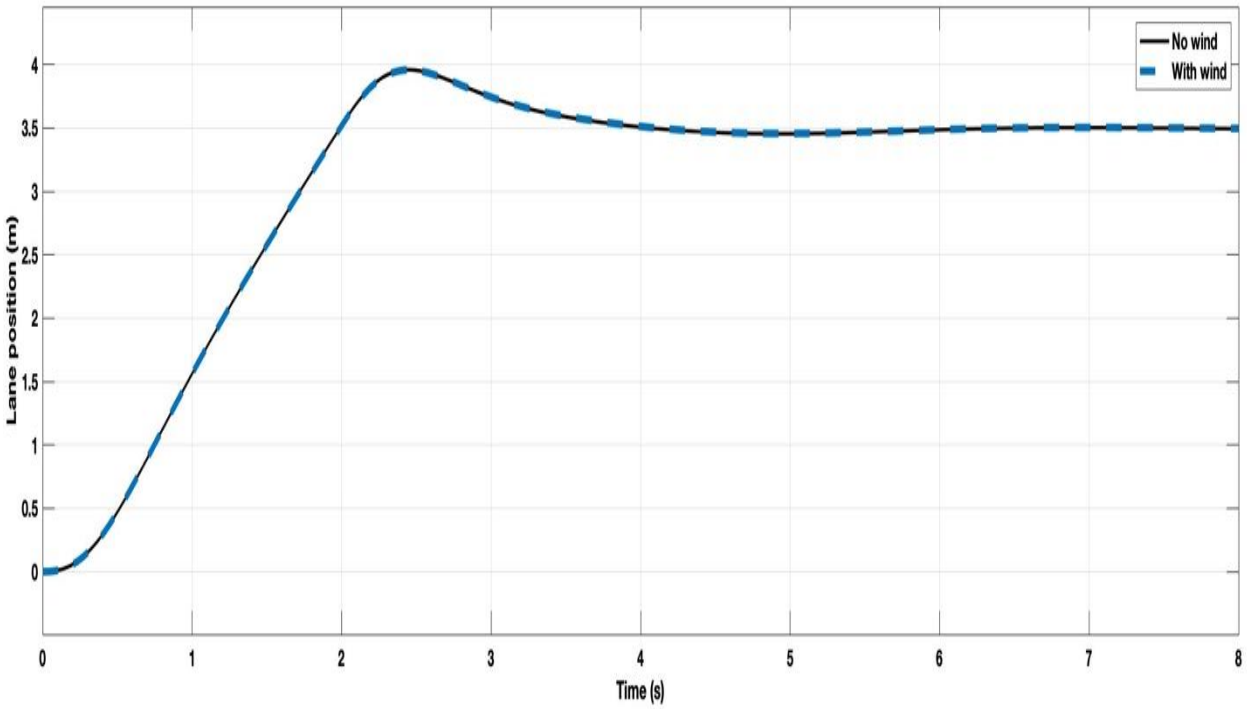

Fig. 6.28. Lane position with/without wind disturbance in the opposite direction.

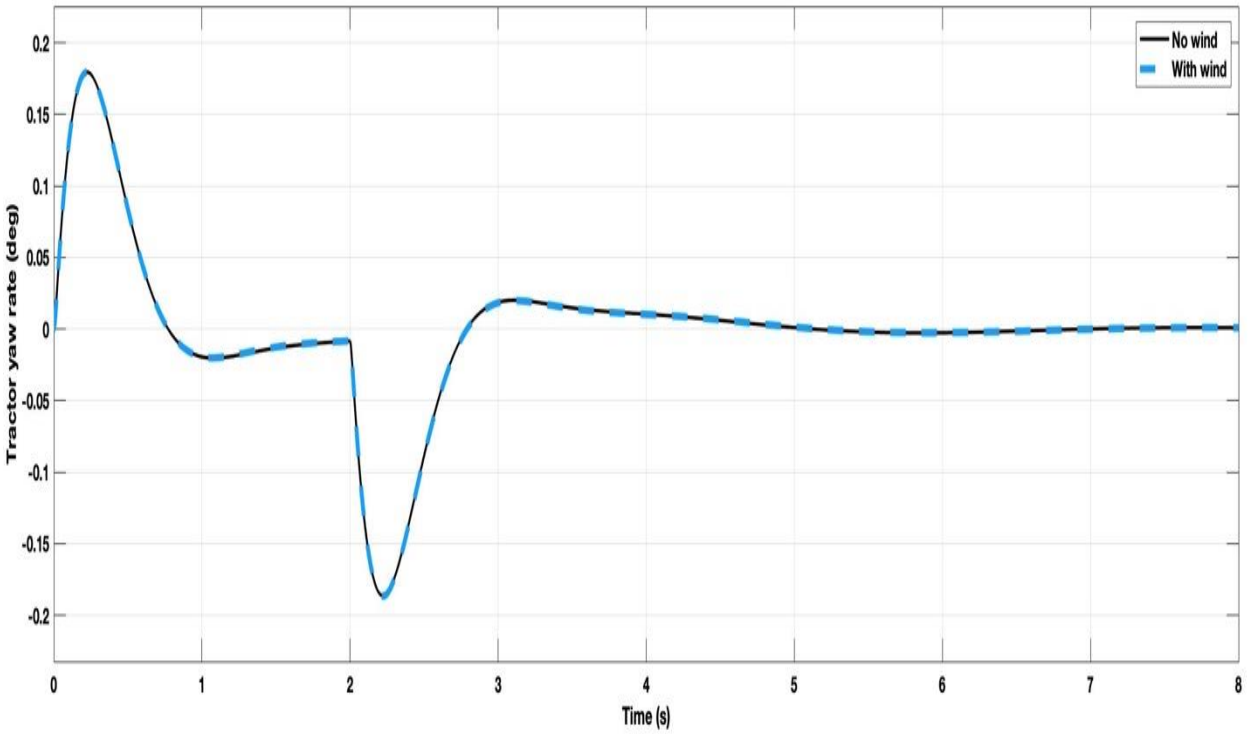

Fig. 6.29. Tractor yaw rate with/without wind disturbance in the opposite direction.

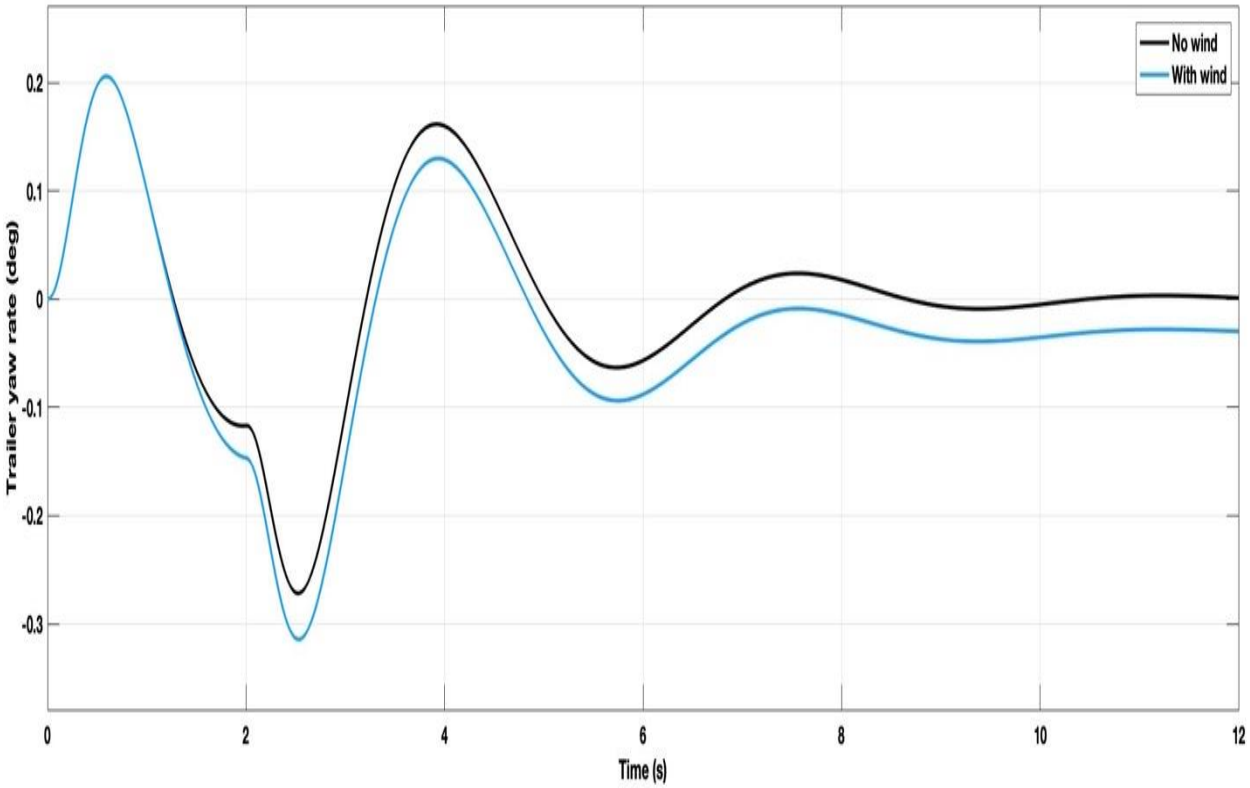

Fig. 6.30. Trailer yaw rate with/without wind disturbance in the opposite direction.

The tractor and trailer lateral velocities are displayed in Fig. 6.31 and Fig. 6.32, as the results shows that the tractor and trailer lateral velocity would marginally increase with the side-wind force acting on the opposite direction of the trailer, while performing the highway single lane change. Hence, these results also confirm the FOSFB performance under side-wind disturbances acting on the trailer opposite direction, as the controller demonstrated the tractor-trailer can perform safety and reject side wind disturbance while travelling at a highway speed.

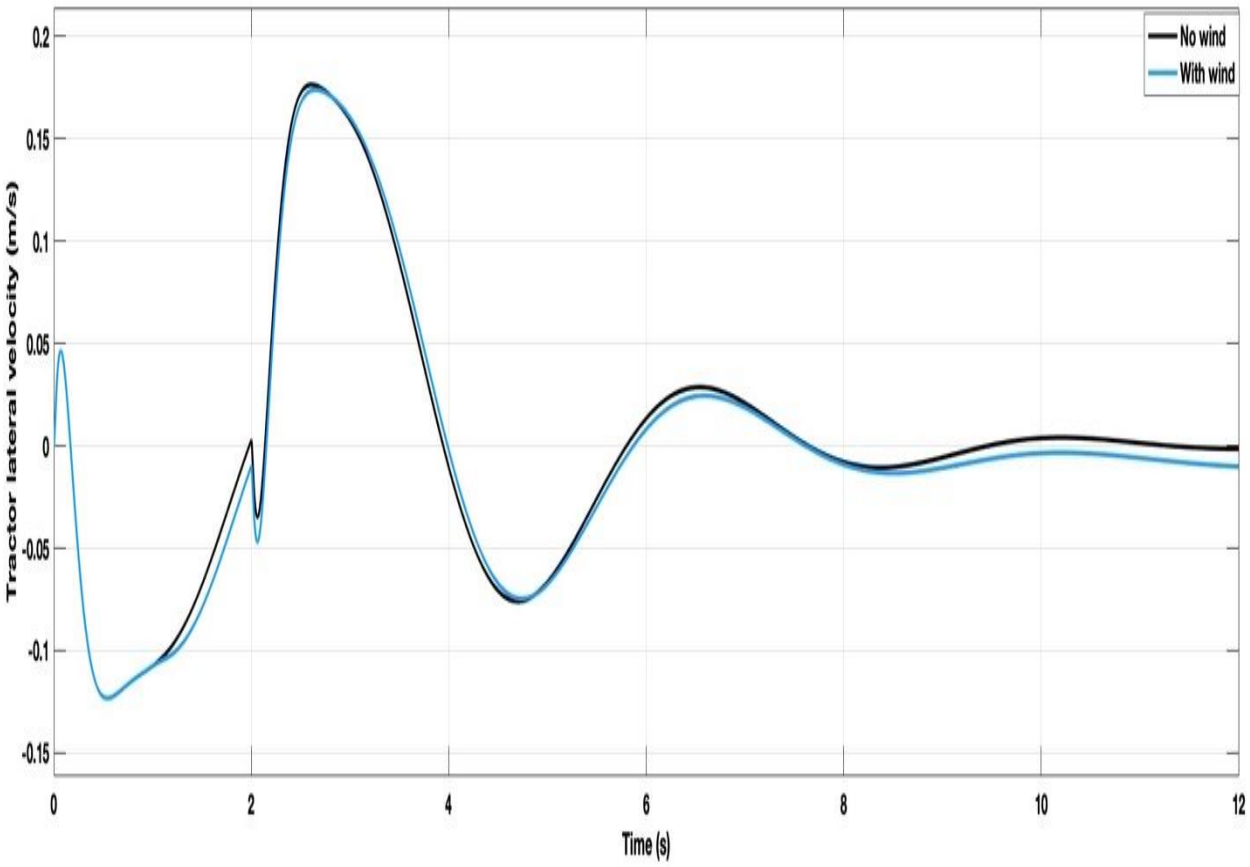

Fig. 6.31. Tractor lateral velocity with/without wind disturbance in the opposite direction.

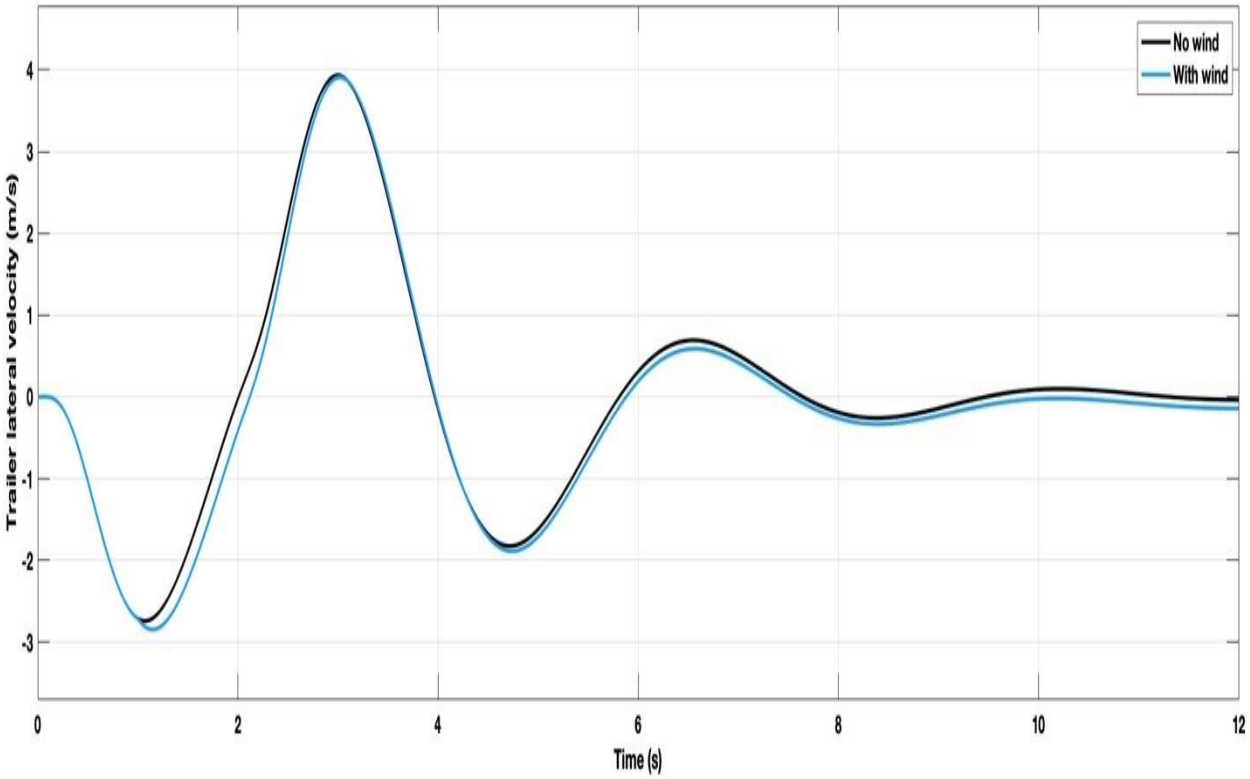

Fig. 6.32. Trailer lateral velocity with/without wind disturbance in the opposite direction.

To conclude this Chapter, where the linear FO controller was applied to the tractor-trailer nonlinear dynamics, which demonstrate the effective of applying the FOSFB controller for the tractor-trailer lateral stability, thus with this new controller design the objective of this research is met by providing an improvement of 20% time response increase over a professional truck driver to changes lanes for an emergency situation, while another objective is met by demonstrating the robustness of the controller for tire stiffness and wind disturbance rejection.

With the fractional order integral control, which included the additional tuning parameter λ that allowed to meet the system requirements and improved the stability margin and response time of the tractor-trailer system. The implanted fractional order controller design would be a new contribution to this field as it has not been examined for this application in any research as of today, as only limited research existed for applying this controller scheme for the controlling the

lateral dynamics of passenger vehicle, while currently no research exists for implanting this controller for tractor-trailer platoons. Hence, in study it has been demonstrated that selecting an optimal fractional order integral value would provide an improved lane position tracking and time response for the tractor-trailer system for an emergency lane change situation and at the same time not degrading other aspects on the system i.e., the lateral acceleration and the articulation angle of the system.

Chapter 7: Conclusion and Future Work

7.1 Conclusion

This section provide a short summary of the work and the findings of this research. A model for a passenger vehicle was presented based on the “bicycle model”. Then this model was extended to model a larger system such as a 3-axle tractor-trailer system, where, the linear and non-linear model for the tractor-trailer system has been analyzed in this dissertation. A highway evasive maneuver scenario was presented, where a new controller design based on fractional calculus: a fractional order state feedback controller was implemented to improve the lateral stability of tractor-trailers in platooning for an emergency lane change.

The concept of active front steering was presented, which can deliver an additional independent steer angle element to the input of the driver that continuously modify the varying steer relation, as this ratio is increased for slow speeds and is decreased for high speeds. The tractor trailer system was controlled through the AFS technique, where the controller design was based on the linear tractor-trailer system, and then the controller was implemented to the highly nonlinear model.

Tractor-trailer platooning technology and the benefits of this operation for heavy commercial articulated vehicles was demonstrated, as this technology is more likely to be fully available for commercial heavy vehicles first on the market due to the prime advantages it can provide for the trucking industry and public safety as opposed to passenger vehicles. Hence the major benefits of the platooning operation include, energy saving, decreased cost for shipping companies, improved safety measurements on the road, reduced traffic congestions and reduced workload on truck drivers.

The tractor-trailer system was analyzed with state feedback controller with only a proportional gain and adding an integrator in the system, as the benefits for adding the integrator term were discussed where the tracking would significantly be improved for tracking a ramp input as the order of the integrator would increase.

The proposed FOPI state feedback controller design was based on the tractor-trailer travelling at a speed of 70 mph, since it is the average highway speed in U.S. highways, where the LQR method was used to obtained the gain values for the state feedback with a higher order fractional integral action, and the a method for choosing the fractional order integrator was presented.

The selection of the optimal fractional order integrator term was based on minimizing the performance index relationship in terms of the tractor-trailer lane position error with the tractor lateral acceleration and the articulation angle with the lane position error. As in was determined that the fractional order integral value equal to 1.4 is the optimal integral value that provides the enhanced lane position tracking for a ramp input and at the same time the stability margin for the tractor-trailer would increase in terms of the articulation angle. Hence for the tractor-trailer system it is critical to have a high stability margin for the lateral evasive maneuver situation in order to maintain the truck regulated during the lane change.

The applied fractional order PI state feedback control scheme through AFS was evaluated with several conditions for an evasive highway lane departure to avoid an obstacle, with variation in the velocity, loading conditions on the trailer, tire cornering stiffens variation and wind disturbance acting on the same and opposite direction of the trailer.

The system with the FO controller improved the time response by 20% as compared to a professional truck driver, which is the main objective of this research. With the proposed controller

the tractor-trailer system would take 6 sec. to completed a lane change safely and being in the center of the lane after the maneuver is completed, while the skilled truck driver averages 7.6 sec. to fully complete the lane departure to avoid the an obstacle in a highway.

Also, the benefits of applying the fractional order integrator as opposed to the classical order integrator were discussed, where with the additional integrator tuning parameter λ, the robustness of the system lane position tracking can be increased, which cannot be obtained with an integer order integrator.

Several other conditions were also presented to confirm the controller robustness against system parameters variations. Simulation results confirmed the controller for maintaining stability for system disturbances such as, wind force disturbance occurring on the trailer and the variation of the tire cornering stiffness.

Applying a fractional order controller for this application is a new contribution to the field as this controller has not been implemented for this system as of today and it will open many new research investigations on fractional order controllers, especially for automated systems. Thus, the fractional integral control has demonstrated the effectiveness of using a small order power for the integrator in order to achieve a higher stability margin and a fast time response for an evasive maneuver circumstance.

7.2 Future work

For future work, the proposed control algorithm can implemented for a real time simulation for a hardware in the loop implantation as this type of fractional order controller for this application has not been implanted as of today in real time. Thus, modeling this type of system as a fractional

order model will be highly beneficial since the trailer-trailer model will be more accurately molded as compared to an integer-order modeling and thus providing more accurate results.

Also another improvement in terms of energy consumption besides the platooning operation, is that the controller scheme can be applied for electric (hybrid) tractor-trailers platoons for increased green technologies and reduced emissions.

8 References

[1] E. Chao, J. Rosen, P. Hu and R. Schmitt, “Freight facts and figures 2017,” U.S. department of transpiration and Bureau of transportation statistics, 2017.

[2] S. Tsugawa, S. Jeschke and S. Shladovers,”A review of Truck Platooning projects for energy savings,” *IEEE Trans. on intelligent vehicles,* vol.1, March 2016.

[3] J.Felez, “Control Design of an articulated truck with autonomous driving in an electrified highway, IEEE 2018.

[4] Q. Li, G. Shi, J. Wei and Y. Lin, "Yaw stability control of active front steering with fractional order PID controller," *International Conference on Information Engineering and Computer Science*, Wuhan, pp.1-4, 2009.

[5] NHTSA national center of statistics and analysis, “Traffic safety facts for large trucks,” NHTSA report DOT HS 812 497, 2018.

[6] U.S Department of Transportation Federal Highway Administration, Nov. 2017 [online]. Available: https://safety.fhwa.dot.gov/roadway_dept/

[7] X. Diao, Y. Jin, L. Ma, S. Ding and H. Jiang, "Composite active front steering controller design for vehicle system," *IEEE Access*, vol. 5, pp. 6697-6706, 2017.

[8] X. Jin, G. Yin and N. Chen, “Gain-scheduled robust control for lateral stability of four-wheel -independent-drive electric vehicles via linear parameter-varying technique,” *Mechatronics,* vol.30 , pp.286-296, 2015.

[9] S. Vempaty and Y. He, “A review of car trailer lateral stability control approaches,” *SAE technical paper,* 2017.

[10] B. Bandyopadhyay and S. Spurgeon, *Advances in sliding model: concept, theory and implementation*, Springer, 2013.

[11] R. McCann and A. Le, "Electric motor based steering for jackknife avoidance in large trucks," *IEEE Vehicle Power and Propulsion Conference,* Issue 7-9 September, 2005.

[12] H. Zhang and J. Wang, “Vehicle lateral dynamics control through AFS/DYC and robust gain-scheduling approach,” *IEEE Trans. on vehicular technology,* Vol. 65, No. 1, Jan., 2016.

[13] A. Riofrio, S. Sanz, M. L. Boada and B. L. Boada, “A LQR-based controller with estimation of road bank for improving vehicle lateral and rollover stability via active suspension,” *Sensors,*vol.17:10, Oct. 2017.

[14] S. Oreh, R. Kazemi and S. Azadi, “A sliding-mode controller for directional control of articulated heavy vehicles,” *Proceedings of the institute of mechanical engineers part d: journal of automobile engineering*, Vol. 228, No. 3, pp.245-262, 2014

[15] S. Fergani, O. Sename and L. Dugard, “ An LPV/H_∞integrated vehicle dynamic controller,” IEEE Trans. on vehicular technology, Vol. 65, No. 4, April, 2016.

[16] J. Wang, M. Tomizuka, “Dynamic analyses and robust steering controller design for automated lane guidance of heavy-duty vehicles,” *Asian journal of control*, Vol. 2, No. 3, pp.140-154, 2008.

[17] C. Ching-Yao and T. Han-Shue, “Feasibility analysis of steering control as a driver-assistance function in collision situations,” IEEE Trans. Intell. Transp. Syst., vol. 2, no. 1, pp. 1–9, Mar. 2001.

[18] M. Nagai, M. Onda, and T. Katagiri, “Simulation of emergency obstacle avoidance situations using genetic algorithm,” JSAE Rev., vol. 18, pp. 158– 160, 1997.

[19] S. Vempaty, E. Lee and Y. He, “Model-reference based adaptive control for enhancing lateral stability of car-trailer systems,” ASME international mechanical engineering congress and exposition, transportation systems, Vol. 12, 2016.

[20] L. Li, H. Wang, J. Lian, X. Ding and W. Cao “ A lateral control method of intelligent vehicle based on fuzzy neural network,” *SAGE journals, advances in mechanical engineering*, Vol. 7, No. 1, 2015.

[21] SAE level of automation available on https://www.nhtsa.gov/technology-innovation/automated-vehicles-safety

[22] US. Department of transportation, National Highway traffic safety Administration, "Critical Reasons for crashes investigated in the national moto vehicle crash causation survey,” February 2015.

[23] D. Blower and J. Woodroofe, “Survey of the status of truck safety: Brazil, China, Australia and United States,” The University of Michigan, transportation research institute, report No. UMTRI-2012-13, May, 2012.

[24] Y. Chen and J. Wang, "Personalized Vehicle Path Following Based on Robust Gain-scheduling Control in Lane-changing and Left-turning Maneuvers," *2018 Annual American Control Conference (ACC)*, Milwaukee, WI, 2018, pp. 4784-4789.

[25] G. Meyer and S.Beiker, *Road vehicle automation 5*, Springer pp.149-162, 2019.

[26] S.Tsugawa," An overview on an automated truck platoon within the energy ITS project," *7th IFAC symposium on advances in automotive control*, vol. 46, no. 21, pp.41-46, 2013.

[27] C. Chen and M. Tomizuka, "Lateral control of commercial heavy vehicles," Vehicle system dynamics, Vol.33, pp.391-420, 2000.

[28] S. Li, G. Wang, B. Zhang, Z. Yu and G. Cui, "Vehicle stability control based on model predictive control considering the changing trend of tire force over the prediction horizon," in *IEEE Access*, Vol. 7, pp.6677-6888, 2019.

[29] R. Rajamani, *Vehicle Dynamics and control.* Switzerland: Springer, 2012.

[30] S. Mammar and D. Koenig, ''Vehicle handling improvement by active steering,'' *Vehicle System Dynamics,International Journal of vehicle mechanics and mobility*., vol. 38, no. 38, pp 211–242, 2002.

[31] P. Falconea, H. Tsengb, F. Borrellic, J. Asgarib, and D. Hrovatb, ''MPC-based yaw and lateral stabilization via active front steering and braking,'' *Vehicle System Dynamics, International Journal of vehicle mechanics and mobility*, vol. 46, no. S.1, pp. 611–628, 2008.

[32] J. Kasselmann and T. Keraned, "Adaptive steering," *Bendix Technical Journal*, vol. 2, pp.26-35, 1969.

[33] A. Farazandeh, A. Ahmad and S. Rzkheja, "Braking and steering performance analysis of a road vehicle with active independent front steering," *International Journal of heavy vehicle systems*, Vol. 22, No. 3, 2015.

[34] X. Na and D. J. Cole, "Application of Open-Loop Stackelberg Equilibrium to Modeling a Driver's Interaction with Vehicle Active Steering Control in Obstacle Avoidance," in *IEEE Transactions on Human-Machine Systems*, vol. 47, no. 5, pp. 673-685, Oct. 2017.

[35] C. March and T. Shim, ''Integrated control of suspension and front steering to enhance vehicle handling,'' Proc. Inst. Mech. Eng. D J. Autom. Eng., vol. 221, no. 221, pp. 377–391, 2007.

[36] X. Ma, P. Wong, J. Zhao and Z. Xie, "Cornering stability control for vehicles with active front steering system using T-S fuzzy based sliding mode control strategy," *Mechanical Systems and Signal Processing*,Vol. 125, pp. 347-364 , 2019.

[37] X. Huang, H. Zhang, G. Zhang and J. Wang, "Robust Weighted Gain-Scheduling H∞ Vehicle Lateral Motion Control With Considerations of Steering System Backlash-Type Hysteresis," in *IEEE Transactions on Control Systems Technology*, vol. 22, no. 5, pp. 1740-1753, Sept. 2014.

[38] M. Nagai and M. Shino, ‘‘Study on integrated control of active front steer angle and direct yaw moment,’’ JSAE Rev., vol. 23, no. 3, pp. 309–315, 2002.

[39] S. Çağlar Baslamisli, İ. Emre Köse & G. Anlaş," Gain-scheduled integrated active steering and differential control for vehicle handling improvement," Vehicle System Dynamics, 47:1, 99-119, 2009

[40] D. Odenthal, T. Bünte and J. Ackermann, "Nonlinear steering and braking control for vehicle rollover avoidance," *1999 European Control Conference (ECC)*, Karlsruhe, 1999, pp. 598-603.

[41] Zhang, J.Y., Kim, J.W., Lee, K.B. and Kim, Y.B. "Development of an active front steering (AFS) system with QFT control," *International Journal of Automotive Technology*, 9(6), pp. 695-702, 2008.

[42] S. Zheng *et al*., "Model predictive control based vehicle stability control via active front steering," *2017 Chinese Automation Congress (CAC)*, Jinan, 2017, pp. 4660-4665.

[43] Koehn, P. and Eckrich, M. (2004) Active steering–the BMW approach towards modern steering technology, SAE Technical Paper no. 2004-01-1105.

[44] R. McCann and S. Nguyen, "Jackknife avoidance in large trucking using active front steering," *SAE Technical paper*, 2004

[45] A.Kumar and D.Kamble, " An overview of active front steering system," International Journal of Scientific & Engineering Research, Vol 3,Issue 6, June, 2012.

[46] Y. Xia, F. Pu, S. Li and Y. Gao, "Lateral path tracking control of autonomous land vehicle based on ADRC and differential flatness," *IEEE Transactions on Industrial Electronics*, vol. 63, no. 5, pp. 3091-3099, May, 2016.

[47] M. Brault, "Americans with disabilities: 2010 household economic studies," United States Census Bureau, July, 2012.

[48] J. Zmud, F. Diaz, P. Lavieri, C. Bhat and R. Pendyala, Research to examine behavioral Responses to automated vehicles, Road Vehicle Automation 5, 2019.

[49] K. Bimbraw, "Autonomous cars: Past, present and future a review of the developments in the last century, the present scenario and the expected future of autonomous vehicle technology," in Proc. Int. Conf. Informat. Control, Automat. Robot. (ICINCO), Colmar, France, Jul. 2015, pp. 191–198.

[50] K. Divakaral, A. Amadi and S. Razavi, " A Cognitive Advanced Driver Assistance Systems Architecture for Autonomous-Capable Electrified Vehicles," IEEE Trans. On transportation electrification, Vol. 5, No. 1, March 2019.

[51] K. Bengler, K. Dietmayer, B. Farber, M. Maurer, C. Stiller, and H. Winner, “Three decades of driver assistance systems: Review and future perspectives,” I*EEE Intelligent. Transpiration System Magzine*, vol. 6, no. 4, pp. 6–22, Oct. 2014.

[52] J. Zmud, I. Sener, C. Simek and P. Gigante, “ Who’s first: early adopters of self-driving vehicles,” Texas A&M Transportation Institute, College station, 2018.

[53] P. Lavieri, V. Garikapati, C. Bhat, R. Pendyala, S. Astroza and F. Dias, “Modeling Individual preferences for ownership and sharing of autonomous vehicle technologies,” Transp. Res Rec 2665:1-10, 2017.

[54] Z. Lenkyseteme GmbH and S. Gmund, “Concept and functionality of active front steering system,” SAE international, 2004.

[55] S. Bin and J. PengKai, "The analysis and modeling of active front steering system," *2011 IEEE 2nd International Conference on Computing, Control and Industrial Engineering*, Wuhan, 2011, pp. 237-242.

[56] R. Isermann, R. Mannale and K. Schmitt, “Collision-avoidance systems PRORETA: Situation analysis and intervention control,” Control Engineering Practice, vol.20, pp.1236-1246, 2012.

[57] Felix Ammah-Tagoe, “Freight in America,” Research and Innovative Technology Administration, Bureau of Transportation Statistics, Jan. 2006.

[58] P. Gaspar, Z. Szabo, J. Bokor and B. Nemeth, *Robust Control Design for Active Driver Assistance Systems a Linear-Parameter-Varying Approach.* Switzerland: Springer International Publishing AG, 2017.

[59] European Truck Platooning, 2016. Available [online] https://www.eutruckplatooning.com/Press/Photos+Volvo/default.aspx

[60] M. Lammert, B. Bugbee, Y. Hou and A. Mack, “Exploring telematics big data for truck platooning opportunities,” *SAE Technical paper*, DOI: 10.4271/2018-01-1083, 2018.

[61] B.McAuliffe, M.Lammert, X. Lu and S. Shladover, “Influences on energy savings of heavy trucks using cooperative adaptive cruise control,” *SAE Technical paper*, DOI: 10.4271/2018-01-1181, 2018.

[62] S. Hoef, “Coordination of heavy-duty vehicles platooning,” Ph.D thesis, Department of Electrical Engineering, KTH Royal Institute of Technology, 2018.

[63] Y.Sugimoto, S. Kuzumaki, SIP-adus an update on Japanese initives for automated driving Road Vehicle Automation 5, Lecture notes in mobilty, 2019.

[64] J. Engstrom, R. Bishop, S.Shadover, M. Murray and L. Rourke, "Deployment of automated trucking: challenges and opportunities," road vehicle automation 5, 2019.

[65] Peloton overview of driver-assistive truck platooning, Illinois transportation and highway engineering conference 2019, available[online] http://www.theconf.com/presentations/2019/Truck%20Platooning%20and%20Automation.pdf

[66] Bureau of labor statistics "Occupational employment statistics: May, 2016 national occupational employments and wage estimates United States," 2017.

[67] International transport forum, "Managing the transition on driverless road freight transport, 2017.

[68] K. Recheru, "Gain scheduling of state feedback in articulated vehicles for jackknife avoidance," Master's thesis, Department of Electrical Engineering, University of Arkansas, 2009.

[69] NHTSA and DOT, Federal Motor Vehicle Safety Standards; Electronic Stability Control System for Heavy Vehicles, Vol.80, No. 120, June, 2015.

[70] J. Woodrooffe, D. Blower,T. Gordon, P. Green, B. Liu, and P. Sweatman, "Safety benefits of stability control systems for tractor-semitrailers," NHTSA Technical Report, DOT HS 811 205, October, 2009.

[71] R. Merala and K. White, "Tractor Semitrailer Left Turns and Lane Changes," *SAE International*, 2010.

[72] Federal Motor Carrier Safety Administration, Publication No. FMCSA-RRA-07-017 https://www.fmcsa.dot.gov/safety/research-and-analysis/large-truck-crash-causation-study-analysis-brief.

[73] A. Tepljakov, *Fractional-order Modeling and Control of Dynamic Systems*. Switzerland. Springer International Publishing AG, 2017.

[74] D. Xue, *Fractional-Order Control Systems Fundamentals and Numerical Implementations.* Berlin/Boston: De Gruyter, 2017.

[75] P. J. Torvik and R. L. Bagley, "On the appearance of the fractional derivative in the behavior of real materials," *Trans. Of the ASME,* Vol. 51, No. 4, pp.294-298, 1984.

[76] S. Karad, S. Chatterji and P. Suryawanshi, " Performance Analysis of Fractional Order PID Controller with the Conventional PID Controller for Bioreactor Control," *International journal of scientific & engineering research*, Vol. 3, No. 6, June-2012.

[77] Podlubny, I., Kostial, I., Kacenak, M., Terpak, J.: Modeling of the Distribution of the Liquid Iron Level in the Blast Furnace Hearth. *METALURGIJA*, vol. 40, no. 2, 2001, pp. 107–109.

[78] Y. Chen, I. Petras and D. Xue, Fractional order control - A tutorial, *American Control Conference*, St. Louis, MO, 2009, pp. 1397-1411.

[79] D. Xue, Y. Chen and D. Atherton, Linear Feedback Control Analysis and Design with MATLAB, SIAM publishing, 2007.

[80] Y. Q. Chen,"Ubiquitous fractional order controls," Proc. 2nd IFAC Symp. Fract. Deriv. Applicat. (FDA'06), Porto, Portugal, July 19–21, vol. 2, pp. 168–173, 2006.

[81] D. Xue, C. Zhao and Y. Chen, "A Modified Approximation Method of Fractional Order System," *International Conference on Mechatronics and Automation*, Luoyang, Henan, 2006, pp. 1043-1048.

[82] I. Pan and S. Das, *Intelligent Fractional Order Systems and Control: An Introduction.* Berlin Heidelberg: Springer, 2013.

[83] K. Miller and B. Ross, *An Introduction to the Fractional Calculus and Fractional Differential Equations*, Wiley, New York, 1993.

[84] I. Podlubny, "Fractional order systems and $PI^{\lambda}D^{\mu}$ controllers," *IEEE Trans. Automat. Contro*l, vol. 44, no.1, pp. 208-214, 1999.

[85] A. Oustaloup, La Commande CRONE, Hermes , Paris, 1991.

[86] A. Oustaloup, La Derivation non entire : theorie, synthese et applications, Hermes Paris, 1995.

[87] I. Podlubny, " Fractional differential equations: an introduction to fractional derivatives, fractional differential equations, to methods of their solution and some of their applications," *Academic Press*, Vol. 198, 1999.

[88] B. M. Vinagre, Y. Q. Chen, and I. Petráš, "Two direct Tustin discretization methods for fractional-order differentiator/integrator," Journal of the Franklin Institute, vol. 340, no. 5, pp. 349–362, 2003.

[89] R. Magin, *Fractional Calculus in Bioengineering*, Begell House Inc. Publishers, Redding, 2006.

[90] T. Hartley, C. Lorenzo, and H. Qammer, "Chaos in a fractional order Chua's system," *IEEE Transactions on Circuits and Systems I: Fundamental Theory and Applications*, vol. 42, no. 8, pp. 485–490, 1995.

[91] R. Hilfer, *Applications of Fractional Calculus in Physics*, World Scientific, Singapore, 2000.

[92] K. Oldham and J. Spanier, *The Fractional Calculus: Theory and Applications of Differentiation and Integration to Arbitrary Order,* Academic Press, New York, 1974.

[93] A. W. Lo, "Long-term memory in stock market prices," Econometrica, vol. 59, no. 5, pp. 1 279–1313, 1991.

[94] K. Ogata, *Modren control engieering*, 5th ed., Prentice hall, 2010.

[95] K. Astrom and R. Murray, *An Introduction to Scientists and Engineers*, Princeton University Press, 2008.

[96] C. Chen, *Linear System Theory and Design*, 3rd ed., Oxford University Press, Inc., New York, 1999.

[97] C. Monje, Y. Chen, B. Vinagre, D. Xue and V. Feliu, *Fractional-order Systems and Controls; Fundamentals and Applications,* Springer, 2010.

[98] Y. Luo and Y. Chen, *Fractional Order Motion Controls*, John Wiley & Sons Ltd., UK, 2012.

[99] A. Dastjerdi, B. Vinagre, Y. Chen and S. HoesseinNia, "Linear fractional order controller; A survey in the frequency domain," *Annual Reviews in Control,* vol. 47, pp.51-70, 2019.

[100] S. Folea, R. Keyser, I. Biras, C. Muresan and C. Ionescu, "Discrete- time implementation and experimental validation of a fractional order pd controller for vibration suppression in airplane wings," *Acta Polytechnica Hungarica,* Vol. 14, No. 1, pp.191-206, 2017.

[101] M. Schnubel *Automotive Suspension & Steering Systems*, 6th Ed., Cengage learning, Stamford, CT, USA., 2015.

[102] R. Dorf and R. Bishop, *Modren Control Systems*, 12th ed., Prentice hall. 2008.

[103] G. Franklin, M. Workman and D. Powell, Digital Control of Dynamic Systems, 3rd rd., Addison-Wesley Longman Publishing Inc., Boston, USA 1997.

[104] R. McCann and A. Le, "Gain Scheduling Control in Commercial Vehicles with Electrohydraulic Power Steering," *SAE Int. J. Commer. Veh.* 1(1):481-487, 2009.

Appendix

This Section displays the generated c code for the applied FOSFB controller to the tractor-trailer nonlinear dynamics.

```
#include "NONlINEAR_TRUCK.h"
#include "NONlINEAR_TRUCK_private.h"

/* Block signals (default storage) */
B_NONlINEAR_TRUCK_T NONlINEAR_TRUCK_B;

/* Continuous states */
X_NONlINEAR_TRUCK_T NONlINEAR_TRUCK_X;

/* Block states (default storage) */
DW_NONlINEAR_TRUCK_T NONlINEAR_TRUCK_DW;

/* Real-time model */
RT_MODEL_NONlINEAR_TRUCK_T NONlINEAR_TRUCK_M_;
RT_MODEL_NONlINEAR_TRUCK_T *const NONlINEAR_TRUCK_M =
&NONlINEAR_TRUCK_M_;

/*
 * Time delay interpolation routine
 *
 * The linear interpolation is performed using the formula:
 *
 *          (t2 - tMinusDelay)         (tMinusDelay - t1)
 * u(t)  =  ----------------- * u1  +  ------------------- * u2
 *             (t2 - t1)                  (t2 - t1)
 */
real_T rt_TDelayInterpolate(
  real_T tMinusDelay,                /* tMinusDelay = currentSimTime - delay */
  real_T tStart,
  real_T *tBuf,
  real_T *uBuf,
  int_T bufSz,
  int_T *lastIdx,
  int_T oldestIdx,
  int_T newIdx,
  real_T initOutput,
  boolean_T discrete,
  boolean_T minorStepAndTAtLastMajorOutput)
{
```

```
  int_T i;
  real_T yout, t1, t2, u1, u2;

  /*
   * If there is only one data point in the buffer, this data point must be
   * the t= 0 and tMinusDelay > t0, it ask for something unknown. The best
   * guess if initial output as well
   */
  if ((newIdx == 0) && (oldestIdx ==0 ) && (tMinusDelay > tStart))
    return initOutput;

  /*
   * If tMinusDelay is less than zero, should output initial value
   */
  if (tMinusDelay <= tStart)
    return initOutput;

  /* For fixed buffer extrapolation:
   * if tMinusDelay is small than the time at oldestIdx, if discrete, output
   * tailptr value,  else use tailptr and tailptr+1 value to extrapolate
   * It is also for fixed buffer. Note: The same condition can happen for transport delay block
where
   * use tStart and and t[tail] other than using t[tail] and t[tail+1].
   * See below
   */
  if ((tMinusDelay <= tBuf[oldestIdx] ) ) {
    if (discrete) {
      return(uBuf[oldestIdx]);
    } else {
      int_T tempIdx= oldestIdx + 1;
      if (oldestIdx == bufSz-1)
        tempIdx = 0;
      t1= tBuf[oldestIdx];
      t2= tBuf[tempIdx];
      u1= uBuf[oldestIdx];
      u2= uBuf[tempIdx];
      if (t2 == t1) {
        if (tMinusDelay >= t2) {
          yout = u2;
        } else {
          yout = u1;
        }
      } else {
        real_T f1 = (t2-tMinusDelay) / (t2-t1);
        real_T f2 = 1.0 - f1;
```

```
      /*
       * Use Lagrange's interpolation formula.  Exact outputs at t1, t2.
       */
      yout = f1*u1 + f2*u2;
    }

    return yout;
  }
}

/*
 * When block does not have direct feedthrough, we use the table of
 * values to extrapolate off the end of the table for delays that are less
 * than 0 (less then step size).  This is not completely accurate.  The
 * chain of events is as follows for a given time t.  Major output - look
 * in table.  Update - add entry to table.  Now, if we call the output at
 * time t again, there is a new entry in the table. For very small delays,
 * this means that we will have a different answer from the previous call
 * to the output fcn at the same time t.  The following code prevents this
 * from happening.
 */
if (minorStepAndTAtLastMajorOutput) {
  /* pretend that the new entry has not been added to table */
  if (newIdx != 0) {
    if (*lastIdx == newIdx) {
      (*lastIdx)--;
    }

    newIdx--;
  } else {
    if (*lastIdx == newIdx) {
      *lastIdx = bufSz-1;
    }

    newIdx = bufSz - 1;
  }
}

i = *lastIdx;
if (tBuf[i] < tMinusDelay) {
  /* Look forward starting at last index */
  while (tBuf[i] < tMinusDelay) {
    /* May occur if the delay is less than step-size - extrapolate */
    if (i == newIdx)
      break;
    i = ( i < (bufSz-1) ) ? (i+1) : 0;/* move through buffer */
```

```
  }
 } else {
  /*
   * Look backwards starting at last index which can happen when the
   * delay time increases.
   */
  while (tBuf[i] >= tMinusDelay) {
    /*
     * Due to the entry condition at top of function, we
     * should never hit the end.
     */
    i = (i > 0) ? i-1 : (bufSz-1);   /* move through buffer */
  }

  i = ( i < (bufSz-1) ) ? (i+1) : 0;
 }

 *lastIdx = i;
 if (discrete) {
  /*
   * tempEps = 128 * eps;
   * localEps = max(tempEps, tempEps*fabs(tBuf[i]))/2;
   */
  double tempEps = (DBL_EPSILON) * 128.0;
  double localEps = tempEps * fabs(tBuf[i]);
  if (tempEps > localEps) {
    localEps = tempEps;
  }

  localEps = localEps / 2.0;
  if (tMinusDelay >= (tBuf[i] - localEps)) {
    yout = uBuf[i];
  } else {
    if (i == 0) {
      yout = uBuf[bufSz-1];
    } else {
      yout = uBuf[i-1];
    }
  }
 } else {
  if (i == 0) {
    t1 = tBuf[bufSz-1];
    u1 = uBuf[bufSz-1];
  } else {
    t1 = tBuf[i-1];
    u1 = uBuf[i-1];
```

```
    }

    t2 = tBuf[i];
    u2 = uBuf[i];
    if (t2 == t1) {
      if (tMinusDelay >= t2) {
        yout = u2;
      } else {
        yout = u1;
      }
    } else {
      real_T f1 = (t2-tMinusDelay) / (t2-t1);
      real_T f2 = 1.0 - f1;

      /*
       * Use Lagrange's interpolation formula.  Exact outputs at t1, t2.
       */
      yout = f1*u1 + f2*u2;
    }
  }

  return(yout);
}

/*
 * This function updates continuous states using the ODE4 fixed-step
 * solver algorithm
 */
static void rt_ertODEUpdateContinuousStates(RTWSolverInfo *si )
{
  time_T t = rtsiGetT(si);
  time_T tnew = rtsiGetSolverStopTime(si);
  time_T h = rtsiGetStepSize(si);
  real_T *x = rtsiGetContStates(si);
  ODE4_IntgData *id = (ODE4_IntgData *)rtsiGetSolverData(si);
  real_T *y = id->y;
  real_T *f0 = id->f[0];
  real_T *f1 = id->f[1];
  real_T *f2 = id->f[2];
  real_T *f3 = id->f[3];
  real_T temp;
  int_T i;
  int_T nXc = 18;
  rtsiSetSimTimeStep(si,MINOR_TIME_STEP);

  /* Save the state values at time t in y, we'll use x as ynew. */
```

```
(void) memcpy(y, x,
            (uint_T)nXc*sizeof(real_T));

/* Assumes that rtsiSetT and ModelOutputs are up-to-date */
/* f0 = f(t,y) */
rtsiSetdX(si, f0);
NONlINEAR_TRUCK_derivatives();

/* f1 = f(t + (h/2), y + (h/2)*f0) */
temp = 0.5 * h;
for (i = 0; i < nXc; i++) {
  x[i] = y[i] + (temp*f0[i]);
}

rtsiSetT(si, t + temp);
rtsiSetdX(si, f1);
NONlINEAR_TRUCK_step();
NONlINEAR_TRUCK_derivatives();

/* f2 = f(t + (h/2), y + (h/2)*f1) */
for (i = 0; i < nXc; i++) {
  x[i] = y[i] + (temp*f1[i]);
}

rtsiSetdX(si, f2);
NONlINEAR_TRUCK_step();
NONlINEAR_TRUCK_derivatives();

/* f3 = f(t + h, y + h*f2) */
for (i = 0; i < nXc; i++) {
  x[i] = y[i] + (h*f2[i]);
}

rtsiSetT(si, tnew);
rtsiSetdX(si, f3);
NONlINEAR_TRUCK_step();
NONlINEAR_TRUCK_derivatives();

/* tnew = t + h
   ynew = y + (h/6)*(f0 + 2*f1 + 2*f2 + 2*f3) */
temp = h / 6.0;
for (i = 0; i < nXc; i++) {
  x[i] = y[i] + temp*(f0[i] + 2.0*f1[i] + 2.0*f2[i] + f3[i]);
}

rtsiSetSimTimeStep(si,MAJOR_TIME_STEP);
```

```
}

/*
 * Output and update for atomic system:
 *    '<S10>/Embedded MATLAB Function1'
 *    '<S12>/Embedded MATLAB Function1'
 */
void NONlINE_EmbeddedMATLABFunction1(real_T rtu_psi, real_T *rty_y)
{
  *rty_y = cos(rtu_psi) * 0.00021945746155369283;
}

/*
 * Output and update for atomic system:
 *    '<S10>/Embedded MATLAB Function15'
 *    '<S12>/Embedded MATLAB Function15'
 */
void NONlIN_EmbeddedMATLABFunction15(real_T rtu_u1, real_T rtu_psi, real_T
  rtu_v1, real_T rtu_v2, real_T rtu_r1, real_T rtu_r2, real_T rtu_Fy1, real_T
  rtu_Fy2, real_T rtu_Fx1, real_T rtu_Fx2, real_T rtu_Fx3, real_T rtu_Fa1,
  real_T rtu_Fa2, real_T rtu_delta, real_T *rty_y)
{
  real_T tmp;
  real_T tmp_0;
  tmp = sin(rtu_psi);
  tmp_0 = cos(rtu_psi);
  *rty_y = (((((rtu_Fx1 * tmp * 2.5551434321583784E-5 + rtu_Fy1 * tmp_0 / 5450.0)
              * sin(rtu_delta) + (rtu_Fy2 * 0.00037089785537421538 - rtu_r2 *
    rtu_u1) * tmp) + (((rtu_Fa1 - rtu_Fx2) / 5450.0 - (rtu_r1 - rtu_r2) *
                      (0.8611 * rtu_r1)) - rtu_r2 * rtu_v1) * tmp_0) + (rtu_Fy1
             * tmp * 2.5551434321583784E-5 - rtu_Fx1 * tmp_0 / 5450.0) * cos
            (rtu_delta)) - (rtu_Fa2 - rtu_Fx3) / 27800.0) + rtu_r2 * rtu_v2;
}

/*
 * Output and update for atomic system:
 *    '<S10>/Embedded MATLAB Function16'
 *    '<S12>/Embedded MATLAB Function16'
 */
void NONlIN_EmbeddedMATLABFunction16(real_T rtu_Fy1, real_T rtu_Fy2, real_T
  rtu_Fy3, real_T rtu_r1, real_T rtu_r2, real_T rtu_v1, real_T rtu_u1, real_T
  rtu_psi, real_T rtu_Fx1, real_T rtu_Fx2, real_T rtu_Fa1, real_T rtu_delta,
  real_T *rty_y)
{
  real_T tmp;
  real_T tmp_0;
```

```
  real_T tmp_1;
  tmp = sin(rtu_psi);
  tmp_0 = cos(rtu_psi);
  tmp_1 = rtu_r2 * rtu_u1;
  *rty_y = (((((((rtu_Fa1 - rtu_Fx2) / 5450.0 - rtu_r2 * rtu_v1) + (-rtu_r1 +
    rtu_r2) * 0.8611 * rtu_r1) * tmp + (rtu_Fx1 * tmp_0 * -2.5551434321583784E-5
    + tmp * rtu_Fy1 / 5450.0) * sin(rtu_delta)) + (-rtu_Fy2 *
    0.00037089785537421538 + tmp_1) * tmp_0) + (rtu_Fy1 * tmp_0 *
            -2.5551434321583784E-5 - tmp * rtu_Fx1 / 5450.0) * cos(rtu_delta))
          + rtu_Fy3 * -5.1685619778417252E-5) - tmp_1;
}

/*
 * Output and update for atomic system:
 *    '<S10>/Embedded MATLAB Function2'
 *    '<S12>/Embedded MATLAB Function2'
 */
void NONlINE_EmbeddedMATLABFunction2(real_T rtu_psi, real_T *rty_y)
{
  *rty_y = cos(rtu_psi) * 0.00056685801919579811;
}

/*
 * Output and update for atomic system:
 *    '<S10>/Embedded MATLAB Function22'
 *    '<S12>/Embedded MATLAB Function22'
 */
void NONlIN_EmbeddedMATLABFunction22(real_T rtu_d11, real_T rtu_d22, real_T
  rtu_d12, real_T rtu_d21, real_T *rty_y)
{
  *rty_y = rtu_d22 * rtu_d11 - rtu_d12 * rtu_d21;
}

/* Model step function */
void NONlINEAR_TRUCK_step(void)
{
  /* local block i/o variables */
  real_T rtb_TransportDelay2;
  real_T rtb_TransportDelay1;
  real_T rtb_TransportDelay;
  real_T rtb_Gain3_c;
  real_T rtb_Gain_j;
  real_T rtb_Gain1_f;
  real_T rtb_y_p;
  real_T rtb_y_a;
  real_T rtb_Integrator;
```

```
  real_T rtb_Add2;
  real_T rtb_y_kl;
  real_T rtb_y_d;
  real_T rtb_y;
  real_T rtb_y_g;
  real_T rtb_y_el;
  real_T rtb_y_en;
  real_T tmp[5];
  int32_T i;
  real_T Gain6_tmp;
  real_T Gain6_tmp_0;
  if (rtmIsMajorTimeStep(NONlINEAR_TRUCK_M)) {
    /* set solver stop time */
    rtsiSetSolverStopTime(&NONlINEAR_TRUCK_M->solverInfo,
                          ((NONlINEAR_TRUCK_M->Timing.clockTick0+1)*
      NONlINEAR_TRUCK_M->Timing.stepSize0));
  }                                    /* end MajorTimeStep */

  /* Update absolute time of base rate at minor time step */
  if (rtmIsMinorTimeStep(NONlINEAR_TRUCK_M)) {
    NONlINEAR_TRUCK_M->Timing.t[0] = rtsiGetT(&NONlINEAR_TRUCK_M-
>solverInfo);
  }

  /* Integrator: '<Root>/Integrator1' */
  NONlINEAR_TRUCK_B.Integrator1 = NONlINEAR_TRUCK_X.Integrator1_CSTATE;

  /* Integrator: '<Root>/Integrator2' */
  NONlINEAR_TRUCK_B.Integrator2 = NONlINEAR_TRUCK_X.Integrator2_CSTATE;

  /* SignalConversion: '<Root>/TmpSignal ConversionAtGain5Inport1' incorporates:
   *  Integrator: '<Root>/Integrator3'
   *  Integrator: '<Root>/Integrator5'
   *  Integrator: '<Root>/Integrator6'
   */
  tmp[0] = NONlINEAR_TRUCK_B.Integrator1;
  tmp[1] = NONlINEAR_TRUCK_B.Integrator2;
  tmp[2] = NONlINEAR_TRUCK_X.Integrator5_CSTATE;
  tmp[3] = NONlINEAR_TRUCK_X.Integrator6_CSTATE;
  tmp[4] = NONlINEAR_TRUCK_X.Integrator3_CSTATE;

  /* Gain: '<Root>/Gain5' */
  rtb_y_p = 0.0;
  for (i = 0; i < 5; i++) {
    rtb_y_p += NONlINEAR_TRUCK_ConstP.Gain5_Gain[i] * tmp[i];
  }
```

```
  /* Integrator: '<Root>/Integrator10' */
  NONlINEAR_TRUCK_B.Integrator10 = NONlINEAR_TRUCK_X.Integrator10_CSTATE;

  /* Step: '<S18>/Step' */
  if (NONlINEAR_TRUCK_M->Timing.t[0] < 0.0) {
    rtb_y_d = 0.0;
  } else {
    rtb_y_d = 1.75;
  }

  /* End of Step: '<S18>/Step' */

  /* Product: '<S18>/Product' incorporates:
   *  Clock: '<S18>/Clock'
   */
  rtb_Integrator = rtb_y_d * NONlINEAR_TRUCK_M->Timing.t[0];

  /* Saturate: '<S7>/Saturation' */
  if (rtb_Integrator > 7.0) {
    rtb_Integrator = 7.0;
  } else {
    if (rtb_Integrator < 0.0) {
      rtb_Integrator = 0.0;
    }
  }

  /* End of Saturate: '<S7>/Saturation' */

  /* Integrator: '<Root>/Integrator9' */
  rtb_y_a = NONlINEAR_TRUCK_X.Integrator9_CSTATE;

  /* Sum: '<Root>/Sum6' incorporates:
   *  Integrator: '<Root>/Integrator9'
   */
  NONlINEAR_TRUCK_B.Sum6 = rtb_Integrator -
NONlINEAR_TRUCK_X.Integrator9_CSTATE;

  /* Sum: '<Root>/Sum10' incorporates:
   *  Integrator: '<Root>/Integrator5'
   */
  NONlINEAR_TRUCK_B.Sum10 = NONlINEAR_TRUCK_B.Integrator2 -
    NONlINEAR_TRUCK_X.Integrator5_CSTATE;

  /* Sum: '<Root>/Add2' incorporates:
   *  Gain: '<Root>/Gain5'
```

```
 *  Gain: '<Root>/Integral Gain 1 '
 *  Gain: '<Root>/Integral Gain 2'
 *  Gain: '<Root>/Proportional Gain '
 *  Gain: '<S1>/Gain'
 *  Gain: '<S1>/Gain1'
 *  Integrator: '<Root>/Integrator6'
 *  StateSpace: '<S3>/Internal'
 *  Sum: '<Root>/Sum5'
 *  Sum: '<S1>/Add1'
 */
rtb_Add2 = (((((((NONlINEAR_TRUCK_X.Internal_CSTATE[0] +
                   NONlINEAR_TRUCK_X.Internal_CSTATE[1]) +
                  NONlINEAR_TRUCK_X.Internal_CSTATE[2]) +
                 NONlINEAR_TRUCK_X.Internal_CSTATE[3]) +
                NONlINEAR_TRUCK_X.Internal_CSTATE[4]) + 0.15848931924611132 *
               NONlINEAR_TRUCK_B.Integrator10) * 0.39999999999999986 +
              1.4229544886448324 * NONlINEAR_TRUCK_B.Integrator10) +
             1.4427847279115398 * NONlINEAR_TRUCK_B.Sum6) - rtb_y_p) + (0.0 *
  NONlINEAR_TRUCK_X.Integrator6_CSTATE + -0.0 * NONlINEAR_TRUCK_B.Sum10);

/* MATLAB Function: '<S11>/Embedded MATLAB Function11' incorporates:
 *  Constant: '<Root>/Constant'
 */
rtb_y_kl = (rtb_Add2 - (1.7424 * NONlINEAR_TRUCK_B.Integrator2 +
  NONlINEAR_TRUCK_B.Integrator1) / 31.30001) * 630000.0;

/* MATLAB Function: '<S13>/Embedded MATLAB Function12' incorporates:
 *  Constant: '<Root>/Constant'
 */
rtb_y_d = -(NONlINEAR_TRUCK_B.Integrator1 - 2.0676 *
            NONlINEAR_TRUCK_B.Integrator2) / 31.30001 * 1.848E+6;

/* TransportDelay: '<Root>/Transport Delay2' */
{
  real_T **uBuffer = (real_T**)
    &NONlINEAR_TRUCK_DW.TransportDelay2_PWORK.TUbufferPtrs[0];
  real_T **tBuffer = (real_T**)
    &NONlINEAR_TRUCK_DW.TransportDelay2_PWORK.TUbufferPtrs[1];
  real_T simTime = NONlINEAR_TRUCK_M->Timing.t[0];
  real_T tMinusDelay = simTime - 0.25;
  rtb_TransportDelay2 = rt_TDelayInterpolate(
    tMinusDelay,
    0.0,
    *tBuffer,
    *uBuffer,
    NONlINEAR_TRUCK_DW.TransportDelay2_IWORK.CircularBufSize,
```

```
    &NONlINEAR_TRUCK_DW.TransportDelay2_IWORK.Last,
    NONlINEAR_TRUCK_DW.TransportDelay2_IWORK.Tail,
    NONlINEAR_TRUCK_DW.TransportDelay2_IWORK.Head,
    0.0,
    0,
    0);
}

/* TransportDelay: '<Root>/Transport Delay1' */
{
  real_T **uBuffer = (real_T**)
    &NONlINEAR_TRUCK_DW.TransportDelay1_PWORK.TUbufferPtrs[0];
  real_T **tBuffer = (real_T**)
    &NONlINEAR_TRUCK_DW.TransportDelay1_PWORK.TUbufferPtrs[1];
  real_T simTime = NONlINEAR_TRUCK_M->Timing.t[0];
  real_T tMinusDelay = simTime - 0.25;
  rtb_TransportDelay1 = rt_TDelayInterpolate(
    tMinusDelay,
    0.0,
    *tBuffer,
    *uBuffer,
    NONlINEAR_TRUCK_DW.TransportDelay1_IWORK.CircularBufSize,
    &NONlINEAR_TRUCK_DW.TransportDelay1_IWORK.Last,
    NONlINEAR_TRUCK_DW.TransportDelay1_IWORK.Tail,
    NONlINEAR_TRUCK_DW.TransportDelay1_IWORK.Head,
    0.0,
    0,
    0);
}

/* TransportDelay: '<Root>/Transport Delay' */
{
  real_T **uBuffer = (real_T**)
    &NONlINEAR_TRUCK_DW.TransportDelay_PWORK.TUbufferPtrs[0];
  real_T **tBuffer = (real_T**)
    &NONlINEAR_TRUCK_DW.TransportDelay_PWORK.TUbufferPtrs[1];
  real_T simTime = NONlINEAR_TRUCK_M->Timing.t[0];
  real_T tMinusDelay = simTime - 0.45;
  rtb_TransportDelay = rt_TDelayInterpolate(
    tMinusDelay,
    0.0,
    *tBuffer,
    *uBuffer,
    NONlINEAR_TRUCK_DW.TransportDelay_IWORK.CircularBufSize,
    &NONlINEAR_TRUCK_DW.TransportDelay_IWORK.Last,
    NONlINEAR_TRUCK_DW.TransportDelay_IWORK.Tail,
```

```
    NONlINEAR_TRUCK_DW.TransportDelay_IWORK.Head,
    0.0,
    0,
    0);
  }

  /* MATLAB Function: '<S12>/Embedded MATLAB Function15' incorporates:
   *  Constant: '<Root>/Constant'
   *  Integrator: '<Root>/Integrator4'
   *  Integrator: '<Root>/Integrator5'
   *  Integrator: '<Root>/Integrator6'
   */
  NONlIN_EmbeddedMATLABFunction15(31.3,
NONlINEAR_TRUCK_X.Integrator6_CSTATE,
    NONlINEAR_TRUCK_B.Integrator1, NONlINEAR_TRUCK_X.Integrator4_CSTATE,
    NONlINEAR_TRUCK_B.Integrator2, NONlINEAR_TRUCK_X.Integrator5_CSTATE,
    rtb_y_kl, rtb_y_d, rtb_TransportDelay2, rtb_TransportDelay1,
    rtb_TransportDelay, NONlINEAR_TRUCK_ConstB.Gain,
    NONlINEAR_TRUCK_ConstB.Gain_d, rtb_Add2, &rtb_y_el);

  /* MATLAB Function: '<S14>/Embedded MATLAB Function2' incorporates:
   *  Constant: '<Root>/Constant'
   *  Integrator: '<Root>/Integrator4'
   *  Integrator: '<Root>/Integrator5'
   */
  rtb_y = -(NONlINEAR_TRUCK_X.Integrator4_CSTATE - 2.3886 *
          NONlINEAR_TRUCK_X.Integrator5_CSTATE) / 31.30001 * 600000.0;

  /* MATLAB Function: '<S12>/Embedded MATLAB Function16' incorporates:
   *  Constant: '<Root>/Constant'
   *  Integrator: '<Root>/Integrator5'
   *  Integrator: '<Root>/Integrator6'
   */
  NONlIN_EmbeddedMATLABFunction16(rtb_y_kl, rtb_y_d, rtb_y,
    NONlINEAR_TRUCK_B.Integrator2, NONlINEAR_TRUCK_X.Integrator5_CSTATE,
    NONlINEAR_TRUCK_B.Integrator1, 31.3, NONlINEAR_TRUCK_X.Integrator6_CSTATE,
    rtb_TransportDelay2, rtb_TransportDelay1, NONlINEAR_TRUCK_ConstB.Gain,
    rtb_Add2, &rtb_y_p);

  /* MATLAB Function: '<S12>/Embedded MATLAB Function1' incorporates:
   *  Integrator: '<Root>/Integrator6'
   */
  NONlINE_EmbeddedMATLABFunction1(NONlINEAR_TRUCK_X.Integrator6_CSTATE,
    &rtb_y_en);

  /* MATLAB Function: '<S12>/Embedded MATLAB Function5' incorporates:
```

```
   *  Integrator: '<Root>/Integrator6'
   */
  rtb_y_g = NONlINEAR_TRUCK_X.Integrator6_CSTATE * 0.00048880610235369285;

  /* MATLAB Function: '<S12>/Embedded MATLAB Function2' incorporates:
   *  Integrator: '<Root>/Integrator6'
   */
  NONlINE_EmbeddedMATLABFunction2(NONlINEAR_TRUCK_X.Integrator6_CSTATE,
&rtb_y_a);

  /* MATLAB Function: '<S12>/Embedded MATLAB Function22' incorporates:
   *  Integrator: '<Root>/Integrator6'
   *  MATLAB Function: '<S12>/Embedded MATLAB Function3'
   */
  NONlIN_EmbeddedMATLABFunction22(rtb_y_en, rtb_y_a,
    -NONlINEAR_TRUCK_X.Integrator6_CSTATE * 0.00029750937839579809, rtb_y_g,
    &rtb_Integrator);

  /* MATLAB Function: '<S12>/Embedded MATLAB Function20' */
  rtb_y_g = (rtb_y_g * rtb_y_el - rtb_y_en * rtb_y_p) / rtb_Integrator;

  /* Product: '<Root>/Product12' incorporates:
   *  Product: '<Root>/Product10'
   *  Trigonometry: '<Root>/Trigonometric Function5'
   */
  Gain6_tmp = cos(rtb_Add2) * rtb_y_kl;

  /* Product: '<Root>/Product13' incorporates:
   *  Product: '<Root>/Product11'
   *  Trigonometry: '<Root>/Trigonometric Function6'
   */
  Gain6_tmp_0 = rtb_TransportDelay2 * sin(rtb_Add2);

  /* Gain: '<Root>/Gain6' incorporates:
   *  Gain: '<Root>/Gain10'
   *  Gain: '<Root>/Gain7'
   *  Gain: '<Root>/Gain8'
   *  Gain: '<Root>/Gain9'
   *  Product: '<Root>/Product12'
   *  Product: '<Root>/Product13'
   *  Sum: '<Root>/Sum4'
   */
  NONlINEAR_TRUCK_B.Gain6 = (((Gain6_tmp * 1.7424 + Gain6_tmp_0 * 1.7424) -
    2.0676 * rtb_y_d) + 0.8611 * rtb_y_g) * 0.00010526315789473685;

  /* MATLAB Function: '<S10>/Embedded MATLAB Function15' incorporates:
```

```
   *  Constant: '<Root>/Constant'
   *  Integrator: '<Root>/Integrator4'
   *  Integrator: '<Root>/Integrator5'
   *  Integrator: '<Root>/Integrator6'
   */
  NONlIN_EmbeddedMATLABFunction15(31.3,
NONlINEAR_TRUCK_X.Integrator6_CSTATE,
    NONlINEAR_TRUCK_B.Integrator1, NONlINEAR_TRUCK_X.Integrator4_CSTATE,
    NONlINEAR_TRUCK_B.Integrator2, NONlINEAR_TRUCK_X.Integrator5_CSTATE,
    rtb_y_kl, rtb_y_d, rtb_TransportDelay2, rtb_TransportDelay1,
    rtb_TransportDelay, NONlINEAR_TRUCK_ConstB.Gain,
    NONlINEAR_TRUCK_ConstB.Gain_d, rtb_Add2, &rtb_y_a);

  /* MATLAB Function: '<S10>/Embedded MATLAB Function16' incorporates:
   *  Constant: '<Root>/Constant'
   *  Integrator: '<Root>/Integrator5'
   *  Integrator: '<Root>/Integrator6'
   */
  NONlIN_EmbeddedMATLABFunction16(rtb_y_kl, rtb_y_d, rtb_y,
    NONlINEAR_TRUCK_B.Integrator2, NONlINEAR_TRUCK_X.Integrator5_CSTATE,
    NONlINEAR_TRUCK_B.Integrator1, 31.3, NONlINEAR_TRUCK_X.Integrator6_CSTATE,
    rtb_TransportDelay2, rtb_TransportDelay1, NONlINEAR_TRUCK_ConstB.Gain,
    rtb_Add2, &rtb_Integrator);

  /* MATLAB Function: '<S10>/Embedded MATLAB Function2' incorporates:
   *  Integrator: '<Root>/Integrator6'
   */
  NONlINE_EmbeddedMATLABFunction2(NONlINEAR_TRUCK_X.Integrator6_CSTATE,
    &rtb_y_el);

  /* MATLAB Function: '<S10>/Embedded MATLAB Function3' incorporates:
   *  Integrator: '<Root>/Integrator6'
   *  Trigonometry: '<Root>/Trigonometric Function10'
   */
  rtb_Add2 = sin(NONlINEAR_TRUCK_X.Integrator6_CSTATE);
  rtb_y_kl = -rtb_Add2 * 0.00029750937839579809;

  /* MATLAB Function: '<S10>/Embedded MATLAB Function1' incorporates:
   *  Integrator: '<Root>/Integrator6'
   */
  NONlINE_EmbeddedMATLABFunction1(NONlINEAR_TRUCK_X.Integrator6_CSTATE,
&rtb_y_p);

  /* MATLAB Function: '<S10>/Embedded MATLAB Function22' incorporates:
   *  Integrator: '<Root>/Integrator6'
   *  MATLAB Function: '<S10>/Embedded MATLAB Function5'
```

```
 */
NONlIN_EmbeddedMATLABFunction22(rtb_y_p, rtb_y_el, rtb_y_kl, sin
  (NONlINEAR_TRUCK_X.Integrator6_CSTATE) * 0.00048880610235369285, &rtb_y_en);

/* Product: '<Root>/Product15' incorporates:
 *  Integrator: '<Root>/Integrator6'
 *  Product: '<Root>/Product6'
 *  Trigonometry: '<Root>/Trigonometric Function9'
 */
rtb_y_p = rtb_y_g * cos(NONlINEAR_TRUCK_X.Integrator6_CSTATE);

/* Product: '<Root>/Product5' incorporates:
 *  MATLAB Function: '<S10>/Embedded MATLAB Function21'
 *  Product: '<Root>/Product7'
 */
rtb_Integrator = (-rtb_y_el * rtb_y_a + rtb_y_kl * rtb_Integrator) / rtb_y_en *
  rtb_Add2;

/* Sum: '<Root>/Sum7' incorporates:
 *  Constant: '<Root>/Constant'
 *  Gain: '<Root>/Gain12'
 *  Integrator: '<Root>/Integrator5'
 *  Product: '<Root>/Product15'
 *  Product: '<Root>/Product4'
 *  Product: '<Root>/Product5'
 *  Sum: '<Root>/Sum8'
 */
```